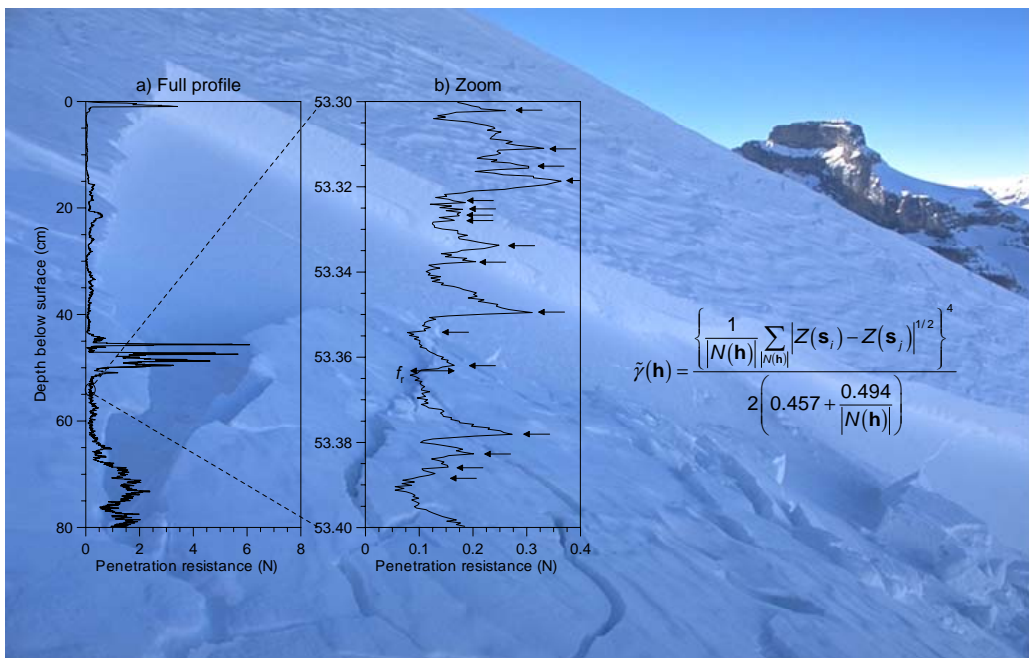

Spatial Variability of Snow Mechanical Properties

with regard to avalanche formation



Kalle Kronholm

**Spatial Variability of Snow Mechanical Properties
with regard to Avalanche Formation**

Dissertation

zur

**Erlangung der naturwissenschaftlichen Doktorwürde
(Dr. sc. nat.)**

vorgelegt der

Mathematisch-naturwissenschaftlichen Fakultät

der

Universität Zürich

von

Kalle Kronholm

aus

Dänemark

Promotionskomitee

Prof. Dr. Wilfried Haerberli (Vorsitz)

Dr. Jürg Schweizer (Leitung der Dissertation)

Dr. Martin Schneebeli (Co-Leitung)

Zürich 2004

Table of Contents

Table of Contents	i
Abstract	v
Zusammenfassung	vii
Preface	ix
Acknowledgements	xi
List of Tables	xiii
List of Figures	xv
List of Symbols	xxi
List of Abbreviations	xxiii
Introduction	1
1.1. Introduction	1
1.2. Motivation.....	1
1.3. Objectives of the study.....	4
1.4. Snow slope stability.....	5
1.4.1. Dry snow slab avalanche formation	5
1.4.2. Slab release processes.....	6
1.5. Scale and scale issues.....	8
1.5.1. A definition of scale.....	8
1.5.2. Problems associated with scale and scaling.....	9
1.6. The snow cover as a sediment.....	11
1.7. Previous studies of slope-scale variability	12
1.7.1. Studies at other scales.....	16
1.7.2. Discussion of previous slope-scale studies.....	17
1.7.3. Conclusions from previous slope-scale studies	19
Methods	21
2.1. Introduction	21

2.2. Research methodology.....	22
2.2.1. Practical limitations and considerations.....	22
2.2.2. Overview of available measurement methods.....	24
2.2.3. Overview of methods for characterizing spatial variability	26
2.2.4. Considerations for the spatial measurement layout	28
2.2.5. Geostatistical optimization of the sampling layout.....	29
2.3. The grid layout.....	32
2.3.1. Measurements in the grid.....	33
2.3.2. Field procedure for the grid measurements.....	34
2.3.3. Slope selection.....	35
2.4. Study area and fieldwork period	35
2.4.1. Fieldwork period	36
2.4.2. Location.....	36
2.4.3. Terrain.....	37
2.4.4. Snow and weather conditions	38
2.5. Ramsonde hardness profile.....	40
2.5.1. Measurement precision	40
2.6. Manually observed stratigraphic snow profile	41
2.6.1. Observations	41
2.6.2. Measurement precision and resolution.....	42
2.7. Snow samples	43
2.8. The snow micro-penetrometer.....	44
2.8.1. Previous SMP versions	46
2.8.2. Measurement errors	46
2.8.3. Analysis of the SMP data on multiple scales.....	47
2.8.4. Penetration resistance of grid-layers	48
2.8.5. Microstructural properties of grid-layers	49
2.8.6. Micro-mechanical properties of grid-layers.....	50
2.8.7. Algorithms for SMP signal analysis	51
2.8.8. Precision of the signal analysis	53
2.9. The rutschblock stability test.....	55
2.9.1. Interpretation of the rutschblock test results.....	57
2.9.2. Rutschblock test limitations	58
2.10. Column-type stability tests.....	58
2.10.1. The stuffblock test	59

2.10.2. The rammrutsch test	59
2.10.3. Values recorded for each fracture	61
2.10.4. Interpretation of point stability test results	62
2.10.5. Measurement errors and limitations	62
2.11. Reconstruction of snow stratigraphy	63
2.11.1. Outline of the procedure	63
2.11.2. The IDL procedure for layer identification	66
2.11.3. Precision of boundary location	66
2.11.4. Grid-layers defined from stability tests	66
2.12. Data analysis	66
2.12.1. Overview of snow cover properties investigated	66
2.12.2. Analysis of stability measurements	67
2.12.3. Analysis of penetration resistance measurements	69
2.12.4. Geostatistical analysis	70
2.12.5. Comments to the geostatistical methods	73
Data	75
3.1. Introduction	75
3.2. The collected data	75
3.2.1. Slope inclination and aspect	75
3.3. Data selection	76
3.3.1. Stability tests	77
3.3.2. Penetration resistance measurements	77
3.4. Snow cover stratigraphy	80
3.4.1. Persistent weak layers PWL-1 and PWL-2	80
3.4.2. Persistent weak layer PWL-3	83
Results	85
4.1. Introduction	85
4.2. Stability test results	85
4.2.1. Comparison of rammrutsch and rutschblock results	86
4.2.2. Variation of point stability	89
4.2.3. Causes of variation in stability	96
4.3. Penetration resistance results	105
4.3.1. Comparison of calculated and observed microstructural properties	106
4.3.2. Grid-layer mechanical properties	107

4.3.3. Variation of penetration resistance	109
4.3.4. Causes of variation in penetration resistance.....	116
4.4. Comparison of point stability and penetration resistance	120
4.4.1. Comparison within each grid-layer	120
4.4.2. Comparison between grid-layers.....	121
Discussion.....	123
5.1. Introduction.....	123
5.2. Measurement methods	123
5.2.1. Stability tests	123
5.2.2. Snow micro-penetrometer	125
5.3. Classification of snow cover stratigraphy.....	128
5.4. Spatial variability.....	130
5.5. Implications for dry snow slab avalanche release.....	135
5.6. Practical consequences.....	135
5.6.1. Grid layout.....	135
5.6.2. Stability evaluation	136
5.6.3. Including spatial variability in models	137
Conclusions	139
6.1. Summary	139
6.2. Conclusions	139
6.3. Outlook	142
References.....	143
Appendix A: Snow profiles	153
Appendix B: Stability test data	165
Appendix C: SMP data.....	177

Abstract

The spatial variability of snowpack mechanical properties strongly influences the fracture initiation and fracture propagation properties of the snowpack, thereby largely controlling the avalanche formation process. The slope-scale spatial variability of the snowpack was investigated on small potential avalanche slopes above timberline near Davos, Switzerland. The characterization of variability was accomplished by combining classical and new measurement methods. The sampling strategy was to optimize the measurement layout for geostatistical analysis. The fracture initiation properties of the snow cover were measured with stuffblock and rammrutsch point stability tests at 24 locations on each slope. High-resolution profiles of penetration resistance were recorded with a novel snow micro-penetrometer at more than 100 locations on each slope. On each slope, a classical stratigraphic profile was made and samples of weak layers were taken. The spatial structure of stability and penetration resistance was modeled as a trend plus residual variation that was described with the semi-variogram. The trend was modeled as a linear regression on the measurement coordinates. A spherical semi-variogram model was used to describe the residual variation.

Twenty weak layers were identified by fractures in point stability tests. The spatial variability of point stability had a spatial structure, mainly in the form of slope-scale trends. The trends accounted for around 40% of the observed spread. The quartile coefficient of variation around the linear trend was around 20% with a maximum of around 50%. This variation around the trend had little spatial structure and was within the measurement error of the tests. The weak layer depth partly explained the variation in stability.

The snow cover stratigraphy was reconstructed from the snow micro-penetrometer profiles. The 21 investigated layers were both weak layers and wind-slabs. The weak layers were identified in all penetrometer profiles on a slope, i.e. they were spatially continuous. A significant spatial trend in penetration resistance was found in most layers. The quartile coefficient of variation around the linear trend was around 15% with a maximum of around 60%. Spatial structure around the linear trend was found in all layers except in a layer of buried surface hoar. The range of spatial auto-correlation varied between 2 m and more

than 10 m. The layer depth partly explained the spatial variation in penetration resistance. Each layer had unique geostatistical properties with regard to penetration resistance. These were likely caused by the different depositional processes acting during each depositional event, thus emphasizing the sedimentary nature of the snow cover.

Comparing the results from the point stability tests and the micro-penetrometer profiles, similar spatial trends at the slope scale were found.

For the first time, the three-dimensional variability of the snow cover was quantified. The results can be used to improve snow cover models that currently do not reflect the spatial variability observed in the field. With regard to the avalanche formation process, the study showed that the weak layers were continuous (through going) at the slope-scale, and that their penetration resistance had a spatial structure with typical length scales of a few meters. Likewise, results from snowpack stability tests had a spatial structure. Therefore, stability tests will not give random results and are useful to assess snow cover stability. The type of variability found suggests that once initiated, a fracture is likely to propagate through the weak layer without being arrested before reaching the critical size where a snow slab avalanche is released.

Zusammenfassung

Die räumliche Variabilität der mechanischen Eigenschaften der Schneedecke beeinflusst wesentlich die Lawinenbildung, und zwar über die Bruchbildung und Bruchausbreitung. Um die räumliche Variabilität der Schneedecke auf der Hangskala zu untersuchen, wurden Messungen in kleinen potentiellen Lawinhängen gemacht, welche alle oberhalb der Baumgrenze in der Nähe von Davos, Schweiz, liegen. Dabei wurden neue und traditionelle Messmethoden kombiniert. Die Messmethodik wurde optimiert im Hinblick auf eine geostatistische Auswertung. Mit Punktstabilitätstests, so genannten Stufblock- und Rammrutsch-Tests, wurden die Bruchbildungseigenschaften an 24 Orten in einem Testhang bestimmt. Mit dem neuartigen Micro-Penetrometer "SnowMicroPen" wurden an über 100 Orten hoch auflösende Profile des Eindringwiderstandes gemessen. Zusätzlich wurde in jedem Testhang ein klassisches Schneeprofil aufgenommen und Proben von schwachen Schichten entnommen. Die räumliche Struktur der Stabilität und des Eindringwiderstandes wurden einerseits als linearer Trend der Ortskoordinaten modelliert, andererseits wurden die Residuen mit einem sphärischen Semi-Variogramm beschrieben.

Aufgrund der Resultate der Stabilitätstests wurden insgesamt 20 schwache Schichten gefunden. Die räumliche Variabilität der Stabilität dieser Schwachschichten hatte eine räumliche Struktur, und zwar vornehmlich in Form eines hangskaligen Trends. Die Trends beschrieben rund 40% der beobachteten Variation. Der Variationskoeffizient der Residuen war ungefähr 20% und erreichte maximal 50%. Diese Variation zeigte kaum eine räumliche Struktur; sie war im Bereich des Messfehlers der Stabilitätstests. Die Variation der Stabilität liess sich teilweise durch die unterschiedlichen Tiefen erklären, in denen die Schwachschichten innerhalb der Schneedecke lagen.

Die Stratigraphie der Schneedecke im Hang wurde aus den Micro-Penetrometer Messungen rekonstruiert. Unter den 21 im Detail untersuchten Schichten befanden sich sowohl Schwachschichten wie auch durch Wind verfrachtete Schneesichten, die typischerweise das abgleitende Schneebrett bilden. Die Schwachschichten konnten in allen Profilen eines Hanges gefunden werden und waren damit räumlich kontinuierlich. Für die meisten Schichten wurde ein signifikanter Trend des Eindringwiderstandes gefunden. Die Variation der Residuen um den

linearen Trend lag im Bereich von 15% mit Maximalwerten bis zu 60%. Für alle Schichten, ausser für eine Schicht von Oberflächenreif, wiesen die Residuen eine räumliche Struktur auf. Die räumliche Autokorrelation variierte zwischen 2 m und mehr als 10 m. Die Tiefe, in denen die Schichten lagen, erklärte wiederum teilweise die Schwankungen des Eindringwiderstandes. Der Eindringwiderstand jeder Schneesicht hatte spezifische und einzigartige geostatistische Eigenschaften. Dies dürfte darauf zurückzuführen sein, dass die Ablagerungsbedingungen während jedem Schneefallereignis unterschiedlich sind. Dies unterstreicht die Sichtweise der Schneedecke als ein Sediment.

Die räumlichen Trends auf der Hangskala waren unabhängig von der Messmethode (Stabilitätstests und Micro-Penetrometer) ähnlich.

In dieser Arbeit wurde Erstmals die dreidimensionale räumliche Variabilität der Schneedecke quantifiziert. Die Resultate bilden die Grundlage um bestehende Schneedeckenmodelle zu verbessern, welche derzeit die räumliche Variabilität nicht berücksichtigen, obwohl diese für die Lawinenbildung wichtig ist. In Bezug auf die Lawinenbildung ist von Bedeutung, dass die Untersuchung zeigte, dass die gefundenen Schwachschichten auf der Hangskala durchgehend vorhanden waren. Der Eindringwiderstand variierte räumlich, jedoch nicht zufällig, sondern wies eine räumliche Struktur mit typischen Längen von einigen Metern auf. Auch die Stabilitätstests zeigten eine räumliche Struktur. Punktuelle Schneedeckenuntersuchungen liefern deshalb nicht zufällige Resultate und sind somit nützlich um die Schneedeckenstabilität abzuschätzen. Aufgrund der gefundenen räumlichen Strukturen kann angenommen werden, dass sich ein Bruch in einer schwachen Schicht über die kritische Grösse hinaus ausbreiten kann, welche für eine Schneebrettauslösung nötig ist, ohne vorher zum Stillstand zu kommen.

Preface

This thesis is divided into six chapters: introduction, methods, data, results, discussion and conclusions.

Chapter 1 introduces the reader to the problems associated with snow slab avalanche release, and then states the specific objectives of the study. Then follows a more detailed introduction to issues that are important for the study: snow slope stability including the avalanche formation process and an overview of the issues associated with scale and scaling. Finally, a review of all previous studies of slope-scale variability of the snow cover is made.

Chapter 2 first explains how the research methodology was made, including an overview of some existing measurement techniques and the practical considerations that had to be made for the field measurements. After that, the study area topography and snow and weather conditions are described. Then follows a description of each of the measurement methods used, and a description of the procedure used to reconstruct snow stratigraphy from the measurements. Finally, the data analysis methods are described.

Chapter 3 gives an overview of the data that was collected over the three winter seasons. It then describes which data were selected for analysis, and why. Finally, some features of the snow cover during the three winters are described.

Chapter 4 presents the results without any discussion. The chapter first describes the results from the stability tests, then the penetration resistance results. Finally, results from the two methods are compared.

Chapter 5 discusses the results. Because some of the methods used in the study were new, the usability of the methods is discussed first. The next section treats observations made on the stratigraphy of the snow cover. Then the results from the spatial variability analysis, the main topic of the thesis, are discussed. This is followed by a discussion of the implications that the observed spatial variability has for the slab avalanche release process. Finally, the practical consequences of the observed spatial variability are discussed.

Chapter 6 gives a brief summary of the study, followed by the conclusions that are made, and finally gives some suggestions for further research in the field.

Some results presented in this thesis have already been presented in peer-reviewed journals and at conferences. Here the ideas and methods are developed further, and more data are analyzed.

Results from point stability tests were first presented on the International Conference on Avalanches and Related Subjects in Kirovsk, Russia, September 2001. A related paper "Spatial variability of snowpack stability on small slopes studied with the stuffblock test" by Kronholm, Schweizer, Pielmeier, and Schneebeli is in press in the peer reviewed *Data of Glaciological Studies* (Kronholm and others, in press-b). At the International Snow Science Workshop, September-October 2002 in Penticton, British Columbia, results from the second year of point stability tests were presented. These data are presented in the paper "Snow stability variations on small slopes" by Kronholm and Schweizer in *Cold Regions Science and Technology* (Kronholm and Schweizer, 2003). The same data are used in this thesis but the analysis presented here is based on robust statistics to automatically handle outliers and small deviations from normality in the data.

Results and methods from the snow micro-penetrometer were first presented at the International Symposium on Snow and Avalanches, held by the International Glaciological Society in Davos, Switzerland, in June 2003. Two papers presenting some of the methods described in this thesis are to appear in *Annals of Glaciology*, Vol. 38. The paper "Spatial variability of penetration resistance in snow layers on a small slope" by Kronholm, Schneebeli and Schweizer (Kronholm and others, in press-a) presents results from the spatial analysis of penetration resistance in several snow layers on a single potential avalanche slope. The same data are analyzed in this thesis together with data from nine other potential avalanche slopes. The paper "Changes in the shear strength and micro-penetration hardness of a buried surface hoar layer" by Birkeland, Kronholm, Schneebeli and Pielmeier (Birkeland and others, in press) investigates temporal and spatial changes in penetration resistance and shear strength of a buried surface hoar layer on a single avalanche slope.

During two winters, fieldwork partly within the framework of this thesis was done to investigate spatial variability of snow stability at the regional scale. The results are not presented in the thesis, but the first analyses were presented at the International Snow Science Workshop, September-October 2002 in Penticton, British Columbia. The results are published in the paper "Verification of regional snowpack stability and avalanche danger" by Schweizer, Kronholm and Wiesinger in *Cold Regions Science and Technology* (Schweizer and others, 2003b).

Acknowledgements

“So, are you going heli-skiing today?” is a question that I have often heard over the last winters. That would have been nice, but the reality was different. Long, cold, early-morning approaches to the slope on which we were to spend most of the day in the shade (or, if we were lucky, got to see the sun for 5 minutes). Being weighed down by heavy backpacks on the way there, and even more so on the way back to the office at the end of the day. Freezing fingers (not to mention toes) after standing around for only half an hour meant there was always someone willing to do the digging. As for the turns needed to get home at the end of the day, they were mostly survival turns, coping with heavy backpacks, breakable crust and rapidly disappearing light down through the trees on “Jürg’s home run”... Despite these miseries, there were always people who were willing to help: even more than once. Most of them were even grinning at the end of the day. Without the following field-crew, this thesis would not have been possible: **Achim Heilig, Alejandro Casteller, Andrea Mayer, Barbara Landl, Beat Haas, Charles Fierz, Christine Pielmeier, Dani Odermatt, Elsebeth Kuriger, Eric Lutz, Esther Hegglin, Ingo Meirold-Mautner, Jordy Hendrikx, Jürg Schweizer, Margret Matzl, Martin Schneebeli, Martina Lütschg, Pascale Rieber, Sebastian Feick and Thilo Lichtenheld.**

Jürg Schweizer and **Martin Schneebeli** provided superb guidance through fire and ice the last three years. From the beginning when the subtleties of geostatistics and snow stability were largely unknown to me, until to the end where the question “what’s next?” came up. I would also like to thank **Wilfried Haerberli** for accepting me as a PhD student at the Department of Geography in Zurich. Without the infrastructure at **SLF** under the direction of **Walter Ammann**, this thesis would not have been possible.

I was lucky to share my office with **Christian Sigrist** and **Christine Pielmeier**. Both were always willing to lay other things aside when I needed it. **Daniela Kasbauer** and **Esther Hegglin** helped with the data analysis. Behind the scene, but as necessary as all others were **Stefan Frutiger** and **Bernhard Zingg** who constructed the rammrutsch setup, **Reto Wetter** who constructed and re-constructed the snow micro-penetrrometer at very short notice when it was needed, and **George**

Krüsi who had the cutting of planar sections down to an art. **Andi Stoffel** was always there to help with GIS questions. For giving me the first opportunity to learn about snow, I am grateful to **Bruce Jamieson**, who accepted having a snow-illiterate flat-lander come to Canada based on little more than an e-mail. Likewise, I would like to thank his field-crew **Ben Johnson, Greg Johnson, Tom Chalmers, Michelle Gagnon** and **Jill Hughes** for having the needed patience to deal with it. For many good discussions (also about snow) I thank **Pascal Hägeli, Karl Birkeland, Chris Landry, Charles Fierz** and **Paul Föhn**. **Jerry Johnson** helped me towards a better understanding of the mechanical interpretation of the snow micro-penetrometer signal. **Matthew Sturm** provided many comments and ideas about spatial variability. Three **anonymous reviewers** provided constructive comments to two journal articles, which at the same time were valuable for the thesis.

On a personal note, many people made sure that life was more than work. Although you might not have been aware of it, I appreciated your presence immensely. Thank you; **Sisse** and **Jon** for sharing the love for cold regions and a great friendship; **Rasmus** (Müssen) for giving me a chance to forget the ring and to hear the sweet sound of baby feet on the floor; **Anders** (Superduck) for good coffee and “padde” support; **Henrik** (den hvide neger) for not reading books; **Bo** for smoking on the balcony and for giving amazing tele-tips; **Grete** for making me want to get a real job with a pension plan; **Lasse** for putting it all in perspective while still sharing the fascination that **Trine** and **Torben** planted.

Finally, thank you **Anne Marie** for letting me share life and the love of mountains with you. This is to you.

List of Tables

Table 1.1. Definition of the process scales used in the present study.	9
Table 1.2. Previous studies of slope-scale spatial variability. Results of relevance for this study are briefly stated. Details of each study are discussed in the text. Results from this study are not included. CV is the coefficient of variation.....	13
Table 2.1. Loading steps and associated rutschblock scores for the rutschblock test (after Schweizer, 2002).	56
Table 2.2. For each rutschblock test, the portion of the isolated block that fractured was recorded as one of three types of release types.	57
Table 2.3. Types of fracture-planes recorded for the rutschblock tests.	57
Table 2.4. Values recorded for each fracture in the stuffblock and rammrutsch point stability tests.	61
Table 2.5. Types of fracture character classified in the stuffblock and rammrutsch tests.....	61
Table 2.6. Stuffblock drop height and associated rutschblock scores (after Birkeland and Johnson, 1999). N is the number of tests used for comparison. Q_1 and Q_3 are the first and third quartile, respectively.	62
Table 2.7. Snow cover properties investigated. The analysis type indicates how the data were analyzed. “spatial” indicates that a full spatial analysis was done. For data of the type “relation”, univariate statistics were used to investigate their relation to the data that were spatially analyzed.	67
Table 3.1. Snow surface inclination and aspect, and the type and number of measurements in the grids carried out over the three winter seasons.	76
Table 3.2. Number of point stability tests N_{test} and number of fractures n_{fract} in the 11 grids and the 21 grid-layers identified from the point stability tests and with more than five fractures within a grid.....	78
Table 3.3. The number of analyzed SMP measurements in the eleven analyzed grids.	79
Table 4.1. Stability, depth and fracture types for grid-layers identified in rutschblock tests and point stability tests.	87

Table 4.2. Column-type stability test results associated with the seven rutschblock loading steps. The stuffblock results are from Birkeland and Johnson (1999). Data for the compression test (Jamieson, 1999) are added for convenience.....	88
Table 4.3. Regression coefficients for the robust bi-linear regression of the drop height on the spatial coordinates ($DH = \alpha x + \beta y + c_t$) for the point stability grid-layers. x and y were in m and DH in cm. ...	90
Table 4.4. Summary statistics for the variation of stability in the grid-layers defined from the point stability tests. DH_{res} indicate the residuals after trend removal.	92
Table 4.5. Regression coefficients from the linear regression of fracture depth (in cm) ($DH = aFD + c_{FD}$) and slope inclination (in degrees) ($DH = b\psi + c_{incl}$) on the drop height (in cm). A robust algorithm was used for the fit.....	97
Table 4.6. Grain shape, grain size, height above ground (at the ramsonde location) and a description of each layer investigated. PWL indicates if the grain shape in the weak layer was persistent or not.	99
Table 4.7. Number and percentage of fractures in the 21 grid-layers identified from the point stability tests and with more than five fractures within a grid.	102
Table 4.8. Observed grain type and grain size, median layer thickness, and a description of each layer investigated.....	105
Table 4.9. Regression coefficients from the linear parametric trend model on the coordinates, and results for the model semi-variogram. The trend model was $\bar{R}' = \alpha x + \beta y + c_t$, where x and y were in meters.	110
Table 4.10. Summary statistics for the transformed penetration resistance in the grid-layers investigated.....	115
Table 4.11. Regression coefficients for ordinary least square fitted linear regression of the grid-layer thickness and depth on the penetration resistance. Coefficients marked in bold type were significant ($P < 0.05$).....	117
Table 4.12. A list of the five layers that were analyzed for variation of stability and penetration resistance. ν is the regression coefficient for a linear regression between drop height and penetration resistance (see text for closer description). The value of ν for grid-layer L1, marked in bold type, was significant ($P < 0.05$).	120

List of Figures

- Figure 1.1. The five most important contributing factors leading to slab avalanche release. Within the snowpack, damage and sintering continuously take place at the bond-scale. The state of damage in the snow cover might thereby increase and decrease until slab release. After Schweizer and Jamieson (2003a) and Schweizer and others (2003a)..... 6
- Figure 1.2. Nomenclature associated with snow slab avalanches (after Perla (1977) and Schweizer and others (2003a)). 7
- Figure 1.3. Spacing, extent and support for the measurement scale. Circles represent measurements. The sampling layout is the one that was used in this study (Section 2.3, p. 32)..... 8
- Figure 2.1. a) Spatial overview and b) the number of point pairs of three possible SMP measurement designs. Grid type 1 was almost exclusively used..... 31
- Figure 2.2. The layout of the measurements in grid type 1, which was used in all the grids analyzed. Before the snow pit was dug, a ramsonde profile was made. In the snow pit, the stratigraphic profile with grain shape, grain size, snow temperature and layer density was made. The rutschblock test (RB) was done above the pit. 113 SMP profiles and 24 column-type point stability tests covered the grid. 32
- Figure 2.3. Typical setting of a grid on a slope. Three of the 12 pit holes for the point stability tests in grid 8 are marked..... 33
- Figure 2.4. Map of the Chörbsch Horn – Hanengretjji study area. The blue triangle indicates the location of the Hanengretjji IMIS weather station. The insert map shows Switzerland with the location of the study area marked. 36
- Figure 2.5. A view of the study area towards the SSW. The study area provided easy access to a number of small north-facing slopes with little skier disturbance. North-facing slopes are in shade. 37
- Figure 2.6. Typical ground cover on the slopes where the measurements were done; alpine meadows with solifluction and patches of scree. The elevation difference between the lake and the ridge is 30 m in the middle of the picture..... 38

Figure 2.7. The automatic IMIS weather station viewed from Hanengretji towards south. From the ridge behind the station, a recent slab avalanche is seen. On the ridge, cornices have formed due to winds from the south. 39

Figure 2.8. Air temperature and snow depth at the Hanengretji IMIS station during the three years where fieldwork was made. The three winter seasons were typical for the study area. 39

Figure 2.9. Two in-situ samples were taken parallel to the snow layers on the vertical wall of the snow pit in grid 20. Removal of weak layer samples from the wall often had to be repeated several times to get an undisturbed sample. 43

Figure 2.10. After removal of the sample from the wall of the snow pit, black diethyl-phthalate was slowly poured into the sample until it was completely saturated. 44

Figure 2.11. The snow micro-penetrometer (SMP) with motor drive, rod, and the two legs for stability. 45

Figure 2.12. The tip of the snow micro-penetrometer (SMP) just before entering the snow. The penetration resistance of the tip is recorded by a force sensor located inside the front of the rod. 46

Figure 2.13. An SMP signal where failures of individual microstructural elements can be identified by a sudden drop in penetration resistance. a) The full SMP profile, and b) a zoom of the signal where arrows mark the failures. At one failure, the rupture force is indicated by f_r 52

Figure 2.14. Simulations of an SMP signal with 10 failures with constant rupture force. a) Constant spacing between the grain contacts. b), c), and d) show different realizations of a signal with random spacing between grains. 54

Figure 2.15. The effect of changing the threshold t_{fail} in the IDL signal analysis routine. Each box for a given threshold represents the values from all 113 SMP profiles in a given grid-layer. The effect of changing the threshold value was layer specific. Whiskers extent to the extreme values while the boxes indicate the quartiles. The median is indicated with a line through the boxes. 55

Figure 2.16. The rutschblock during loading in step 4; jump from above the block with skis. 56

Figure 2.17. The setup for the rammrutsch test. 60

Figure 2.18. Two transects through grid 23 with the SMP profiles in each transect side-by-side. The upper panel is a transect in the cross-slope direction from orographic right to left. The lower panel is a

- transect from the top of the grid to the bottom of the grid. Layers *a* to *k* could be followed through the snow cover within the grid. 64
- Figure 2.19. Planar sections and nearby SMP profile from grid 23. The five grid-layers can be identified in planar sections and in the SMP signal. The exact definition of the layer boundaries was difficult because many boundaries were gradual transitions between adjacent layers (e.g. between 23a and 23b). Some layers had high slope-perpendicular variability (e.g. 23e). Sample A: GR02-A, Sample B: GR02-B..... 65
- Figure 2.20. The distribution of the transformed penetration resistance data \bar{R}' , for a) grid-layer 23c with a fitted normal distribution, and b) grid-layer 23e, which included an outlier. Data from the grid-layers either were very close to a normal distribution like in a) or had a small skew as in b)..... 69
- Figure 2.21. An example of sample semi-variogram (circles) and model semi-variogram (line) with the descriptive parameters c_o , c_s and a_s indicated (see text for a description of each parameter). γ is the semi-variance..... 73
- Figure 3.1. Comparison of a) a high quality SMP profile from grid 23, and b) an unusable SMP profile from grid 24. The inserted profiles show a closer zoom to a part of the profiles. The depth scales are the same on the full profiles and the zoomed profiles, respectively. ... 79
- Figure 3.2. Snow depth and air temperature during the rain event that lead to the crust around which PWL-1 and PWL-2 were later formed. Data are from the Hanengretji IMIS station for 20 November 2001 to 3 January 2002 recorded every 30 minutes. A running average is fitted to the temperature data..... 81
- Figure 3.3. Stratigraphic snow cover profile from grid 15. The persistent weak layer PWL-1 is at $H = 72$ cm above the upper crust. PWL-2 is at $H = 64$ cm, below the lower crust. 82
- Figure 3.4. Snow depth and air temperature during deposition and burial of the surface hoar layer PWL-3. Data from the Hanengretji IMIS station for 17 November 2002 to 12 January 2003 recorded every 30 minutes. A running average is fitted to the temperature data... 83
- Figure 3.5. Stratigraphic snow cover profile from grid 23. The buried surface hoar layer PWL-3 is near $H = 110$ cm. 84
- Figure 4.1. Relation between the rutschblock score and the drop height from the stuffblock tests (SB) and the rammrutsch tests (RR). The spread for each RB score is partly due to areal variation in the RR

and SB drop height values. N is the number of tests used for the calculation. 88

Figure 4.2. Sample semi-variograms for the drop height values in grid-layers 15A, 18C, 23A and 24A. These four examples of sample semi-variograms were among a few that had enough point pairs to give reasonable qualitative results..... 91

Figure 4.3. The semi-interquartile range as a function of the median drop height in each grid. a) Before and b) after trend removal. 93

Figure 4.4. Drop heights for a) stuffblock tests in grid-layer 14A, and b) rammrutsch tests in grid-layer 18A, in which points with very low stability were found. Grid-layer 18A collapsed while working on the slope. The two grid-layers shown were among those with the highest variation of all..... 94

Figure 4.5. Picture of a vertical wall in a transect across the tensile fracture that formed after fracture of grid-layer 18A. The numbers on the ruler are 1 cm apart. Downhill from the tensile fracture, the thickness of the fractured layer decreased with approximately 0.5 cm. The horizontal slab displacement was around 1 cm at the tensile fracture. The stratigraphic snow cover profile is shown in Figure 4.6. 95

Figure 4.6. Stratigraphic profile and hand hardness from grid 18. The fracture happened above the upper crust at 50 cm above the ground where the RB score was 5. For a translation of the German terms, see Appendix A. 95

Figure 4.7. a) Temporal change of the drop heights in grid-layer 18A after fracture. Numbers indicate the chronological order of the tests. b) The location of the RR tests with the numbers corresponding to a). Slab failure occurred after test number 4 was finished. Open circles in b) indicate the locations where no fracture was produced by the stability tests in grid-layer 18A. 96

Figure 4.8. The semi-interquartile range of the stability (drop height) SIQR as a function of the median slab thickness (fracture depth) *FD* for each of the 21 grid-layers. 98

Figure 4.9. Median semi-interquartile range SIQR of drop height as a function of median fracture depth *FD* for all grid-layers (all), persistent weak layers (PWL), and for the non-persistent weak layers (N-PWL). PWL is further separated into the three persistent weak layers PWL-1, PWL-2, and PWL-3. a) The relationship for the absolute drop height values, and b) for the residuals after trend removal..... 100

- Figure 4.10. a) The semi-interquartile range SIQR as a function of grain size. A log-linear fit is shown. b) The fracture depth as a function of the grain size, with a log-linear fit shown for all data (hatched line) and for grid-layers with a grain size smaller than 4 mm (full line). Data from grid-layer 23A (surface hoar) is left out of the plots because of its very large grain size (15 – 22 mm). The first grain shape given in Table 4.6 is shown. The observed grain size plotted is the largest value in Table 4.6. 101
- Figure 4.11. Histogram of the number of fractures in the 66 grid-layers identified in the point stability tests..... 103
- Figure 4.12. The percentage of possible fractures in each grid-layer as a function of grain size. Data from grid-layer 23A with $F = 100\%$ is left out because of its very large grain size (surface hoar with grain size 15 – 22 mm)..... 104
- Figure 4.13. a) The microstructural element length L_n and b) L_s calculated from the SMP profiles as a function of the observed grain size in each grid-layer. For the observed grain size, the mean of the largest grains are given (largest value in Table 4.8). For L_n and L_s , the median calculated size of all measurements in the grid is plotted. Data from grid-layer 23f is left out due to the large observed grain size (15 – 22 mm, $L_n = 1.2$ mm and $L_s = 0.23$ mm). The first grain shape from Table 4.8 is used as label for each grid-layer. 106
- Figure 4.14. The density calculated from the SMP profiles as a function of the measured density in each grid-layer. For the SMP density, the median calculated density of all SMP measurements in the grid is plotted. When layers with facets were not considered, the linear regression gave $P < 0.001$ 107
- Figure 4.15. Median elastic modulus from each grid-layer calculated from the SMP profiles as a function of the density measured in the pit. a) The calculated elastic modulus. Ellipses indicate the suggested grain-shape specific log-linear relationships between density and elastic modulus. b) The calculated modulus multiplied with 150 together with the data summarized by Mellor (1975) in grey..... 108
- Figure 4.16. Median compressive strength from each grid-layer calculated from the SMP profiles as a function of the density measured in the pit. Data for unconfined compressive strength summarized by Mellor (1975) are shaded in grey. 109
- Figure 4.17. a) Penetration resistance as a function of the x and b) the y coordinate. c) Linear (thick grey contour lines) and quadratic (thin

black contour lines) trend surfaces for grid-layer 22d. Circles in c) indicate the location of SMP measurements, with open circles indicating the location of outliers that were removed before the analysis. 112

Figure 4.18. Examples of the three types of spatial structure found in the grid-layers after removal of a slope-scale trend. a) Pure nugget semi-variogram model for grid-layer 23f. b) Model semi-variogram increasing without bound for grid-layer 23e. c) And d) model semi-variogram for grid-layers 20a and 23b for which a sill was reached and a range could be determined. 113

Figure 4.19. A comparison of the eight semi-variograms which reached a sill at a range < 10 m. a) Grid-layers in grids 15, 20 and 23, and b) grid-layers in grid 14. Note the difference in the two γ scales. 114

Figure 4.20. a) The effect of layer thickness and b) layer depth on penetration resistance for grid-layer 23c. The ordinary least squares linear fit for each regression is given. 116

Figure 4.21. a) The semi-interquartile range SIQR for the transformed penetration resistance, and b) the median transformed penetration resistance as a function of the median layer thickness for the 20 grid-layers investigated. 118

Figure 4.22. a) The range a_s and b) the nugget c_0 as a function of the median layer thickness. The log-linear regression line shown in a) excludes the thickest layer of mixed forms. 118

Figure 4.23. The quartile coefficient of variation of transformed penetration resistance as a function of the median penetration resistance, which has been back transformed. 119

Figure 4.24. The average drop height DH in each stability pit as a function of the transformed penetration resistance in the fracture layer in the pit. a) For grid-layer L1, and b) for grid-layer L5. L1 did not fracture at all stability test locations. 121

Figure 4.25. A comparison of a) the semi-interquartile range for the stability test results and the transformed penetration resistance in the five grid-layers that were analyzed for both measurement methods. b) A comparison of the regression parameter β from the linear trend model for the stability results and the SMP measurements. Positive values of β means an increase in the measured value in the up-slope direction. Labels refer to the grid-layer name (Table 4.12). 122

List of Symbols

Symbol	Description	Unit
A_s	Effective surface area of the micro-penetrometer tip	mm ²
a_s	Range of the model semivariogram	m
c_o	Nugget variance of the model semi-variogram †	(log N) ²
c_s	Sill variance of the model semi-variogram †	(log N) ²
c_t	Constant from linear grid-scale trend fitting	m
D	Depth below the snow surface	cm
DH	Drop height at fracture for column-type stability tests	cm
E	Elastic modulus calculated from the SMP measurements	kPa
FD	Fracture depth (below surface) for column-type stability tests	cm
f_r	The rupture force of a microstructural element	N
H	The vertical coordinate of a snow cover measurement, measured from the ground	cm
h	Lag distance between two measurement locations used for semivariogram calculation	m
HS	The height of snow on the ground, normally measured vertically	cm
L_n	The average length of microstructural elements in contact with the SMP tip calculated from the penetration resistance signal	mm
L_s	The shape-dependent grain size calculated from the penetration resistance signal	mm
n_{fail}	Number of microstructural element fractures caused by the penetration of the SMP tip	-
Q_1, Q_3	The first and the third quartile †	-
$r_{b,max}$	The maximum radius of the micro-penetrometer tip	mm
R_{ram}	Penetration resistance of the Swiss ramsonde	N
R	Penetration resistance of the snow micro-penetrometer	N
\bar{R}	Mean penetration resistance within a layer	N
\tilde{R}	Median penetration resistance within a layer	N
\mathbf{s}	Location of a measurement (x, y)	-
t_{fail}	Threshold value used to locate fractures in the SMP signal	N mm ⁻¹
x	Coordinate of a measurement in the cross-slope direction	m
y	Coordinate of a measurement in the up-slope direction	m
$Z(\mathbf{s})$	The value of a variable at location \mathbf{s} †	-
z_{top}	The depth below the snow surface of the top of a layer	cm
z_{btm}	The depth below the snow surface of the bottom of a layer	cm
z_p	The slope-perpendicular distance moved by the SMP	cm
α	Constant multiplier on x from linear grid-scale trend fitting †	-
β	Constant multiplier on y from linear grid-scale trend fitting †	-
$\tilde{\gamma}(\mathbf{h})$	Sample semivariogram based on measurement data †	(log ₁₀ (N)) ²
$\bar{\gamma}(\mathbf{h})$	Model semivariogram fitted to a sample semivariogram †	(log ₁₀ (N)) ²
μ	Friction coefficient between ice grains and the SMP tip	-
ρ_0	Snow density	kg m ⁻³
Σ	Compressive strength calculated from the SMP signal	kPa

List of Symbols

Symbol	Description	Unit
θ	Half the included angle of the SMP tip	°

Notes to the list of symbols: ‡ The unit of the transformed values: Since the transformation was \log_{10} , the variance and semivariance values reflect the transformation. † The unit depends on the value.

List of Abbreviations

Abbreviation	Description
CT	Compression stability test
CV	Coefficient of variation
IDL	Interactive Data Language
PWL	Persistent weak layer
QLCT	Quantified loaded column stability test
QCV	Quartile coefficient of variation
RB	Rutschblock stability test
res	Subscript res indicates a value calculated from data where the slope-scale trend has been removed
RR	Rammrutsch stability test
SB	Stuffblock stability test
SIQR	The semi-interquartile range
SLF	Swiss Federal Institute for Snow and Avalanche Research
SMP	Snow micro-penetrator

Chapter 1

Introduction

“The fact that a weak layer exists is not enough information to analyze the avalanche hazard. The spatial variation of its thickness and strength is critical to determining the likelihood of the initiation of a failure and whether or not the failure will propagate or die out. Thus the usual “point” analysis in pits may have to be supplemented by information gathered over some area. In fact, the extension to areal information is one of the outstanding problems for all studies of snow.”

S. C. Colbeck (1991)

1.1. Introduction

This chapter introduces the snow avalanche problem, and gives the motivation for this study. First, a brief motivation of the study (Section 1.2) leads up to the definition of the objectives (Section 1.3). Thereafter follows a more in-depth introduction to some of the background information about the processes leading to snow avalanche release (Section 1.4) and about scale-related issues that are important for all studies of spatially distributed variables (Section 1.5). Section 1.6 introduces the important concept of the snow cover as a sedimentary deposit. Finally, section 1.7 is a review of the available literature on spatial variability of the seasonal snow cover, ending with the conclusions that can be drawn from previous studies.

1.2. Motivation

Natural hazards are a threat to humans and infrastructure in mountainous regions. Among these hazards are snow avalanches, landslides, mudflows, rock falls, ice avalanches and glacier floods (e.g. Haeberli and others, 1989). In the Swiss Alps, snow avalanches cause an average of 26 fatalities per year (Tschirky and others, 2000). The worldwide annual average is estimated to 250 fatalities per year (Schweizer and others, 2003a). Of the Swiss fatalities, 90% can be

attributed to avalanches triggered by recreationists such as e.g. skiers, snowboarders and climbers. The fatal human-triggered avalanches are in 90% of the Swiss cases triggered by the victims themselves (Schweizer and Lütshg, 2001). Slab avalanches are the most dangerous type of avalanches (McClung and Schaerer, 1993).

Avalanche forecasting has been defined as “the prediction of current and future snow instability in space and time” and its goal to “minimize the uncertainty about instability introduced by the temporal and spatial variability of the snow cover” (McClung, 2000). Avalanche forecasting is done by recreationists (by evaluating information from observations of the snow cover from e.g. snow profiles, stability tests and signs of instability such as running cracks or “whumpf” sounds) and by experienced avalanche forecasters (by evaluating snow and meteorological information from a larger area).

The spatial variability of the snow cover has long been recognized, both in the vertical direction (layering) and in the horizontal direction (variation within individual layers) (Seligman, 1936). At a regional scale, the result of spatial variability is that snow cover stability is not constant, but spatially variable (Schweizer and others, 2003b). Even at the slope-scale, local stability is not always constant (e.g. Conway and Abrahamson, 1984; Kronholm and Schweizer, 2003). This poses problems for recreationists and professional forecasters alike. For the recreationists, the question is “where can I make observations about the snow cover that are representative for a slope and a region?”, and further, “is the avalanche danger on all slopes in the region the same, or are some slopes stable enough to ski, while others are not?” For an avalanche forecaster who works at larger scales, e.g. a mountain range, the question is “is the avalanche danger for the forecast-area the same, or are there local variations within the area that I must consider in my forecast?” The spatial variability of the snow cover is highly relevant to snow stability evaluation at all scales.

At the regional scale, two numerical snow cover stratigraphy models have been used for operational avalanche forecasting: the French SAFRAN-Crocus-MÉPRA (SCM) model chain (Durand and others, 1999), and the Swiss SNOWPACK model (Lehning and others, 1999). Based on meteorological data and weather forecasts, the SCM model simulates average snow cover profiles for separate elevations, aspects and slope inclinations. The simulation is done for separate regions (each of around 500 km²). For each of the resulting sub-regions, it is assumed that the simulated average profile is representative. Avalanche forecasting is based on the simulated profiles. The

SNOWPACK model uses meteorological data from a network of stations to simulate the snow cover stratigraphy at each station. Recently, it has been attempted to predict snow cover stability from the SNOWPACK simulations (Lehning and others, in press). Spatial interpolation of the SNOWPACK model results relies on expert knowledge from avalanche forecasters. Both numerical models use the existence of weak layers as an indicator of instability, an approach also used by Schweizer and Wiesinger (2001) for manually recorded profiles. Although the numerical snow stratigraphy models provide information about the regional variation of the snow cover, they cannot predict slope-scale variability of the snow cover, which is where the slab release processes take place.

At the slope-scale, slab avalanche release depends on the existence of a weak layer within the snow cover (McClung and Schaerer, 1993), but also the horizontal variability of the weak layer is critical to slab release (Colbeck, 1991). All numerical slab release models reviewed by Schweizer (1999) include a pre-existing crack to initiate fracture propagation in weak layer with spatially homogeneous strength. Deficit zones are areas on a slope where the slab is no longer supported at the base by the weak layer, but is held in place by the peripheral strength of the slab. In the release models, the deficit zone expands as a crack propagates outwards from the existing deficit zone through the weak layer. Eventually the peripheral strength of the slab above might be overcome and a slab is released. All field studies have found that spatial variability exists, but only one study by Conway and Abrahamson (1984) suggests that deficit zones exist. As pointed out by Conway and Abrahamson (1984) as well as subsequent researchers, the methods used in the study are questionable, and the existence of deficit zones therefore not considered as proven. This is not surprising, since sintering will probably heal deficit zones within a short time (Salm, 1975). To provide the necessary variation in stress and strain needed for a crack to develop, Schweizer (1999) suggested including stochastic variation of layer properties instead of deficit zones in future slab release models. So far, this has not been attempted. Horizontal spatial variation in layer properties not only determines whether a crack can be initiated in a weak layer, but also control whether the crack can subsequently propagate through the layer (Colbeck, 1991), and, finally whether the spatially variable peripheral strength of the slab can be overcome. The spatial variability of the snow cover is, therefore, critical for slab avalanche release. Still, the spatial variability of layer properties has never been quantified.

The primary agents controlling spatial variability at the regional scale and at the slope-scale are not the same. Downscaling of the regional spatial variation given by the numerical snow stratigraphy models through regional-scale meteorological parameters to the slope scale will therefore be difficult. At the slope scale, spatial variability is primarily caused by local wind effects (Seligman, 1936; Kronholm and others, in press-a). At the basin-scale, different slope aspects cause large variations in radiation, which plays a major role in the metamorphic processes within the snow cover (Bader and others, 1939) and in the building of weak layers near the snow surface (Seligman, 1936). Over even larger scales such as multiple mountain ranges, the general weather patterns and large differences in elevation might produce a completely different snow cover from one part of a range to another (Sturm and others, 1995; Mock and Birkeland, 2000; Hægeli and McClung, 2003).

Snow cover spatial variability in the vertical and horizontal directions is not only relevant for the mechanical properties (such as snow stability) of the snow cover. Spatial variability of mechanical properties is also important for over-snow trafficability of vehicles and animals. Spatial variation of structural properties is important for water, heat, vapor and airflow and for the spectral properties of snow (Colbeck, 1991). Simply stated, “the extension to areal information is one of the outstanding problems for all studies of snow” (Colbeck, 1991).

1.3. Objectives of the study

Before this study, no conclusive measurements of spatial variability of mechanical snow cover properties were available. The aim of the study was to **characterize quantitatively the spatial variability of stability and related mechanical properties on typical avalanche slopes**, with millimeter-resolution in the slope-perpendicular direction (different layers) and meter-resolution in the slope-parallel direction (within individual layers). To achieve the aim, the study had the following objectives:

- 1) Choose the appropriate field methods
- 2) Design an appropriate measurement setup for the field measurements
- 3) Carry out enough field measurements to provide sufficient data for a sound statistical analysis

- 4) Use appropriate statistical methods to characterize spatial variability
- 5) Compare the results from the various measurement methods to each other
- 6) Discuss the results in terms of implications for dry snow slab avalanche release

1.4. Snow slope stability

Snow avalanches can be divided into slab avalanches and loose snow avalanches (e.g. McClung and Schaerer, 1993, p. 61). Loose snow avalanches start from a point and move down the slope as a mass without cohesion while spreading out to a triangular shape. They normally involve only the upper part of the snow cover. Slab avalanches involve the release of cohesive blocks of snow by cracks propagating through the snow cover. Slab avalanches normally involve a large proportion of the depth of the snow cover and are normally far more dangerous to people and property than loose snow avalanches. Slab avalanches can further be divided into dry and wet snow avalanches. Dry slab avalanches can be naturally triggered, e.g. by new snowfall, or by artificial triggers such as skiers or explosives. Although the slab release mechanisms are the same for the two types of triggers, the loading rates and the area of loading are different. Artificial triggers generally apply localized near surface rapid loading (Schweizer and others, 2003a), whereas natural triggers load the snow cover at slower rates and over larger areas. This is important because the mechanical properties of snow are rate-dependent (e.g. McClung, 1977). Dry snow slab avalanches are responsible for more fatalities and damage to property than wet snow avalanches, with the exception of coastal mountainous areas such as western Norway.

1.4.1. Dry snow slab avalanche formation

Avalanche formation is the interplay between terrain, meteorological conditions and the snow cover, ultimately leading to the release of avalanches. After avalanche release, avalanche motion and finally deposition occurs. Avalanche formation processes have recently been reviewed by Schweizer and others (2003a). Slab release depends on the existence of a weak layer below a thicker cohesive slab within the snow cover (McClung and Schaerer, 1993, p. 80). Investigations of the snow cover stratigraphy are therefore a key to understanding slab release.

1.4.2. Slab release processes

A conceptual model of slab avalanche formation is presented by Schweizer and others (2003a). The model involves all scales over which the active processes operate, from the scale of a bond to the scale of a slope on which the avalanche is released (Figure 1.1). At the bond scale, damage processes and sintering processes might take place at the same time. The damage processes decrease the strength of the snow by breaking and weakening bonds, whereas sintering increases snow strength by building new bonds and strengthening existing ones. If only the damage process and not the sintering process were active, avalanches would continuously be released from snow-covered slopes.

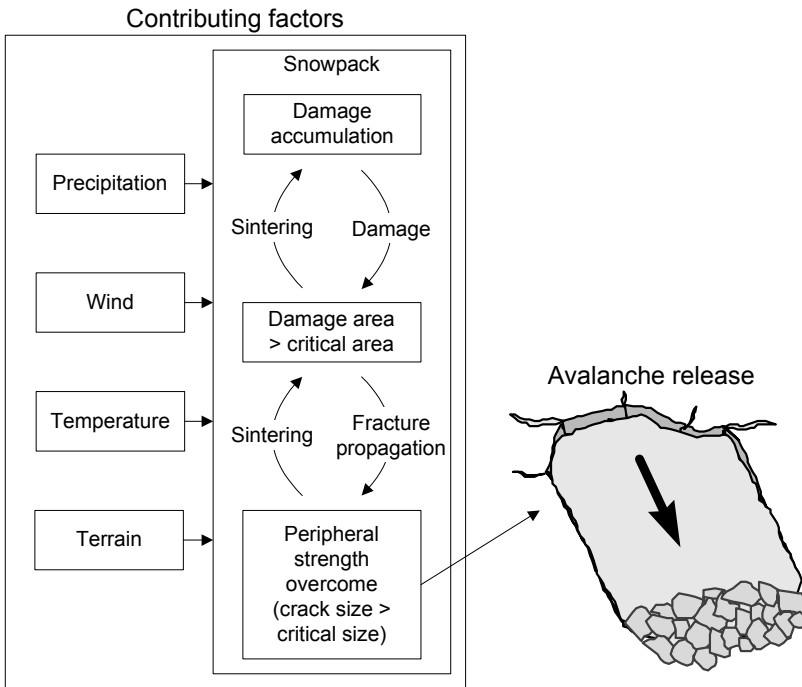


Figure 1.1. The five most important contributing factors leading to slab avalanche release. Within the snowpack, damage and sintering continuously take place at the bond-scale. The state of damage in the snow cover might thereby increase and decrease until slab release. After Schweizer and Jamieson (2003a) and Schweizer and others (2003a).

As snow cover damage accumulates, a crack or fracture is formed along a weak layer or a weak interface in the snow cover. If the propagation potential of the snow cover and weak layer allows, the crack will propagate and spread along the weak layer or interface. If the crack reaches a certain size, it will rapidly propagate along the weak layer. The slab above the crack is only stabilized by the peripheral strength of the snow around the circumference of the crack and a negligible frictional force at the base of the slab. The expanding crack might reach a size where the peripheral strength of the slab is overcome by the gravitational pull. In that case, a slab avalanche will be released. If a crack does not become large enough for an avalanche to release, it will likely heal within hours or even faster (Schweizer, 1999).

The spatial variability of 1) slab strength (in tension at the crown, shear at the flanks and compression at the stauhwall, Figure 1.2), 2) weak layer continuity and 3) shear strength play an important role in the slab release processes.

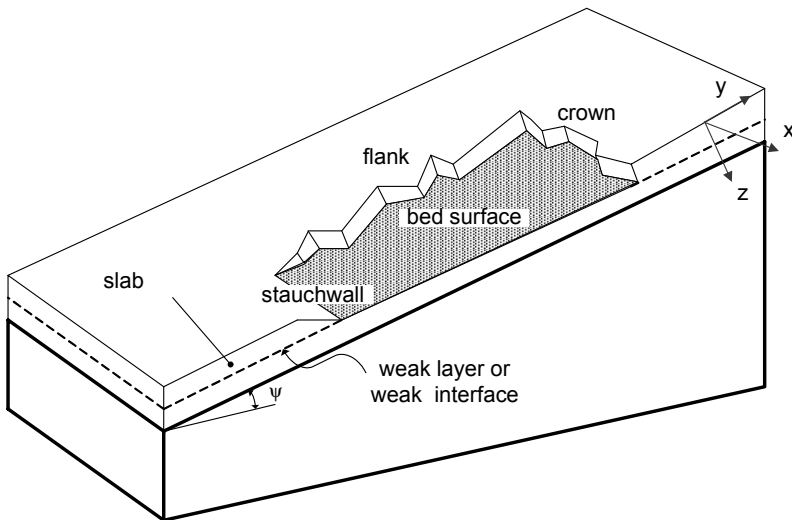


Figure 1.2. Nomenclature associated with snow slab avalanches (after Perla (1977) and Schweizer and others (2003a)).

1.5. Scale and scale issues

1.5.1. A definition of scale

Blöschl and Sivapalan (1995) review scale issues related to snow hydrology, and Blöschl (1999) discusses these issues in detail. He proposes a framework, which is applicable for all studies dealing with scale issues. The framework operates with three types of scales: process scale, measurement scale and model scale. The **process scale** is the true spatial scale of a process, also called the scale of the natural variability. The **measurement scale** is the spatial scale of the instrument used to measure the process of interest. The **model scale** is the scale of a model used to describe the process. The measurement scale and the model scale as defined by Blöschl and Sivapalan (1995) are identified by the scale triplet: spacing, extent and support (Figure 1.3).

To give an intuitive meaning to the different scales studied here, logical names are given to each of the scales used (Table 1.1). The scales are hierarchical with the larger scales fully containing the smaller ones.

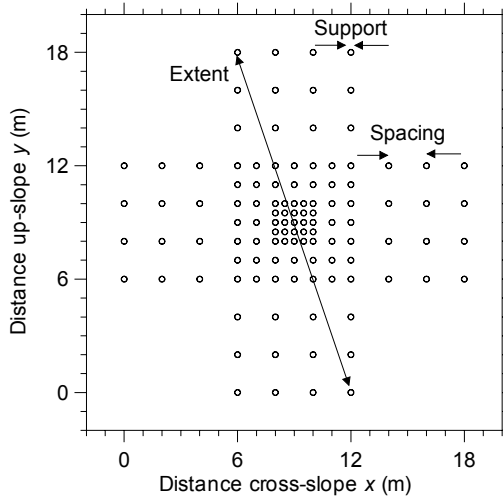


Figure 1.3. Spacing, extent and support for the measurement scale. Circles represent measurements. The sampling layout is the one that was used in this study (Section 2.3, p. 32).

Table 1.1. Definition of the process scales used in the present study.

Process scale	Characteristics	Length
Grain-scale	The size of individual microstructural elements in the snow cover, e.g. grains and clusters of grains.	0.1 mm – 1 cm (10^{-4} – 10^{-2} m)
Layer-scale	The scale of the typical snow layer thickness.	1 cm – 10 cm (10^{-2} – 10^{-1} m)
Snowpack-scale	The scale of the typical snow cover thickness.	10 cm – 5 m (10^{-1} – 5×10^0 m)
Slope-scale	The size of typical avalanche slopes. Radiation is constant due to constant aspect. Precipitation is constant, but snow can be redistributed by wind at this scale.	5 m – 100 m (5×10^0 – 10^2 m)
Basin-scale	An area with slopes of different aspects, inclinations and elevations. Radiation varies, precipitation is constant.	100 m – 1 km (10^2 – 10^3 m)
Regional scale	Precipitation varies.	1 km – 10 km (10^3 – 10^4 m)
Mountain range	At this scale, spatial snow cover patterns exist and are due to the tracks of individual storms.	10 km – 100 km (10^4 – 10^5 m)

1.5.2. Problems associated with scale and scaling

The spatial dimensions in Table 1.1 are one-dimensional lengths, but can be extended to two and three dimensions by simply assuming that the length is equal in all dimensions. For snow however, the typical scales are anisotropic at most scales. Using the layer-scale, which is investigated in this study, as an example, the slope-perpendicular length-scale is smaller than the slope-parallel length-scale because the layers are draped out over ground. The scales given in Table 1.1 must therefore be taken as first approximations only.

Scaling here refers to the change from one scale to another. Scaling represents a problem for all studies that span multiple scales because most natural properties are scale-dependent (e.g. Bian and Walsh, 1993). In this study, there are two major scaling issues: 1) the scaling of a process measured with different supports (i.e. snow stability inferred from different methods), and 2) the relation between property-scaling (e.g. the scaling of penetration resistance) and process-scaling (e.g. the scaling of snow stability).

Scaling of snow stability

A variable that has high variation measured at one support might have less variation measured at a larger support, i.e. variability is a function of measurement support (e.g. Blöschl, 1999). Different methods for determining snow stability exist (Section 2.2.2, p. 24). These have

different supports, and spatial variability results can therefore not be directly compared. In addition, the scaling of stability itself presents a problem. Three scales that are often used in avalanche forecasting are point stability, slope stability and regional snowpack stability. **Point stability** is proportional to the additional load a small (compared to a slope), isolated snow block will withstand before fracturing. **Slope stability** is inversely proportional to the probability that an avalanche will release on a given slope. **Regional snowpack stability** is proportional to the probability and frequency of avalanche release in a given region. For avalanche forecasters and recreationists, it is relevant to know the relation between point stability, slope stability and regional snowpack stability. As described in Section 1.4, three separate processes act together to release a slab avalanche: fracture initiation, fracture propagation and peripheral fracture (Schweizer and others, 2003a). Point stability tests measure the fracture initiation properties of the weak layer and slab, but the fracture propagation properties of the snow cover are not tested. Further, the test result does not include information about the peripheral strength of the slab. A point stability test can therefore not be directly up-scaled to predict slope stability. If many point stability tests are made on a slope with large variability, the slope stability is not the mean of the stability test results. The minimum test result is then a better estimation of slope stability. If the weak layer is continuously present and weak over a slope, and the spatial variability low, the result of a stability test will likely be a good measure of slope stability. Test skiing and the use of explosives are two ways to increase measurement support and hence to test the slope stability. The regional snowpack stability is influenced by the different aspects, which lead to different snow cover stratigraphy over the region. Regional snowpack stability therefore consists of a distribution of slope stabilities (Munter, 2003; Schweizer and others, 2003b).

Process-scaling and property-scaling

In this study, point stability and penetration resistance are investigated as the two main variables. Whereas penetration resistance is a true snow cover property, point stability involves a number of processes that are all included in a point stability measurement result. First, the methods used to determine stability and penetration resistance have different support. The variability found in one type of measurement can therefore not be expected to unconditionally correlate with the other measurement type. Second, the scaling of stability will be different from the scaling of penetration resistance because of the different processes involved in the stability measurement as discussed above.

1.6. The snow cover as a sediment

The almost exact analogy between snow and sedimentary deposits studied by geologists and soil scientists has long been identified (Seligman, 1936, p. 271; Bader and others, 1939; Colbeck, 1991). A snow layer has been defined as “A stratum of snow that is different in at least one respect from the strata above and below” (Colbeck and others, 1990, p. 9). The primary layers are the outcome of a sequence of weather events. Each event influences the spatial variability of the primary snow layers. Secondary layers can be created within the snow cover. The agents that affect the variability of layers can be divided into internal agents that work within the snow cover and those that are external (Sturm and Benson, in press; Harper and Bradford, 2003). In an alpine environment, a third group of agents that introduce catastrophic changes in the snow cover, e.g. avalanches and falling cornices, are also important.

The external agents include wind, temperature, snowfall rate and solar radiation. Aeolian snow transport is considered to be the most active agent in introducing spatial variability in a dry snow cover (Seligman, 1936, p. 273; Sturm and Benson, in press), and have been held responsible for spatial variability found in some previous studies (Conway and Abrahamson, 1984; Föhn, 1989; Jamieson, 1995). The external agents drive the snow-internal metamorphism by e.g. introducing temperature gradients. The external agents are coupled to the terrain through slope aspect and inclination, elevation and the amount of exposure to wind.

The primary internal agent is the temperature, which drives the vapor-flux responsible for metamorphosis of the grains. Other agents such as free water can change the properties of the layers within the snowpack.

Snow cover variability exists in both the slope-perpendicular (vertical) and in the slope-parallel direction (horizontal). Vertically, the main variability is due to the snow layers, but there is also slope-perpendicular variability within each layer (Pielmeier and Schneebeli, 2003). Horizontally, the thickness and depth of each layer changes (Birkeland and others, in press), and layers might disappear at certain locations (Sturm and Benson, in press). The structural (e.g. grain shape and size) and mechanical properties (e.g. hardness, shear strength and compressive strength) of a layer change in the slope-parallel direction. This study examines both the slope-perpendicular and the slope-parallel variability.

1.7. Previous studies of slope-scale variability

A number of field studies have investigated the spatial variation of snow cover stability, penetration resistance and other mechanical and structural properties. An overview is given in Table 1.2, followed by a discussion of each study.

In addition to the studies mentioned in Table 1.2, three earlier studies have reported the coefficient of variation for their shear strength measurements (Perla, 1977; Sommerfeld and King, 1979; Föhn, 1987b). These are given more as a measurement error than an index of the spatial variability of the shear strength and are not summarized here.

Conway and Abrahamson (1984, 1988) measured tensile and shear strength along avalanche crowns released by ski cutting just prior to their measurements and on slopes that had not failed. They used a modified shear frame embedded on the top of an approximately 30 cm x 30 cm freestanding column of snow. They comment that the test might have introduced a bending moment in the column. Where measurements were made immediately after fracture and close to the crown, weak layer conditions might be unrepresentative of slope stability before triggering: cracks in the weak layer might have spread further than where the tensile crack formed the crown, yielding very low stability test results. From the measurements, the point stability index was calculated and the spatial variability investigated with classical statistics and by visualization. In a further analysis of their data, Conway and Abrahamson (1988) suggest looking at the data as random variable with spatial autocorrelation. Opposite other studies, tests that failed during preparation were included in the results with a stability index of 1. They found large variations in the stability index, changing from a deficit zone to a pinning area (non-deficit zone) over 0.5 m to 1 m. For all 93 stability indices calculated for eight slopes that had failed, the mean was 1.57 and the coefficient of variation CV was 82%. For 18 slopes that had not failed, the mean stability index of the 63 measurements was 4.25 with a CV of 65%. They suggest that the smallest point stability index found on a slope might be more critical for evaluating slope stability than the mean point stability index. Further, Conway and Abrahamson (1984) argue that the critical length of deficit zones within a weak layer was < 1 m, although a re-analysis of their data (Conway and Abrahamson, 1988) suggests that this length was > 2.9 m.

Table 1.2. Previous studies of slope-scale spatial variability. Results of relevance for this study are briefly stated. Details of each study are discussed in the text. Results from this study are not included. CV is the coefficient of variation.

Study	Property	Results
Conway and Abrahamson (1984)	Stability index	<ul style="list-style-type: none"> - Large changes in stability over 0.5 m - “Outliers” not discarded - CV, stable slopes: 65% - CV, unstable slopes: 82% - Critical length of deficit zone < 1 m
Conway and Abrahamson (1988), same data as above	Stability index	<ul style="list-style-type: none"> - Critical length of deficit zone > 2.9 m - Measurements should be spaced less than 0.5 m apart to capture variability - Measurements should span at least 3 m - The pattern of point stability on a slope is important for slope stability
Föhn (1989)	Stability index	<ul style="list-style-type: none"> - CV, stable slopes: < 30% with outliers excluded, < 38% when outliers included - Concluded that small deficit zones were not enough to make slopes unstable
Jamieson and Johnston (1993), Jamieson (1995)	Rutschblock score	<ul style="list-style-type: none"> - With 97% probability, a rutschblock score on the uniform part of a slope is within ± 1 score of the slope median score - One of nine slopes investigated included a small area of very weak surface hoar, possibly a deficit zone - Despite this area, the slope did not fail during measurements
Birkeland and others (1995)	Penetration resistance	<ul style="list-style-type: none"> - CV of average penetration resistance was 28% to 58%
Chernouss (1995)	Density, snow depth	<ul style="list-style-type: none"> - Spatial autocorrelation was calculated for four different snow properties
Takeuchi and others (1998)	Penetration resistance	<ul style="list-style-type: none"> - No quantification of horizontal variability - A dry snowpack showed more spatial continuity in layer hardness than wet snow
Jamieson and Johnston (2001)	Shear strength	<ul style="list-style-type: none"> - CV of shear strength from 3% to 66% with a mean of 15% - Larger variation in avalanche release areas than level study plots
Stewart (2002) and Stewart and Jamieson (2002)	Stability	<ul style="list-style-type: none"> - Patches of below and above average stability were found in most of the 39 grids - No spatial autocorrelation length was found - CV max: 82%, min: 10%, mean: 50%
Landry (2002) and Landry and others (2003)	Shear strength, stability	<ul style="list-style-type: none"> - CV of weak layer shear strength was between 10% and 50%, with a mean of 24% - Stability variation was in the same range - High and low values of shear strength were found in adjacent tests
Harper and Bradford (2003)	Stratigraphy	<ul style="list-style-type: none"> - Thick (5 – 10 cm) layers are continuous over tens of meters, whereas thin layers (1 – 10 mm) are not - No quantification of horizontal variability
Birkeland and others (in press)	Penetration resistance	<ul style="list-style-type: none"> - No spatial trend in penetration resistance of a buried surface hoar layer - Median penetration resistance varied 45% and layer thickness around 30%

With their results, Conway and Abrahamson (1984, 1988) triggered a debate over the use of a stability test as an appropriate method to judge snow slope stability. The issue is still nowadays heatedly debated. The results of Conway and Abrahamson (1984) are used to demonstrate that results from a single stability test cannot be extrapolated and therefore does not have predictive value for snow stability at larger scales.

Föhn (1989) calculated the stability index from shear strength measurements of weak layers with a standard shear frame. He excluded suspicious measurements from the calculations and found that the CV for the stability index was usually $< 30\%$, which was the same order of magnitude as other snow cover parameters such as snow depth, depth of the weak layer, density of the slab. Small deficit areas of < 1 m were not found if the standard procedure where shear samples which rupture during preparation were excluded from the analysis. Föhn (1989) also carried out rutschblock tests (Föhn, 1987a), which test an area of 3 m^2 , on typical avalanche slopes. Even though a few rutschblock tests on some slopes showed low point stability, this was not enough to release slab avalanches during subsequent test skiing and explosive testing. He therefore concluded that single, small deficit areas were not enough to make slopes unstable as found by Conway and Abrahamson (1984, 1988).

Jamieson and Johnston (1993) did multiple rutschblock tests on potential avalanche slopes. They found that the rutschblock score is within ± 1 score with 97% probability. Despite such a narrow distribution, the rutschblock scores had a CV of 10% to 25%. The study was extended by Jamieson (1995, p. 159-169) who did multiple rutschblock tests on nine potential avalanche slopes. The rutschblock scores on one slope (6 March 1991) included an area of particularly weak surface hoar, where the rutschblock scores were 1 and 2 while the slope median was 3. Slope inclinations ranged from 25° to 30° . Despite this weak area, the slope did not fail during the measurements, as would have been expected from the results by Conway and Abrahamson (1984, 1988). On the same slope, the maximum score was 5, thus giving a large range of scores. None of the other slopes included areas of very low rutschblock scores.

Birkeland and others (1995) used a penetrometer to measure penetration resistance of the snow cover at two sites. The surface area of the measuring tip was 10 mm (Dowd and Brown, 1986). Penetration resistance was measured every 5 mm in the vertical direction. Lower values of the average penetration resistance of the snow cover were

related to the presence of underlying rocks. The CV of the average penetration resistance varied between 28% and 58%. No spatial analysis of the data was done. The study is unique in that many measurements of a snow cover variable were carried out in a short time. However, the average penetration resistance cannot be related to the variations in weak layer shear strength, which are important for snow slope stability.

Chernouss (1995) investigated the spatial correlation of total snow thickness, new snow thickness, new snow shear strength and density in avalanche start zones with the correlogram (e.g. Webster and Oliver, 2001). The most spatially variable parameter was snow thickness followed by shear strength and density. Unfortunately, the measurement methods are not well described and all references are in Russian, so the results are hard to assess.

Takeuchi and others (1998) used a push-pull force gauge to measure the penetration resistance of snow on a vertical snow pit wall. The diameter of the tip was 7 mm. Measurement spacing was 5 cm in the vertical direction and 10 cm in the horizontal direction. They did not quantify the spatial variability of the penetration resistance of the pit wall, but noted that in a dry snow cover with small grains, the horizontal variability in penetration resistance was smaller than in wet snow layers of larger grains. However, the profiles were made in different locations, and the difference in variability could be due to other factors.

Jamieson and Johnston (2001) used shear frames of different sizes (0.01, 0.025 or 0.05 m²) to measure shear strength of weak layers. For all 809 sets of 7–12 measurements, the CV ranged from 3% to 66% with an overall mean of 15%. For level study sites chosen for a uniform snow cover, mean CV was 14%, whereas for measurements in avalanche start zones, mean CV was 18%. The variability found was generally lower than previous studies with shear frame tests. No spatial analysis of the data sets was done.

Stewart (2002) and Stewart and Jamieson (2002) used the drop hammer stability test to investigate the spatial variability of snow stability in avalanche start zones. Closely spaced stability tests of 30 cm x 30 cm isolated snow columns were done in 39 grids. Within each grid, no significant correlation was found between stability and slab thickness, *HS* and slope inclination. However, the mean stability of each grid was correlated with mean slab thickness. Spatial analyses showed clusters of low and high stability in most grids, but no correlation length of stability was found. Clusters were defined as areas where four or more adjacent tests had stability distinctly higher or lower than the stability outside the

cluster. A distinct difference was defined as a drop height difference of 10 cm at fracture.

Landry (2002) and Landry and others (2003) used the quantified loaded column stability test (Landry and others, 2001) to measure the spatial variability of snow stability on seven potential avalanche slopes with eleven grids. The test loads a 30 cm x 30 cm isolated snow column until fracture. CV of weak layer shear strength was between 10% and 50% with a mean of 24%. Stability variation was within the same range. Large variations in stability were found on some slopes. At least on one slope, a visual estimate suggests that the large variability found is the effect of a slope-scale trend. However, no spatial analysis of the stability results was done.

Harper and Bradford (2003) studied snow stratigraphy on a glacier with radar, closely (vertically) spaced density measurements, back-lit snow sections and manual stratigraphic mapping. The extent of the study area was 20 m. They found that thicker, major layers (5 – 10 cm) were spatially continuous over tens of meters, while thinner layers (1 – 10 mm) were spatially discontinuous. No quantification of variability within each layer was done.

Birkeland and others (in press) used a micro-penetrometer (Schneebeli and Johnson, 1998) to study the penetration resistance of a buried surface hoar layer on two days on the same slope. The extent of the grid sampled each day was 30 m, with a minimum spacing of 1 m the first day, and 0.5 m the second day. On the first day, 86 measurements were done, and 129 on the second. The mean thickness of the layer was 8 mm with a CV of 34% on the first day of measurements. The CV decreased to 24% after six days, although the thickness of the layer did not change. The median penetration resistance of the layer over the slope did not change significantly between the two days and the CV of median penetration resistance stayed around 45%. There was no spatial trend in the penetration resistance. Although it was not mentioned, a spatial analysis of the penetration resistance data with the semi-variogram (e.g. Cressie, 1993) showed no autocorrelation between the measurement points. Shear strength variations for the same weak layer recorded on the same two days with the QLCT test (Landry and others, 2001) of 30 cm x 30 cm had a CV of 10% on both days.

1.7.1. Studies at other scales

In addition to the studies mentioned above, other studies have investigated spatial variability at larger scales. Birkeland (1997, 2001) describe the variability of stability in a small mountain range in terms of

terrain, and modeled stability using a digital elevation model in a GIS. A GIS approach was also used by Stoffel and others (1998) to study the spatial distribution of avalanches from a long time series of recorded avalanches in a small region in Switzerland. Kozak and others (2001) investigate the spatial variability of snow slab hardness in a small region and try to model the hardness with meteorological parameters (Kozak and others, 2002). Hägeli and McClung (2003) explore the spatial patterns of avalanche occurrences in a mountain range in Canada. Pielmeier (2003) and Pielmeier and Schneebeli (2003) investigate spatial variability at the layer-scale, and include a visual comparison of several adjacent penetration resistance profiles. Sturm and Benson (in press) analyze previous studies of snow cover variability at various scales. They conclude that the scale at which the largest variation occurs is around 100 m, and that layers are continuous over large distances. Snow cover variability has been studied in Antarctica (Richardson and Holmlund, 1999; Stenberg and others, 1999; Sturm and others, 1998) and in the Arctic (Benson and Sturm, 1993).

1.7.2. Discussion of previous slope-scale studies

Previous studies of snow cover spatial variability at the slope scale all show that spatial variability exists, but only few studies quantify the variability. In the studies where the variability is quantified, there is no agreement on the level at which spatial variability is “high” and when it is “low”. For example, Conway and Abrahamson (1984, 1988), find that stability variation is highly spatially variable with a variation of around 80% on avalanched slopes and 65% on non-avalanched slopes (with “outliers” included). Stewart (2002) and Stewart and Jamieson (2002) report stability coefficients of variation CV with a maximum of around 80% and a mean of 50%, but find the stability on the studied slopes “spatially consistent”, implying low spatial variability. Landry (2002) and Landry and others (2003) find stability variation that was lower than the CV found by Stewart: max 50%, mean 24% on small slopes. Still, they conclude that extrapolation of stability results from a snow pit to a slope is not possible for 30% of the snow pits, implying high spatial variability of stability. The methods used in these three examples all test the stability of a weak layer over an area that is approximately the same; 30 cm x 30 cm. In the study of variability in rutschblock test results by Jamieson and Johnston (1993) and Jamieson (1995), the result – 97% of scores within ± 1 score of the slope median – suggests that the slope-scale variability is rather small. Yet, 2 RB scores span around 30% of the ordinal scale used for the RB scores, and the CV of the scores on individual slopes is up to 25%. This is still lower than the three examples

above, but it has to be considered that the rutschblock test integrates an area more than 30 times larger than the tests used in the examples above. The lower variability of the rutschblock test is therefore expected.

One reason for the contrasting interpretations might be that most studies do not consider the spatial structure of the stability data. The CV does not include any information on spatial auto-correlation. Kronholm and Schweizer (2003) show that the CV can be misleading as a measure of stability variation if there are spatial trends in point stability on a slope. Conway and Abrahamson (1984) pointed out the importance of the spatial distribution of stability and suggested analyzing the stability data with random field theory, which they later did (Conway and Abrahamson, 1988). However, a quantification of spatial variability at the slope-scale has been left out by most studies, with the exception of Stewart (2002). When the results from the previously mentioned studies are visually compared, it appears that the results found by Stewart (2002) vary at a large spatial scale (he found significant slope-scale trends on 11 of 39 slopes), whereas the results from Conway and Abrahamson (1984, 1988) and Landry (2002) vary at a smaller spatial scale. Intuitively, small-scale variability “feels” larger than large-scale variability, although the variability measured by the non-spatial CV is the same. It is therefore crucial that the characterization of the variation of a spatially distributed variable, like point stability, includes some measure of the spatial scale of the variation. Non-spatial measures of variation are not sufficient for a thorough characterization (Conway and Abrahamson, 1984, 1988).

Large spatial variability and completely spatially random stability test results imply that stability test results cannot be spatially extrapolated and interpolated as suggested by Landry (2002). This contradicts the findings by Föhn (1987b) and Chalmers and Jamieson (2001, 2003). In both studies, results of stability measurements in selected observation sites can reasonably well be used to predict avalanche activity in a surrounding area.

The studies by Conway and Abrahamson (1984, 1988), Stewart (2002) and Landry (2002) were done in different snow climates and different types of study plots. Only Landry (2002) made one set of measurements away from his usual study area in Montana, US. This set of measurements was done near Rogers Pass, Canada, where Stewart (2002) and his team carried out their measurements. In the data set from Canada, Landry (2002) finds the same kind of large-scale stability variation that Stewart (2002) reports. The variability observed in a study might therefore depend on the study site (e.g. its exposure to wind) and

the snow climate (e.g. snow depth). However, more studies must be made to test this hypothesis.

Another reason for the different results is the differing interpretation of measurement results in the studies. Conway and Abrahamson (1984, 1988) include stability tests that fail during preparation in their statistical summary as deficit zones with low stability. Most other studies discard such measurements because they are considered as erroneous measurements. The argument is that fracture might be produced during sample preparation, e.g. when inserting a shear frame, in which case some unintended loading of the targeted weak layer can take place. Indeed, samples that fail during preparation might be an indication that the location is weak, although this is not necessarily always the case.

Most previous studies have investigated point stability, with true stability tests that integrate information about the slab and the weak layer. Of the studies that focus on a specific layer, most have focused on the strength of weak layers. The study by Harper and Bradford (2003) is the first that at the slope-scale investigates multiple layers in the snow cover at a time, but they do not quantify the variability. Pielmeier (2003) also investigated multiple snow layers in the snow cover, but at a smaller scale than the present study.

1.7.3. Conclusions from previous slope-scale studies

Previous studies of snow cover spatial variability have investigated different snow cover properties with different measurement types. This makes the results difficult to compare. The results by Conway and Abrahamson (1984, 1988) lead to a belief that snow cover stability is highly variable with points of very high stability adjacent to points of very low stability. However, the interpretation of results differs from most other studies and the fracture process conditions at the study sites might not be representative of the stability before triggering. The studies by Landry and his field-crew (Landry, 2002; Landry and others, 2003) seem to partly support the results reported by Conway and Abrahamson (1984, 1988) although no spatial analysis was done. Munter (2003) focuses on the reports of high variability and postulates that the snow cover is a highly variable and completely random patchwork of areas of high stability mixed with areas of low stability. This is not supported by a number of other field studies (Föhn, 1989; Jamieson and Johnston, 1993; Jamieson, 1995; Stewart, 2002; Stewart and Jamieson, 2002), which show that stability is spatially variable, but that the variation has a spatial structure, although the structure has never been completely quantified. In addition, it has been shown that stability measurements in

study plots are correlated with avalanche activity (Föhn, 1987b; Jamieson, 1995; Jamieson and Johnston, 1998; Chalmers and Jamieson, 2001, 2003). Regarding slab avalanche release, it is important to note that most studies conclude that distinct layers are spatially continuous rather than discontinuous. The reasons for the different results are not clear, but four factors seem to play a role: a) the different test methods used in different studies, and b) interpretation of results; c) different studies investigate snow stability and snow properties in different snow climates and in different types of observation sites; and d) the lack of a true spatial analysis of the measurement results. Despite the inconsistencies, the following conclusions can be made:

- 1) Spatial variability exists.
- 2) The CV of point stability at the slope-scale ranged from 10% to 82% but was normally around 20% to 30%.
- 3) Spatial patterns of variation are important for the characterization of variability and should be quantified in the future.
- 4) Most studies suggest that point stability has spatial structure, which means that stability results can be extrapolated to some area but the precision might depend on the study site.

Chapter 2

Methods

2.1. Introduction

Mechanical and structural properties vary between snow layers in the vertical direction and within each layer in the horizontal direction (Colbeck, 1991). A complete description of mechanical and structural properties of the snow cover must be able to characterize this variation: measurements of bulk properties in one location do not suffice.

The goal of the study was to measure mechanical and structural properties of the snow cover with grain-scale resolution in the slope-perpendicular direction and snowpack-scale resolution in the slope-parallel direction. The measurements should enable a quantitative characterization of the slope-scale spatial variability for individual layers.

At present, no single technique makes it possible to measure spatial variability of properties related to snow stability with at high resolution and at the relevant scales simultaneously. To achieve the goal of this study, it was necessary to combine a number of techniques. The first step in the study was therefore to develop a research methodology that integrated various measurement types (Section 2.2). To have a data set that was ideal for a characterization of spatial variability and still kept within certain practical limits (Section 2.2.1), the measurements were placed in an optimized grid layout (Section 2.3). Once the grid design was determined, fieldwork began in a selected study area (Section 2.4) where slope selection was based on certain criteria (Section 2.3.3). Within each grid, a ramsonde hardness profile was measured (Section 2.5), a manual stratigraphic snow cover profile recorded (Section 2.6), snow samples collected (Section 2.7), snow micro-penetration profiles recorded (Section 2.8) and stability tests done (Sections 2.9 and 2.10). The snow cover stratigraphy within the grids was reconstructed (Section 2.11) and the variability of point stability and penetration resistance

characterized using the geostatistical corner stone, the semi-variogram (Section 2.12).

2.2. Research methodology

In the beginning of the project, no complete methodology was available. It therefore had to be developed by considering the objectives of the project and the methods available.

2.2.1. Practical limitations and considerations

Spatial scale

For the slab release processes, the variability of interest is up to and including the slope scale. At these scales, the fracture initiation and fracture propagation properties control whether a slab will release or not. At larger spatial scales variability also exists, but for the slab release processes those scales are not of primary interest. The focus of the study was on variability from the grain-scale to the slope-scale. Measurements therefore had to be done in the field on potential avalanche slopes.

Temporal scale

Snow cover properties may change within hours or days (e.g. Bader and others, 1939). To minimize the influence of temporal changes in structural and mechanical properties, all datasets were to be obtained within a day. This limited the number of potential measurement methods.

Relevant snow cover properties

The aim of the study was to investigate the spatial variability of snow cover properties relevant for snow slope stability. The stability of a slope cannot be measured directly, but can be estimated with results from point stability tests. Such tests give information about the ability to initiate a fracture in a weak layer by integrating slab and weak layer properties in the test result. Whether a fracture will propagate depends on the spatial variability of the weak layer properties. In order to measure the weak layer properties directly, other methods are needed. As discussed below, not many methods allow measuring properties of individual layers. Instead of limiting the study to measuring specific mechanical properties, the limiting factor was more the instruments that can be used to describe individual layers, which was one aim of the study.

Layers and layer boundaries

In manually recorded profiles, boundaries between adjacent layers are distinct owing to the methods used (Section 2.6). As pointed out by Pielmeier and Schneebeli (2003), such distinct layer boundaries are not found when measuring with high spatial resolution. Rather, between adjacent layers the layer properties (such as hardness) change gradually in most cases. These transition zones are important for processes, e.g. water and vapor flow or temperature gradients (Colbeck, 1991) and must be captured for a complete description of the snow cover. Thin layers of 1 to 5 mm often exist in the snow cover (Pielmeier and Schneebeli, 2003). Such layers are often responsible for slab avalanches. To identify thin layers and the gradual transitions between adjacent layers, the slope-perpendicular resolution of the measurement methods must be high.

Spatial layout of measurements

Standard spatial sampling schemes are available (e.g. Webster and Oliver, 2001), but most assume that information on the scales of variability of the measured variable are available. This was not the case. Further, the spatial layout had to be practical for the field crew. Measurements could for example have been placed randomly on a slope but this would not have been practical. With most sampling schemes, it is common to revisit an area where sampling density was not large enough in the first measurement campaign. On snow slopes, this is not possible because of the fast temporal changes that might occur in the snow cover and because the original snowpack was destroyed after the first measurement campaign. The spatial layout of the measurement on a slope is discussed further in Sections 2.2.4 and 2.3 below.

Study area

The selected study area should have untracked slopes and fast access to allow the field crew to spend enough time on a slope to finish all planned measurements in a day. The access had to be safe.

Safety

Measurements on potential avalanche slopes can be dangerous. To ensure safety of the field team, fieldwork could not be done on slopes when the snow cover was unstable. Further, only short slopes with a gradual run-out could be used, since the consequences of an avalanche release are smaller.

2.2.2. Overview of available measurement methods

The suitability of all available instruments and measurement methods was considered at the beginning of the study. The selection of the methods and instruments was based on 1) the dependence of the result on operator experience, 2) the time needed for one measurement, and 3) the field applicability of the method. Some of these methods are briefly described by Pielmeier (2003, p. 3).

Manually observed snow profile

The classical way to describe the snow layering (i.e. the vertical snow cover variability) is to record a manually observed pit profile (e.g. Colbeck and others, 1990). At the SLF, a snow pit on a slope is traditionally accompanied by a ramsonde hardness profile (Haefeli in Bader and others, 1939) and a rutschblock test (Föhn, 1987a). For a detailed description of individual layers in the snow cover (grain shape, size, density, hardness and temperature), the method takes about 1 to 2 hours. The precision of the method depends on the observers' experience and the purpose of the profile. Equipment needed for a complete snow profile (ramsonde, scale, magnifying lens, crystal screen and density measuring kit) weighs around 4 kg and fits inside a backpack.

Shear frame

The shear frame is used to measure the shear strength of weak layers or of weak interfaces (de Quervain, 1950; Jamieson and Johnston, 2001). A single measurement takes around 5 minutes but initial digging of a pit considerable longer. The method is to a certain degree operator dependent (Jamieson and Johnston, 2001), but is considered the best way to measure weak layer shear strength. The equipment needed for the test fits in a backpack and weighs around 1 kg.

Stability tests

A stability test indicates the stability of the snow cover at the location where it is done. Load applied on the snow surface of an isolated block or column of snow is increased until fracture occurs in a weak layer. Many different stability tests are in use. The area tested by the rutschblock test (RB) (Föhn, 1987a) is 3 m², and the test takes 10 to 20 minutes if combined with a snow cover profile. Most other stability tests e.g. the quantified loaded column test (QLCT) (Landry and others, 2001), the compression test (CT) (Jamieson, 1999), and the stuffblock test (SB) (Birkeland and Johnson, 1999) test an area of 0.09 m² (typically 30 cm x 30 cm). The rammrutsch test (RR) used by

M. Schneebeli (Schweizer and others, 1995) tested an area of 0.25 m² (50 cm x 50 cm). These smaller stability tests require 5 to 10 minutes once a snow pit has been dug. All stability tests require only little experience to do, whereas practice is needed for correct interpretation of the results. The QLCT test and the RR test require materials that weigh around 2 kg whereas the materials for the other tests weigh less than 1 kg.

Snow micro-penetrometer

The snow micro-penetrometer (SMP) (Schneebeli and Johnson, 1998) measures slope-perpendicular profiles of penetration resistance. Measurements are made every 4 μm. The diameter of the measuring tip is 5 mm. The penetration resistance has been shown to theoretically give information about the compressive strength of the snow and its elastic modulus (Johnson and Schneebeli, 1999; Schneebeli, 2001). The theory had only been tested on a limited number of field measurements before the study. No relationship between the SMP penetration resistance and snow cover stability had been found at the beginning of the study. However, differences in hardness between two adjacent layers might be important for shear failures along layer interfaces (Schweizer, 1993; Schweizer and Jamieson, 2003b). The operation of the instrument requires moderate practice. The SMP fits into a backpack and weighs around 6 kg. One SMP measurement takes around 3 minutes once the SMP has been assembled. Prior to the study, the SMP had not been extensively used in the field. Software for visualization of the SMP resistance profile was available, but practical experience with quantitative interpretation of the SMP signal was limited.

Radar

A few studies have used radar to investigate snow stratigraphy (Gubler and Hiller, 1984; Harper and Bradford, 2003), but no systematic studies have been made at the slope scale. It is not possible to investigate the properties of individual layers and thin layers with low density (e.g. critical weak layers) are not identified in the radar signal. The instruments available at the beginning of the study had a weight of 5 to 10 kg and were too large to be carried in a backpack.

Near-infrared photography

In the near-infrared spectrum, the snow reflectivity strongly depends on the grain size (Colbeck, 1991). A special camera can be used to investigate reflectivity variation on the snow surface or on vertical walls in a snow pit. The acquired information covers an area, not a line as the

information from e.g. the SMP. The method requires special light conditions to give good results. The equipment weighs around 1 kg. At the start of the study, the method was not well developed.

Choosing the methods

The radar instruments were too heavy and bulky to bring into the field. Signal analysis was also not mature enough for intensive use of the instruments. Radar measurements were therefore not done. Similarly, near-infrared photography was not well developed and was not used here. For a good description of snow cover stratigraphy, at least 100 measurements were needed (Sections 2.2.3 and 2.2.4). Only the SMP would enable 100 measurements in a day and it was therefore used to study the spatial variability of layer properties. The SMP was also the only fast instrument with which it was possible to identify thin layers in the snow cover. Because the SMP penetration resistance signal had not been comprehensively related to snow cover properties used to assess strength, and accordingly stability, a complete manually observed profile was done for comparison. Snow samples for analysis in the cold lab provided detailed microstructural information about some layers. To evaluate the snow stability, stability tests were needed. These should also provide data for spatial analysis. To obtain as many stability test results as possible, stability tests that were fast to execute were preferred over slower ones. For the first winter, the SB test was chosen because it did not need as much equipment as the other methods. However, results from the first winter showed that the test setup did not give consistent results (Section 2.10.5). For the second and third winter, the rammrutsch test (in a slightly modified version) was chosen. This method got around some of the error sources in the SB test, but required heavier equipment than the SB test.

2.2.3. Overview of methods for characterizing spatial variability

The processes that cause spatial variation in the snow cover do so in a physically controlled deterministic way. If these processes were quantitatively known, it should be possible to describe the snow cover with a deterministic model. However, the current understanding of the processes is far from complete and the interaction between these processes might be non-linear, making the outcome so complex that it might seem random. To describe the spatial variation of the snow cover an alternative to a purely deterministic description must therefore be sought.

Spatial variability can only partly be described by classical statistics. Classical descriptors such as the variance (σ_0^2), the standard deviation σ_0 and the coefficient of variation CV describe the dispersion of the variable Z around its average, typically the arithmetic mean \bar{Z} or the median \tilde{Z} . However, variables with equal values for the classical statistical descriptors can be spatially continuous (i.e. they vary smoothly) or spatially discontinuous (i.e. they exhibit rapid fluctuations over short distances) in space. A continuous variable will show large uniform patches in space whereas a discontinuous variable will show small uniform patches. In addition to the classical descriptors, the spatial continuity of a variable must also be characterized.

Techniques to statistically describe the spatial variability of a variable are well developed. Possible ways to characterize spatial continuity are by using geostatistics (e.g. Cressie, 1993), random field theory (e.g. Vanmarke, 1977), Fourier analysis (Cressie, 1993, p. 117), wavelet transformations (Haar (1910) in Sahimi, 2003) or through the fractal dimension D (Mandelbrot (1982) in Cressie, 1993, p. 729). Fourier analysis should only be applied if there is reason to believe that the data are oscillatory, and requires much data (Cressie, 1993, p. 117). The fractal dimension only describes small-scale variability (Cressie, 1993, p. 312), while the approach by Vanmarke concentrates on the large-scale variation (Cressie, 1993, p. 119). Wavelet analysis requires large amounts of data, which was not available for the horizontal spatial variation. However, wavelets might be a possible way to analyze individual SMP profiles.

Geostatistics have successfully been used in e.g. mining and agricultural applications, and hydrology (e.g. Blöschl, 1999) to describe spatial and temporal variability of 1, 2 and 3-dimensional data. It is backed up by a large body of theory (e.g. Cressie, 1993). Section 2.12.4, p. 70 describes the geostatistical methods used in this study. Geostatistics relies on the idea that a variable changes continuously in space. When a variable is measured at two closely spaced points, the difference between measurements is small, whereas when the measurement points are spaced further apart, the difference in the measurements is larger. The cornerstone of geostatistics is the semi-variogram (Figure 2.21, p. 73), which describes the variance in the data as a function of the distance between the measurement locations. The semi-variogram can be characterized through three parameters: the range, the nugget variance (or simply the nugget) and the sill variance (or simply the sill). The range of a variable is a measure of the average spatial distance over which measurements of a variable are correlated. A

spatially continuous variable has a large range whereas a discontinuous variable has a small range. The sill is a measure of the magnitude of variance of the variable at distances greater than the range. The nugget is a measure of the small-scale variability of the variable. For the semi-variogram to give accurate results, a reasonable number of measurement points must be used in the analysis. The lower limit for a statistically sound determination of the semi-variogram for two-dimensional data is 50 to 100 (Webster and Oliver, 2001, p. 90). However, this number depends on the relative position of the measurement locations and the distribution of the data.

2.2.4. Considerations for the spatial measurement layout

To optimize the spatial information for the statistical analysis (Section 2.12.4, p. 70), the spatial layout of the measurements was considered in terms of the scaling triplet: support, extent and spacing as described in Section 1.5, p. 8 (Blöschl and Sivapalan, 1995).

Support

The support of a measurement is the area or volume over which the measurement is integrated. In general, a smaller support gives a higher variance than a larger support. Choosing the support for a measurement method is a dilemma: with a large support, the result provides a good average description of the variable, but little information of the small-scale statistical variation of the variable, and vice versa. A reasonable measurement support must be chosen after considering the aim of the study. Upon choosing the SMP and the small stability tests as the main measurement methods, the support was fixed. The support of the SMP was small compared to the support of the stability tests.

Extent

The extent is the maximum distance between two measurements in the sampling layout. A spatial analysis will not be able to detect spatial patterns with a length scale larger than the extent. The extent should be larger than 10 m, since this is expected to be the maximum limit for fast fracture propagation (Schweizer, 1999).

Spacing

The sample spacing is the slope-parallel distance between the individual measurements in the sampling layout. Webster and Oliver (2001, p. 92) discuss the problem of selecting the optimal sample spacing. The optimal spacing depends on the variability of the property measured. The measurements must have a spacing that is small enough to capture

the minimum expected variability in the property (analogous with the Nyquist frequency for oscillatory data). The minimum spacing between measurements could not be determined from previous field measurements (Section 1.5). The scales of variation thus had to be estimated by considering the main natural agents (thereby excluding skiers, avalanches, etc.) responsible for variations in snow layer properties. Before the spring, where percolation of melt-water might introduce small-scale variability in snow layer properties, the main agents were thought to be wind, radiation and temperature (Kronholm and others, in press-a; Sturm and Benson, in press). The two last agents are relatively constant at the slope-scale, and assumed constant over the relatively planar slopes investigated. In the study area, surface forms associated with wind have length-scales from a few centimeters for small ripples, to tens of meters for large dunes. Horizontal variability at length-scales smaller than 1 m can be studied under controlled conditions in a lab. To accurately determine horizontal variability at a length-scale of 1 m, the smallest spacing had to be 0.5 m or smaller.

There is a trade-off between spacing and extent. The number of measurements that could be done in a day had a maximum limit (100 to 140, see Section 2.2.5 below). Decreasing the spacing would therefore also decrease the extent of a measurement layout. By varying the spacing over the sampled area (nested sampling), it was possible to partly work around this problem. A minimum spacing of 0.5 m was chosen as a compromise between having a large extent and the smallest possible spacing.

2.2.5. Geostatistical optimization of the sampling layout

For the geostatistical optimization of the measurement locations over a slope, the goal was to optimize the semi-variogram. A good graphical representation (a map) of the results was secondary. The most important criterion for the semi-variogram was that the number of point pairs with pair-wise distances between 1 and 10 m was large. For a complete description of calculation of the semi-variogram, see Section 2.12.4 and Cressie (1993).

Layout of SMP measurements

First, the layout of the SMP measurements was considered. Preliminary tests showed that between 100 and 140 measurements could be done in one day. A regular spatial sampling plan (a grid) was preferred over random sampling of more than 100 measurements because a grid is 1) easier to implement on a snow slope, and 2) usually better suited for

kriging (Cressie, 1993, p. 319). A nested spatial sampling plan is recommended if little is known about the spatial variation (e.g. Webster and Oliver, 2001, p. 93), which was the case. No standard way exists to choose an optimal sampling scheme. Based on these considerations, a number of possible sampling plans were designed and compared. All had three conditions in common: 1) there were between 100 and 140 SMP measurement locations, 2) the resulting omni-directional semi-variogram consisted of a reasonable number of point pairs to a distance of at least 10 m, and 3) the measurements were in a regular grid. The locations of SMP measurements in three possible sampling plans are shown in Figure 2.1. The figure also shows the number of point pairs for various lag-distances.

Grid types 1 and 3 (Figure 2.1) had minimum spacing of 0.5 m and were therefore preferred over grid type 2. Grid type 3 required large slopes for measurements. Smaller slopes were easier to find and safer for the field crew, so grid type 1 was almost exclusively used.

Layout of stability tests

Second, the location of stability tests within grid type 1 and 3 was chosen. Unlike the SMP measurements, these tests required the digging of a snow pit, which was time-consuming. In the second winter, it was decided to locate the stability tests in pairs of two in each pit. This also allowed an estimation of the small-scale variability of point stability. The maximum number of tests that could be done in a day was around 25, which would allow around 12 pits within a grid.

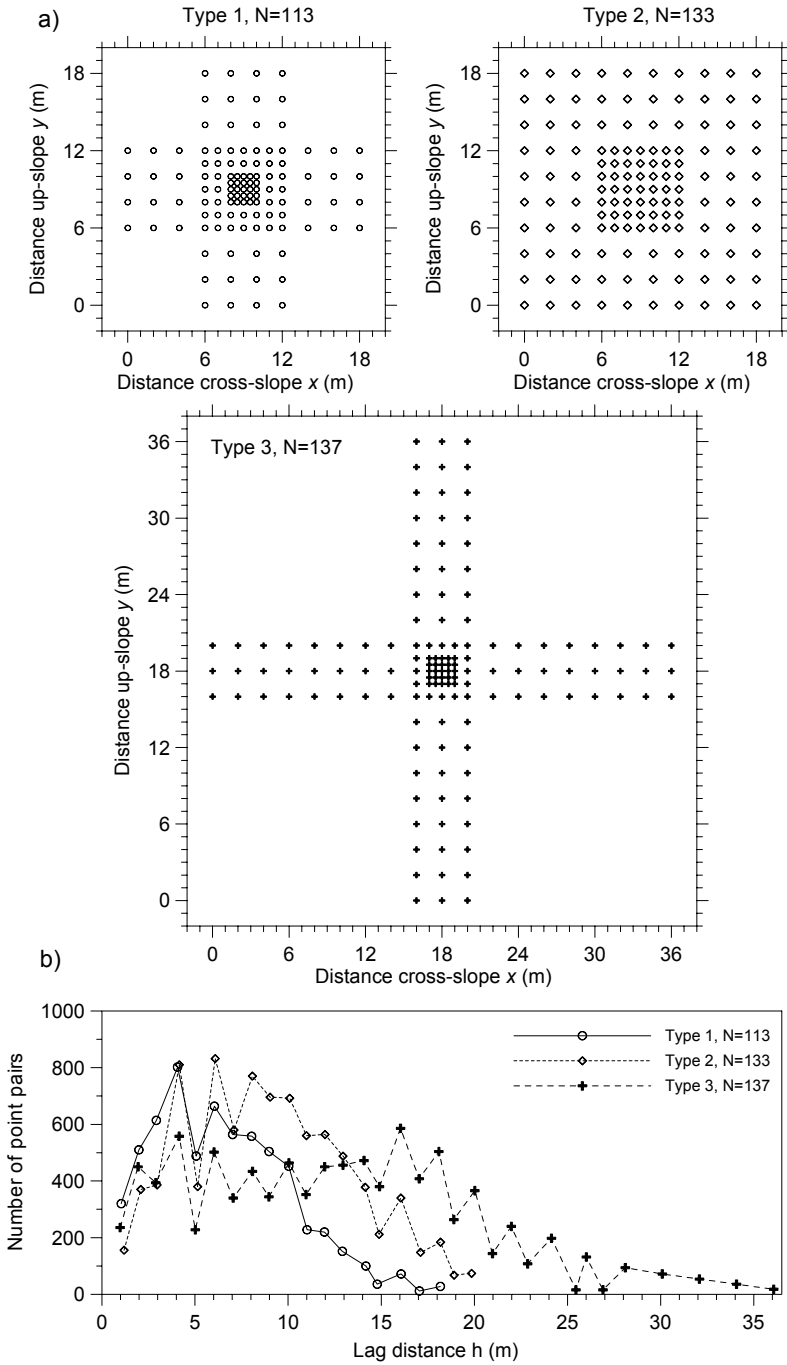


Figure 2.1. a) Spatial overview and b) the number of point pairs of three possible SMP measurement designs. Grid type 1 was almost exclusively used.

2.3. The grid layout

After the considerations mentioned above, the spatial layout of the measurements was defined (Figure 2.2). All grids analyzed in this study were of type 1 (Figure 2.1) and had the same spatial layout of the measurements. In the beginning of the first winter season, grid type 2 (Figure 2.1) was used on three field days (Table 3.1, p. 76). No data from these days were analyzed, and only the layout of grid type 1 is therefore shown. The grid (nicknamed the “Schweizer Kreuz”) spanned 18 m in both the cross-slope direction (x) and the up-slope direction (y). The up-slope and cross-slope extent (in the sense of (Blöschl, 1999), Section 1.5.1, p. 8) was therefore 18 m, and the maximum extent a little more than 18 m. A grid normally covered a large part of the slope (Figure 2.3).

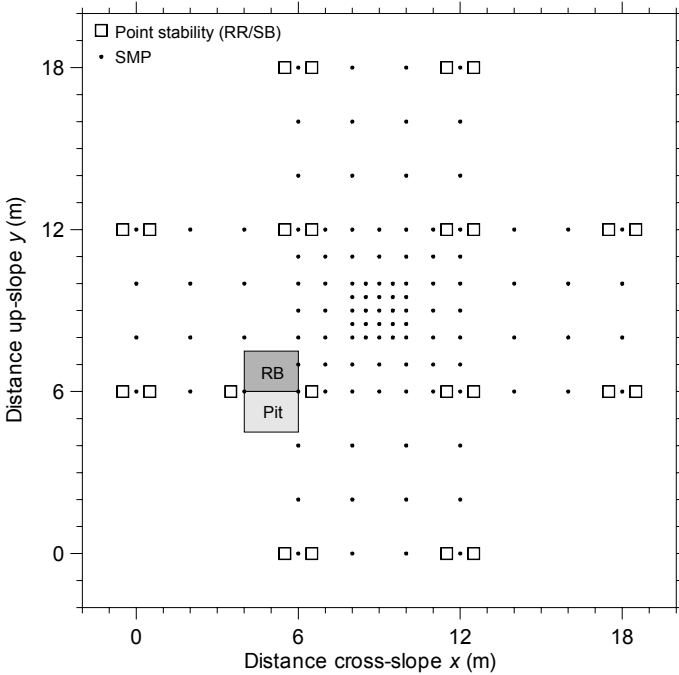


Figure 2.2. The layout of the measurements in grid type 1, which was used in all the grids analyzed. Before the snow pit was dug, a ramsonde profile was made. In the snow pit, the stratigraphic profile with grain shape, grain size, snow temperature and layer density was made. The rutschblock test (RB) was done above the pit. 113 SMP profiles and 24 column-type point stability tests covered the grid.

2.3.1. Measurements in the grid

A ramsonde hardness profile (Section 2.5) was made below the left leg of the grid (Figure 2.2). The ramsonde was left standing, and a pit was opened with the vertical ramsonde in one corner. In the pit, a manual stratigraphic profile was made (Section 2.6). All depths from this profile referred to the depth-scale on the ramsonde, starting from zero at the ground. Above the pit, a rutschblock stability test was done (Section 2.9) to pinpoint weak layers. Samples of these weak layers were taken in the pit, and occasionally at other locations in the grid (Section 2.7). Within the grid, 113 snow micro-penetrometer (SMP) measurements (Section 2.8) were spaced 0.5 m to 2 m apart in a nested pattern. Next to each SMP measurement, the vertical snow depth HS was measured with an avalanche probe. In all 12 corners of the grid, column-type stability tests (Section 2.10) were done in pairs, yielding 24 tests. The two tests in a pair were 1 m apart in the cross-slope direction, and located on each side of the center of a small pit. Each of the 12 stability test pits was 6 m apart in the x and y direction.

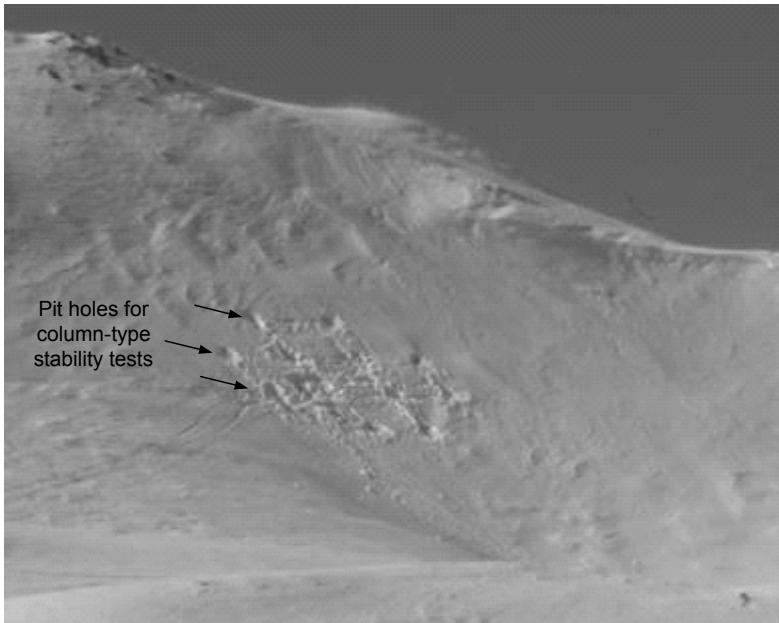


Figure 2.3. Typical setting of a grid on a slope. Three of the 12 pit holes for the point stability tests in grid 8 are marked.

Distances between the measurement points were measured parallel to the snow surface with a measuring tape. The location of each measurement was marked with a bamboo-stick. The precision of each location was better than ± 20 cm in both the x and y direction. All measurements were normally done in less than 6 hours.

2.3.2. Field procedure for the grid measurements

Two points were crucial for each grid to be successful in terms of i) finishing all measurements in a day, ii) making the measurements in the correct locations, and iii) leaving the snow undisturbed at measurement locations. First, it was important to think through every detail of the grid layout before stepping onto the slope. Second, the field team had to be well organized. A strict schedule was therefore followed. After a slope was selected, the most experienced field person would traverse the slope such that the tracks were immediately below $y = 6$ m in the grid coordinate system (Figure 2.2). A quick overview of the snow depth along the line was made with an avalanche probe. If the snow depth was very irregular, a new slope was searched. If the snow depths were regular, the snow pit was located where snow depth was a little below the average along the line $y = 6$ m. However, selecting the pit location should still leave room for the grid to extent to both sides without placing the outer points in very deep or shallow snow cover. One team (the pit team) with the most experienced field person then started the ramsonde profile and the stratigraphic profile with the second person recording. A second team (the SMP team) first marked the rough outline of the grid to make orientation easier. When this was done, one person marked the locations of the SMP measurements and at the same time measured snow depths in the left leg of the grid. The other person did the SMP measurements at the marked locations. After the SMP measurements in the left leg were finished, the rutschblock test could be done by the pit team. After finishing SMP measurements in the left grid leg, the SMP team worked through the lower leg, the middle part of the grid, the right leg and finally the top leg. After the pit team had finished the pit and the rutschblock test, they started the point stability tests. These were typically done in the same order as the SMP measurements: left leg; bottom leg; middle; right leg and finally the top leg. Because the pit team knew the general layering of the snow cover, it was normally easy for them to relate the layers and interfaces that failed in the stability tests to the stratigraphy in the pit. The team that finished first took the snow samples over the interfaces and layers that were judged interesting in terms of stability by the pit team. Although the measurements could be

done by four persons, a fifth person was occasionally present to replace persons with cold feet and empty stomachs.

2.3.3. Slope selection

Selection of the slopes was done in the field by the most experienced field person in the group. The criteria for the selection depended on the avalanche danger observed on the field day and on the snowpack characteristics. The preferred slopes

- a) had a northerly aspect
- b) had an inclination between 35° and 45°
- c) had at least one weak layer be present in the snow cover
- d) showed no signs of natural (e.g. previous avalanches) or human (e.g. ski tracks) disturbance
- e) had a relatively homogeneous snow cover thickness and a ground cover without large rocks
- f) were rather short, typically less than 50 m high and free from large concave features and cliffs below

a), b) and c) ensured that the selected slopes were typical avalanche slopes (McClung and Schaerer, 1993; Schweizer and Lütshg, 2001). If the snow cover on the slopes was very inhomogeneous, it was expected that fracture propagation could not take place. Because the aim was to sample potential avalanche slopes, only slopes with homogeneous snow cover were of interest in the study. This was attempted (but not ensured) by selecting slopes that satisfied d) and e). From the frequent visits to the study area, the field team knew which slopes had been disturbed, and these were avoided, fulfilling d). Point e) was achieved by using an avalanche probe to measure snow depths across a slope before any other measurements were started. To ensure the safety of the field team, f) was always fulfilled.

2.4. Study area and fieldwork period

The study area was selected due to a large number of suitable slopes with a variety of slope aspects and slope inclinations and due to relatively easy access. In the first two winters, access was provided by ski lifts followed by a one-hour ski tour. During the third winter, the ski lifts were closed and the area was accessed with helicopter. Despite the relatively easy access, the area is not heavily used by skiers.

2.4.1. Fieldwork period

Field measurements were done in the same study area during the winter seasons 2000 – 01, 2001 – 02 and 2002 – 03. Each winter season was restricted to January, February and March. On each field day, one slope was selected for investigation (Section 2.3.3). The measurements were done in a grid, each of which was finished in a day.

2.4.2. Location

The study area is located near Davos in the eastern part of the Swiss Alps (Figure 2.4). The area covers approximately 3 km x 1 km and is located in the Chörbsch Horn – Hanengretji region 4 km west of Davos (Figure 2.4).

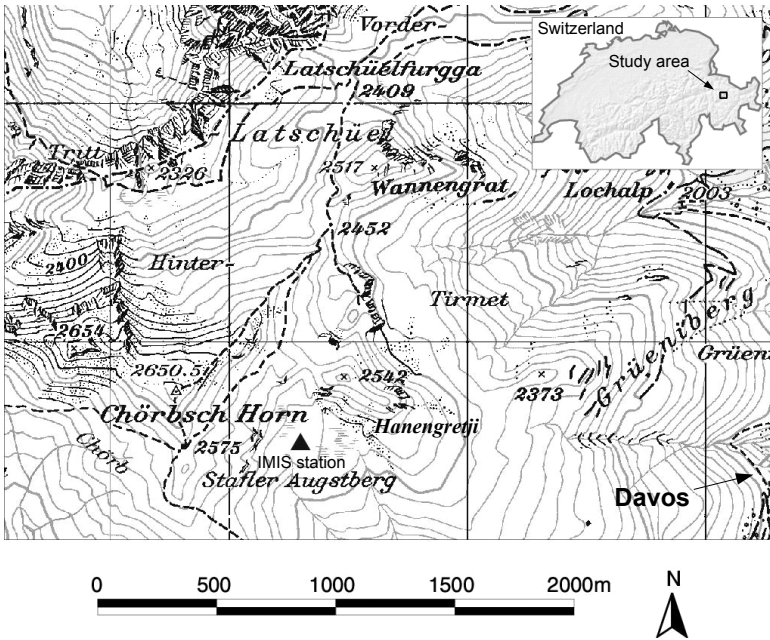


Figure 2.4. Map of the Chörbsch Horn – Hanengretji study area. The blue triangle indicates the location of the Hanengretji IMIS weather station. The insert map shows Switzerland with the location of the study area marked.

2.4.3. Terrain

Elevation within the area is between 2350 and 2650 m a.s.l., well above the timberline (Figure 2.5), which around Davos is at 2000 m a.s.l. The area is located in a small mountain range with a broad ridge running NE–SW. The topography is steep with peaks reaching 2700 m a.s.l., while the valleys on either side of the ridge have elevations between 1300 and 1500 m a.s.l. The slopes in the study area are grassy with solifluction or covered with rocks with a diameter of 2 – 30 cm (Figure 2.6). Occasionally larger rocks were present on the ground within the grids. In an area 13 km east of the area studied here, Haeberli (1975) found permafrost down to 2300 m a.s.l., especially at the base of west to north-exposed slopes, where avalanche snow usually remains far into summertime and cools the ground. At the base of the short slopes studied here, avalanche debris seldom remains much longer than the normal snow cover. In the profiles, the temperature at the bottom of the snow cover was never colder than -2°C .

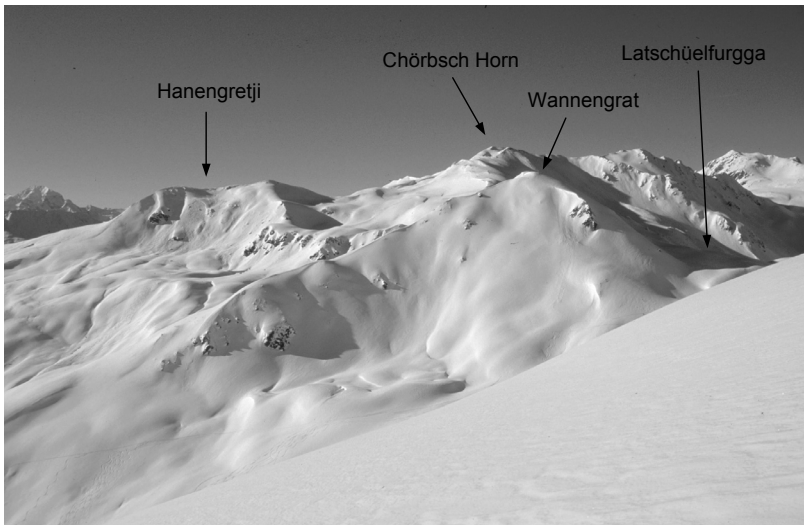


Figure 2.5. A view of the study area towards the SSW. The study area provided easy access to a number of small north-facing slopes with little skier disturbance. North-facing slopes are in shade.



Figure 2.6. Typical ground cover on the slopes where the measurements were done; alpine meadows with solifluction and patches of scree. The elevation difference between the lake and the ridge is 30 m in the middle of the picture.

2.4.4. Snow and weather conditions

Winter precipitation in the region is normally brought by low-pressure systems approaching from the north. This results in regional-scale variations in snow depth with more snow in the mountain regions north of Davos and less snow in the regions to the south (Schweizer and others, 2003b). During the first winter, most precipitation came from the south.

An automated IMIS type weather station (Lehning and others, 1999) was located within the study area on a small horizontal shoulder between Chörbsch Horn and Hanengretji (Figure 2.4, Figure 2.7). Snow and wind conditions at the station are shown for the three winter seasons in Figure 2.8. The maximum snow depth around 2 m is typical for the area, but large variations occur on the basin-scale from slope to slope due to snowdrift. On wind-exposed slopes, the snow cover might be only 0.5 m, while lee slopes might have more than 4 m snow cover. Due to the large relief, basin-scale wind patterns play a large role in the redistribution of snow within the area. In the pass “Latschüelfurgga” (Figure 2.4), the wind was mostly stronger than in the rest of the area, due to the strong funneling effect of the pass.

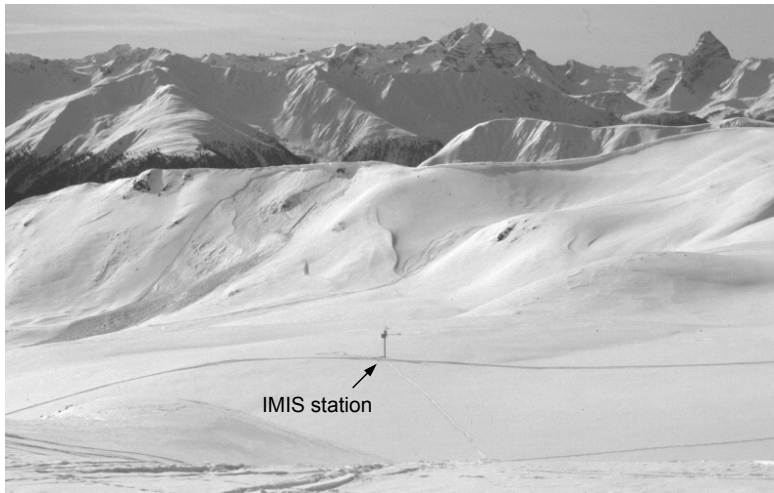


Figure 2.7. The automatic IMIS weather station viewed from Hanengretji towards south. From the ridge behind the station, a recent slab avalanche is seen. On the ridge, cornices have formed due to winds from the south.

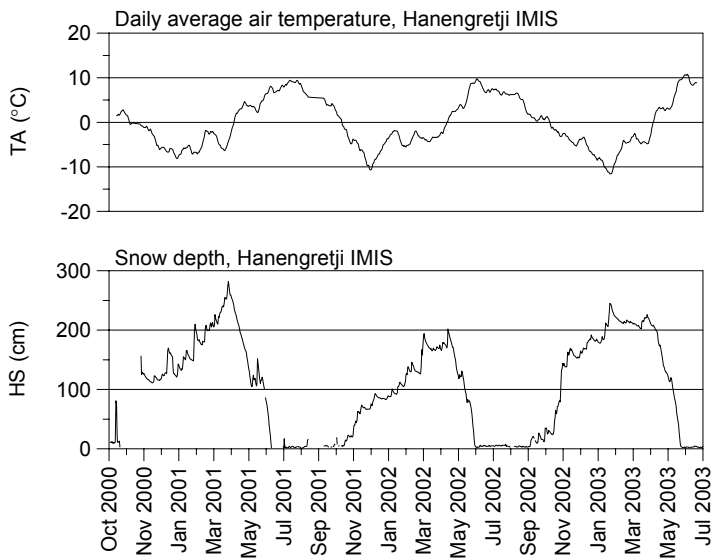


Figure 2.8. Air temperature and snow depth at the Hanengretji IMIS station during the three years where fieldwork was made. The three winter seasons were typical for the study area.

2.5. Ramsonde hardness profile

In each grid, a hardness profile was made with the Swiss ramsonde (Haefeli in Bader and others, 1939). The ram profile indicates the penetration resistance of the snow cover. It is commonly used as a hardness index through a vertical section of the snowpack (e.g. McClung and Schaerer, 1993, p. 143). The hardness profile is used for a quick overview of the consolidation of the snow cover, and can be used to classify the snow cover into different classes (Schweizer and Wiesinger, 2001).

A one meter rod with a weight of $Q = 10$ N was placed vertically on the snow surface and the initial penetration recorded. The tip measured 4 cm diameter and had an included angle of 60° . After the initial penetration, a drop hammer with weight $P = 10$ N and a thin rod for the guidance of the drop hammer was put on top of the ramsonde and the resulting total depth of penetration recorded. This was followed by a number of drops of the drop hammer from a specific height with resulting penetration of the snow cover. At frequent intervals, the number of drops n , the drop height dh and the total penetration was recorded. When the snow provided little penetration resistance to the ramsonde, the total depth of penetration was recorded after a few drops from a small drop height. The drop height and the number of drops were adjusted to the penetration resistance of the snow cover. If the snow cover was deeper than 1 m, additional rods of 1 m in length were added on top of the first rod. q is the number of rods used. The mean ram penetration resistance R_{ram} in N between two recordings was calculated from the difference in penetration depth between two recordings Δ by

$$R_{ram} = \frac{n \times dh \times P}{\Delta} + P + (q \times Q). \quad (\text{Eq. 2.1})$$

2.5.1. Measurement precision

Due to the large ramsonde tip, the ram profile does not show thin weak layers, which might be critical for stability. Other methods must be used to detect such layers, and the ram profile must be used as an overview of the consolidation of the snow.

Equation 2.1 simplifies the physics of the ramsonde – snow interaction because it neglects the energy losses that occur during the consecutive drops of the drop hammer (Gubler, 1975). Despite this, the equation is used as a standard to calculate the penetration resistance. The ram penetration resistance was plotted as a function of depth alongside the description of the stratigraphic layers in the snow cover.

2.6. Manually observed stratigraphic snow profile

Manually observed stratigraphic profiles (manual snow profiles) of snow properties (layering, grain shape and size, hand hardness, temperature and layer density) were done in a snow pit according to the methods described by Colbeck and others (1990). One profile took 1 to 2 hours to complete, depending on the depth and the complexity of the layers in the snow cover. The snow pits were dug so that the wall was in shade to prevent fast metamorphism of the exposed snow grains. The ramsonde was left standing in one corner of the pit.

2.6.1. Observations

The recording of stratigraphic layers served to describe the sequence and the properties of each separate layer in the snow cover. The separation of layers was based on visual and sensible variations in snow hardness and snow texture. The vertical location of layer boundaries was measured from the bottom of the profile ($H = 0$ cm) towards the top of the snow cover ($H = HS$) by referring to the scale on the ramsonde. For each layer identified the grain shape and size and hand hardness were recorded. Density was recorded if the layer was not too thin.

Grain shape and size

Snow grain shape and size were identified using a crystal screen and an 8x or a 10x magnifying glass. With the exception of crusts, grain shape was recorded according to international standards (Colbeck and others, 1990). For crusts, the international standard only recognizes melt-forms (\circ) within the crust (\odot). In this study, other grain types, typically facets (\square) or rounded facets (\triangle), often observed in the crusts, were recorded. This practice is standard for observations by SLF researchers, and further differentiates the international classification for crusts. Up to two shapes were recorded for each layer. If the quantity of two different shapes were equal, they were recorded as e.g. [\square \triangle]. In some layers, one shape dominated, but a second shape was also observed. For such a layer, the shapes would be recorded as e.g. $\square(\triangle)$, where the shape in brackets was the secondary shape. The grain size for a layer was given an upper and a lower bound. The lower bound was estimated as the mean grain size, the upper bound as the mean size of the largest grains (Baunach and others, 2000).

Hand hardness

Hand hardness was classified according to the five main classes in the international standard (Colbeck and others, 1990); F: fist, 4F: four

fingers, 1F: one finger, P: pencil, K: knife and I: ice. Additionally, intermediate hardness values between these five classes (e.g. 4F – 1F) were also used.

Density

The layer density (ρ) was recorded as the mean of two samples. Occasionally, a large difference between the two samples was found, and another two or three samples were made. Then the density was calculated as the average of all samples. Two types of metal samplers were used: a cylindrical type with a volume of 100 cm³ (diameter = 3.7 cm, length = 9.3 cm) and a rectangular type with a volume of 100 cm³ (6 cm x 3 cm x 5.5 cm). On each field day, only one type of sampler was used. For layers that were thinner than the minimum dimension of the density sampler, the density was measured by cutting out a sample of the layer, measuring the dimensions and weighing it. For very weak or brittle thin layers, such as buried surface hoar, it was not possible to measure layer density. These layers did not have their density measured separately but were included either in the layer above or below.

Temperature

Snow temperature was measured at regular intervals of 5 cm near the top of the snowpack, typically the upper 15 – 30 cm. In the rest of the profile, the measurements were 10 cm apart.

2.6.2. Measurement precision and resolution

The precision and resolution of a manually observed stratigraphic profile depends on the observer and the purpose of the profile. For the purpose of stability evaluation, a stratigraphic profile of only the major layers may suffice, as long as all weak layers are included. For verification of snow cover models, a detailed stratigraphic profile is needed. In this study, the profiles included most stratigraphic details.

The precision of the observed grain shape and size and hand hardness is impossible to quantify. It depends on layer properties, on the experience of observer, the weather (snow, temperature and sun), on the purpose of the profile and on the layer properties. The thickness of thin layers might be accurate to 1 mm, whereas the thickness of thicker layers might be accurate to 1 cm.

Each manual profile was recorded by one of three experienced observers. One observer (J. Schweizer) did around 80% of all profiles in this study, the other two observers around 10% each.

2.7. Snow samples

During the second and third winter, snow samples were taken in the field. In-situ samples of primarily weak layers were taken in a 5 cm x 5 cm x 7 cm container, which was inserted in a vertical wall with its upper edge parallel to the layering (Figure 2.9). After removal of the container, the weak layer was checked to see if it was still intact. For very weak layers, the removal of the container was very delicate and the sampling procedure sometimes had to be repeated several times to get an undisturbed sample.

In one corner of the container, the snow was removed from the top to the bottom to make room for the tip of a funnel. Diethyl-phthalate dyed with Sudan Black was slowly poured through the funnel (Figure 2.10) until the snow was completely saturated and the container full. To prevent the snow sample from melting and the diethyl-phthalate from freezing, it was kept at -3°C in a thermos until use.



Figure 2.9. Two in-situ samples were taken parallel to the snow layers on the vertical wall of the snow pit in grid 20. Removal of weak layer samples from the wall often had to be repeated several times to get an undisturbed sample.



Figure 2.10. After removal of the sample from the wall of the snow pit, black diethyl-phthalate was slowly poured into the sample until it was completely saturated.

To ensure that no air pockets were left in the diethyl-phthalate filled sample, it was left undisturbed for 15 minutes. The sample was then lifted into an insulated box, which was half filled with dry-ice. After freezing, the cast could be transported to the cold-lab at SLF, where it was stored.

In the cold-lab, a cube from the center of the sample was cut out to avoid possible disturbances of the edges of the sample during sample preparation. The cube was placed in a microtome and the surface leveled and photographed with a digital camera. Finally, the image was binarized to distinguish between ice and pore-space (Good, 1987; Dozier and others, 1987). The resulting images showed a 1.5 cm wide and 5 cm high section perpendicular to the layering in the original cast, with the weak layer in the middle.

2.8. The snow micro-penetrometer

An improved version of the snow micro-penetrometer (SnowMicroPen, SMP) described by Schneebeli and Johnson (1998) was used to measure slope-perpendicular profiles of the snow cover penetration resistance. The SMP consisted of microcomputer and a rod that was driven into the snow at constant speed of 20 mm s^{-1} by a motor drive

(Figure 2.11). Two legs were attached to the motor drive and pushed into the snow to keep the unit stable. The microcomputer was controlled by the operator through a touch-screen on the front of the box containing the processor.

The penetration resistance was measured every $4\ \mu\text{m}$ with a piezo-electric force sensor at the front of the rod (Figure 2.12). The cone-shaped measuring tip had a 60° included angle and a maximum diameter of 5 mm. The resolution of the sensor was better than $10^{-3}\ \text{N}$, the range 40 N. The standard deviation of the signal noise in air was around $10^{-3}\ \text{N}$. The temperature of the force sensor was recorded every 0.5 mm to check for large temperature drift. The SMP was powered by an external 12 V, 7 Ah battery, which was typically stored in the operators' pocket to keep it warm.

Penetration resistance (R) and sensor temperature for each profile were saved in separate files on a memory card together with the average penetration speed and the date and time of the measurement. In the office, the files were transferred and stored on a file server. The SMP penetration resistance profiles were measured perpendicular to the snow surface (as judged by the operator) to avoid the tip slipping on hard layers. A single measurement took around 3 minutes after the SMP was mounted.

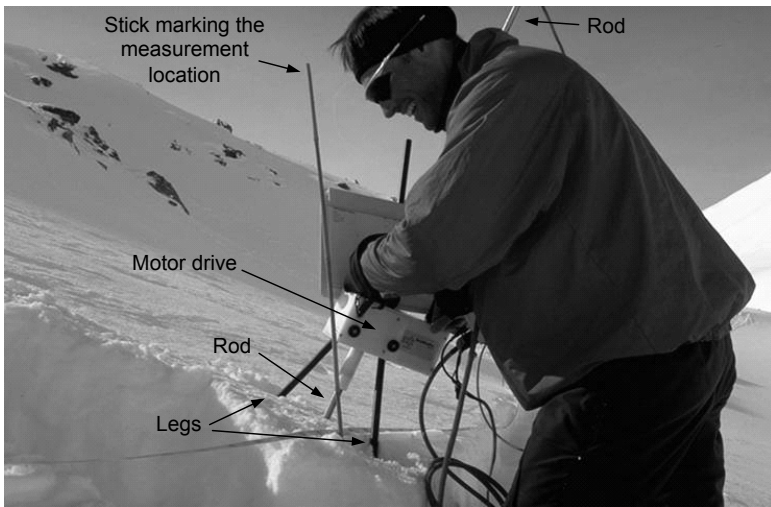


Figure 2.11. The snow micro-penetrometer (SMP) with motor drive, rod, and the two legs for stability.

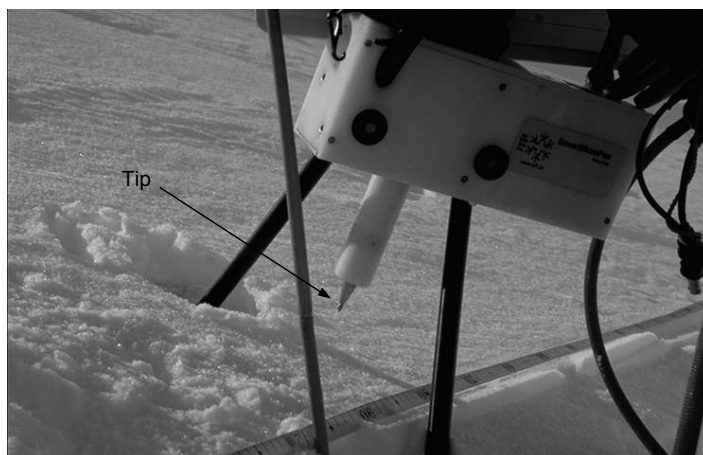


Figure 2.12. The tip of the snow micro-penetrometer (SMP) just before entering the snow. The penetration resistance of the tip is recorded by a force sensor located inside the front of the rod.

2.8.1. Previous SMP versions

During the first winter season, the field team used a version of the SMP that differed from the version described above. The main difference was that the older version had a force sensor with a range of 500 N, which was more sensitive to temperature than the version described above. In most measurements from the first winter, the temperature gradients in the snow cover caused a large drift in the SMP force signal. It was attempted to filter the drift out of the signal, but because the data from the following two winters were good and sufficient for the analysis, the SMP data from the first winter were not analyzed.

2.8.2. Measurement errors

It was attempted to measure the penetration resistance profiles perpendicular to the snow surface. Failure to do so would lead to apparent layer thicknesses greater than the actual layer thicknesses. The penetration angle of the rod was estimated to be less than $\pm 5^\circ$ from the ideal penetration angle. This results in an overestimation of layer thickness estimates of less than 0.5%. This error was considered negligible in the further analyses.

During penetration of very hard layers in the snow cover, the SMP operator put a lot of weight on the SMP motor box to keep the

penetration speed constant. If too little weight were applied, the SMP motor box lifted, resulting in decreased speed of the SMP tip. If too much weight were applied, the legs would sink further into the snow, causing an increase of the penetration speed of the SMP tip. When either happened, the operator would repeat the measurement. However, in some cases the lifting or sinking of the motor box might have gone unnoticed. The resulting small sections with penetration speed that differed from the average were probably around 1 cm. No such sections were noticed in the analyzed SMP penetration signals.

The piezo-electric sensor in the SMP was weakly temperature dependent. Tests carried out in the cold lab showed that changes in the temperature of the sensor resulted in a drift of the force signal. The force drift was influenced by the rate of change of the temperature. In conditions typical for the snow cover measured in this study, with temperatures typically between -15°C and 0°C and relatively low temperature gradients in the sensor temperature, the drift of the force signal was estimated to be lower than 0.05 N, typically around 0.02 N.

To reduce bending moments in the force sensor, which would result in erroneous force measurements, the SMP tip ran tightly but with negligible friction through the hole in the conical front of the rod. In some cases, water entered the small space between tip and conus and froze, resulting in incorrect measurements of penetration resistance. The resulting signals appeared as low-pass filtered true signals and they were easily identified by visual inspection in the office but unfortunately not in the field. This occurred in about 50% of all measurements, and affected most measurements in a grid. Despite the tight fit of the tip through the hole in the front of the rod, bending moments were sometimes introduced on the force sensor. Such moments caused negative force readings, which typically occurred as single spikes. This was primarily observed in layers with large grains, where bending moments were produced as the tip was in contact with only a single grain, and thus being pushed to one side.

2.8.3. Analysis of the SMP data on multiple scales

The SMP data can be analyzed on multiple scales. At the snowpack-scale, the SMP profiles give information about the consolidation of the snow, much like the ramsonde (Section 2.5). At the layer-scale, the SMP data can be used to identify all stratigraphic layers thicker than 1 mm in the profile. At the grain-scale, individual bond fractures can be identified due to the high slope-perpendicular resolution of the signal. The grain-

scale information from the SMP signal can be used to calculate structural and mechanical properties of the snow.

In this study, the SMP data were analyzed at the layer-scale and at the grain-scale. First, individual layers within the grids (grid-layers) were identified from the SMP signals and followed through the snow in each grid. The procedure is described in detail in Section 2.11, p. 63. Second, the microstructural and micromechanical properties were calculated and analyzed for each grid-layer as described in Sections 2.8.4 to 2.8.6.

2.8.4. Penetration resistance of grid-layers

Penetration resistance was measured at 4 μm intervals from the top z_{top} to the bottom z_{btm} of a grid-layer at each measurement location in the slope-parallel x - y plane, $R_{x,y,z_{\text{top}}:z_{\text{btm}}}$. To simplify the three-dimensional problem to a two-dimensional case, the spatial variability of the mean penetration resistance within a layer was analyzed. The penetration resistance data $R_{x,y,z_{\text{top}}:z_{\text{btm}}}$ were transformed to normality with a lognormal transformation. Negative force readings occasionally occurred due to a bending moment on the sensor. Negative measurements, which were found in around 10% of all analyzed layers, were replaced by positive values from a median filtered signal. Pielmeier and Schneebeli (2003) also investigate penetration resistance, and their data show that penetration resistance data follow a lognormal distribution. They did not look at the distribution within separate grid-layers. It is reasonable to assume that the distribution within each grid-layer follows the same distribution as multiple grid-layers. Further investigation is required to describe the distribution of penetration resistance within grid-layers, but it was outside the scope of this study. For each x - y location within a grid-layer, the mean of the transformed penetration resistance $\bar{R}'_{x,y,z_{\text{top}}:z_{\text{btm}}}$ was calculated and transformed back to the non-normally distributed data-space to $\bar{R}_{x,y,z_{\text{top}}:z_{\text{btm}}}$ or simply \bar{R} . From $R_{x,y,z_{\text{top}}:z_{\text{btm}}}$ also the median \tilde{R} was calculated for each x - y position and grid-layer. The spatial variation of \bar{R} was investigated (Section 2.12.3, p. 69). The mean penetration \bar{R} was compared to the stability test results to investigate any relation between point stability in a grid-layer and the penetration resistance signal from that layer (Section 4.4, p. 120).

2.8.5. Microstructural properties of grid-layers

Using a mechanical model based on a theory for indentation of foams (described in detail in Section 2.8.6 below), the average microstructural element length L_n was calculated from the SMP signal. Depending on the snow type a microstructural element can be a single snow grain (e.g. large depth hoar crystals) or a number of grains bound together in a three-dimensional matrix by bonds (e.g. snow which has been through mild melt-freeze cycles). The calculation of L_n from the SMP penetration resistance relies on having a high-resolution penetration resistance signal so that the failure of each microstructural element can be seen. In the SMP signal shown in Figure 2.13, failures of individual microstructural elements are marked with arrows.

By assuming that the microstructural elements are isotropic, Johnson and Schneebeli (1999) suggest that L_n can be related to the number of element failures n_{fail} over a traveled distance of Δz , and the area of the SMP measuring tip A_s by

$$L_n = \left(\frac{\Delta z}{n_{fail}} A_s \right)^{1/3}. \quad (\text{Eq. 2.2})$$

The IDL (Interactive Data Language) procedure `calc_phys` was written to locate all failures of microstructural elements within the defined layers and return the average microstructural element length for each layer (Section 2.8.7). The travel distance Δz in equation 2.2 above was therefore equal to the distance between z_{top} and z_{btm} . The algorithm was based on the algorithm outlined by Schneebeli (2001). For a description of the procedure, see Section 2.8.7.

Johnson and Schneebeli (1999) further suggested that the grain size L_s can be calculated from L_n by

$$L_s = L_n \frac{\rho_0}{\rho_s}, \quad (\text{Eq. 2.3})$$

where ρ_0 is the snow density and ρ_s is the density of ice. The density of the layers might change within the grid, so ρ_0 was calculated from the SMP signal to calculate a location-specific L_s . Pielmeier (2003, p. 95) found that the median SMP penetration resistance was related to snow density by $\tilde{R} = 0.0033 e^{(0.018 \times \rho_0)}$ ($P < 0.001$), or

$$\rho_0 = 55.6 \ln(\tilde{R}) + 317.4, \quad (\text{Eq. 2.4})$$

where ρ_0 is in kg m^{-3} and \tilde{R} is N. Density and penetration resistance measurements were averaged over 25 cm. The regression was found for

snow with densities between 150 and 520 kg m⁻³. For the lower snow densities, there is a large scatter in the data, possibly due to different microstructures. No attempt was made to correct for changes in snow microstructure in the measurements.

The IDL procedure `calc_phys` calculated ρ_0 and L_s for each defined layer (Section 2.8.7). The values calculated from the SMP signal were compared to the values measured in the snow profile pit. No spatial analysis was done.

2.8.6. Micro-mechanical properties of grid-layers

Micro-mechanical properties of the snow (compressive strength and elastic modulus) were interpreted using the statistical mechanical model for indentation of snow proposed by Johnson and Schneebeli (1999).

Model overview

The model is based on the indentation of elastic foam (Ashby and others, 1986; Gibson and Ashby, 1997). It assumes that the total force on the SMP tip is the sum of the resistance force of each microstructural element in contact with the tip, and that failures of all individual elements in contact with the SMP tip can be identified in the SMP penetration resistance profile. By making a number of simplifying assumptions about the number and size of the elements and their distribution along the face of the tip, the micromechanical properties of the snow can be calculated. For a complete discussion of the model, see Johnson and Schneebeli (1999) and Johnson (2003b).

Model assumptions

Five assumptions are made in the model:

- 1) Compaction of fractured microstructural elements in front of the tip is not contributing to the penetration force of the tip. The microstructural elements fracture and fall into the interstitial pore space if the snow is porous enough. At a certain snow density, the fractured microstructural elements will not be able to move out of the way of the tip and will lock up, causing compaction in front of the tip. At the low densities found in the natural snow cover in this study, it is reasonable to assume that no compaction occurred.
- 2) As the tip penetrates the snow, each microstructural element that contacts the tip will be elastically deflected and finally fail with the rupture force f_r . Assuming a linear increase in reaction force from a microstructural element from the first contact with the tip to the time of failure of the element, the mean force contribution by each

microstructural element will be half that of the force at rupture. This assumption is too simple to describe the reaction of the three-dimensional structure with which the tip interacts. Until more investigations are made on this topic, no better description exists.

- 3) All elements are isotropic. While little is known about the shape of the elements interacting with the SMP tip, some grain shapes, e.g. surface hoar and chains of depth hoar likely form elements that are not isotropic. More research is needed to investigate the validity of this assumption.
- 4) All elements contacting the tip will rupture. The deformation rate achieved with the SMP tip is $10^1 - 10^2 \text{ s}^{-1}$, which is at least a factor of 10^4 higher than the deformation rate of 10^{-3} s^{-1} where snow is considered to deform in brittle mode. The assumption is therefore reasonable.
- 5) All element failures can be identified in the SMP signal. This assumption is discussed further in Section 2.8.7 below. Whether the assumption holds or not, depends on whether the interpretation of the SMP signal is correct.

Model equations

Based on Johnson and Schneebeli (1999) and Johnson (2003a) the compressive strength of the snow Σ can be calculated as

$$\Sigma = \frac{2\bar{R}}{A_s (\sin \theta + \mu \cos \theta)}, \quad (\text{Eq. 2.5})$$

where θ is half the included angle of the SMP tip (30°) and μ is the frictional coefficient between the SMP tip and the snow grains. The friction coefficient for the steel tip was set to 0.25 following Mellor (1975, p. 284). The elastic modulus for each snow layer E is calculated by

$$E = \frac{\bar{f}_r}{\bar{L}_n^2 (\sin \theta + \mu \cos \theta)}, \quad (\text{Eq. 2.6})$$

where \bar{f}_r is the average rupture force for the microstructural element within the layer, corresponding to the drop in force associated with each element failure (Figure 2.13). \bar{L}_n is the average microstructural element length in the layer, calculated from equation 2.2.

2.8.7. Algorithms for SMP signal analysis

To apply the model to the SMP penetration resistance signal, failures of individual microstructural elements were identified in the SMP signal with

the IDL procedure `calc_phys`. The algorithm was based on the algorithm described by Schneebeli (2001). The procedure also calculated the microstructural properties of the snow within the layers as described in Section 2.8.5 above.

Within each defined layer, the first derivative of the SMP penetration resistance dR/dz was calculated over the depth Δz . A failure of a microstructural element was identified as a resistance recording where $dR/dz < t_{fail}$, where t_{fail} was a negative threshold value described in Section 2.8.8 below. The average distance between failures within the layer L_n was calculated (equation 2.2), together with the average drop in penetration resistance f_r caused by failure of an element (Figure 2.13). From these two values and the mean penetration resistance within a layer, Σ and E were calculated from equations 2.5 and 2.6, respectively.

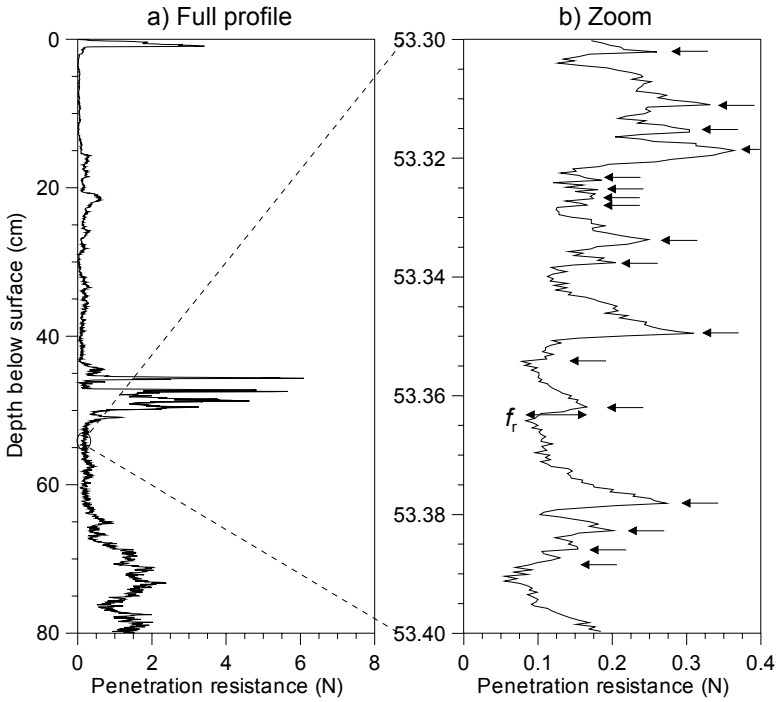


Figure 2.13. An SMP signal where failures of individual microstructural elements can be identified by a sudden drop in penetration resistance. a) The full SMP profile, and b) a zoom of the signal where arrows mark the failures. At one failure, the rupture force is indicated by f_r .

The calculations were done by the IDL procedure `layer_analysis` for one grid-layer at a time. For all SMP profiles in a grid, where the grid-layer was defined, the investigated properties of the layer (Table 2.7, p. 67) were calculated and written to an ASCII file. Together with the data, the spatial coordinates (x, y) of each measurement were also written to the file, which could then be used for further analysis (Section 2.12, p. 66).

2.8.8. Precision of the signal analysis

Calculation of the compressive strength Σ (equation 2.5) did not depend on microstructural information from the SMP signal, but was directly proportional to the mean penetration resistance within a grid-layer. The mean penetration resistance was influenced by temperature-gradient induced drift in the force signal that was expected to cause an absolute drift of less than ± 0.05 N, typically around ± 0.02 N. The denominator in equation 2.5 is 3.17×10^{-5} , so the absolute uncertainty in Σ is ± 1.3 kPa. The relative uncertainty depends on the penetration resistance of the actual layer.

The precision in the calculation of the elastic modulus E (equation 2.6) depended on the precision with which microstructural and micro-mechanical information could be extracted from the SMP signal. Two types of simulations were done to test how well the applied IDL routines recovered structural properties of a SMP signal for use in calculation of E . 1) A Monte-Carlo simulation was made to study how well the IDL procedure identified the failures in a simulated signal. 2) A sensitivity analysis of the cut-off value t_{fail} was made.

Monte-Carlo simulation of failure picking routine performance

One assumption in the model used to calculate the structural and mechanical properties of the grid-layers is that all failures are identified in the SMP signal. The performance of the IDL routine for picking failures in a signal was tested by simulating an SMP signal with \bar{f}_r and \bar{L}_n as input values. First the signal analysis routine `calc_phys` was tested on a signal with constant spacing between the grain contacts ($\bar{L}_n = L_n$) and constant rupture force ($\bar{f}_r = f_r$), shown in Figure 2.14a. The properties of the signal (\bar{f}_r and \bar{L}_n) were recovered 100%. Second, the simulated spacing between the grain contacts was randomized using a uniform distribution. Consequently, random values of L_n and of f_r (Figure 2.14b) to d) were obtained. The IDL routine was run on 1000 SMP realizations, and the mean and the coefficient of variation of the 1000 resulting values

of \bar{f}_r and \bar{L}_n calculated. The `calc_phys` algorithm underestimated \bar{f}_r by 0.001%, while the CV of \bar{f}_r was 0.6%. \bar{L}_n was overestimated with 0.006% and the calculated \bar{L}_n had a CV of 0.4%.

Sensitivity of the calculated elastic modulus to t_{fail}

The threshold value t_{fail} was used to locate failures of microstructural elements in the SMP signal. Element failures were identified where $dR/dz < t_{fail}$. The value of t_{fail} influenced the values of L_n and therefore E . When t_{fail} was set to -2.0 N mm^{-1} , the failures that were identified by the routine were those that were also manually identified from the signal. By decreasing t_{fail} , the number of failures that were identified in the signal also decreased, giving higher values of L_n and normally of f_r . The sensitivity of E to changes in t_{fail} was layer specific (Figure 2.15). The effect of t_{fail} on the elastic modulus was not investigated further. To accurately determine E from SMP signals, t_{fail} requires more attention.

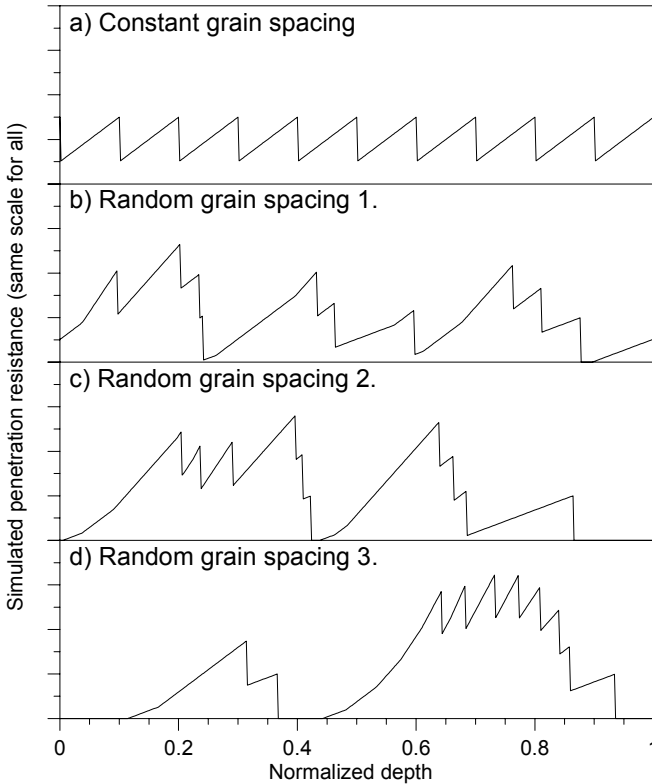


Figure 2.14. Simulations of an SMP signal with 10 failures with constant rupture force. a) Constant spacing between the grain contacts. b), c), and d) show different realizations of a signal with random spacing between grains.

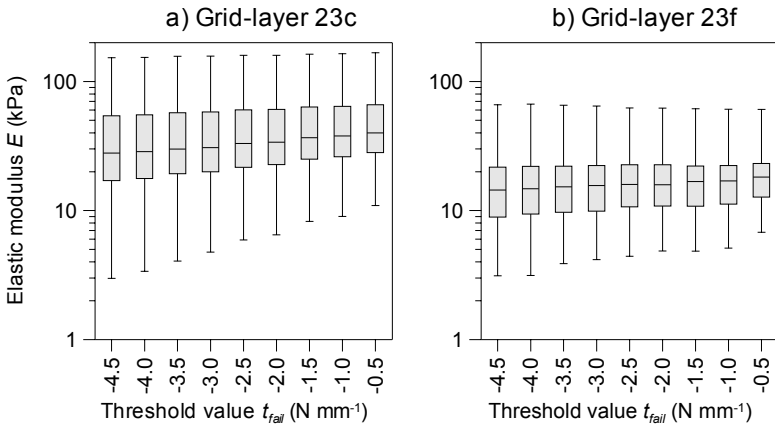


Figure 2.15. The effect of changing the threshold t_{fail} in the IDL signal analysis routine. Each box for a given threshold represents the values from all 113 SMP profiles in a given grid-layer. The effect of changing the threshold value was layer specific. Whiskers extent to the extreme values while the boxes indicate the quartiles. The median is indicated with a line through the boxes.

For all calculations in this study, t_{fail} was initially set to -2.0 N mm^{-1} . In all grid-layers in grid 21, this threshold level did not identify any failures. This could be due to the SMP tip not moving freely through the tip of the rod (also described in Section 2.8.2, p. 46). For all grid-layers in grid 21, t_{fail} was set to -1.0 N mm^{-1} .

2.9. The rutschblock stability test

In the rutschblock (RB) test, an isolated snow column was loaded in successive steps by a skier until fracture. The loading-step at fracture indicates the snow stability. The test was described by Föhn (1987a). In this study, the test was performed following the procedure described by Schweizer (2002). A block measuring 2 m across the slope and 1.5 m up the slope (Figure 2.16) is isolated by digging trenches at the sides and cutting the back with a thin rope. The surface-parallel area is 3 m^2 . The front face was the snow-pit wall. The block is isolated to a depth larger than the deepest suspected weak layer, and often all the way to the ground. The minimum slope angle recommended for the test is 30° (Föhn, 1987a). With certain precautions, it might be useable for locating weak layers on slopes with inclinations down to 20° (Jamieson and Johnston, 1993).



Figure 2.16. The rutschblock during loading in step 4; jump from above the block with skis.

After isolation, the block is loaded in successive steps (Table 2.1). Each fracture was associated with a RB score, corresponding to the loading step required to produce the fracture (Table 2.1). If the test is done after completing a stratigraphic profile, as recommended by Föhn (1987a), the test takes 10 to 20 minutes (see also Jamieson and Johnston, 1993).

Table 2.1. Loading steps and associated rutschblock scores for the rutschblock test (after Schweizer, 2002).

RB score	Loading step
1	The block slides during isolation of the block by digging or cutting.
2	The skier approaches the block from above and gently steps down onto the upper third of the block.
3	Without lifting the heels and skis, the skier drops three times from a straight leg to a bent-knee position, pushing downwards and compacting surface layers.
4	The skier jumps with skis from above the block onto the compacted spot on the block.
5	The skier jumps another two times with skis from above the block landing on the compacted spot.
6	With skis removed, the skier jumps three times from above on the compacted spot or near the corners.
7	None of the previous six loading steps produced a fracture.

Table 2.2. For each rutschblock test, the portion of the isolated block that fractured was recorded as one of three types of release types.

Fracture type	Description
Complete	The complete block slid along the weak layer.
Partial	Only a part of the block, typically below the operators' skies, slid along the weak layer or weak interface.
Corner	Only a corner or an edge of the block broke off.

For each fracture, the portion of the block that slid was noted as one of three release types (Table 2.2). For each fracture, the fracture-plane was characterized as one of three possible types (Table 2.3). Finally, each fracture was associated with a layer or interface recorded in the stratigraphic profile.

Table 2.3. Types of fracture-planes recorded for the rutschblock tests.

Fracture plane type	Description
Planar	A completely planar (even; smooth) fracture surface along the fracture plane.
Rough	Small roughness elements are present along the fracture plane, but the fracture plane is well defined.
Irregular	The fracture plane is not well defined but has a very irregular appearance. This often happens by the collapse of thick layers.

2.9.1. Interpretation of the rutschblock test results

In this study, the purpose of the RB test was two-fold: 1) to locate weak layers or weak interfaces critical to rapid near surface loading, 2) to associate each of these weak layers with a stability-level, consisting of the RB score, the release type and the fracture-plane type.

The RB test produces fractures in the weakest layers or interfaces in the snowpack (Föhn, 1987a). Because the load is a skier producing a rapid, near surface impact, the test is most appropriate for interpretation of artificially triggered slab avalanches and not natural avalanches. In general, rutschblock scores 1, 2 and 3 indicate unstable conditions, scores 4 and 5 are associated with intermediate conditions, and scores 6 and 7 indicate that conditions are relatively stable. It is recommended that the RB test results should always be combined with a snow profile and other observations of snow stability (Föhn, 1987a; Jamieson and Johnston, 1993). When combined with a stratigraphic profile and a ramsonde hardness profile, a more formal description of snow stability can be given according to a five-level stability-rating scheme (Schweizer and Wiesinger, 2001).

For fracture propagation to proceed from an initial failure area, a critical failure area must be reached. For fast fracture propagation, the critical length is thought to be 1 to 10 m (Schweizer, 1999). With an area of 3 m², the RB test might therefore give indications about the fracture propagation properties of a snow cover unlike the smaller column-type stability tests described in Section 2.10 below.

2.9.2. Rutschblock test limitations

Jamieson and Johnston (1993) and Schweizer (2002) discuss the precision and limitations of the rutschblock test. Correct interpretation of the RB test results requires that:

- one person must watch the block from below to observe all fractures in the isolated column
- the person jumping must be of average size; 60 to 80 kg
- the operators' skis do not penetrate deeper than 10 cm from the top of the critical weak layer

In this study, all rutschblock tests fulfilled these requirements. For practical purposes, e.g. winter recreation, some limiting factors of the RB test should be considered. Although the tested area is larger than the point stability tests described below, it only tests the stability of a limited area of a slope. RB test results might vary on a slope, but by locating tests in representative locations, RB scores can be expected to be within ± 1 RB score of the slope median score (Jamieson and Johnston, 1993). Stability evaluation should not be based on a single RB test. Slope inclination is expected to influence the RB score by increasing the score 1 step for each 10° decrease in slope inclination. However, this effect is often masked by effects of spatial variability (Jamieson and Johnston, 1993). In some cases, the negligence of the peripheral strength of the slab might underestimate stability.

2.10. Column-type stability tests

Two types of stability tests used in the study were different from the rutschblock test (Section 2.9 above) in two aspects: 1) they tested a smaller area, and 2) the load was not a skier. The first means that the fracture propagation properties of the snow cover could not be deduced from the tests, as might be possible in the case of the RB test. The second means that the impact needed to produce a fracture cannot be intuitively related to skier triggering. These types of stability tests are called column-type stability tests.

During the first two winter seasons, the stuffblock (SB) test as described by Birkeland and Johnson (1999) was used to measure point stability. During the second and third winter seasons, a modified version of the rammrutsch test (RR) used by M. Schneebeli and described in Schweizer and others (1995) was used. Both test types took around 10 minutes to complete. The RR test was preferred over the SB test because the impact energy was directed more precisely onto the column and less energy was lost at the impact of the drop weight with the plate (Section 2.10.5). The RR setup was finished late in the second winter season, preventing us from using it two full seasons.

The two column-type stability tests applied a load to an isolated column of the snow cover to produce a fracture along a weak interface or in a weak layer in the isolated column. The impact load required to produce a fracture is an index for snow stability at the test location. For both tests, a 30 cm by 30 cm snow column was isolated from the surrounding snow cover. The dimensions were measured parallel to the snow surface. The column was isolated by cutting all four sides with a snow saw and progressively loaded until fracture occurred. The slope inclination was measured in each pit with column-type stability tests.

After a fracture, the snow above the fractured weak layer was removed and the top of the snow column was cut horizontal. Impacts were continued from a drop height level above the height where the previous fracture occurred. Multiple fractures occurred in most of the tests.

2.10.1. The stuffblock test

In the stuffblock test (Birkeland and Johnson, 1999), a stuff-sack filled with 4.5 kg snow provided the drop weight. The drop height was measured with a string with markings every 10 cm that was sewn onto the bottom of the stuff-sack. Before the first impact, the top of the snow column was leveled with a shovel. The shovel was then placed on top of the column and the stuff-sack dropped from increasing heights in 10 cm intervals onto the column until a fracture occurred in a weak layer or along a weak interface. If a weak layer fractured as the shovel and filled stuff-sack were placed on top of the column, a drop height of 0.5 cm was recorded. If a weak layer fractured during isolation of the column, a drop height of 0 cm was recorded.

2.10.2. The rammrutsch test

The modified rammrutsch setup (Figure 2.17) was similar to a device used by M. Schneebeli (Schweizer and others, 1995) and is almost

identical to the drop hammer test used by Stewart (2002). It consisted of a 1.5 cm x 30 cm x 30 cm foam plate with a 1 mm thick aluminum plate glued to the upper and lower sides. For the preliminary tests, the top of the isolated snow column was not leveled before the first impact. To prevent the plate from slipping on the inclined snow surface, four L-shaped fins were fixed to the bottom aluminum plate around the edge of the plate and three across the plate. The preliminary tests showed better results if the top of the column was leveled, in particular for soft surface layers, so this was done in all subsequent tests, and for all snow types. On top of the plate, a 1 m rod similar to the one used for the ramsonde was mounted.

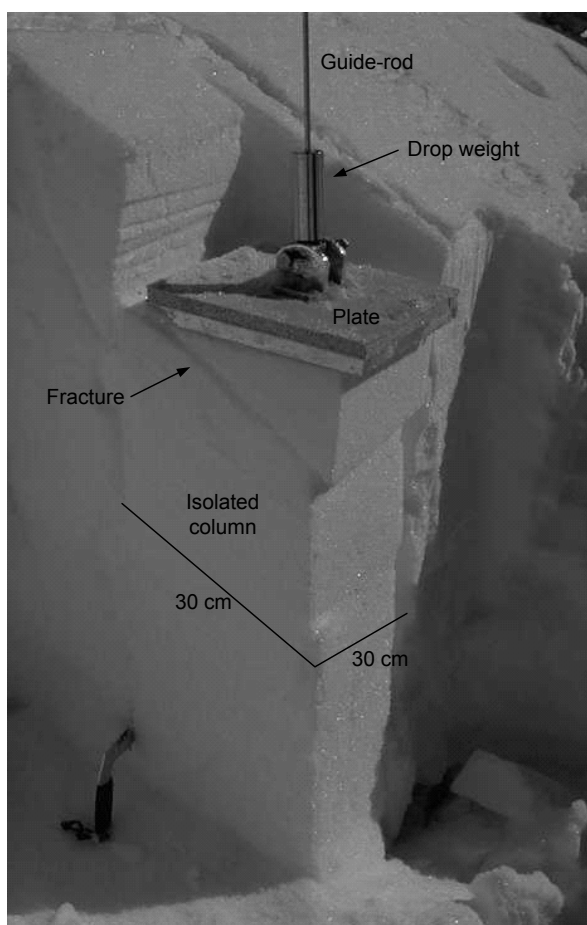


Figure 2.17. The setup for the rammrutsch test.

The dynamic impacts were made with the same 1 kg drop weight that was used for the ramsonde. The drop heights were progressively increased in 5 cm intervals until a fracture occurred. If a weak layer was identified near the snow surface, the first drop height was 1 cm. If a weak layer fractured as the plate was placed on top of the column, a drop height of 0.5 cm was recorded. If a weak layer fractured during isolation of the column, a drop height of 0 cm was recorded.

2.10.3. Values recorded for each fracture

For each fracture produced by the column-type stability tests, a number of values were recorded to describe the depth of the weak layer and the impact energy associated with each fracture (Table 2.4). To identify the same weak layers in the snow cover within a grid, the layer or interface in which the fracture occurred was identified by the height (above the ground) of the weak layer in the manual profile. Finally, the fracture character for each fracture was recorded (Table 2.5).

Table 2.4. Values recorded for each fracture in the stuffblock and rammrutsch point stability tests.

Description	Symbol	Unit
The drop height at which the fracture occurred	<i>DH</i>	cm
The depth of the weak layer in the snowpack	<i>FD</i>	cm
The amount of compaction that occurred below the shovel at the impact that led to fracture	<i>CO</i>	cm
The amount of damping snow between the shovel and the weak layer	<i>DA</i>	cm
The stratigraphic layer or interface in which the fracture occurred	-	-

Table 2.5. Types of fracture character classified in the stuffblock and rammrutsch tests.

Type	Description
C	Well defined clean (smooth; planar) fracture plane
P	A clean fracture only partially covers the weak layer in the column
COL	Collapse of a thicker layer; typically happened in depth hoar
SIR	Small irregularities along the fracture plane, < 1 cm
LIR	Large irregularities along the fracture plane, < 1 cm
STP	The fracture plane stepped between two weak layers

2.10.4. Interpretation of point stability test results

The drop height recorded for each fracture was interpreted as the point stability for the layer or interface that fractured. For the RB test, there is a well-defined stability scale for each RB score (Table 2.1, p. 56). Birkeland and Johnson (1999) related the drop height recorded from the SB test to the RB score in side-by-side tests. They found that for increasing RB scores, the associated SB test drop heights also increased (Table 2.6). The RR test had not been intensively used before this study. To interpret the drop heights in terms of RB stability score and other stability tests, a comparison was made for grid-layers that produced fractures in both the RR test and in the RB test (Section 4.2.1, p. 86).

Table 2.6. Stuffblock drop height and associated rutschblock scores (after Birkeland and Johnson, 1999). N is the number of tests used for comparison. Q_1 and Q_3 are the first and third quartile, respectively.

RB score	Stuffblock drop height DH			
	Q_1 (cm)	Median (cm)	Q_3 (cm)	N
1	-	-	-	0
2	0	10	10	13
3	10	10	20	27
4	20	30	40	44
5	30	40	50	28
6	30	40	60	20
7	60	80	80	16

Conway and Abrahamson (1984) observed that while isolating snow columns for stability measurements, a fracture was sometimes produced in the weak layer before the column was loaded. Areas where the weak layer shear strength was smaller than the shear stress due to gravity were called “deficit areas”. One such observation was made in this study, and recorded as $DH = 0$ cm.

2.10.5. Measurement errors and limitations

One person supervised or carried out all tests within a grid to ensure that they were done the same way. Five causes of inaccuracies were identified in the tests. 1) The same amount of snow should be shoveled off a column after each fracture. If this was not done, the amount of damping snow between the top of the column and the fracture plane was different, causing different amounts of energy dissipation in the column. 2) The stuff-sack sometimes landed on the side of the column instead of

the middle. This happened primarily when the sack was dropped from large heights. The problem was avoided in the RR test. 3) The snow in the stuff-sack was observed to harden considerably during testing. Hardening of the snow increased the impact energy transferred to the isolated column and could thereby change the drop heights. 4) In snow columns where there was a very weak layer deep in the snow cover, the tests might not have produced fractures in any weak layers above. If in other parts of the grid the deep weak layer was stronger, the upper weak layers might have fractured. To avoid this problem, one particular weak layer could have been targeted (Landry and others, 2001; Landry and others, 2003), in which case only information about fractures in one particular weak layer were recorded. Because the goal was to describe the stability of as many layers as possible, this practice was not followed. 5) Below the plate in the RR test, loose snow was observed to accumulate between the fins. This might have dampened the impact from the drop weight.

The RR test had less potential errors and was therefore preferred over the SB test. The absolute error of the drop height was estimated to be better than ± 10 cm in general, but less for shallower weak layers that fractured with fewer impacts than deeper layers (see the cause number 5 above). No measurements of the accuracy of the tests were done.

2.11. Reconstruction of snow stratigraphy

The stratigraphy of layers within the grids (grid-layers) was reconstructed from the SMP penetration resistance profiles. Grid-layers were identified by the grid number followed by a lower-case letter, e.g. 23i. The procedure has been briefly described by Schneebeli and others (1999), Pielmeier and Schneebeli (2003), Kronholm and others (in press-a) and Birkeland and others (in press). Here, the procedure is described in more detail.

2.11.1. Outline of the procedure

The layer boundaries were defined in a hierarchical order. First, the most distinct layers within a grid were defined. Together with the snow surface and the ground (if the SMP profile was deep enough), the most distinct layers provided upper and lower limits for the less distinct layers that were harder to identify in the SMP profiles. The distinct layers were mostly harder than the surrounding layers, but some softer layers, primarily of buried surface hoar, were also quite distinct.

The upper and lower boundaries of a layer were defined by visual inspection of each SMP profile. The boundaries of each grid-layer in an SMP profile were defined by progressively zooming closer (on the computer screen) to the slope-perpendicular location where the layer was expected to be. In the beginning of the zooming process, the slope-perpendicular location of a grid-layer was estimated based on the full penetration resistance profile and the manually observed stratigraphic profile. In case adjacent layers had already been defined in the SMP profile, these helped in the location procedure for less distinct layers. In some grids, the stratigraphy was difficult to trace through the grid because the SMP profiles changed by a large amount from one location to the next. For the snow cover within these grids, SMP resistance profiles from up/down-slope and cross-slope transects plotted side-by-side (Figure 2.18) helped to interpret stratigraphy. In the beginning of the zooming process, the microstructure of each grid-layer could not be recognized on the computer screen.

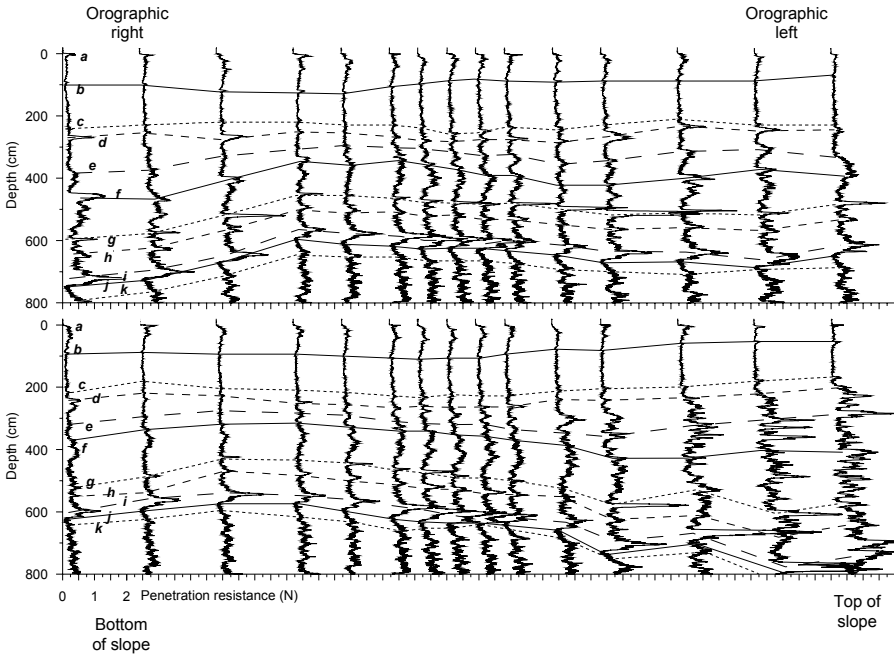


Figure 2.18. Two transects through grid 23 with the SMP profiles in each transect side-by-side. The upper panel is a transect in the cross-slope direction from orographic right to left. The lower panel is a transect from the top of the grid to the bottom of the grid. Layers a to k could be followed through the snow cover within the grid.

As the zoom-level increased, the resolution of the penetration resistance in the grid-layer improved so that the microstructure of the layer could be recognized (Figure 2.19). At this point, the planar sections (if available for the given grid-layer) from the in-situ diethyl-phthalate samples were compared to the microstructure seen in the SMP signal and the exact location of the layer boundaries defined (Figure 2.19).

As pointed out by Pielmeier and Schneebeli (2003), the layer boundaries seen in the SMP signal are often not as distinct as the boundaries recorded in a stratigraphic profile. Some boundaries were therefore hard to identify precisely because the length of transition in penetration resistance between adjacent layers was wide. Other boundaries were easy to identify because the transition length was small.

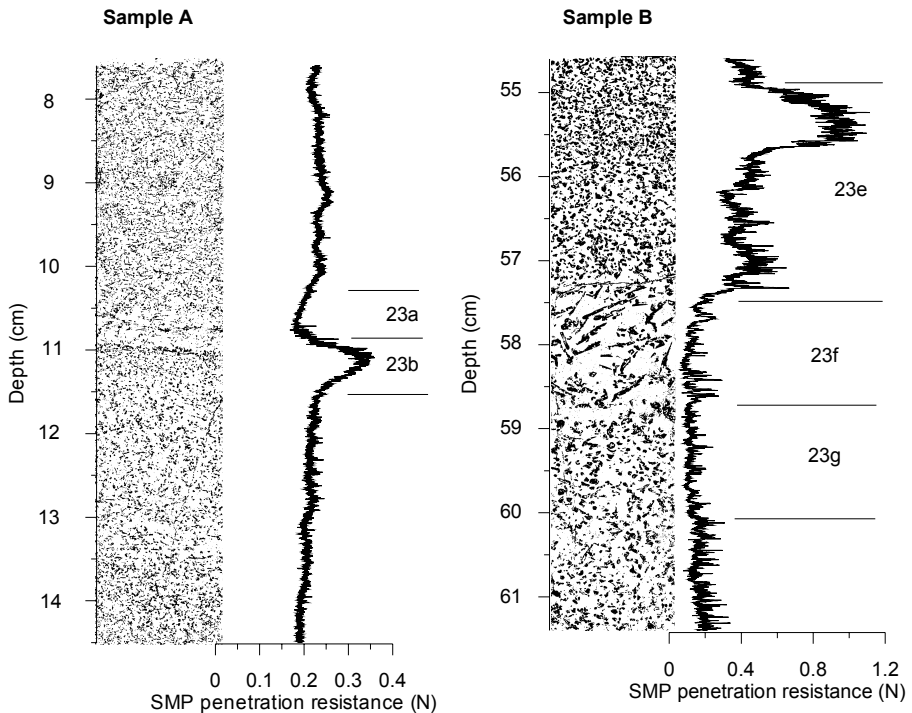


Figure 2.19. Planar sections and nearby SMP profile from grid 23. The five grid-layers can be identified in planar sections and in the SMP signal. The exact definition of the layer boundaries was difficult because many boundaries were gradual transitions between adjacent layers (e.g. between 23a and 23b). Some layers had high slope-perpendicular variability (e.g. 23e). Sample A: GR02-A, Sample B: GR02-B.

2.11.2. The IDL procedure for layer identification

Definition of layer boundaries was done interactively with the IDL procedure `define_layer`. This procedure allowed the user interactively to zoom in and out on a section of an SMP profile. When the user had found the boundaries of the desired layer, these boundaries were identified with the cursor. The procedure then stored the boundary depths together with the name of the layer in a separate ASCII file that could later be associated with the SMP file. During the zooming process, all boundaries that had already been defined for the SMP record were shown on the screen to ease the identification procedure.

2.11.3. Precision of boundary location

Most layer boundaries were observed to be gradual transitions between adjacent layers rather than sharp transitions (Figure 2.19). This was also noted by Pielmeier (2003) and Pielmeier and Schneebeli (2003). Transitions were observed to be up to a few millimeters thick. The boundaries were defined in the middle of the transition between adjacent layers (e.g. between 23a and 23b in Figure 2.19). Birkeland and others (in press) showed that the calculated grid-layer properties of a buried surface hoar layer did not change significantly if the layer thickness was increased by 5% or narrowed by 5%. It is assumed that the same is the case for other grid-layer types, but this has to be investigated further.

2.11.4. Grid-layers defined from stability tests

With the SMP profiles, all distinct layers (both hard and soft) in the snow cover within the grid could be identified. With the stability test results, weak layers or weak interfaces were defined. Grid-layers defined from the stability tests were not defined with an upper and lower boundary, but with a fracture depth below the snow surface. The data associated with these grid-layers were the drop heights required to produce a fracture and the other data recorded for each fracture (Section 2.10, Column-type stability tests).

2.12. Data analysis

2.12.1. Overview of snow cover properties investigated

For each grid, a number of snow cover properties were investigated (Table 2.7). The data were divided in two groups: one for which a spatial analysis was done to characterize the spatial structure of the variation.

For the second group, no spatial analysis was done, but their relation to the first group was investigated with univariate statistics.

2.12.2. Analysis of stability measurements

For the grid-layers defined from the point stability measurements, there was only a limited number of stability point data for analysis. The number of points depended on the number of stability tests done in each grid, and on how many fractures these tests produced in a grid-layer. In the grid-layers for which an analysis was done, the number of points ranged from 7 to 25. This placed two constraints on the type of analysis methods that could be applied. First, it could not be accurately determined whether the data were normally distributed. Stewart (2002) showed that his stability test results were not normally distributed. The data were therefore described with non-parametric statistics, which do not assume a certain distribution of the data and are resistant to outliers. Second, it has been empirically determined that results of spatial statistics might be erratic for data with less than 50 to 100 measurements (Webster and Oliver, 2001, p. 90). The spatial analysis made with the stability test results must therefore be interpreted carefully.

Table 2.7. Snow cover properties investigated. The analysis type indicates how the data were analyzed. “spatial” indicates that a full spatial analysis was done. For data of the type “relation”, univariate statistics were used to investigate their relation to the data that were spatially analyzed.

Property	Analysis type	Measurement method	Symbol	Unit
Drop height at fracture = point stability	spatial	SB, RR	DH	cm
Fracture depth of fracture = slab thickness	relation	SB, RR	FD	cm
Snow depth	relation	Probing	HS	cm
Layer thickness	relation	SMP	d	mm
Mean penetration resistance	spatial	SMP	\bar{R}	N
Median penetration resistance	relation	SMP	\tilde{R}	N
Microstructural element length	relation	SMP	L_n	mm
SMP calculated grain size	relation	SMP	L_s	mm
Compressive strength	relation	SMP	Σ	kPa
Elastic modulus	relation	SMP	E	kPa

Non-spatial variability of point stability

Robust statistical methods were used to describe the variability of point stability of each grid-layer. The central tendency was described by the median \widetilde{DH} , and the first and third quartiles, Q_1 and Q_3 (e.g. Spiegel and Stephens, 1999, p. 61, 63). The absolute spread of the data (similar to the standard deviation σ from parametric tests) was described using the semi-interquartile range SIQR defined by Spiegel and Stephens (1999, p. 90) as

$$\text{SIQR} = \frac{Q_3 - Q_1}{2}. \quad (\text{Eq. 2.7})$$

The semi-interquartile range is the range of the middle 50% of the measurements. The relative spread (similar to the parametric coefficient of variation CV) was described with the quartile coefficient of variation QCV (Spiegel and Stephens, 1999, p. 108)

$$\text{QCV} = \frac{1/2(Q_3 - Q_1)}{1/2(Q_3 + Q_1)} = \frac{Q_3 - Q_1}{Q_3 + Q_1}, \quad (\text{Eq. 2.8})$$

where $1/2(Q_3 + Q_1)$ in the denominator is a robust measure of the central tendency of the data. The counter is the semi-interquartile range. The robust absolute and relative measures of spread are not directly comparable with the standard deviation and the coefficient of variation. However, for moderately skewed data an empirical relation between SIQR and the standard deviation σ exist (Spiegel and Stephens, 1999, p. 93):

$$\text{SIQR} \approx \frac{2}{3}\sigma. \quad (\text{Eq. 2.9})$$

Under the assumption that the point stability data are only moderately skewed, the numerator in equation 2.8, is not far from the arithmetic mean. An approximation to the CV can be calculated by

$$\text{CV} \approx \frac{3}{2}\text{QCV} \quad (\text{Eq. 2.10})$$

for a comparison with CV values from other studies.

Spatial variability of point stability

The spatial variability of the point stability measurements was characterized with geostatistical methods, described in Section 2.12.4.

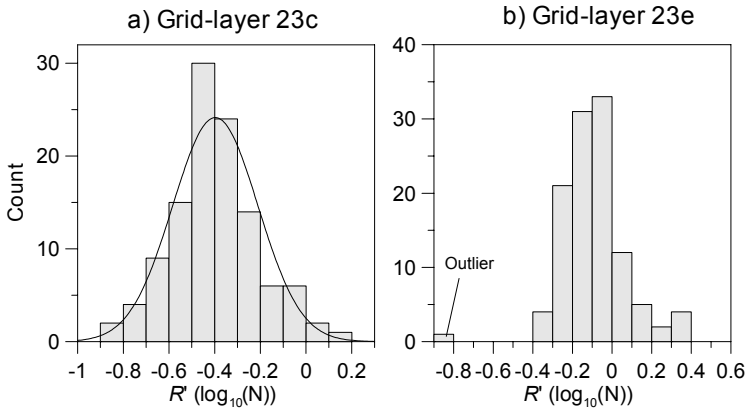


Figure 2.20. The distribution of the transformed penetration resistance data \bar{R}' , for a) grid-layer 23c with a fitted normal distribution, and b) grid-layer 23e, which included an outlier. Data from the grid-layers either were very close to a normal distribution like in a) or had a small skew as in b).

2.12.3. Analysis of penetration resistance measurements

The mean penetration resistance data \bar{R} from each of the grid-layers had more data than the stability measurements.

Transformation to normality

Before analysis, the \bar{R} values from each grid-layer were analyzed, the data were checked for normality. It was found that a \log_{10} transformation brought the distribution of most transformed data sets \bar{R}' close to normality. Data from around half of the grid-layers were visually close to normality after transformation, and passed the Kolmogorov–Smirnov goodness-of-fit test for normality with $P < 0.05$ (e.g. grid-layer 23c, Figure 2.20a). However, the remaining half had a small tail to either left or right (e.g. grid-layer 23e, Figure 2.20b) and did not pass the Kolmogorov–Smirnov test. Other transformations were also tested, but the \log_{10} transformation provided the best overall results. The skew prompted the use of robust statistics for the further analysis.

Detection and removal of outliers

An outlier was defined as a point measurement that did not follow the same distribution as the rest of the data in a grid-layer. Outliers were detected by QQ-plots (the quantiles of the data as a function of the quantiles of a normal distribution), box-plots and histograms. In the histogram in Figure 2.20b, one point in grid-layer 23e was identified as an outlier. Data points initially identified as outliers were in most cases

caused by a wrong manual definition of layer boundaries. In these cases, the boundary was re-defined, and the calculation repeated with the new boundaries. In the remaining cases, the cause was a drift in the SMP signal (Section 3.3.2, p. 77). The drift caused the outliers to have both higher and lower penetration resistance compared to the rest of the grid-layer data. Outliers caused by signal drift were excluded from further analysis.

Non-spatial variability of penetration resistance

Even after \log_{10} -transformation, not all data were normally distributed. The non-spatial absolute spread of the transformed data was therefore described using the semi-interquartile range, equation 2.7, while the relative spread was described with the quartile coefficient of variation, equation 2.8. The robust statistics also automatically handled any outliers that had been left undetected, if there were any.

Spatial variability of penetration resistance

The spatial variability of the penetration resistance measurements was characterized with geostatistical methods, described in Section 2.12.4 below.

2.12.4. Geostatistical analysis

A geostatistical analysis takes into account the location of each measurement in addition to the measurement result. The transformed data from the SMP \bar{R} and the drop heights DH were analyzed using the same methods. In this section, both variables are denoted as $Z(\mathbf{s})$, where $\mathbf{s}=(x, y)$ are the coordinates of each measurement location within the grid. The analysis was done as described by e.g. Cressie (1993).

The data were divided into a trend $t(\mathbf{s})$ and its randomly varying residuals $\varepsilon(\mathbf{s})$ such that

$$Z(\mathbf{s}) = t(\mathbf{s}) + \varepsilon(\mathbf{s}). \quad (\text{Eq. 2.11})$$

The decomposition served two purposes: 1) to describe the variation of the data at two scales; a relatively large scale (the grid-scale) and a smaller scale (the sub-grid-scale), and 2) to ensure that $\varepsilon(\mathbf{s})$ was stationary (the variables have a constant mean and variance over the grid) as required for further geostatistical analysis. This decomposition into variation at two different scales cannot be specified uniquely (i.e. there is no true or correct way to define a trend), but depends on the way the trend is defined (Cressie, 1993, p. 162).

Spatial trend

The spatial trend model must be robust to outliers and (slight) departure from normality in the data. Cressie (1993, p. 46) suggests using median polishing to describe the trend. However, this method does not provide a simple way to describe the trend surface. Webster and Oliver (2001, p. 75) suggest that a linear regression on the spatial coordinates or a quadratic or higher order polynomial can be fitted to the data to identify the trend. The spatial trend was modeled as linear, which does not mean that the trend was linear. A higher order trend surface could also have been used, but the limited number of *DH* data-points did not allow for a higher order trend analysis, because it would have left very little random variation in the residuals. In addition, the results from such a model would not have been as easy to interpret. The regression was described by

$$t(\mathbf{s}) = \alpha x + \beta y + c_t, \quad (\text{Eq. 2.12})$$

where α , β and c_t are regression coefficients. y was positive in the up-slope direction, and x was positive to the orographic left (Figure 2.2, p. 32).

To automatically deal with atypical data points, the regression was fitted with the robust MM (Modified Maximum-likelihood-type) method (Yohai and others, 1991) implemented in the S-Plus function `lmRobMM` (Marazzi, 1993, p. 201; MathSoft, 1999). In the S-Plus version used for the data analysis, there was no implementation of a robust F estimate of the regression models. This has been implemented in the newer version of the S-Plus software (Insightful Corporation, 2001, p. 41-45). This means that there was no option to describe the significance of the regression in a robust way. Instead, the R^2 value is given for the regressions to describe how much of the variance was explained by the trend models. The individual regression coefficients are given significance (P) values.

Recently, the global D-statistic has been suggested as a statistical test for presence or absence of a trend in geostatistical data (Pardo-Igúzquiza and Dowd, 2003). The D-statistic tests the null-hypothesis that the data have a constant mean over the area. Because the method was only available late in the progression of this study, it was not used.

Random variation

The residuals from the trend analysis $\varepsilon(\mathbf{s})$ were considered to vary randomly around the linear trend. The spatial structure was analyzed using the semi-variogram (e.g. Webster and Oliver, 2001). The semi-

variogram $\gamma(\mathbf{h})$ is a tool to quantify spatial variability. It estimates the average squared difference between two measurements at increasing intervals of lag distance \mathbf{h} , a vector that can be defined by a distance and a direction. An assumption for the semi-variogram is that the data are stationary, which implies two things. First, the expected value over the area must be constant (constant mean), which was attempted by removing any spatial trend present in the data. Second, the average squared difference between two measurements must depend only on the distance between the two measurements and not on the absolute position of the measurements. This was assumed the case.

A sample semivariogram $\tilde{\gamma}(\mathbf{h})$ was calculated using a robust method to remove contamination by outliers as suggested by (Cressie and Hawkins, 1980; Cressie, 1993, p. 75):

$$\tilde{\gamma}(\mathbf{h}) = \frac{\left\{ \frac{1}{|N(\mathbf{h})|} \sum_{i,j} |Z(\mathbf{s}_i) - Z(\mathbf{s}_j)|^{1/2} \right\}^4}{2 \left(0.457 + \frac{0.494}{|N(\mathbf{h})|} \right)}. \quad (\text{Eq. 2.13})$$

Each semivariogram was calculated for n classes of lag distances \mathbf{h} . Each class contained $|N(\mathbf{h})|$ point pairs at locations \mathbf{s}_i and \mathbf{s}_j . The summation in the counter is made for each class. The robust semi-variogram ensures that outliers in the data are handled automatically by giving them low weight in the calculation of the semivariance. The robust method therefore generally gives lower semivariance values than the classical (non-robust) semivariogram. An example of a semi-variogram is shown in Figure 2.21.

The sample semivariogram was modeled with a spherical semivariogram model $\bar{\gamma}(\mathbf{h})$ plus a constant c_o such that

$$\bar{\gamma}(\mathbf{h}) = \begin{cases} 0 & \mathbf{h} = 0, \\ c_o + c_s \left[\frac{3\mathbf{h}}{2a_s} - \frac{1}{2} \left(\frac{\mathbf{h}}{a_s} \right)^3 \right] & 0 < \mathbf{h} \leq a_s, \\ c_o + c_s & \mathbf{h} > a_s. \end{cases} \quad (\text{Eq. 2.14})$$

The reason for using spherical models is given in Section 2.12.5. The model semi-variogram was described by the parameters $\theta = (c_o, c_s, a_s)$ (Figure 2.21). The sill variance c_s is a measure of the variation of the data around the grid-scale trend. The lag distance where the model semivariogram reaches the sill is the range a_s . The range is the

maximum distance over which there is spatial autocorrelation. The nugget variance c_0 is caused primarily by variance over shorter distances than the minimum measurement spacing $\min|\mathbf{s}_i - \mathbf{s}_j|$ and by measurement error.

The fitting of $\bar{\gamma}(\mathbf{h})$ to $\tilde{\gamma}(\mathbf{h})$ was done by the weighted least squares method (Cressie, 1993, p. 94) implemented in the S+SpatialStats function `variogram.fit` (Kaluzny and others, 1998).

At large lag distances \mathbf{h} , the number of point pairs in each lag distance class $|N(\mathbf{h})|$ became relatively small. It has been recommended that only lag distance classes with more than 30 point pairs be used to fit the model semi-variograms (Journel and Huijbregts, 1978, p. 194). For the \bar{R}' data, this recommendation could be fulfilled (Figure 2.1, p. 31). Classes with 30 or less point pairs were not included in the fit of the model semi-variograms. For the DH data, no model semi-variograms were fitted to the sample semi-variograms. The sample semi-variograms were therefore calculated using all lag classes with at least one point pair although this might cause erratic results.

2.12.5. Comments to the geostatistical methods

The procedure followed in this study, fitting the same type of semivariogram model to a number of data sets, is different from the procedure followed in normal geostatistical problems. In most studies using geostatistical methods, a number of model types are tested on a single or a few data sets. The best model is selected and used for prediction of values (kriging) at locations where no measurements were made.

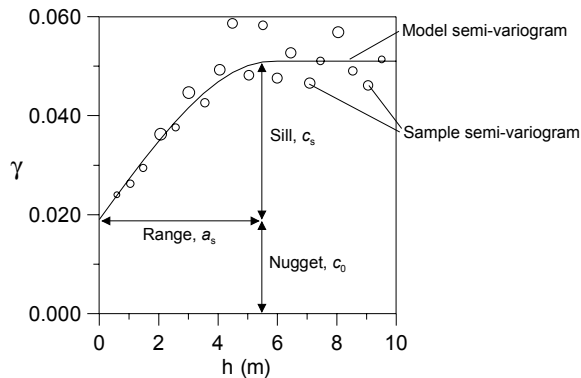


Figure 2.21. An example of sample semi-variogram (circles) and model semi-variogram (line) with the descriptive parameters c_0 , c_s and a_s indicated (see text for a description of each parameter). γ is the semi-variance.

My aim was different: I wanted to describe and compare the spatial structure of many layers in the snow cover. This was done with the model semivariograms. To ensure that the parameters of the model semivariograms were directly comparable, I chose to use only one type of semivariogram model for the analyses. This seems a reasonable choice because the results of kriging are much the same for any reasonable choice of semivariogram model (Webster and Oliver, 2001, p. 127).

In a preliminary analysis, spherical, exponential, rational quadratic, and power models (e.g. Cressie, 1993, p. 61) were fitted to sample semivariograms calculated for the penetration resistance of eight grid-layers. The parameters a_s , c_o and c_s from the fitted models to each layer varied slightly. For most grid-layers, the spherical model provided the best visual fit. Choosing one or more semivariogram models by the visual fit and then fitting them with statistical methods to the data has been recommended by e.g. Cressie (1993, p. 94) and Webster and Oliver (2001, p. 128).

Chapter 3

Data

3.1. Introduction

This chapter presents the metadata before the results are presented in the next chapter. One challenge in this study was the variety of data types that were to be kept track of and related. Section 3.2 describes which measurements were done in each of the grids, and the snow surface topography of the places where the grids were located. Within each grid, column-type stability tests and penetrometer measurements served as the core data to describe the spatial variability of the snow. Because of technical problems with the equipment, only a part of the core data were selected for analysis as described in Section 3.3. The typical snow cover stratigraphy, which each winter included a number of persistent weak layers, is described in Section 3.4.

3.2. The collected data

During the three winter seasons, 24 grids were measured (Table 3.1). During the winter season 2000 – 2001, 13 grids were measured, 8 during the 2001 – 2002 season, and 3 during the 2002 – 2003 winter season.

3.2.1. *Slope inclination and aspect*

Four of the 24 grids, all from the first winter, were made on flat ground. Of the twenty grids measured on slopes, three had a southern component to the aspect, and 11 were slopes in the north sector (NW-N-NE). Slope inclinations were around 30°, generally steeper towards the top of the slope and gentler towards the bottom.

Table 3.1. Snow surface inclination and aspect, and the type and number of measurements in the grids carried out over the three winter seasons.

Grid	Date dd-mm-yyyy	Asp.	Inclin. ψ (°)	SMP	SB	RR	Cast	RB score	Data used
1	18-01-2001	ENE	20-29	93	14	-	-	6	-
2	19-01-2001	(flat)	0	113	12	-	-	-	-
3	29-01-2001	(flat)	0	113	12	-	-	-	-
4	31-01-2001	E	29-34	113	12	-	-	4/6-7	-
5	02-02-2001	NW	30-36	113	12	-	-	5	-
6	12-02-2001	N	25-34	113	12	-	-	5	-
7	13-02-2001	(flat)	0	113	12	-	-	-	-
8	16-02-2001	E	33-39	113	12	-	-	4	-
9	19-02-2001	NNW	28-36	113	13	-	-	4/6-7	-
10	21-02-2001	SSW	30-35	113	12	-	-	6	-
11	16-03-2001	N	20-44	117	14	-	-	4	-
12	19-03-2001	(flat)	0	137	13	-	-	-	-
13	28-03-2001	NE	26-41	137	15	-	-	5	-
14	09-01-2002	ESE	28-41	47	26	-	3	3/5	Y
15	15-01-2002	NNE	24-32	113	24	-	2	5	Y
16	29-01-2002	ENE	23-30	113	17	-	3	3	Y
17	18-02-2002	NNW	25-32	104	-	24	-	4	Y
18	01-03-2002	NNW	25-34	113	-	24	-	2/5	Y
19	05-03-2002	N	23-28	113	-	24	3	4	Y
20	08-03-2002	N	22-37	113	-	24	-	3	Y
21	13-03-2002	WNW	29-35	113	-	24	2	5	Y
22	13-01-2003	NNW	28-38	113	-	24	2	6-7	Y
23	17-01-2003	NE	30-43	113	-	25	3	4/5/6-7	Y
24	19-02-2003	SW	33-36	113	-	24	-	6-7	Y

Notes: The range of inclinations given is the minimum and maximum inclinations measured at the locations of the point stability tests. Abbreviations are SMP: number of snow micro-penetrometer measurements, SB: number of stuffblock tests, RR: number of rammrutsch test, Cast: number of snow samples cast in diethyl-phthalate, RB score: score of the rutschblock test. Grids 11, 12 and 13 were of a different grid type spanning 36 m (Section 2.2.5, p. 29).

3.3. Data selection

Data from grids 14 to 24 were analyzed. Data from grids 1 to 13 were not analyzed because

- Only 12 to 15 point stability tests were done within each of these grids (Table 3.1). Most of the layers that could be defined from the point stability tests do not provide enough fractures for a statistical analysis.
- The SMP used for the 13 grids had an older force sensor that had various problems as described in Section 2.8, p. 44.

- The measurement locations within the first two grids were not precise. Determining the location of each measurement required considerable practice that was acquired only after the first two grids.
- The eleven grids provided enough data for the analysis.

All selected data sets (penetration resistance and stability) were checked for a temporal trend in the results. Such a temporal trend could have been caused by diurnal changes of mechanical properties of the upper part of the snow cover. No temporal trends were found.

3.3.1. Stability tests

In the eleven grids analyzed, 262 stability tests were done, resulting in 420 fractures (Table 3.2). Each fracture was assigned to a weak layer or a weak interface in the snow cover within a grid. A weak layer or a weak interface identified from the stability tests within a grid is called a “grid-layer” and identified by the grid number followed by an upper case letter, e.g. 23A. From the point stability tests, 66 grid-layers were identified in the eleven grids. To avoid erratic results from the statistical analyses, only data from grid-layers with more than five fractures were analyzed. This restriction left twenty-one grid-layers for analyses (Table 3.2).

3.3.2. Penetration resistance measurements

In four of the eleven grids analyzed, the SMP had mechanical problems that prevented data analysis of the penetration resistance signal (Table 3.3). In all measurements in these grids, the tip was frozen to the inside of the SMP head. This normally occurred on warm days or on days where the measurements were done in the sun. When the tip of the SMP was outside the snow cover, melt water would run down the rod towards the tip and into the space between the tip and the inside of the SMP head. In the snow, the water froze because the snow cover was still cold. Profiles recorded on these days were not useable for analysis because they contained both a smoothing of the signal at the grain-scale and drift at the layer-scale (Figure 3.1). In grid 14, less than half of the planned SMP measurements were done because the batteries were not fully charged.

Table 3.2. Number of point stability tests N_{test} and number of fractures n_{fract} in the 11 grids and the 21 grid-layers identified from the point stability tests and with more than five fractures within a grid.

Grid and grid-layer	n_{fract}	N_{test}
Grid 14	36	26
14A	16	-
Grid 15	30	24
15A	18	-
Grid 16	38	17
16A	14	-
16B	9	-
16C	7	-
Grid 17	32	24
17A	22	-
17B	8	-
Grid 18	49	24
18A	15	-
18B	10	-
18C	20	-
Grid 19	59	24
19A	7	-
19B	14	-
19C	19	-
19D	10	-
Grid 20	32	24
20A	17	-
Grid 21	29	24
21A	18	-
Grid 22	33	26
22A	14	-
22B	15	-
Grid 23	5	25
23A	25	-
23B	25	-
Grid 24	29	24
24A	24	-
<i>Total</i>	<i>21 grid-layers: 327</i>	<i>11 grids: 262</i>
	<i>11 grids: 420</i>	
<i>Median</i>	<i>21 grid-layers: 15</i>	<i>11 grids: 24</i>

Table 3.3. The number of analyzed SMP measurements in the eleven analyzed grids.

Grid	Analyzed profiles	Comments
14	47	Battery died after 47 measurements.
15	113	-
16	113	-
17	0	The tip might have been frozen, causing some dampening of the force signal.
18	0	The tip froze, causing large drift in the force signal.
19	0	The tip froze, causing large drift in the force signal.
20	113	-
21	113	-
22	113	Minor drift in some SMP signals.
23	113	-
24	0	The tip froze, causing large drift in the force signal.

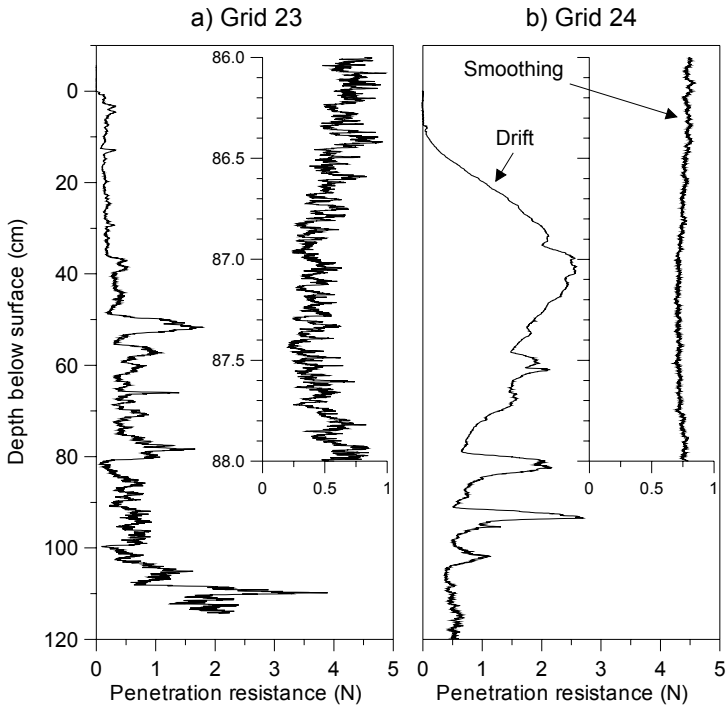


Figure 3.1. Comparison of a) a high quality SMP profile from grid 23, and b) an unusable SMP profile from grid 24. The inserted profiles show a closer zoom to a part of the profiles. The depth scales are the same on the full profiles and the zoomed profiles, respectively.

Within each grid with useable SMP measurements, one or more layers were identified from the penetration resistance signal. These grid-layers are numbered with the grid number and a lower case letter, e.g. 23b. Twenty grid-layers were analyzed, primarily weak layers but also wind slabs.

3.4. Snow cover stratigraphy

The manually recorded stratigraphic profiles from grids 14 to 24 are shown in Appendix A. These profiles also provide information about RB fractures and the ramsonde hardness profile.

In the 2001 – 2002 winter season, two persistent weak layers PWL-1 and PWL-2 were found in the snow cover. In the 2002 – 2003 winter season, a surface hoar layer PWL-3 was found in the snow cover.

3.4.1. Persistent weak layers PWL-1 and PWL-2

In early December 2001, rain and wet snow moistened the snow surface up to an elevation of about 2800 m a.s.l. in the study area. After freezing, this produced two (in some places three) separate crusts above each other (Figure 3.3). These crusts were found in all grids from the investigated area the rest of the winter season 2001 – 2002. Above the upper crust, faceted crystals formed (Birkeland, 1998; Colbeck and Jamieson, 2001; Jamieson and van Herwijnen, 2002), producing a 2 to 5 cm thick weak layer. A number of natural and skier-triggered avalanches failed in this layer, and it remained critical for most of the winter. This persistent weak layer is called PWL-1.

Faceting also took place below the lower crust (Colbeck, 1991; Fierz, 1998). Until the beginning of March 2002, only few fractures were produced in this weak layer, and it was not as active as sliding layer for avalanches as PWL-1. The persistent weak layer that developed below the lower crust is called PWL-2. As the winter progressed, the faceted crystals (\square) in both weak layers metamorphosed into depth hoar (\wedge) or mixed forms (\diamond), or a combination of these grain types.

These two persistent weak layers were present within the snow cover in all grids measured in 2002 although we did not produce fractures in them at all point stability test locations.

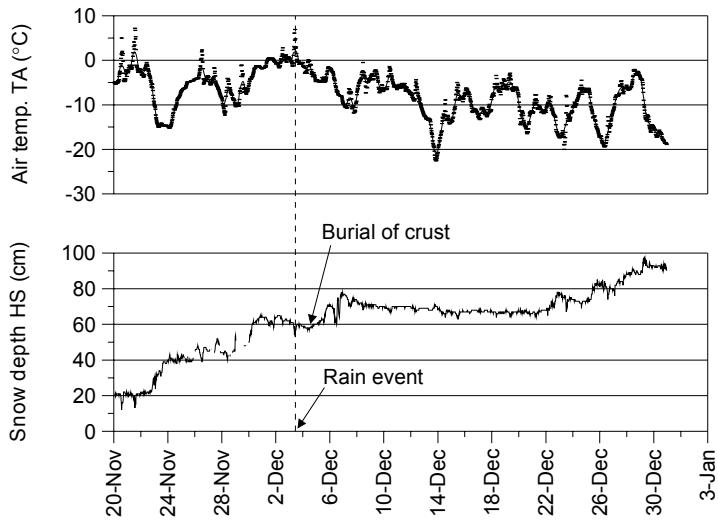


Figure 3.2. Snow depth and air temperature during the rain event that lead to the crust around which PWL-1 and PWL-2 were later formed. Data are from the Hanengretji IMIS station for 20 November 2001 to 3 January 2002 recorded every 30 minutes. A running average is fitted to the temperature data.

Handprofil

Ort: **GR Steintälli - Strela - Davos**

Datum/Zeit: **15.01.2002 10:00**

Profilnr: 1

Beobachter: Schweizer/Fierz

Station: 164

Temp.: -9.0 °C

Höhe ü. M.: 2415 m

Koordinaten: 779510 / 186525

sonnig (0/8)

Exposition: NNE

Neigung: 28 Grad

Windrichtung:

-stärke: 0 km/h

Wetter/Niederschlag: sonnig

LKNr: 1197 Bemerkungen: bei Grid #2 / unterhalb Ski

Gesamtwasserwert: 355.1 mm (HS: 126.0 cm)

Mittl. Raungew.: 282 kg/m³

Mittl. Rammwiderstand: 54 N

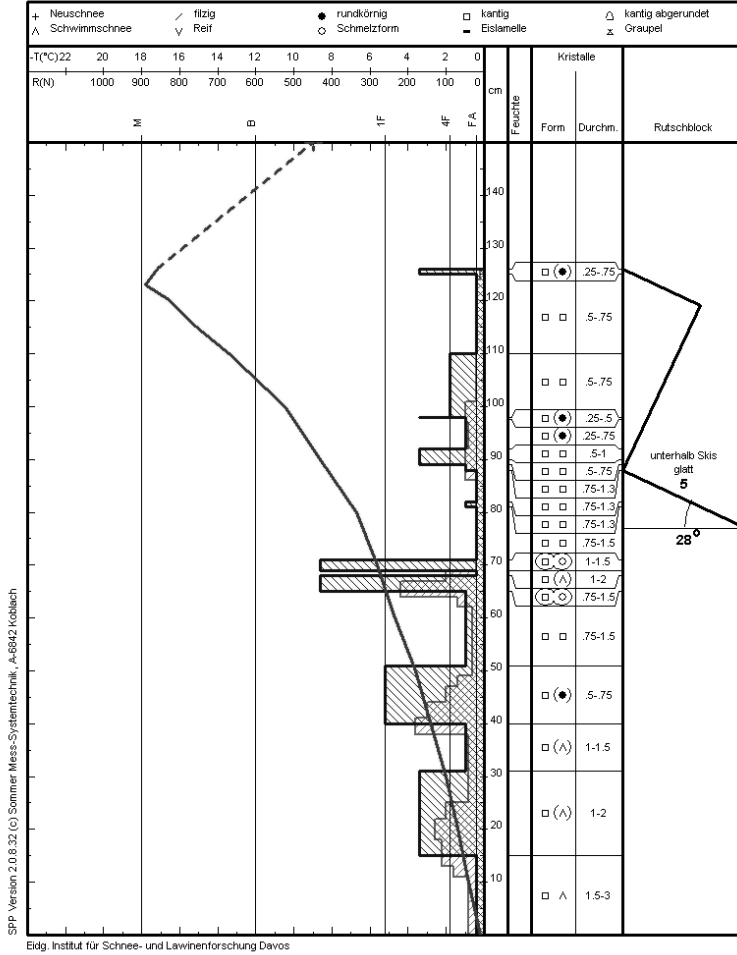


Figure 3.3. Stratigraphic snow cover profile from grid 15. The persistent weak layer PWL-1 is at $H = 72$ cm above the upper crust. PWL-2 is at $H = 64$ cm, below the lower crust.

3.4.2. Persistent weak layer PWL-3

In early December 2002 after a few cold, clear nights, a layer of surface hoar grew on the snow surface in the region around Davos. The surface hoar was buried by snowfall later in December (Figure 3.4). The persistent weak layer formed by the buried surface hoar is called PWL-3 (Figure 3.5). It was active as sliding layer for natural and skier-triggered avalanches through most of the remaining winter season 2002–2003. The surface hoar crystals eventually metamorphosed into depth hoar and mixed forms.

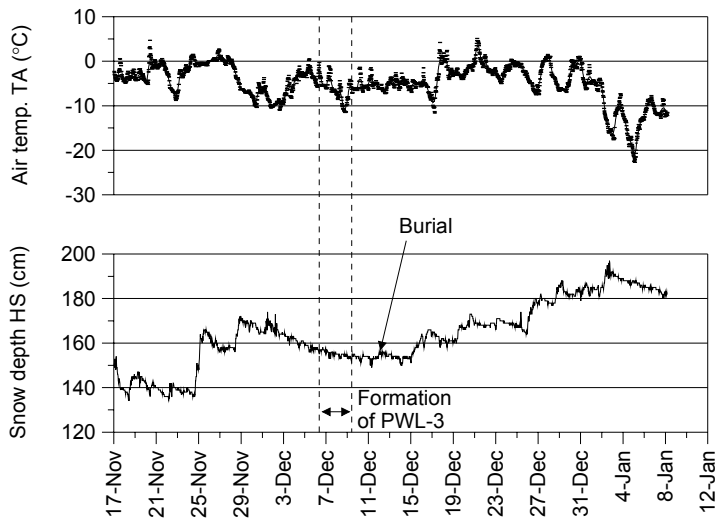


Figure 3.4. Snow depth and air temperature during deposition and burial of the surface hoar layer PWL-3. Data from the Hanengretjji IMIS station for 17 November 2002 to 12 January 2003 recorded every 30 minutes. A running average is fitted to the temperature data.

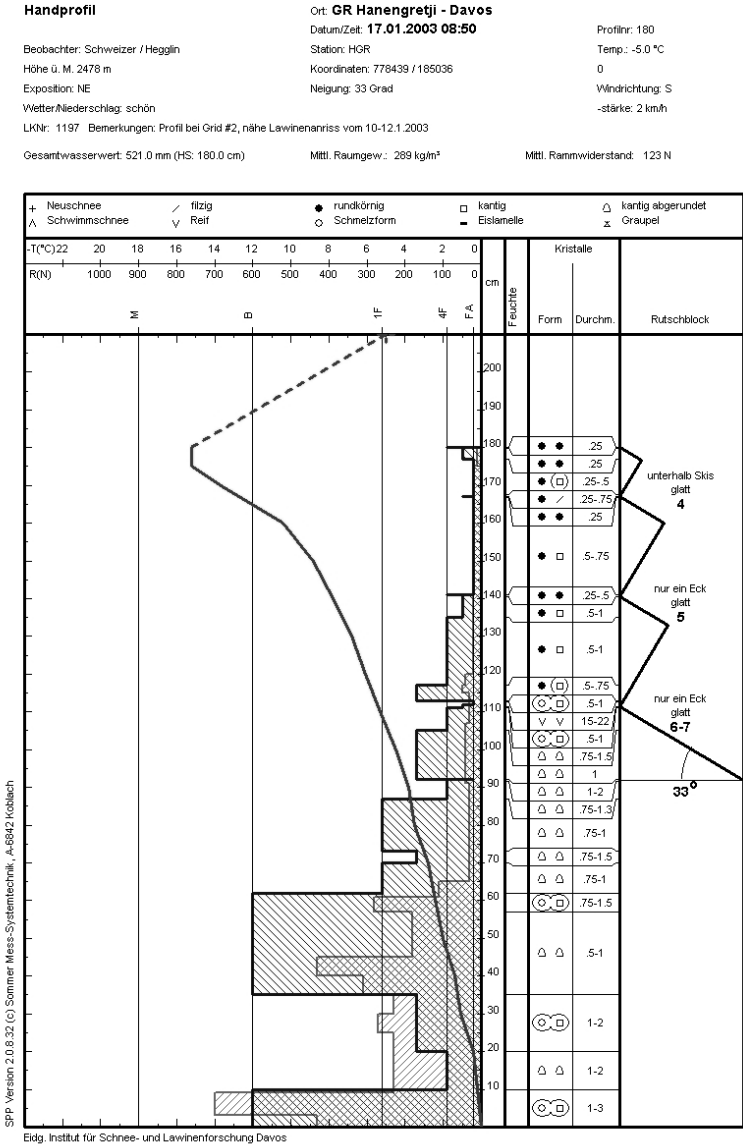


Figure 3.5. Stratigraphic snow cover profile from grid 23. The buried surface hoar layer PWL-3 is near $H = 110$ cm.

Chapter 4

Results

4.1. Introduction

Measurements of two different properties were made to characterize their spatial variability within each grid. Column-type stability tests were made to measure point stability and its spatial variation. Point stability results integrate information about slab and weak layer properties. To describe the spatial variability of individual layers, micro-penetrometer measurements were made. The penetration resistance profiles provided grain-scale resolution (mm) in the slope-perpendicular direction and the measurements were spaced close enough to give resolution (m) at the snowpack-scale in the horizontal direction. The two methods measure different snow cover properties, and results are therefore presented separately. Section 4.2 presents the results from the stability tests, while results from the micro-penetrometer are presented in Section 4.3.

None of the two methods had been extensively used in the field before, so first it was necessary to relate the results from each method to results from previously used instruments and methods. The results from this comparison are presented in Section 4.2.1 for the rammrutsch stability test, and in Sections 4.3.1 and 4.3.2 for the micro-penetrometer. Once the two measurement methods were established, the spatial variability of point stability (Section 4.2.2) and penetration resistance (Section 4.3.3) was characterized using geostatistical methods. The influence of various snow cover properties on the spatial variability of stability (Section 4.2.3) and penetration resistance (4.3.4) was then investigated. Finally, in Section 4.4 the spatial variability found by the two methods are compared.

4.2. Stability test results

To establish the rammrutsch test (RR) as a true stability test, the results were compared and scaled to the results of the better-known rutschblock

(RB) results (Section 4.2.1). Once a relationship was established, the spatial variability of point stability was characterized (Section 4.2.2). Finally, possible causes of the observed variability were investigated (Section 4.2.3).

4.2.1. Comparison of rammrutsch and rutschblock results

The stuffblock (SB) test results are related to rutschblock (RB) results and can be used in combination with other observations to evaluate snow stability (Birkeland and Johnson, 1999). To test the validity of the rammrutsch (RR) test as a stability test, the RR drop heights were compared with the RB test results. In 14 grid-layers, fractures were produced by both the point stability tests and by the RB tests (Table 4.1). In three additional grid-layers, fractures were produced by the RB tests but not the point stability tests (Table 4.1). Jamieson (1999) assigns such “no fracture” stability tests an arbitrary, high stability value. I have chosen to leave the three grid-layers out of the analysis. That way an arbitrarily assigned value does not carry weight in the analysis. In the 12 grid-layers where fractures were produced by the point stability tests but not by the RB tests, the RB score was set to 7; the “no fracture” RB score. Data for the 29 layers available for analysis are shown in Table 4.1.

Based on results from the SB tests from grids 14, 15 and 16, the SB tests had a higher median associated with the RB scores than the RR tests (Figure 4.1). In the following analysis, results from the two tests are therefore treated separately.

The RR results for a weak layer were related to the RB score for the same weak layer (Figure 4.1). Except between RB score 4 and 5 there was an increase in the RR results for increasing RB scores. A closer examination of the RR results from the three grid-layers associated with RB score 4 did not give an answer to the high median RR drop height for these grid-layers. Considering only the fractures on either side of the RB test in each of the three grids with a RB score 4 gives drop heights of 20 and 35 cm for grid-layer 17A, 35 cm for grid-layer 19D, and two tests with $DH = 1$ cm for grid-layer 23B. Thus, the median drop height does not change from 20 cm when only considering the RR tests on either side of the RB test.

Table 4.1. Stability, depth and fracture types for grid-layers identified in rutschblock tests and point stability tests.

Grid-layer	Point stability tests				RB		
	Test type	No. fract. n_{fract}	Median <i>FD</i> (cm)	Median <i>DH</i> (cm)	Score	fract. type	fract. surf. type
14A	SB	16	48.5	35.0	3	corner	planar
14B	SB	4	37.5	20.0	5	partial	planar
15A	SB	18	35.5	40.0	7	-	-
15B	SB	5	32.0	40.0	5	partial	planar
16A	SB	14	58.0	50.0	7	-	-
16B	SB	9	22.0	10.0	3	partial	planar
16C	SB	7	21.0	10.0	7	-	-
17A	RR	22	52.5	35.0	4	complete	planar
17B	RR	8	27.0	35.0	7	-	-
18A	RR	15	57.0	15.0	5	partial	planar
18B	RR	10	54.0	22.5	7	-	-
18C	RR	20	14.5	5.0	2	complete	planar
19A	RR	7	28.0	30.0	7	-	-
19B	RR	14	64.0	32.5	7	-	-
19C	RR	19	18.0	15.0	7	-	-
19D	RR	10	34.0	45.0	4	partial	planar
20A	RR	17	62.0	20.0	7	-	-
20B	RR	4	28.0	10.0	3	complete	planar
20C	RR	0	-	-	3	complete	planar
21A	RR	18	50.0	32.5	7	-	-
21B	RR	0	-	-	5	partial	planar
22A	RR	14	23.5	40.0	7	-	-
22B	RR	15	9.0	10.0	6	corner	rough
23A	RR	25	79.0	20.0	6	corner	planar
23B	RR	25	9.0	1.0	4	partial	planar
23C	RR	1	30.0	20.0	5	partial	planar
24A	RR	24	92.5	35.0	7	-	-
24C	RR	1	42.0	35.0	6	corner	irregular
24D	RR	0	-	-	6	corner	irregular

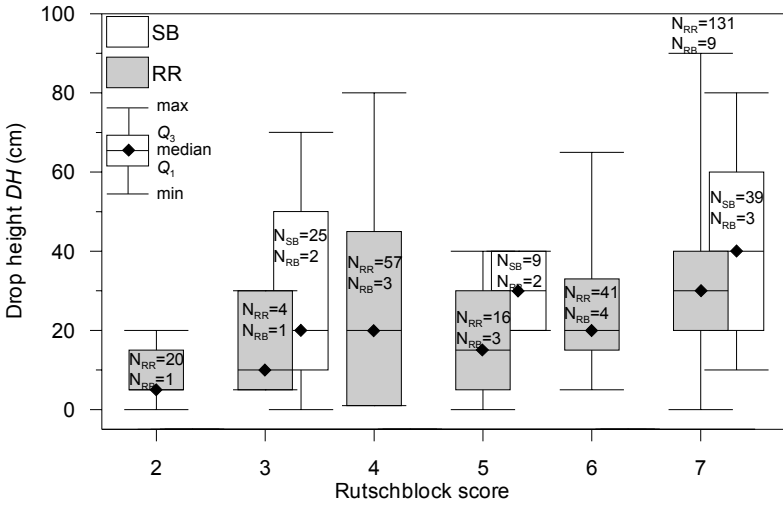


Figure 4.1. Relation between the rutschblock score and the drop height from the stuffblock tests (SB) and the rammrutsch tests (RR). The spread for each RB score is partly due to areal variation in the RR and SB drop height values. N is the number of tests used for the calculation.

Despite the high median RR drop height for RB score 4, Figure 4.1 suggests that the RR test can be used to evaluate snow cover stability in the same manner as the RB test, at least for RB scores greater than 1. The RR drop height values corresponding to the RB scores and other stability tests are compiled in Table 4.2. As for all other point stability test, additional stability related information must be considered when evaluating snow cover stability with the rammrutsch test.

Table 4.2. Column-type stability test results associated with the seven rutschblock loading steps. The stuffblock results are from Birkeland and Johnson (1999). Data for the compression test (Jamieson, 1999) are added for convenience.

Rutschblock score	Stuffblock test (drop height, cm)			Rammrutsch test (drop height, cm)			Compression test (number of taps)
	Median	Q ₁	Q ₃	Median	Q ₁	Q ₃	
1	-	-	-	-	-	-	-
2	10	0	10	5	5	15	0-13
3	10	10	20	10	5	25	14-16
4	30	20	40	-	-	-	17-18
5	40	30	50	15	5	30	19-20
6	40	30	60	20	15	30	21-25
7	80	60	80	30	20	40	>25

4.2.2. Variation of point stability

Spatial variability in the column-type stability test results was found to exist. The variability was characterized with the geostatistical methods described in Section 2.12.4, p. 70 by analyzing the data as a random field with autocorrelation.

Spatial trends

Spatial trends spanning the grids were investigated with a robust linear regression given by equation 2.12, where DH is in cm and x and y in m (Table 4.3). y is positive uphill and x is positive to the orographic left (Figure 2.2, p. 32). Due to the few fractures (e.g. 16C) and the small spread of the drop heights in some grid-layers (e.g. 23B), the robust S-Plus fitting routine used, `lmRobMM` (Marazzi, 1993, p. 201; MathSoft, 1999), did not provide reasonable trend estimates for all grid-layers. For grid-layers 16C, 19A and 23B where the routine produced an error message, an ordinary least squares fit was used instead.

Significant ($P < 0.05$) linear spatial trends in either direction (α or β significant), or in both directions (α and β significant) were found for seven out of the 21 grid-layers. For these seven grid-layers, no typical pattern was found: α and β were positive for some grid-layers and negative for others. The variance explained by the regression models was generally low with a median of $R^2 = 0.36$.

The median regression coefficient in the up-slope direction (y) was negative, implying a general decrease of stability towards the top of the grids. In the cross-slope direction, there was not a typical direction of the trend. The median of the absolute regression coefficients shows that spatial trends were generally stronger in the up/down-slope direction than in the cross-slope direction. Trends in two grid-layers within the same grid were in a few cases observed to be in opposite directions (e.g. β for 18A and 18B).

Table 4.3. Regression coefficients for the robust bi-linear regression of the drop height on the spatial coordinates ($DH = \alpha x + \beta y + c_i$) for the point stability grid-layers. x and y were in m and DH in cm.

Grid-layer	α (cm m ⁻¹)	β (cm m ⁻¹)	c_i (cm)	R^2
14A	4.65	0.64	-14.4	0.74
15A	-0.69	0.12	45.1	0.11
16A	-0.01	-3.93	85.1	0.54
16B	-0.06	-0.44	17.0	0.15
16C [‡]	-0.88	-0.47	29.8	0.65
17A	0.65	-1.34	43.0	0.38
17B	0.98	-1.14	28.2	0.58
18A	-1.33	2.21	11.0	0.41
18B	-0.55	-1.74	34.2	0.10
18C	0.07	0.86	-0.5	0.16
19A [‡]	-2.47	-1.25	73.5	0.56
19B	-0.16	-3.95	83.5	0.65
19C	0.31	-0.48	17.9	0.12
19D	-1.14	-1.26	59.7	0.42
20A	2.22	-2.96	43.5	0.24
21A	-0.05	-1.57	51.4	0.21
22A	-0.67	-0.18	49.5	0.15
22B	0.46	-0.42	9.1	0.63
23A	-0.83	0.24	29.7	0.20
23B [‡]	-0.20	0.08	3.3	0.36
24A	-0.82	-1.23	56.1	0.35
Median	-0.16	-0.48	-	0.36
Median abs [†]	0.67	1.14	-	-

Notes: [‡] The ordinary least squares method was used to fit the regressions. Coefficients marked in **bold type** were significant ($P < 0.05$). [†] Median|abs| is the median of the absolute values.

Spatial structure after trend removal

Robust sample semi-variograms were calculated for the residuals from the trend analysis. All sample semi-variograms are shown in Appendix B, and four examples are shown in Figure 4.2. Because of the limited number of fractures used for each semi-variogram (≤ 25), they should be interpreted carefully. For the same reason, it was not attempted to fit any model semi-variograms to the sample semi-variograms. Only a few sample semi-variograms had enough combinations of point pairs to make them reasonable to interpret qualitatively. Of these semi-variograms, most had increasing semi-variance at increasing lag-distances but none reached a sill within a lag distance of 10 m. This indicates that even with the linear trend removed the drop heights were not stationary (i.e. the local mean changed over the slope) or that the range was longer than 10 m. The semi-variance at 1 m lag-distance was

often more than 50% of the semi-variance at lag distances between 8 and 10 m indicating that the additional spatial structure left in the drop height residuals after trend removal was small. Further spatial analysis, such as fitting a model semi-variogram, would therefore bring little additional information to the spatial analysis.

Non-spatial statistical description of variation

Most previous studies use classical statistics to describe spatial variability. Here, the variability of DH was characterized by the quartiles (Minimum, Q_1 , Median, Q_3 and Maximum), the semi-interquartile range SIQR (equation 2.7) and the quartile coefficient of variation QCV (equation 2.8). These values together with the median fracture depth FD are given for each grid-layer in Table 4.4.

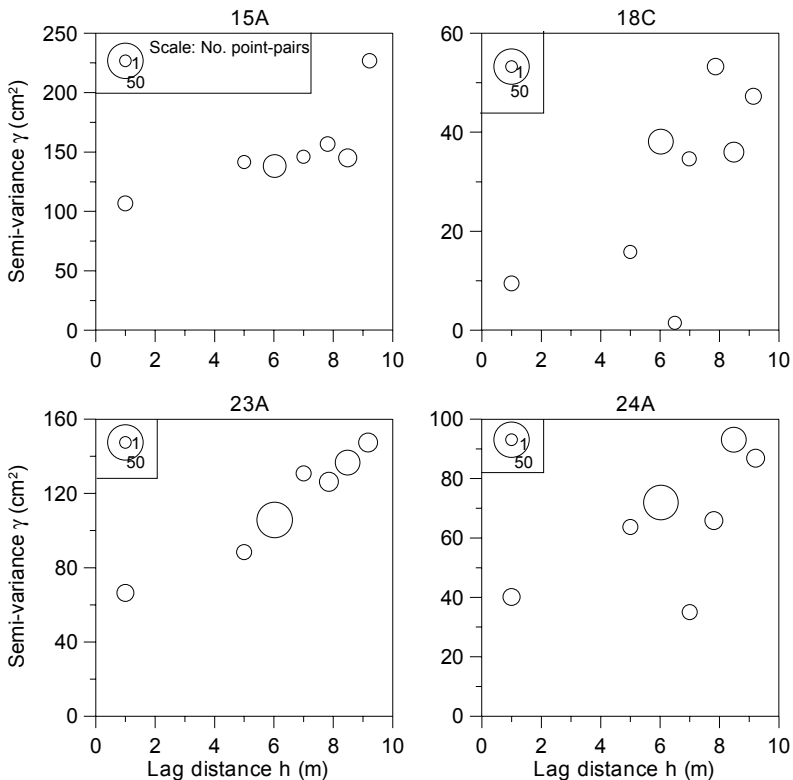


Figure 4.2. Sample semi-variograms for the drop height values in grid-layers 15A, 18C, 23A and 24A. These four examples of sample semi-variograms were among a few that had enough point pairs to give reasonable qualitative results.

Table 4.4. Summary statistics for the variation of stability in the grid-layers defined from the point stability tests. DH_{res} indicate the residuals after trend removal.

Grid-layer	FD (cm)	Drop height DH (cm)					SIQR (cm)		QCV (%)	
		Median	Min	Q_1	Med	Q_3	Max	DH	DH_{res}	DH
14A	48.5	0	10.0	35.0	52.5	70	21.3	4.6	68	14
15A	35.5	20	30.0	40.0	47.5	60	8.8	7.4	23	19
16A	58.0	10	20.0	50.0	67.5	80	23.8	3.6	54	8
16B	22.0	0	10.0	10.0	20.0	20	5.0	4.9	33	35
16C	21.0	10	10.0	10.0	15.0	30	2.5	0.9	20	8
17A	52.5	20	26.3	35.0	45.0	80	9.4	6.8	26	19
17B	27.0	20	20.0	35.0	41.3	45	10.6	4.6	35	13
18A	57.0	0	5.0	15.0	30.0	40	12.5	4.5	71	32
18B	54.0	5	7.5	22.5	33.8	40	13.1	5.4	64	23
18C	14.5	0	5.0	5.0	11.3	20	3.1	3.0	38	43
19A	28.0	0	20.0	30.0	35.0	60	7.5	3.0	27	9
19B	64.0	5	21.3	32.5	53.8	75	16.3	8.5	43	23
19C	18.0	5	10.0	15.0	25.0	45	7.5	6.3	43	36
19D	34.0	10	35.0	45.0	50.0	70	7.5	11.3	18	26
20A	62.0	5	15.0	20.0	55.0	65	20.0	6.1	57	23
21A	50.0	15	25.0	32.5	43.8	90	9.4	8.9	27	25
22A	23.5	25	35.0	40.0	50.0	60	7.5	9.1	18	22
22B	9.0	5	5.0	10.0	15.0	15	5.0	1.3	50	11
23A	79.0	5	20.0	20.0	35.0	65	7.5	6.1	27	22
23B	9.0	1	1.0	1.0	2.0	10	0.5	0.9	33	47
24A	92.5	20	25.0	35.0	45.0	55	10.0	3.6	29	10
Median	35.5	5	20.0	30.0	41.3	60	8.8	4.9	33	22

The semi-interquartile range SIQR in the drop heights varied from 0.5 cm to 23.8 cm with a median of 8.8 cm before trend removal. The SIQR was proportional to the median drop height up to a drop height of around 20 cm (Figure 4.3a). After removal of a linear trend, the absolute spread generally decreased especially for large values of SIQR (Figure 4.3b). With the exception of one value from grid-layer 19D, which increased after trend removal, the values of $SIQR_{res}$ were below 10 cm. For some grid-layers where the linear trend model was not appropriate, the SIQR and QCV increased after trend removal.

For the SB tests, the median SIQR was 8.8 cm (4.6 cm after trend removal) while for the RR tests the median was 8.4 cm (5.8 cm after trend removal). The median for all 21 grid-layers was 8.8 cm (4.9 cm after trend removal). Two grid-layers with SB tests (14A and 16A) had the highest SIQR before trend removal, but these high values were reduced by the trend removal.

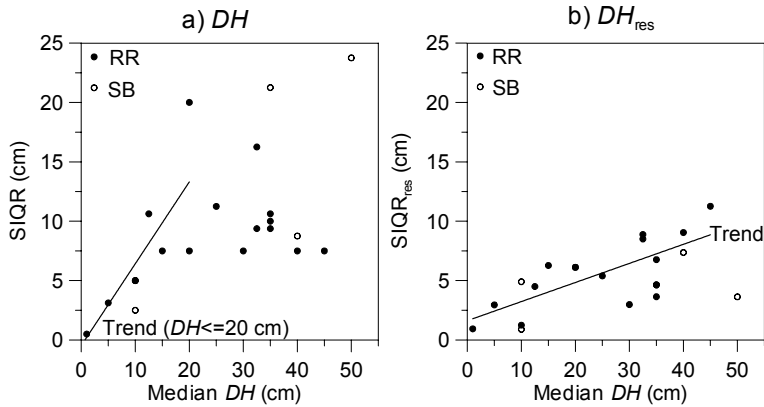


Figure 4.3. The semi-interquartile range as a function of the median drop height in each grid. a) Before and b) after trend removal.

The quartile coefficient of variation QCV varied from 18% to 71% with a median of 33%. Using equation 2.10, this corresponds to a standard (parametric) coefficient of variation CV with a minimum of 27% and a maximum of 107% with a median of 50%. After trend removal, the median QCV dropped to 22%, corresponding to a CV of 33%.

Observations of areas with very low stability

One stability test location where the column collapsed during column preparation ($DH = 0$ cm) was observed in grid-layer 14A (Figure 4.4a). The test point was located 5 m from a point with $DH = 60$ cm. This spatial gradient in drop height might be explained by the depth of the layer. At the stable test location, the layer was almost twice as deep as at the less stable test location. In general, the depth of grid-layer 14A was larger in the right-hand side of the grid ($x > 8$ m) than in the left side of the grid.

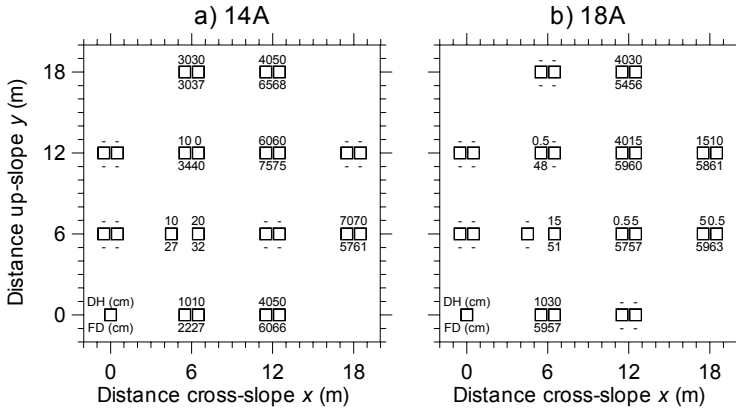


Figure 4.4. Drop heights for a) stuffblock tests in grid-layer 14A, and b) rammrutsch tests in grid-layer 18A, in which points with very low stability were found. Grid-layer 18A collapsed while working on the slope. The two grid-layers shown were among those with the highest variation of all.

While working in grid 18, grid-layer 18A (PWL-1) collapsed with a loud “whumpf”. Because the slope was small and supported below, the slab above the weak layer did not slide more than a few centimeters although a slope-perpendicular tensile fracture was formed above the grid (Figure 4.5). The failure happened around 13:38 as a person took a step onto a harder layer in the slab (between $H = 70$ cm and 80 cm in Figure 4.6) near the middle of the grid. Before the slab failure, tests 1, 2 and 3 did not fracture in grid-layer 18A while test number 4 fractured at a drop height of 15 cm (Figure 4.4b and Figure 4.7). Immediately after slab failure, tests 5 and 6 produced low stability values of 0.5 and 5 cm respectively. This was expected because the weak layer strength must have been reduced after the fracture. Surprisingly, tests 7 and 8 did not fracture in grid-layer 18A, and tests 9 and 10 had drop heights of 15 and 30 cm respectively. Low drop heights were again found in tests 11 and 12. I expect that the fracture in grid-layer 18A did not propagate further down the slope than somewhere between $y = 0$ m and $y = 6$ m. If tests 9 and 10 are not considered in Figure 4.7a, which shows the temporal change in drop heights, it appears that between 15:00 and 16:00, the drop heights increased rapidly from around 5 cm to around 40 cm. This changes the interpretation of the stability from a RB score 2 (unstable) to a RB score 7 (stable). The increase could be due to sintering of the grains in grid-layer 18A.

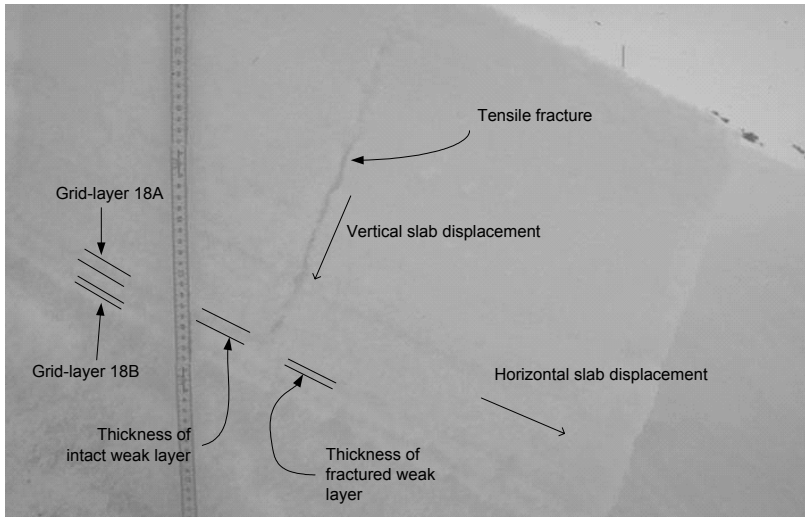


Figure 4.5. Picture of a vertical wall in a transect across the tensile fracture that formed after fracture of grid-layer 18A. The numbers on the ruler are 1 cm apart. Downhill from the tensile fracture, the thickness of the fractured layer decreased with approximately 0.5 cm. The horizontal slab displacement was around 1 cm at the tensile fracture. The stratigraphic snow cover profile is shown in Figure 4.6.

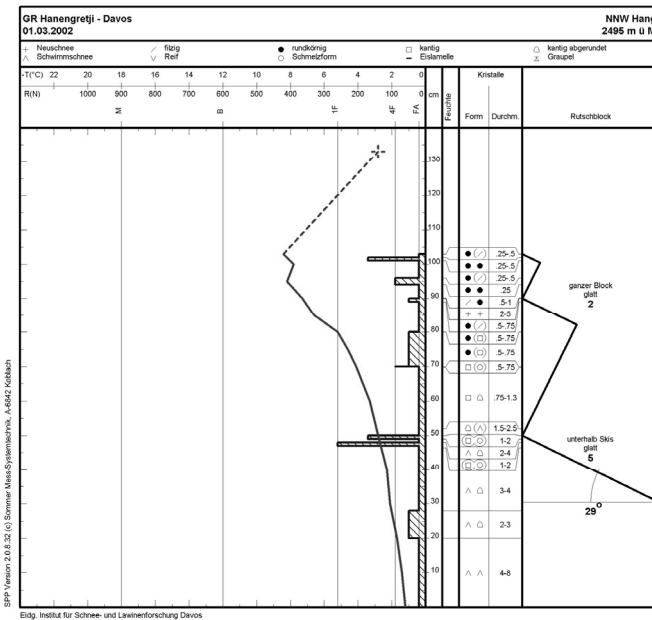


Figure 4.6. Stratigraphic profile and hand hardness from grid 18. The fracture happened above the upper crust at 50 cm above the ground where the RB score was 5. For a translation of the German terms, see Appendix A.

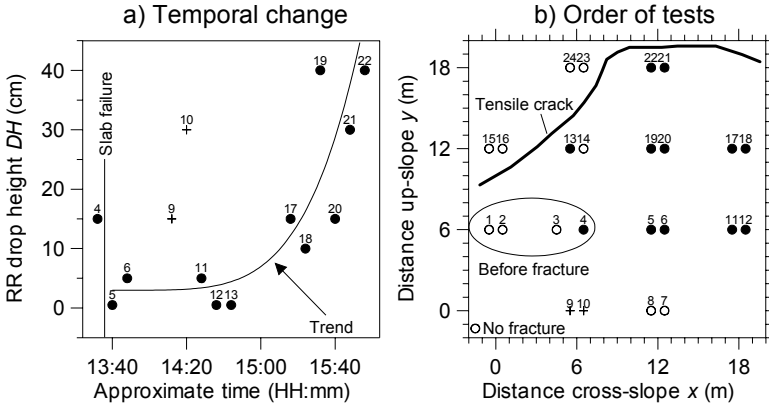


Figure 4.7. a) Temporal change of the drop heights in grid-layer 18A after fracture. Numbers indicate the chronological order of the tests. b) The location of the RR tests with the numbers corresponding to a). Slab failure occurred after test number 4 was finished. Open circles in b) indicate the locations where no fracture was produced by the stability tests in grid-layer 18A.

4.2.3. Causes of variation in stability

Possible factors that might influence the variation of point stability were investigated. These factors were slab thickness, slope inclination and grain type. Finally, it was investigated whether the fracture character type and the number of fractures in a grid-layer were related to its spatial variability.

Slab thickness

By rapid near surface loading of a slab above a weak layer, energy is dissipated in the slab before reaching the weak layer. A relation between the slab thickness and the drop height at fracture was therefore anticipated and investigated for a) fractures within each grid-layer, and b) between the median drop height and slab thickness for all grid-layers.

In 9 of the 21 grid-layers, a significant ($P < 0.05$, robust linear regression) correlation between fracture depth and drop height was found (Table 4.5 below). All nine significant regression coefficients were positive, indicating greater drop height for thicker slabs.

When comparing the median drop height and the median slab thickness for all grid-layers (Table 4.4), there was a non-significant positive relation (linear least square, $P = 0.053$, $R^2 = 0.18$). Between the

median slab thickness and Q_3 for the drop height, the relation was significant (linear least square, $P = 0.003$, $R^2 = 0.38$). Thus, when comparing different weak layers, the slab thickness alone does not explain the observed variability.

The precision of the stability tests was expected to decrease with the slab thickness resulting in larger variation for thicker slabs (Section 2.10.5, p. 62). An increase in the semi-interquartile range SIQR for deeper slabs is evident from Figure 4.8a. However, once the slope-scale trend was removed, the relationship no longer existed (Figure 4.8b).

Table 4.5. Regression coefficients from the linear regression of fracture depth (in cm) ($DH = aFD + c_{FD}$) and slope inclination (in degrees) ($DH = b\psi + c_{incl}$) on the drop height (in cm). A robust algorithm was used for the fit.

Grid-layer	Regression using FD (a) (-)	Regression using ψ (b) ($cm (^{\circ})^{-1}$)
14A	0.88	-13.79
15A	1.27	1.28
16A	1.04	-6.65
16B	-0.96	-1.33
16C	1.77[†]	-0.00
17A	1.24	-3.71
17B	1.46	-0.85
18A	-2.03	2.26
18B	1.02	-2.82
18C	0.31	-0.80
19A	0.56	-23.00
19B	0.60	-7.58
19C	5.00	-3.18
19D	0.89 [†]	-11.94
20A	0.52	-3.10
21A	0.81	-2.85
22A	0.10	1.24
22B	0.96	-0.92
23A	2.23	0.40
23B	0.42[†]	0.14 [†]
24A	0.25	-1.54
<i>Median</i>	<i>0.71</i>	<i>-1.54</i>

Notes: Variables marked in **bold type** were significantly correlated to drop height ($P < 0.05$). [†] Coefficients were estimated with a least square fitted linear regression instead of a robust regression.

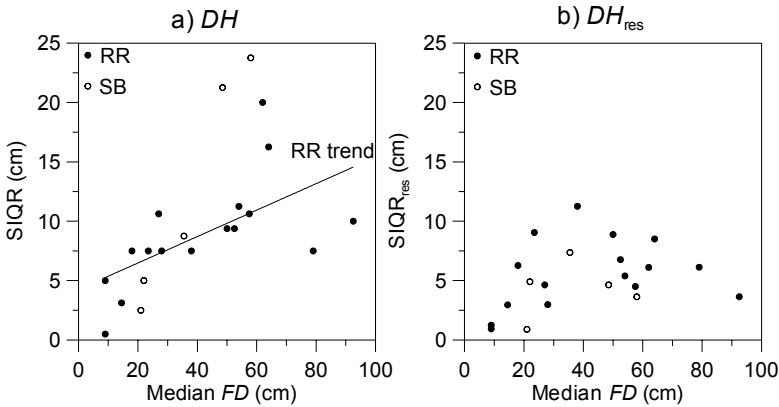


Figure 4.8. The semi-interquartile range of the stability (drop height) SIQR as a function of the median slab thickness (fracture depth) FD for each of the 21 grid-layers.

Slope inclination

The shear stress on a weak layer from the slab above and any additional weight such as a skier is proportional to the sine of the slope inclination. The influence of the snow surface inclination on the point stability (DH) in each grid-layer was investigated. In four of the 21 grid-layers, there was a significant negative correlation ($P < 0.05$, robust linear regression), although in one grid-layer (16C), the coefficient was very close to zero (Table 4.5). Sixteen of the 21 correlation coefficients were negative. One possible reason for the few significant correlations is that the spread of the slope angles on a given slope was small (Table 3.1, p. 76).

Grain shape

The grain shape and size in a layer reflects the processes that have acted on the layer before and after deposition (e.g. wind and metamorphism, respectively). The spatial variability of these processes is likely to influence the variability of the snow. Based on the grain types, the 21 layers were divided into persistent weak layers (PWL) (surface hoar, faceted crystals, mixed forms and depth hoar) and other weak layers (Jamieson, 1995, p. 11) (Table 4.6). The persistent layers were further divided into the three layers PWL-1, PWL-2 and PWL-3 described in Section 3.4, p. 80. PWL-1 and PWL-2 were found in all grids measured in 2002, but did not always produce more than 5 fractures. In the three grids measured in 2003, PWL-3 was found and analyzed in all three grids (Table 4.6). Of the 21 grid-layers investigated, 16 consisted of persistent grain shapes.

Table 4.6. Grain shape, grain size, height above ground (at the ramsonde location) and a description of each layer investigated. PWL indicates if the grain shape in the weak layer was persistent or not.

Grid-layer	Grain shape	Grain size (mm)	PWL	FD (cm)	H (cm)	Description
14A	□(∧)	1-2	PWL-1	48.5	92	Fractures occurred in the interface between PWL-1 and a thin crust above
15A	□	0.75-1.5	PWL-1	35.5	76	Fractures occurred within the weak layer
16A	□(∧)	1-3	PWL-1	58.0	71	Fractures occurred in the interface between PWL-1 and the crust below
16B	∕	0.5-0.75	No	22.0	132	Partially decomposed crystals above a crust
16C	□	0.5-1	Yes	21.0	129	Interface between two layers of small facets
17A	◻(∧)	3-5	PWL-1	52.5	67	Fractures occurred in the interface between PWL-1 and the crust below
17B	●□	0.5-1	No	27.0	92	Fractures occurred in an interface between small rounded and small facets above a thin crust
18A	◻(∧)	1.5-2.5	PWL-1	57.0	50	Fractures occurred in the interface between PWL-1 and the crust below
18B	∧◻	3-4	PWL-2	54.0	46	Fractures occurred in the interface between PWL-2 and the crust above
18C	+	2-5	No	14.5	90	Large new snow crystals above a thin (wind?) crust
19A	◻◻	0.75-1.25	PWL-1	28.0	13	Fractures occurred in the interface between PWL-1 and the crust below
19B	∧(◻)	2-4	PWL-2	64.0	8.5	Fractures occurred in the interface between PWL-2 and the crust above
19C	∕	0.5-0.75	No	18.0	65	Partially decomposed crystals above a harder layer with small round and partially decomposed crystals
19D	◻(◻)	0.75-1.25	Yes	34.0	42	Thin layer of rounded facets at the new snow/old snow interface
20A	∧	2-5	PWL-2	62.0	39	Fractures occurred in the interface between PWL-2 and the crust above
21A	∧◻	2-2.5	PWL-2	50.0	37	Fractures occurred in the interface between PWL-2 and the crust above
22A	∨∧	2-4	PWL-3	23.5	104.5	Surface hoar which was only consistently present in the lower part of the grid
22B	□	0.5-1	Yes	9.0	117	Facets below a harder layer of facets and rounded crystals
23A	∨	15-22	PWL-3	79.0	111.5	Large surface hoar crystals present everywhere in the grid. In the lower right ramrutsch test, the layer was collapsed before doing the test
23B	●∕	0.25-0.75	No	9.0	167	Fractures within a thin layer of partly defragmented crystals on top of a thin (wind?) crust
24A	◻(∨)	2.5-5	PWL-3	92.5	114	A thin layer of surface hoar that had metamorphosed into mixed forms

Considering RR and RB tests together, the median semi-interquartile range SIQR (variation) for the persistent weak layers (9.4 cm) was 88% larger than the median for the non-persistent layers (5.0 cm) before trend removal (Figure 4.9a). After trend removal, this difference decreased (SIQR_{res} of 5.8 cm and 4.6 cm respectively, Figure 4.9b). When PWL-1 (facets), PWL-2 (facets) and PWL-3 (buried surface hoar) were considered separately, the median for PWL-1 was 10.0 cm (4.6 cm after trend removal, i.e. for DH_{res}), for PWL-2 the median was 13.8 cm (7.3 cm after trend removal) and for PWL-3 it was 7.5 cm (6.1 cm after trend removal) (Figure 4.9). The SIQR for PWL-2 was almost twice as large as for PWL-3. Non-persistent grid-layers had smaller SIQR of stability than persistent grid-layers before trend removal.

There was a relation between the slab thickness and the SIQR (Figure 4.8). Because non-persistent grid-layers were found closer to the surface than the persistent grid-layers (Figure 4.9), it was difficult to determine whether a large SIQR was caused by the grain type (persistent or not) or by a large fracture depth. From Figure 4.9a it appears that PWL-3 has a lower variability than expected from the large median fracture depth. After removal of the trend, the difference in variability for the three persistent weak layer types was small with PWL-1 having the lowest variability. The slope-scale trends in drop height were more important for drop height variation than the grain type.

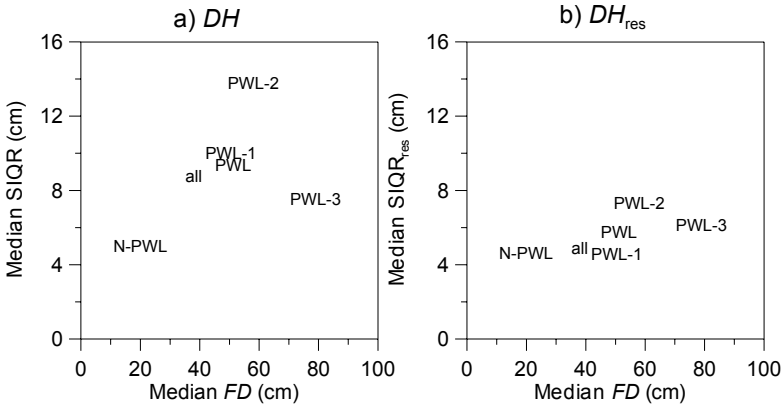


Figure 4.9. Median semi-interquartile range SIQR of drop height as a function of median fracture depth FD for all grid-layers (all), persistent weak layers (PWL), and for the non-persistent weak layers (N-PWL). PWL is further separated into the three persistent weak layers PWL-1, PWL-2, and PWL-3. a) The relationship for the absolute drop height values, and b) for the residuals after trend removal.

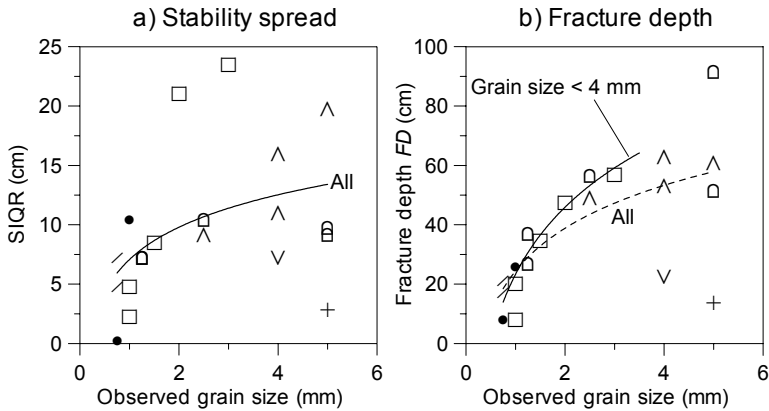


Figure 4.10. a) The semi-interquartile range SIQR as a function of grain size. A log-linear fit is shown. b) The fracture depth as a function of the grain size, with a log-linear fit shown for all data (hatched line) and for grid-layers with a grain size smaller than 4 mm (full line). Data from grid-layer 23A (surface hoar) is left out of the plots because of its very large grain size (15 – 22 mm). The first grain shape given in Table 4.6 is shown. The observed grain size plotted is the largest value in Table 4.6.

Grain size

The drop height SIQR showed some relation to the grain size for grains smaller than 4 mm (Figure 4.10a). For larger grains, there was more scatter in the relation. After removal of trends, the relationship was no longer apparent (not shown).

For grains smaller than 4 mm, there was a strong relation between the grain size and the fracture depth (Figure 4.10b).

Table 4.7. Number and percentage of fractures in the 21 grid-layers identified from the point stability tests and with more than five fractures within a grid.

Grid or grid-layer	Number of tests N_{test}	Number of fractures n_{fract}	Percentage of fractures F	Fracture character types
Grid 14	26	36	-	C:32, P:2, LIR:1, STP:1
14A	-	16	62	C:16
Grid 15	24	30	-	C:21, P:5, LIR:1, COL:3
15A	-	18	75	C:13, P:4, COL:1
Grid 16	17	38	-	C:32, P:6
16A	-	14	82	C:12, P:2
16B	-	9	53	C:7, P:2
16C	-	7	41	C:7
Grid 17	24	32	-	C:27, P:4, STP:1
17A	-	22	92	C:19, STP:1, P:2
17B	-	8	33	C:8
Grid 18	24	49	-	C:44, COL:4, STP:1
18A	-	15	63	C:14, STP:1
18B	-	10	42	C:6, COL:4
18C	-	20	83	C:20
Grid 19	24	59	-	C:49, P:4, COL:6
19A	-	7	29	C:7
19B	-	14	58	C:9, COL:5
19C	-	19	79	C:19
19D	-	10	42	C:8, P:2
Grid 20	24	32	-	C:25, P:3, COL:4
20A	-	17	71	C:16, P:1
Grid 21	24	29	-	C:23, P:1, COL:5
21A	-	18	75	C:15, COL:2, P:1
Grid 22	26	33	-	C:33
22A	-	14	54	C:14
22B	-	15	58	C:15
Grid 23	25	53	-	C:53
23A	-	25	100	C:25
23B	-	25	100	C:25
Grid 24	24	29	-	C:28, P:1
24A	-	24	100	C:24
<i>Total</i>	262	327	-	<i>Total: C:367, P:26, COL:22, STP:3, LIR:2 Analyzed: C:299, P:14, COL:12, STP:2</i>
<i>Median</i>	24	15	63	-

Fracture character types

Of the 420 fractures produced, 87% (367) had a planar fracture (type C), 6% (26) were only partly fractured along a planar surface (type P), and 5% (22) involved a collapse of a thicker snow layer (COL) (Table 4.7). Other fracture character types only occurred a few times. Of the 327 fractures in the 21 weak layers analyzed, 91% (299) were planar (type C), 4% (14) of type P, 4% (12) involved collapses of layers and 1% (2) was stepped between two fracture planes (Table 3.2). Three classes of fracture types would be sufficient to describe the main types of fractures.

The proportion of planar fractures produced in weak layers with more than five fractures within a grid was higher than the proportion of planar fractures in layers with five or fewer fractures within a grid. For statistical comparison with the chi-squared test (e.g. Spiegel and Stephens, 1999, p. 261), the 327 fractures in the analyzed grid-layers were divided into two groups: planar fractures (type C) and other types (P, COL, STP and LIR). The 93 fractures that were not analyzed were divided into the same groups. The chi-square test showed a significantly different distribution of fracture types in the two groups ($P < 0.001$). In weak layers with more than five fractures, the fracture type were in 91% of the cases planar (type C), whereas the fractures in weak layers with five or fewer fractures only were planar in 73% of the cases.

The percentage of planar fractures (type C) in each grid-layer was not related to the grain shape, the observed grain size, the median fracture depth, or the median drop height for each grid-layer.

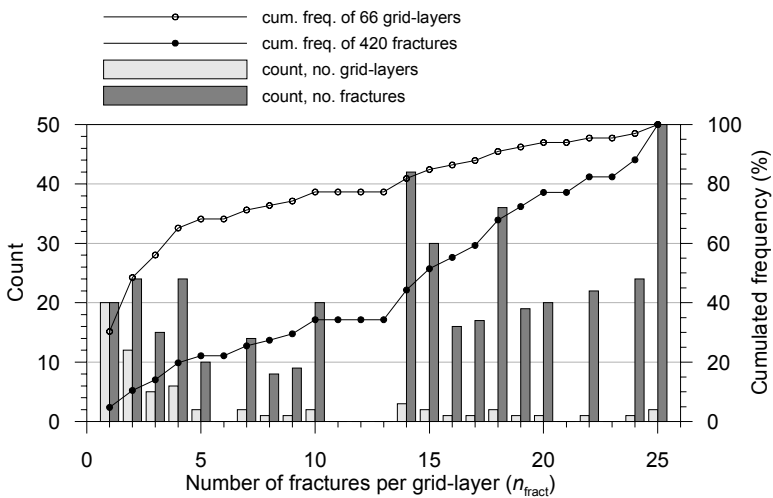


Figure 4.11. Histogram of the number of fractures in the 66 grid-layers identified in the point stability tests.

Number of fractures

Of the 420 fractures produced, 327 (78%) were in 21 weak layers (32% of the grid-layers) with more than five fractures. These 21 grid-layers were the ones that were analyzed. A large proportion of the grid-layers did not consistently produce fractures within the grids. In 20 grid-layers (30% of grid-layers), only one fracture was produced, comprising 5% of the 420 fractures recorded (Figure 4.11). The cumulated frequency of the proportion of grid-layers with a certain percentage of fractures rises sharply of to five fractures per grid-layer and then levels off (open circles in Figure 4.11). The cumulated frequency for the proportion of fractures within weak layers (filled circles in Figure 4.11) is almost linear. When the relative number of fractures F was used instead of the actual number of fractures, the results were similar to those shown in Figure 4.11.

There was a relation between the grain size and the percentage of fractures in a weak layer (Figure 4.12). If data from grid-layer 23A was left out, the relation was not significant (ordinary least squares, $P = 0.093$). If all data was used, the trend was significant ($P = 0.038$), but the data from grid-layer 23A (grain size = 22 mm, $F = 100\%$) gave a strong leverage point and was defined as an outlier.

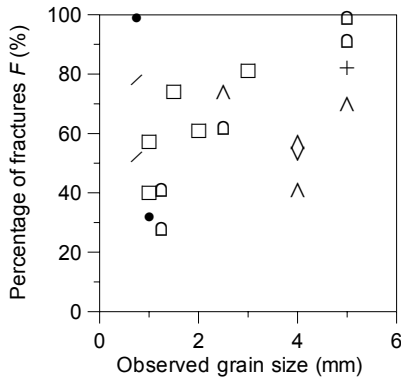


Figure 4.12. The percentage of possible fractures in each grid-layer as a function of grain size. Data from grid-layer 23A with $F = 100\%$ is left out because of its very large grain size (surface hoar with grain size 15 – 22 mm).

4.3. Penetration resistance results

In this section, the results from the snow micro-penetrometer (SMP) profiles are described. First, results from the calculations of the microstructural parameters from the SMP signal using the model proposed by Johnson and Schneebeli (1999) (Section 2.8.5, p. 49) are described in Section 4.3.1. Then the results from the mechanical calculations from the same model are stated in Section 4.3.2, p. 107. Finally, the results from spatial variability analysis of the penetration resistance are presented in Section 4.3.3, p. 109. All calculations were done for 20 grid-layers, which were identified as described in Section 2.11, p. 63. A description of each grid-layer is found in Table 4.8 below.

Table 4.8. Observed grain type and grain size, median layer thickness, and a description of each layer investigated.

Grid-layer	Grain type	Grain size (mm)	ρ (kg m ⁻³)	H^\dagger (cm)	Thickness (mm)	PWL	Comment
14a	□(∧)	1-2	287	92	15.9	PWL-1	
14b	□(∧)	1-3	287 [‡]	87	7.9	Yes	Between crusts
15a	□	0.75-1.5	263	76	3.9	PWL-1	
15b	□(∧)	1-2	263 [‡]	69	10.2	Yes	Between crusts
16a	□□	1-2	268 [‡]	70	10.1	Yes	Between crusts
20a	□	0.75-1.5	250	45	125.4	PWL-1	
20b	∧	2-4	250 [‡]	43	9.8	Yes	Between crusts
21a	∧□	1.5-2	241	40	99.2	PWL-1	
21b	∧□	1.5-3	235 [‡]	39	8.5	Yes	Between crusts
21c	∧□	2-2.5	229	37	51.8	PWL-2	
22b	⊖⊖	1.5	340	115	8.1	Yes	Above buried surface hoar
22c	⊖⊖	1.5	370	19	6.5	Yes	
22d	□□	1-1.25	288	77	9.3	Yes	Not in manual profile
23a	•/	0.25-0.75	164	167	5.7	No	
23b	•	0.25	202	167	9.4	No	
23c	•	0.25-0.5	243 [‡]	141	25.0	No	
23d	•□	0.5-1	257 [‡]	130	12.8	No	Not in manual profile
23e	⊖⊖	0.5-1	295	112	31.0	Yes	
23f	∨	15-22	200	112	10.9	PWL-3	
23g	⊖⊖	0.75-1.5	255	110	26.3	Yes	

[‡] The density of these layers was estimated from the adjacent similar layers. [†] H is the approximate height of the layer above the ground in the snow pit (Appendix A).

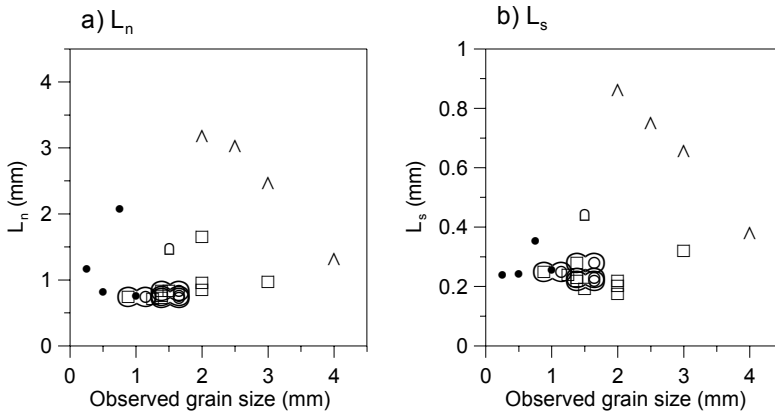


Figure 4.13. a) The microstructural element length L_n and b) L_s calculated from the SMP profiles as a function of the observed grain size in each grid-layer. For the observed grain size, the mean of the largest grains are given (largest value in Table 4.8). For L_n and L_s , the median calculated size of all measurements in the grid is plotted. Data from grid-layer 23f is left out due to the large observed grain size (15 – 22 mm, $L_n = 1.2$ mm and $L_s = 0.23$ mm). The first grain shape from Table 4.8 is used as label for each grid-layer.

4.3.1. Comparison of calculated and observed microstructural properties

The microstructural properties calculated from the SMP signal were grain size and density. These were compared to the manual observations.

Grain size

The two calculated descriptors of grain size from the SMP grid-layers were compared to the manually observed grain size from the corresponding layer (Table 4.8). These descriptors were L_n , the microstructural element length and L_s , a shape-dependent grain size. See e.g. Section 2.8.5, p. 49 for a description of the procedure. From Figure 4.13 it is apparent that none of these grain size descriptors has a good correlation with the observed grain size.

Density

The calculated density was compared to the measured density for each grid-layer. The density of some layers could not be measured with the density sampler either because the layers were too thin or because the layers were not recorded in the manual profile. For these layers, the density was estimated from adjacent similar layers. For most of the

layers in question, there was a nearby layer with similar grain shape and size, from which the density could be estimated. The error resulting from this estimation was small.

Within the range of densities between 150 to 450 kg m⁻³ found in the analyzed layers, the density calculated from the SMP profiles agreed well with the measurements in the snow pit, except for five out of six layers with facets (□) (Figure 4.14). If the six layers with facets were not considered, a linear fit between calculated ρ_{calc} and measured density ρ_{meas} gave $\rho_{calc} = 56.2 \text{ kg m}^3 + 0.78\rho_{meas}$ (shown in Figure 4.14), with $P < 0.001$.

4.3.2. Grid-layer mechanical properties

The calculated mechanical properties were the elastic modulus and the compressive strength. These values were compared to data from other studies. The temperature of the snow cover during the measurements was not considered in this analysis.

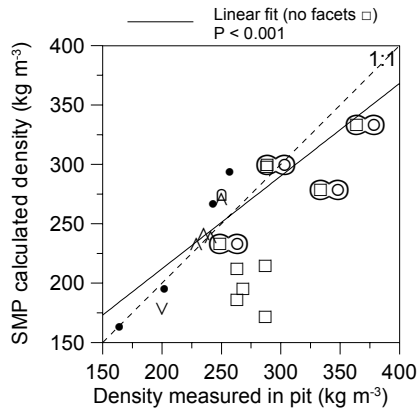


Figure 4.14. The density calculated from the SMP profiles as a function of the measured density in each grid-layer. For the SMP density, the median calculated density of all SMP measurements in the grid is plotted. When layers with facets were not considered, the linear regression gave $P < 0.001$.

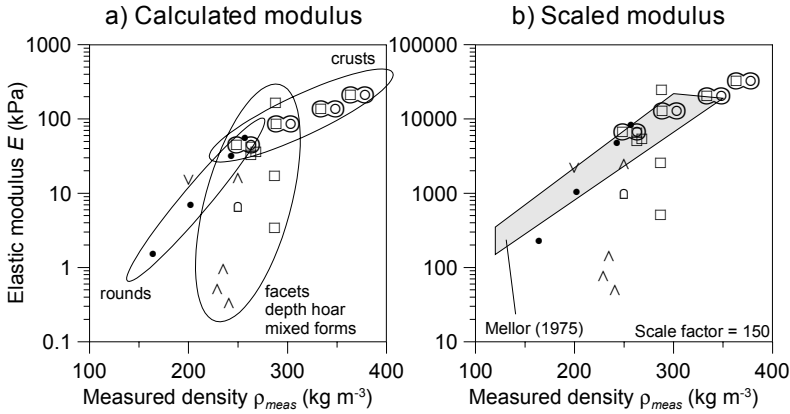


Figure 4.15. Median elastic modulus from each grid-layer calculated from the SMP profiles as a function of the density measured in the pit. a) The calculated elastic modulus. Ellipses indicate the suggested grain-shape specific log-linear relationships between density and elastic modulus. b) The calculated modulus multiplied with 150 together with the data summarized by Mellor (1975) in grey.

Elastic modulus

Calculations were made with the IDL algorithms as described in Section 2.8.6, p. 50. The median of the elastic modulus calculated from each SMP profile spanned three orders of magnitude from 0.35 to 230 kPa (Figure 4.15a). Crusts showed the highest values and depth hoar the lowest, with surface hoar, facets and round grains in between. There was a strong log-linear relationship between the elastic modulus and density. This relation was partly controlled by grain shape as indicated by ellipses for round grains (•), crusts (⊙) and facets (□) combined with depth hoar (△) in Figure 4.15a.

The elastic modulus calculated from the SMP profiles were two orders of magnitude smaller than the data summarized by Mellor (1975) and Shapiro and others (1997). The values given by Mellor are indicated by the grey area in Figure 4.15b, together with scaled values of the calculated elastic modulus. A scaling factor of 150 gave the best visual fit to the Mellor (1975) data for most of the grid-layers. Still, as shown in Figure 4.15a, some grain shapes, mainly depth hoar (△) did not follow the log-linear density trend indicated by Mellor (1975).

Compressive strength

The compressive strength calculated from the SMP profiles had a strong log-linear relation with density (Figure 4.16). Because of the way the compressive strength is calculated (equation 2.5), the distribution of the

calculated density data shown in Figure 4.14 is similar to the distribution of the compressive strength shown on a logarithmic scale in Figure 4.16. The agreement with the data summarized by Mellor (1975) is good for most grain shapes. As for the density shown in Figure 4.14, a cluster of five layers with facets (\square) did not follow the same log-linear trend as the other grain types. For this cluster, the compressive strength was around 75% lower than the value expected for layers of similar density but with different grain shape.

4.3.3. Variation of penetration resistance

The spatial variability of the mean penetration resistance in a layer $\bar{R}'_{x,y,z_{top}:z_{btm}}$ ($\equiv \bar{R}'$) was calculated as described in Section 2.12.3, p. 69.

First, the data were transformed to normality and any outliers removed. Next, the spatial variability was investigated with the geostatistical methods described in Section 2.12.4, p. 70, by first describing any slope-scale trends, and finally analyzing the residuals with the semi-variogram.

Description of spatial trend

A grid-scale trend in \bar{R}' was described as a linear function of the x and y coordinates (in m), where y was positive uphill and x was positive to the orographic left (Figure 2.2, p. 32). Significant ($P < 0.05$) linear trends happened more often in the up/down-slope direction (11 layers) than in the cross-slope direction (8 layers, Table 4.9).

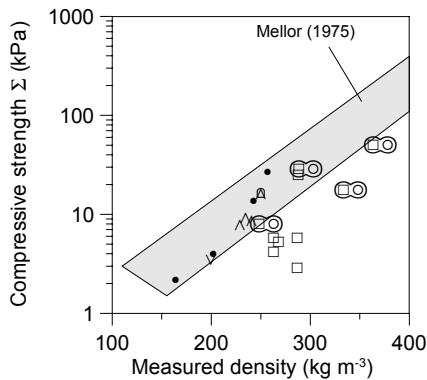


Figure 4.16. Median compressive strength from each grid-layer calculated from the SMP profiles as a function of the density measured in the pit. Data for unconfined compressive strength summarized by Mellor (1975) are shaded in grey.

Table 4.9. Regression coefficients from the linear parametric trend model on the coordinates, and results for the model semi-variogram. The trend model was $\bar{R}' = \alpha x + \beta y + c_t$, where x and y were in meters.

Grid-layer	α^\ddagger	β^\ddagger	c_t^\ddagger	R^2	Range, a_s (m)	Partial sill, c_s	Nugget, c_0	Total sill, $c_s + c_0$
14a	0.081	0.027	-2.117	0.28	5.3	0.248	0.008	0.256
14b	-0.017	0.048	-0.798	0.05	7.9	0.192	0.145	0.337
15a	0.019	-0.010	-0.883	0.07	2.1	0.032	0.038	0.07
15b	-0.006	-0.004	-0.929	0.03	>>10	-	0.023	-
16a	0.003	-0.025	-0.748	0.15	>>10	-	0.019	-
20a	-0.001	-0.010	-0.176	0.10	5.2	0.010	0	0.01
20b	-0.001	-0.008	-0.262	0.10	3.6	0.004	0.005	0.009
21a	-0.025	-0.029	-0.164	0.75	14.1	0.033	0	0.033
21b	-0.022	-0.026	-0.186	0.71	10.0	0.021	0	0.021
21c	-0.019	-0.046	-0.099	0.66	>>10	-	0	-
22b	0.004	0.032	-0.555	0.04	>>10	-	0.087	-
22c	-0.011	0.007	0.171	0.00	>>10	-	0.099	-
22d	0.000	0.019	-0.365	0.06	>>10	-	0.017	-
23a	-0.036	-0.012	-0.762	0.21	6.3	0.038	0.039	0.077
23b	-0.014	0.009	-0.884	0.17	5.8	0.028	0.024	0.052
23c	0.001	0.032	-0.703	0.17	14.5	0.035	0.005	0.04
23d	-0.004	0.050	-0.593	0.30	7.2	0.041	0.037	0.078
23e	-0.006	0.028	-0.290	0.22	>>10	-	0.006	-
23f	-0.022	0.002	-0.831	0.24	-	0	0.053	0.053
23g	-0.007	0.031	-0.860	0.25	10.6	0.016	0.008	0.024

Regression coefficients where $P < 0.05$ are shown in bold type. Units are: ‡ ($\log_{10}(N)$ m^{-1}), ‡ ($\log_{10}(N)$), ‡ ($(\log_{10}(N))^2$).

Most of the significant ($P < 0.05$) regression coefficients in the up-slope direction were negative (7 of 11), indicating that an increase in \log_{10} -transformed values of \bar{R} (and therefore in the mean layer penetration resistance \bar{R}) in the down-slope direction was more typical than an increase in the up-slope direction. The trends were not in the same direction for all snow layers within a grid, but differed for individual snow layers within a grid: in layer 23a, the up-slope trend was negative, while the other investigated layers in the same grid had positive trends in the up-slope direction. However, all other layers with significant trends within the same grid had the same direction of any significant trends.

The linear model of the trend was not always appropriate. Scatter plots of the data (with outliers removed) from grid-layer 22d are shown for the x and y direction in Figure 4.17. A least squares fit of a quadratic regression of the form $\bar{R}' = c_1 + c_2x + c_2y + c_3xy + c_4y^2 + c_5x^2$ to the data gave $P < 0.001$ for grid-layer 22d. The resulting quadratic surface is

shown together with the linear trend model in Figure 4.17. Near the top of the grid (larger values of y), the local trend reversed. The linear trend model was not able to capture such trends. Grid-layer 22d was a typical example of the non-linear trends in the 20 grid-layers. In general, near the edges of many grids, especially near the bottom or top like in grid-layer 22d, the local trend changed, or even reversed. For such grid-layers, the trend would have been better described with a higher order trend model than the first order (linear) trend model used here.

Spatial structure after trend removal

The spatial structure of the residuals from the trend analysis was described with the semi-variogram. All grid-layers were checked for directional anisotropy in the four directions 0° , 45° , 90° and 135° , with $\pm 22.5^\circ$ tolerance. Three grid-layers (21a, 21b and 23b) showed minor anisotropy with a slightly shorter range in the up-slope direction (0°) than in the cross-slope (90°) direction. In all three cases, the difference in range was < 1 m and the difference in the sill was $< 0.001 (\log_{10}(N))^2$. These differences were likely within the error of the estimation of the range and sill. All model semi-variograms were therefore fitted to omnidirectional sample semi-variograms. All model semi-variograms are shown in Appendix D, and four typical examples in Figure 4.18.

Three types of spatial structures were found after removal of the linear trend: 1) pure nugget semi-variance, 2) semi-variograms that increased without bound, and 3) semi-variograms with range $a_s < 10$ m. Examples of each of the three types are shown in Figure 4.18.

Pure nugget: As the only grid-layer, the residuals of grid-layer 23f (buried surface hoar, Table 4.8, p. 105) did not show any additional spatial structure after the linear trend removal. The variance remaining after the trend removal (nugget plus sill) was close to the median value for all grid-layers at $0.053 (\log_{10}(N))^2$.

Unbounded: Seven grid-layers were modeled by virtually unbounded semi-variograms. These would have been better modeled by power- or linear functions (e.g. Cressie, 1993). For these grid-layers, the linear trend-model did not effectively describe the grid-scale trend or the range was larger than the 10 m used for the semi-variogram model.

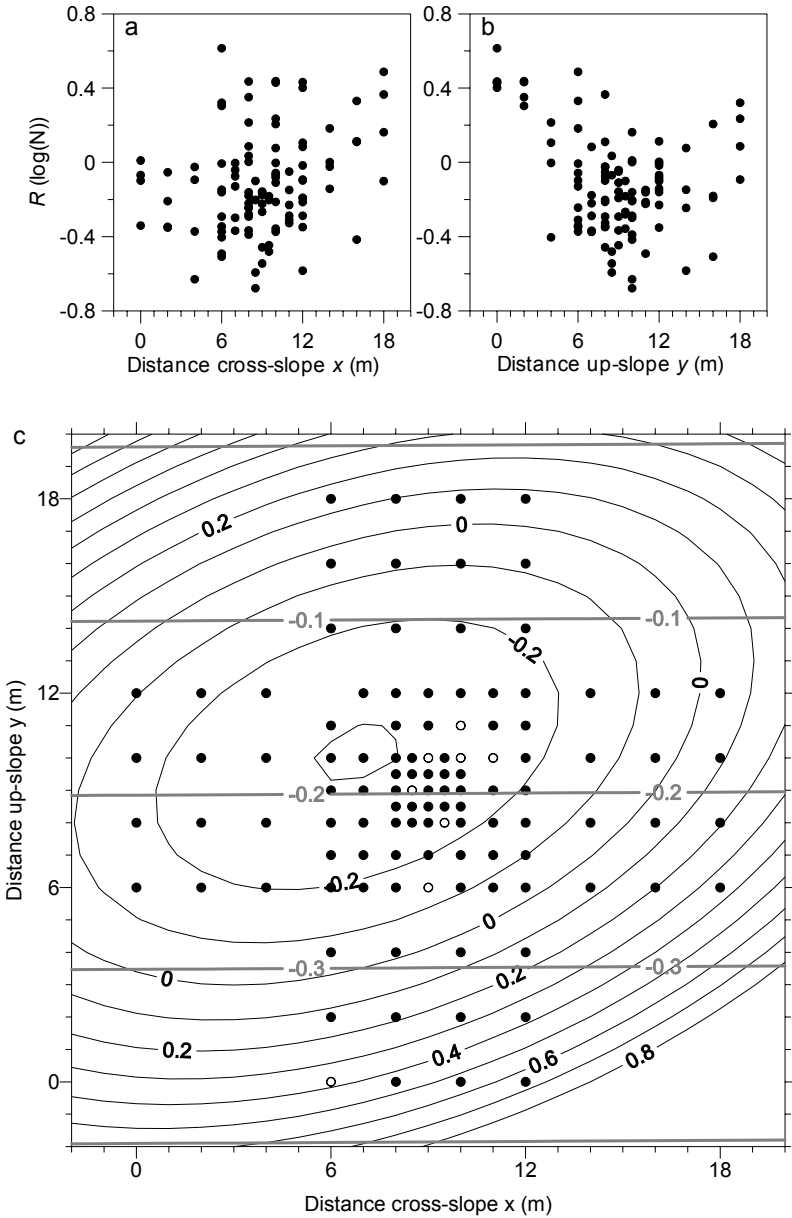


Figure 4.17. a) Penetration resistance as a function of the x and b) the y coordinate. c) Linear (thick grey contour lines) and quadratic (thin black contour lines) trend surfaces for grid-layer 22d. Circles in c) indicate the location of SMP measurements, with open circles indicating the location of outliers that were removed before the analysis.

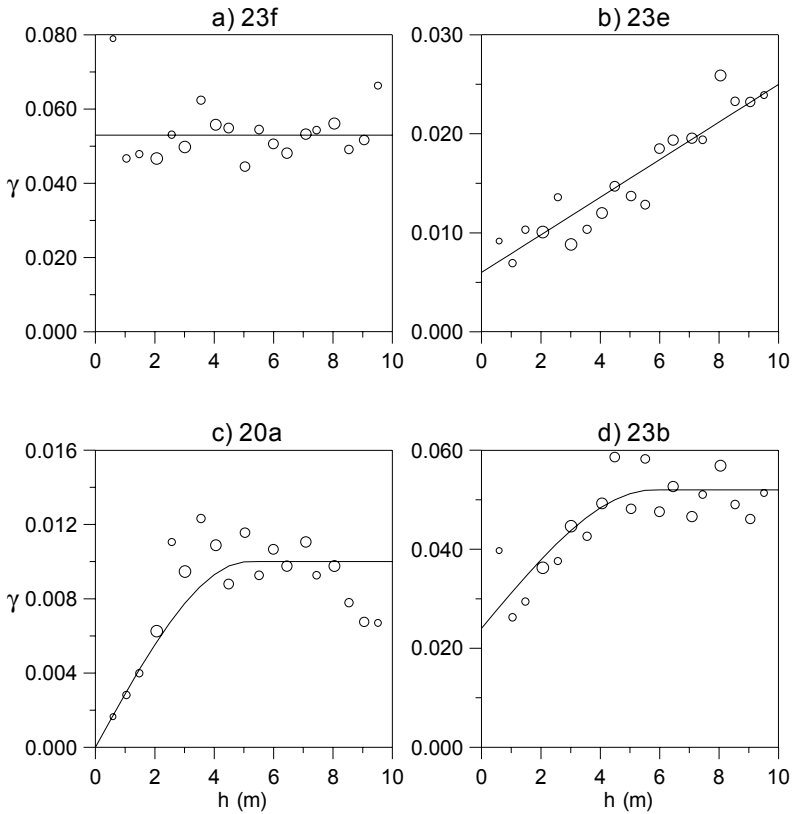


Figure 4.18. Examples of the three types of spatial structure found in the grid-layers after removal of a slope-scale trend. a) Pure nugget semi-variogram model for grid-layer 23f. b) Model semi-variogram increasing without bound for grid-layer 23e. c) And d) model semi-variogram for grid-layers 20a and 23b for which a sill was reached and a range could be determined.

Identifiable range: In the 12 remaining grid-layers, a range could be estimated. However, in four of those, the estimated range was ≥ 10 m. Although the sample semi-variograms indicate a sill towards at the longest lag distances used for the model, extrapolation of the models beyond the 10 m lag distance was uncertain. Still, it must be expected that for these four grid-layers, the range was smaller than the extent of the grid. The model semi-variograms for the eight remaining grid-layers are shown in Figure 4.19. The smallest range found was around 2 m.

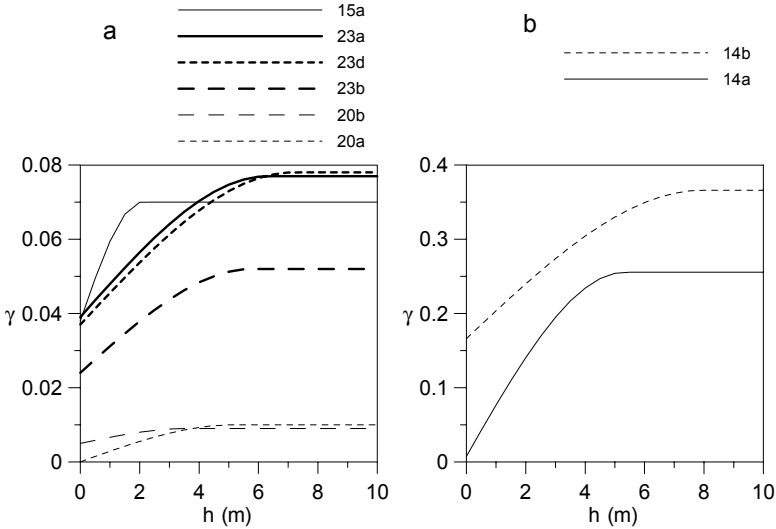


Figure 4.19. A comparison of the eight semi-variograms which reached a sill at a range < 10 m. a) Grid-layers in grids 15, 20 and 23, and b) grid-layers in grid 14. Note the difference in the two γ scales.

Grid-layers 14a and 14b had total sill variances that were an order of magnitude larger than in the remaining grid-layers. The median of the transformed penetration was within the range of the other grid-layers (Table 4.10).

Grid-layer 22b had the highest nugget variance of the model semi-variograms (Table 4.9). In this grid-layer, the linear model was inadequate for a good description of the trend (Figure 4.17). When the residuals from the quadratic trend surface were used to calculate the sample semi-variogram, the model parameters for the model semi-variogram changed considerably. Instead of an almost pure nugget model, a spatial structure with range $a_s = 6.4$ m and sill $c_s = 0.004 (\log_{10}(N))^2$ was found. The nugget $c_0 = 0.03 (\log_{10}(N))^2$ was in the same order of magnitude as the other nuggets (Table 4.9), except for the grid-layers in grid 14.

For some semi-variograms (e.g. grid-layers 23f and 23b, Figure 4.18), the smallest lag-distance had a high semi-variance compared to the value for next-lowest lag-distance. The reason for this is not clear, but it could be due to disturbance of the snow cover while measuring in the inner part of the grid where the measurement locations were close together.

Non-spatial statistical description of variation

The variability of the penetration resistance in each grid-layer was described with non-parametric non-spatial statistics (Table 4.10). The statistics are given for the data before and after removal of a trend. The QCV values in Table 4.10 must be interpreted carefully because they depend on the central tendency of the data, which might be close to zero (e.g. grid-layer 22c).

The median semi-interquartile range SIQR and the quartile coefficient of variation QCV both dropped around 50% after removal of slope-scale trends. The two grid-layers from grid 14 had more variation than the grid-layers in the other grids both before and after trend removal.

Table 4.10. Summary statistics for the transformed penetration resistance in the grid-layers investigated.

Grid-layer	N	Median		Before trend removal		Residuals	
		\bar{R}' ($\log_{10}(N)$)	$10^{\bar{R}'}$ (N) [‡]	SIQR ($\log_{10}(N)$)	QCV [†] (%)	SIQR _{res} ($\log_{10}(N)$)	QCV _{res} [†] (%)
14a	46	-1.130	0.074	0.39	33	0.24	18
14b	38	-0.783	0.165	0.36	66	0.11	18
15a	105	-0.814	0.153	0.20	25	0.04	6
15b	110	-1.011	0.097	0.09	9	0.02	2
16a	111	-0.916	0.121	0.13	13	0.05	5
20a	113	-0.309	0.490	0.07	22	0.02	7
20b	109	-0.328	0.470	0.05	16	0.02	5
21a	109	-0.594	0.255	0.13	22	0.08	13
21b	108	-0.565	0.272	0.11	20	0.08	12
21c	103	-0.634	0.232	0.11	19	0.10	14
22b	101	-0.357	0.439	0.26	58	0.06	28
22c	91	0.100	1.259	0.19	268	0.02	17
22d	103	-0.161	0.690	0.17	98	0.05	25
23a	110	-1.195	0.064	0.17	14	0.07	6
23b	112	-0.961	0.109	0.13	13	0.04	4
23c	112	-0.413	0.386	0.11	27	0.06	16
23d	108	-0.164	0.686	0.25	134	0.10	55
23e	111	-0.102	0.791	0.08	74	0.06	59
23f	106	-1.050	0.089	0.16	15	0.04	4
23g	113	-0.656	0.221	0.10	15	0.06	10
<i>Median</i>	-	<i>-0.614</i>	<i>0.243</i>	<i>0.13</i>	<i>22</i>	<i>0.06</i>	<i>13</i>

[‡] The back-transformed value of the median. [†] The QCV values should be interpreted carefully because the statistical distribution of the data is centered close to zero, sometimes giving unreasonable high values of relative spread.

4.3.4. Causes of variation in penetration resistance

Three possible causes of the variation in penetration resistance were investigated: layer thickness, layer depth, layer hardness, and the manually observed grain size of the layers. The variability descriptors that were investigated were the semi-interquartile range of the transformed penetration resistance \bar{R}' SIQR, and the nugget c_0 . The range a_s and sill c_s were investigated for semi-variograms that reached a sill within 15 m.

Layer thickness

The effect of layer thickness on the variability of penetration resistance was investigated a) within each grid-layer, and b) for the median penetration resistance between all the grid-layers.

For 15 of the 20 investigated grid-layers, there was a significant ($P < 0.05$) linear relationship between the thickness of the layer and its transformed penetration resistance (Table 4.11). For 12 of the 15 significant relations, the regression coefficient was positive, indicating a higher penetration resistance for the thicker parts of the grid-layers (e.g. grid-layer 23c shown in Figure 4.20a).

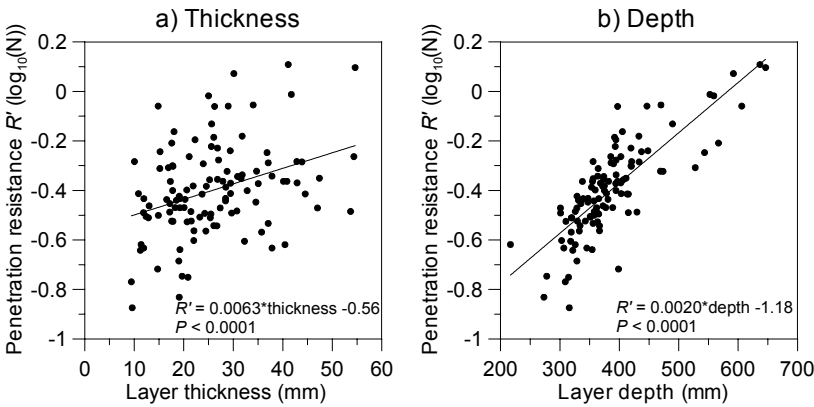


Figure 4.20. a) The effect of layer thickness and b) layer depth on penetration resistance for grid-layer 23c. The ordinary least squares linear fit for each regression is given.

Table 4.11. Regression coefficients for ordinary least square fitted linear regression of the grid-layer thickness and depth on the penetration resistance. Coefficients marked in bold type were significant ($P < 0.05$).

Grid-layer	N	Thickness ($\log_{10}(N) \text{ mm}^{-1}$)	Depth ($\log_{10}(N) \text{ mm}^{-1}$)
14a	46	0.0101	0.0013
14b	38	-0.1030	-0.0004
15a	105	-0.0485	-0.0008
15b	110	0.0291	0.0004
16a	111	0.0313	0.0005
20a	113	0.0002	0.0003
20b	109	0.0084	0.0002
21a	109	0.0010	0.0002
21b	108	0.0224	0.0002
21c	103	0.0006	0.0001
22b	101	0.0239	0.0019
22c	91	-0.0857	-0.0023
22d	103	0.0212	0.0015
23a	110	0.0268	0.0039
23b	112	0.0279	0.0043
23c	112	0.0063	0.0020
23d	108	0.0207	0.0024
23e	111	0.0095	0.0011
23f	106	-0.0090	0.0006
23g	113	0.0045	0.0011

When the grid-layers were compared to each other, there was a large scatter in the relation between the median layer thickness, the non-spatial spread SIQR (Figure 4.21a) and the median \bar{R}' (Figure 4.21b). However, there was an indication that thinner layers had a larger SIQR than thicker layers.

For the spatial variability descriptors, there was a relation between the range and the layer thickness (Figure 4.22a). For thinner layers, the range was smaller than for thicker layers. A \log_{10} -linear fit was not significant ($P = 0.11$) when all points were included. However, if the thick layer of mixed forms (\square) were not included in the fit, the fit was significant ($P = 0.008$, ordinary least squares).

The nugget variance was related to the median layer thickness with higher nugget values for thinner layers. When the four data points with zero nugget were left out, a \log_{10} - \log_{10} regression gave $P = 0.003$.

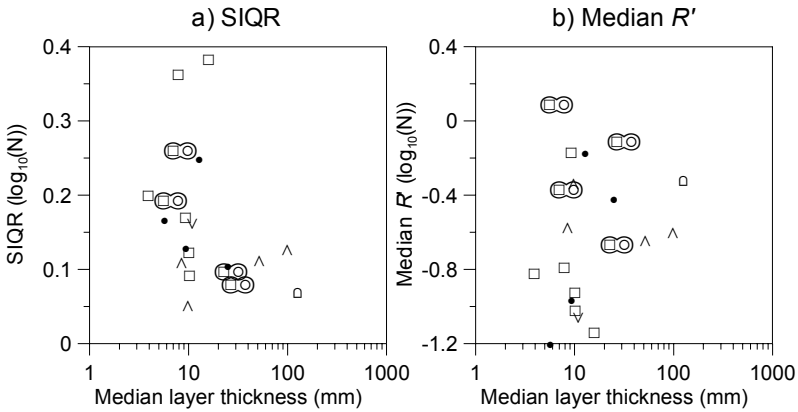


Figure 4.21. a) The semi-interquartile range SIQR for the transformed penetration resistance, and b) the median transformed penetration resistance as a function of the median layer thickness for the 20 grid-layers investigated.

Layer depth

The effect of layer depth on the variability of the penetration resistance was investigated for a) each individual grid-layer, and b) the median for all grids. The layer depth was calculated from each SMP profile in the surface perpendicular direction. The depth was from the snow surface to the top of the layer.

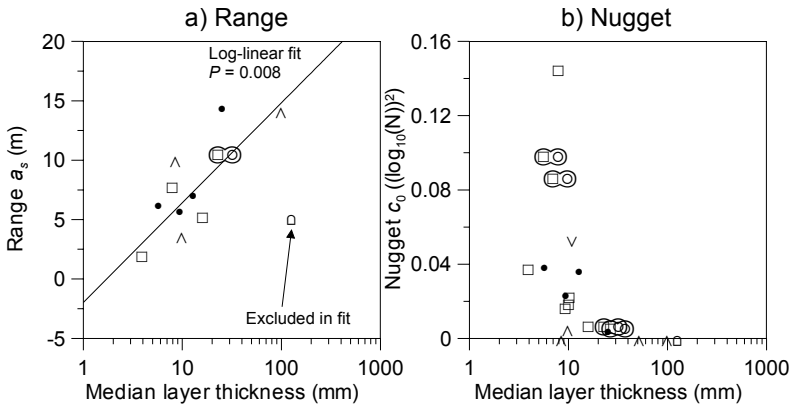


Figure 4.22. a) The range a_s and b) the nugget c_0 as a function of the median layer thickness. The log-linear regression line shown in a) excludes the thickest layer of mixed forms.

For individual grid-layers, there was a significant ($P < 0.05$), linear relation between the depth of the layer at a certain location and its penetration resistance at that location, for 17 out of the 20 grid-layers (Table 4.11). One of the fits with least scatter is shown in Figure 4.20b for grid-layer 23c. The regression coefficients in 15 of the 17 grid-layers were positive, indicating that at locations where the layer was deeper in the snow cover, the penetration resistance was larger than where the layer was shallower.

The median layer depth for the grid-layers showed no significant relations with the non-spatial and the spatial variability parameters.

Layer penetration resistance

Layers with higher penetration resistance had higher quartile coefficients of variation, both before and after trend removal ($P < 0.001$) (Figure 4.23).

Manually observed grain size

Neither the spatial variability descriptors nor the non-spatial descriptors were related to the manually observed grain size in each layer (i.e. the variation in penetration resistance was not related to grain size).

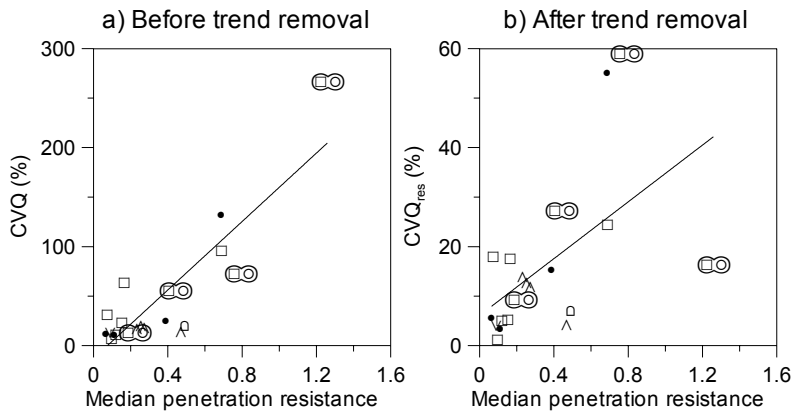


Figure 4.23. The quartile coefficient of variation of transformed penetration resistance as a function of the median penetration resistance, which has been back transformed.

Table 4.12. A list of the five layers that were analyzed for variation of stability and penetration resistance. ν is the regression coefficient for a linear regression between drop height and penetration resistance (see text for closer description). The value of ν for grid-layer L1, marked in bold type, was significant ($P < 0.05$).

Layer	SMP grid-layer	Stability grid-layer	Grain shape	Grain size (mm)	Depth H (cm)	ν (cm (log ₁₀ (N)) ⁻¹)
L1	14a	14A	□(∧)	1-2	91.9	40.01
L2	15a	15A	□	0.75-1.5	76	-28.25
L3	21c	21A	∧ □	2-2.5	37	78.01
L4	23a	23B	• /	0.25-0.75	167	2.40
L5	23f	23A	∨	15-22	111.5	21.63

4.4. Comparison of point stability and penetration resistance

Of the 21 grid-layers defined from the stability tests and the 20 grid-layers defined in the SMP profiles, five grid-layers were the same layer in the snow cover. These five weak snow layers are named L1 to L5 as shown in Table 4.12. The data from the five layers were compared in two ways. First, the data from each individual grid was investigated. At the locations where both a stability test and a SMP profile were made, their results were compared. Second, the variability of the stability tests and the variability measured by the SMP were compared for the five layers.

4.4.1. Comparison within each grid-layer

For each of the grid-layers L1 to L5 the relation between drop height and penetration resistance was investigated. The point stability tests were done in pairs of two in 12 pits in each grid (Figure 2.2, p. 32). Between each stability test pair, an SMP profile was measured. The average drop height of the two stability tests in each of the 12 pits was compared to the transformed penetration resistance in the pit. Instead of the average drop height, the minimum and maximum drop height in each pit was also investigated. The results for the minimum and maximum drop height were similar to the results from the average drop height (see below). The comparison was done for each of the five layers. The regression was $DH = \nu \bar{R}' + C_{DH,R}$, where DH was in cm and \bar{R}' in log₁₀(N).

Only in grid-layer L1 there was a significant correlation ($P < 0.05$) between DH and penetration resistance (Table 4.12). The correlation was positive, indicating that the largest drop heights were associated with the harder parts of the weak layer. The layer consisted of facets and some depth hoar crystals (Table 4.12). In four of the five grid-layers, the relation between drop height and penetration was also positive.

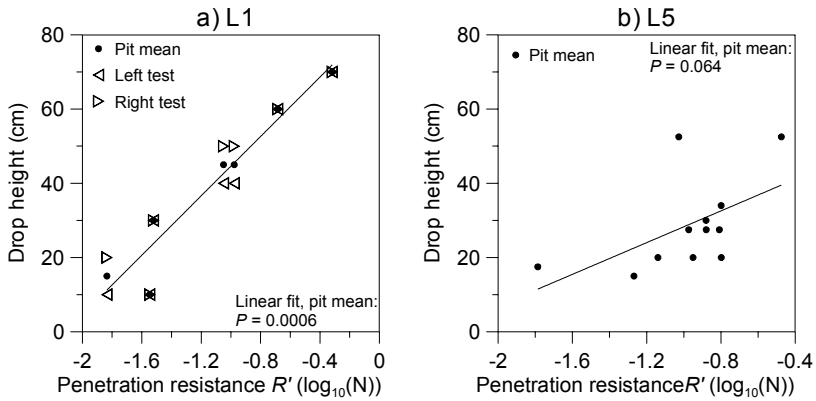


Figure 4.24. The average drop height DH in each stability pit as a function of the transformed penetration resistance in the fracture layer in the pit. a) For grid-layer L1, and b) for grid-layer L5. L1 did not fracture at all stability test locations.

4.4.2. Comparison between grid-layers

For each of the five grid-layers L1 to L5, the stability variation was compared to the variation of penetration resistance. The following descriptors of variability were compared: the trend in the up-slope (y) and the cross-slope direction (x), the semi-interquartile range before (SIQR) and after trend removal (SIQR_{res}) and the quartile coefficient of variation before (QCV) and after trend removal (QCV_{res}). Of these parameters, only the QCV was independent of the units used and could be directly compared. For the other parameters, the aim was to investigate whether the values were proportional. Because there were only five grid-layers for the comparison, no quantification of the relationships were made. The data from the grid-layers were compared visually.

Only the SIQR and the up-slope trend showed any relation between the two methods, while the remaining descriptors of variability showed only scatter. Figure 4.25a) indicates that the SIQR of the transformed penetration resistance was proportional to the SIQR for the drop height. However, without grid-layer L1, the points in Figure 4.25a) would be randomly scattered. The comparison of the regression coefficient β for the up-slope direction is shown in Figure 4.25b). Positive values of β indicate an increase of measured values (drop height and penetration resistance) in the up-slope direction. The trends were proportional, but the limited number of grid-layers used does not allow a thorough analysis of the relation.

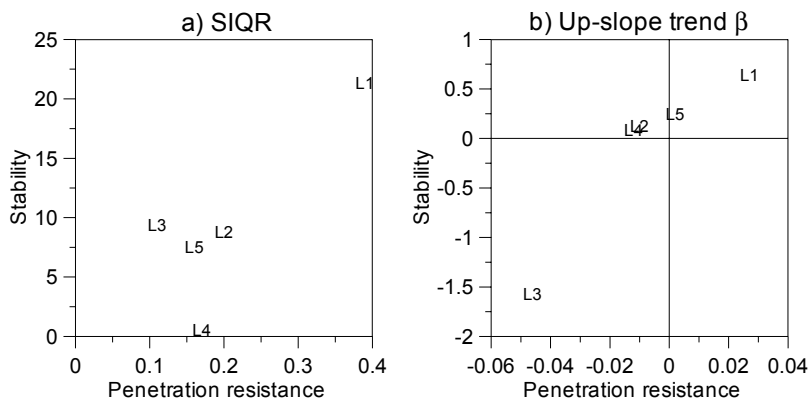


Figure 4.25. A comparison of a) the semi-interquartile range for the stability test results and the transformed penetration resistance in the five grid-layers that were analyzed for both measurement methods. b) A comparison of the regression parameter β from the linear trend model for the stability results and the SMP measurements. Positive values of β means an increase in the measured value in the up-slope direction. Labels refer to the grid-layer name (Table 4.12).

Chapter 5

Discussion

5.1. Introduction

The aim of this study was to quantify the spatial variability of the snow cover on typical avalanche slopes. This was achieved by a number of objectives. The first objective was to choose the appropriate measurement methods. The rammrutsch stability test RR and the snow micro-penetrometer SMP had never before been extensively used in the field before this study. The suitability of the two methods for the study is discussed in Section 5.2. The two methods were found usable for the aim of the study. Objectives 2 to 5, to measure and characterize spatial variability, were accomplished by making spatially distributed measurements in a grid that covered a large part of small slopes, and analyzing the results with geostatistical methods. Before discussing the results from the spatial analysis of stability and penetration resistance in Section 5.4, some problems and limitations with the snow stratigraphy definition used in the present study are discussed in Section 5.3. The final objective of the study is to discuss possible implications of snow cover spatial variability for dry snow slab avalanche release, which is done in Section 5.5. Finally, some practical implications of the results from this study are discussed in Section 5.6.

5.2. Measurement methods

Because the two main measurement methods used in this study, the rammrutsch test and the snow micro-penetrometer, had not been used intensively in the field before, it was appropriate to ask whether they worked, and what they measured.

5.2.1. Stability tests

The primary aim of field based snow stability evaluation with respect to fast surface loading is to identify the existence of critical weak layers or

weak interfaces within the snow cover. If no critical weak layer exists, the snow cover can be considered relatively stable (stability class "very good" in Schweizer and Wiesinger, 2001), because slab avalanches begin with a shear failure of a weak layer (McClung, 1987). Secondary, but still important, is an estimation of the amount of extra load it will take to initiate a fracture in the weak layer. Snow stability tests identify weak layers and measure the extra load needed to initiate a brittle fracture in a weak layer or weak interface at the test location.

The rutschblock RB stability test (Föhn, 1987a) is the most widely used stability test to identify weak layers and assess the extra load needed to initiate a fracture (Schweizer, 2002). The results from the rammrutsch RR test were compared with the results from the RB test. The median RR drop height generally increased with increasing RB scores for the same weak layer (Figure 4.1, p. 88). The RR test results can therefore be used to interpret point stability of the snow cover in a similar way to the RB test. Influence of the slope inclination on the test results was only found for a few grid-layers. Stewart (2002) used the drop hammer stability test to study stability variations. The test is very similar to the rammrutsch test used in this study. Stewart (2002) also found limited dependence between stability and slope inclination. Jamieson and Johnston (1993) found that the slope inclination does not affect the RB test score as long as the slope inclination is more than 30°. Due to energy dissipation through the snow column, the drop height was expected to increase with increasing slab depth. Such a relationship was found for about half of the grid-layers (Table 4.5, p. 97). None of the significant regressions were negative (increasing drop height with decreasing slab thickness) as reported by Stewart (2002) for a few grid-layers. No relation between slab thickness and drop height was found when comparing all grid-layers in this study. This emphasizes that the relation between drop height and slab thickness is unique for each weak layer, i.e. the weak layer properties are important for the variation of weak layer properties.

The spread of the drop height values for each RB score was considerable, with a drop height interquartile range for RB scores 3 to 7 of at least 20 cm (Figure 4.1, p. 88). A drop height of e.g. 20 cm was within the quartile range for RB scores 3 to 7. Such a large spread is not unique for the RR test. In all comparisons of stability test results, there is a large scatter (Jamieson, 1999; Birkeland and Johnson, 1999; Stewart, 2002). The scatter is not only due to different measurement types with different measuring support; some of the tests have the same support and are very similar from the type of impact. In the present study, the

amount of data used for the comparison between the RR test and the RB test was limited. Further, the spread of RR drop height values found in this study was largely due to spatial variation of point stability within the grids. In order to achieve a better relation between the RR and the RB results, more tests must be done, preferably close to each other. The point stability tests within a grid identified the same weak layers (Figure 4.12, p. 104) although the snow micro-penetrometer profiles showed that most layers were found in all measurements within a grid. The practical implications of this result are discussed further in Section 5.6, p. 135.

The median SB drop heights for a given RB score were higher than the median RR drop heights for the same RB score (Figure 4.1, p. 88). Considering the larger drop weight of 4.5 kg for the SB test compared to the drop weight of 1 kg for the RR test this might seem surprising. However, the snow filled in the stuff-sack was soft and reduced the impact energy considerably by deforming at the impact with the shovel. The hardness of the snow in the stuff-sack changed during the day due to mechanical breakdown and sintering of the grains, which especially on warm days was noticed by the operator. Because the energy transfer from the stuff-sack to the column changed with the hardness of the snow in the stuff-sack, SB results could vary over a day and between days. Variability in the SB results was therefore not only caused by the snow cover. This was the main reason for switching to the RR test in the beginning of the second winter.

The median fracture depth showed some relation with the semi-interquartile range of the drop height (Figure 4.8, p. 98). The relationship was no longer present after removing the slope-scale trend found in the drop height ($SIQR_{res}$). This was surprising because the increased number of blows from the drop hammer and the increased number of fractures between the studied weak layer and the surface was hypothesized to increase the sources of error for deeper weak layers. The results are promising for the interpretation of the stability tests, because the instrument proved less susceptible to errors in thicker slabs than expected.

5.2.2. Snow micro-penetrometer

Microstructural properties

The empirical relationship between the snow micro-penetrometer (SMP) penetration resistance and snow density proposed by Pielmeier (2003) gave good results (Figure 4.14, p. 107). This is encouraging because most mechanical snow cover properties are related to density (Mellor,

1975). However, as Mellor points out, the texture of the snow also influences the relationship.

The two descriptors of grain size calculated from the snow micro-penetrometer (SMP) profiles showed a large scatter when compared with the manually observed grain size observed for the grid-layers in the snow pit (Figure 4.13, p. 106). There are at least four reasons for this. First, and most important, it might not be appropriate to compare the manually observed and the calculated grain sizes. The manually observed grain size is a measure of the grain size of individual grains, even though these can be bonded tightly together, while the SMP signal measures the size of microstructural elements, which can consist of multiple grains. I would therefore expect that the microstructural element length L_n calculated from the SMP should be larger than the observed grain size, and that this effect would be strongest for layers with well-bonded grains such as crusts. Figure 4.13a shows that this is not the case: L_n is consistently smaller than the observed grain size in crusts. In general, L_n overestimates the manually recorded grain size as often as it underestimates it. Because L_s is calculated from L_n (and as a function of density), it is clear that also L_s does not agree well with the observed grain size. Second, manually observing grain size is a difficult task that is subjective and observer-dependent (Baunach and others, 2000). However, most profiles were made by one experienced observer, and the grain size observations should be both consistent and exact. Third, the procedure of locating fractures in the signal (Section 2.8.7, p. 51) could be incorrect despite the promising results shown by the analysis of simulated signals (Section 2.8.8, p. 53). The size of the SMP tip is an order of magnitude larger than the smallest grains observed in the natural snow cover. In layers with small grains, there will be many grains in contact with the tip at any time, and the fracture of small microstructural elements will happen very often. Locating every fracture is crucial to the correct interpretation of the microstructural element length. Fourth, the calculation of L_n assumes isotropic microstructural elements. While this assumption is acceptable for some grain shapes it does not hold for other grain shapes such as well-developed depth hoar grains, which are observed to build vertical chains of grains, making anisotropic elements. A way to integrate information about possible grain anisotropy is to include a statistical descriptor of grain anisotropy in the model used to determine the microstructural properties (Johnson, 2003a). A recent expansion of the mechanical theory used in this study (Johnson and Schneebeli, 1999) by Johnson (2003b) might provide a better description of the snow microstructure. It is suggested that the new theory be applied to the SMP signal in a further study. Getting the

description of the microstructural elements right is an important step for a correct determination of the mechanical snow cover properties such as the elastic modulus.

Mechanical properties

The calculated values for the elastic modulus E for the grid-layers show a strong log-linear relation to density (Figure 4.15a, p. 108) also found in other studies (e.g. Mellor, 1975, p. 258). However, the elastic modulus values calculated from the SMP profiles in this study were two orders of magnitude smaller than the values summarized by Mellor (1975). There are three reasons for this discrepancy. First, the results summarized by Mellor (1975) are not directly comparable to the measurements in the present study in terms of the methods used. In the density range of interest for this study, between 100 and 400 kg m⁻³, the data summarized by Mellor (1975) come from tests with slower deformation rates, which plays a role because the elastic modulus depends on strain rate. Second, the mechanical theory used to calculate the elastic modulus in this study (Johnson and Schneebeli, 1999) describes the snow – tip interaction in a way that might be too simple. However, the observed log-linear relationship between an independently measured density and E is assuring that the theory can be used to calculate at least an index of the elastic modulus of snow. The highest values found in the present study are in the lower range of the four values reported by Johnson and Schneebeli (1999). Based on the larger data set by Mellor (1975), the elastic modulus of snow is probably 100 to 200 times larger than the values calculated in the present study. A scaling factor of 150 is proposed. The mechanical model presented by Johnson (2003b) might better describe the interaction of the tip and the snow grains. The use of this model might also help the interpretation of the SMP signal in terms of elastic modulus in the future. Third, E is temperature dependent (Mellor, 1975). A direct comparison of E measured at different temperatures must therefore be made with caution. In the present study, the temperature during SMP measurements was not considered. However, the temperature-dependence of E is not enough to explain the scaling factor of 150 needed to scale the presently calculated values of E to previously reported values.

Even if the calculated elastic modulus is only an index value, the results presented here suggest that for a narrow density range, there is a wide range of values of elastic moduli (Figure 4.15a, p. 108). This has recently also been shown by Schneebeli (in press), who reports a large range of values for calculated elastic moduli for snow within a constant density. Independent measurements of the effect of grain shape and

density on elastic modulus are currently underway (Hempel, 2003) and should be compared with SMP measurements of the same snow.

The compressive strength of the layers was in good agreement with values summarized by Mellor (1975) (Figure 4.15b). Five of the six layers with facets as the primary grain shape had a lower compressive strength than expected from the data summarized by Mellor (1975), who did not include faceted grains in the summary. The layers with depth hoar had a higher compressive strength than five of the six layers with facets. A similar result was found by Bradley and others (1977) and later by Schneebeli and others (1999). The results from the present study confirm that compressive strength as well as the elastic modulus is dependent on grain shape.

The use of the SMP for field measurements of mechanical snow cover properties is promising. However, more validation of the properties calculated from the SMP must be done with independent measurements. In addition to the elastic modulus and compressive strength discussed here, the interpretation of shear strength of weak layers should also be attempted, since this would enable a more direct link to snow stability. Once the interpretation of relevant snow mechanical properties from the SMP signal has been validated, a spatial analysis of important properties, e.g. shear strength of weak layers, can be done. The results of such an analysis will be an important step towards more realistic input to numerical models of snow cover stability, which currently have very simple assumptions about the variability of the snow cover (Schweizer, 1999).

5.3. Classification of snow cover stratigraphy

Before discussing the spatial variability results, the important issue of defining stratigraphy is discussed, based on the observations (not specific measurements and investigations) made during the study.

The snow stratigraphy (layering) constitutes the slope-perpendicular (vertical) variability of the snow cover (Seligman, 1936; Colbeck, 1991). In this study, stratigraphic layers were defined from the SMP profiles and from the stability tests. The method of defining stratigraphy from the SMP signal has previously been briefly discussed by Pielmeier and Schneebeli (2003), Birkeland and others (in press) and Kronholm and others (in press-b). However, there is a need to deal more intensively with the problem of classifying the snow cover into layers. The following discusses four limitations of the present analysis of spatial variability of layer properties.

First, it must be made clear that the problem of defining layers is not unique to the layers seen in the SMP profiles. Manual snow cover profiles are made by classifying the observed layers in a snow pit based on grain shape, grain size and hardness. It is well known that the recorded stratigraphy depends on the purpose of the profile, although this is seldom stated. A profile of a snow cover recorded by an avalanche forecaster who is interested in the presence of weak layers for evaluating snow stability will likely not include the same layers as a profile made by a hydrologist who is interested in the water content of the snow cover and the routing of melt water within the snow.

Second, the layers defined from the SMP signal were the most prominent ones in the snow cover (Section 2.11, p. 63, Figure 2.18, p. 64). It was not attempted to analyze all layers within each grid. This introduces a bias towards layers that are present everywhere because the layers that are not found everywhere in a grid are not as easy to deal with. From the geostatistical side, the problem is how to describe a layer that not only has varying properties, but also is sometimes present, sometimes not. From the practical side, the discontinuous layers are problematic because the layer cannot be assumed present in all SMP profiles, something that was found to be helpful while defining the layer boundaries. The first problem can be solved by using appropriate geostatistical methods, while the second problem requires a more sophisticated and user-friendly way of displaying the SMP signals for the operator or finding a way to automatically construct layers from each SMP profile. It was not attempted to solve these problems in the present study, but in order to describe the variability of all layers within the snow cover, a solution must be found. For such an analysis, other methods of defining layer boundaries and of analyzing their properties must be used.

Third, the penetration resistance varied in the slope-perpendicular direction within each of the defined layers (Figure 2.19, p. 65), as also described by Pielmeier and Schneebeli (2003). I avoided this three-dimensional variability by only characterizing the slope-parallel variability of the mean penetration resistance in the slope-perpendicular direction within each layer. This approach completely ignores the observed slope-perpendicular variation in the penetration resistance at the layer-scale. To characterize the three-dimensional variability of snow layers, a three-dimensional geostatistical analysis similar to that done for reservoir modeling (e.g. Sahimi, 2003) or in mining (e.g. Journel and Huijbregts, 1978) could be done.

Fourth, boundaries between layers were observed to be gradual transitions between layers rather than sharp interfaces, as also observed

by Pielmeier and Schneebeli (2003) and Birkeland and others (in press). This is partly due to the size of the tip, but Pielmeier and Schneebeli (2003) estimated that the layers thicker than 1 mm can be detected from the SMP signal. In the present study, layer transitions were observed to be 1 to 5 mm thick with a median around 2 mm (Kronholm and others, in press-a). The observed transitions of penetration resistance between layers are therefore real and not an artifact of the instrument support (the size of the SMP tip). Pielmeier and Schneebeli (2003) calculate the slope-perpendicular force gradients between adjacent layers because it is recognized that hardness differences in adjacent layers are important for slab avalanche release (Schweizer, 1993; Schweizer and Lütschg, 2001). They do not relate their results with measurements of point stability. If gradients of penetration resistance between adjacent layers are important for slab avalanche release, the transition zones must be studied in more detail and characterized. Such an investigation is possible with the data from the present study, but was not undertaken.

5.4. Spatial variability

The aim of this study was to quantify spatial variability of penetration resistance and stability on typical avalanche slopes. Previous studies of point stability all show that stability varies on the slope-scale, but none of the studies had quantified the variation in a spatial setting. This was because the studies either did not have enough measurements on each investigated slope (e.g. Conway and Abrahamson, 1984, 1988) or did not use spatial statistics to characterize the variability (Jamieson and Johnston, 1993; Jamieson, 1995). To have enough stability tests on a slope, fast column-type stability tests were used for these measurements. Other mechanical snowpack properties than stability are also known to be spatially variable both in the slope-perpendicular and in the slope-parallel direction (Colbeck, 1991). Because snow layers are the result of distinct meteorological events, the variability was expected to differ for individual layers. As pointed out by Pielmeier and Schneebeli (2003), layers are the basic unit in the snow cover, and should be studied separately for a complete description of the snow cover variability. The only instrument that allowed such a characterization was the snow micro-penetrometer (SMP) (Schneebeli and Johnson, 1998), which measures the penetration resistance of snow. Hence, for individual layers the spatial variability of penetration resistance was studied.

The spatial structure of stability and penetration resistance on the investigated slopes showed complex but not random patterns. The patterns were described as a slope-scale trend plus residual variation. The trend was modeled as a linear function of the measurement position. Most investigated grid-layers had slope-scale trends. The residuals were analyzed as a random field with spatial autocorrelation by characterizing their spatial structure with the semi-variogram.

One column-type stability test out of 585 tests (165 the first winter, 420 the second and third) fractured during preparation of the snow column. Another few columns fractured by placing the stability test equipment (shovel or plate) on the isolated column. Locations of low point stability always had adjacent tests that were also of low stability. Deficit zones where numerous tests beside each other fractured during column preparation were observed by Conway and Abrahamson (1984) near the crown lines of fresh avalanches. Such areas were not observed in this study, where measurements were done on slopes that had not avalanched. In view of fast sintering first predicted by Salm (1975) and restated by Schweizer (1999), and demonstrated for a collapsed weak layer (Figure 4.7, p. 96) investigated in this study, deficit zones (if they exist) are not likely to persist for long in the snow cover, and the chance of measuring one in the field is small. Except for Conway and Abrahamson (1984), no other studies of stability have found areas of deficit neither with column-type stability tests (Birkeland, 2001; Stewart, 2002; Landry, 2002) nor with the rutschblock stability test (Föhn, 1989; Jamieson and Johnston, 1993; Jamieson, 1995). Considering these results, it seems more likely that such deficit zones evolve during the fracture process only and are not inherently present on snow slopes. Further, realizing that the preparation of snow columns is delicate work it is suggested that column-type stability tests where the column fractures during preparation should not be interpreted as deficit zones, but as locations of low point stability. The procedure of including or excluding snow columns that fractured during sample preparation must be clearly stated.

Slope-scale trends constituted a large part of the observed variability for both stability and penetration resistance. The semi-interquartile range SIQR for both stability and penetration resistance decreased on average by 50% after trends were removed (Table 4.4, p. 92 and Table 4.10, p. 115). Similarly, the quartile coefficient of variation QCV decreased on average by about 30% after trend removal. Slope-scale trends in stability have been found in other studies. Conway and Abrahamson (1988) mention that their stability results from one

slope appeared to have a spatial trend in stability. Slope-scale trends in stability were also found by Stewart (2002, p. 80) and Landry (2002, p. 87) although he only briefly mentions it. The trends found on the slopes have three important consequences. 1) Although stability is spatially variable, this variation is not random over short distances as suggested by Munter (1997, 2003), but has spatial structure. 2) Non-spatial descriptors of variability have little meaning as already pointed out by Conway and Abrahamson (1984). 3) Methods for evaluation of stability in the field must account for such trends (Section 5.6 below).

The maximum coefficient of variation CV for stability of 107% found in the present study (Table 4.4, p. 92, corrected with equation 2.10) was higher than any previously reported value for column-type stability tests, except those by Conway and Abrahamson (1984). As described above, they assigned tests that fractured during preparation a very low value, and their measurements were made at the crowns of fresh avalanches. However, the median CV of 50% in the present study was comparable to the values reported by Stewart (2002). Other studies (e.g. Landry, 2002) report lower values. These values all include a slope-scale trend. In the absence of a trend, the median CV in this study was 33%, which is close to the variation reported by Föhn (1989) and Landry (2002), although the study sites used by Landry (2002) were on slopes that were quite sheltered from wind.

Significant linear trends in stability and penetration resistance were more often observed in the up/down-slope direction than in the cross-slope direction (Table 4.3, p. 90 and Table 4.9, p. 110). This was likely a consequence of the relatively short slopes chosen for the measurements. The slopes were normally shorter (length in the *y*-direction) than they were wide (length in the *x*-direction) (e.g. Figure 2.3, p. 33). The upper and/or lower part of the grids was therefore more likely to be influenced by edge effects than the sides of the grids. Jamieson and Johnson (1993) found that towards the top of slopes their point stability results changed, and suggested that this was due to different wind and solar exposure, causing a change in stratigraphy. The effect is likely similar at the bottom of slopes. Conway and Abrahamson (1984) and Föhn (1989) also suggest that wind is an important cause of spatial variability of stability. The practical implications for this are discussed in Section 5.6 below.

Trends in grid-layers within the same grid were mostly in the same direction. This was the case for both stability and penetration resistance (Table 4.3, p. 90 and Table 4.9, p. 110). This suggests that the topography affects the trends more than the depositional factors such as

wind speed and direction, which are often different for each depositional event, or that the topography modifies the effect of the depositional factors during the depositional event. Stewart (2002) performed stability tests in the same three study sites in two following winters, but did not find the same spatial patterns. He attributes this to different slab characteristics, which were strongly related to his stability results. This suggests that topography exercises a strong control on stability patterns but that other factors also influence these patterns.

There were too few stability tests done within each grid to produce reliable semi-variograms except for a few grid-layers where most stability tests produced fractures. These grid-layers showed little spatial structure of the residuals after trend removal (Figure 4.2, p. 91) (Kronholm and Schweizer, 2003). Stewart (2002) also calculated semi-variograms for his drop hammer stability results and reports that no spatial structure was found, even with more than 100 tests, a constant spacing of 60 cm and an extent of around 15 m. There are two explanations for the lack of spatial structure. First, there might be no additional spatial structure apart from a slope-scale trend. Second, the semi-interquartile ranges for the drop height residuals after trend removal had a median around 5 cm (Figure 4.3, p. 93), which is close to the precision of the test method. In this case, to describe any structure apart from a trend, a better (more precise) test would therefore be needed in order to decrease the nugget variance, which is associated with measurement errors (Cressie, 1993). The practical relevance of both cases is that if the slope-scale stability trend can be described, the variation around this trend (the residuals) is not important for stability evaluation. Further, if the trend can be described, spatial extrapolation of point stability is possible, at least at the slope-scale.

The 21 semi-variograms calculated from the SMP measurements showed many types of spatial structure around the spatial trend. It was found that the spatial structure of penetration resistance does not depend on grain type, with the possible exception of buried surface hoar. Buried surface hoar is a common weak layer in slab avalanches. The buried surface hoar layer 23f had no additional spatial structure in the penetration resistance after removal of the significant linear slope-scale trend. All other layers had a spatial structure around the trend. Surface hoar is known to form only during low wind speeds (Hachikubo and Akitaya, 1997). Based on just one example, I suggest that absence of wind during the deposition process leads to spatially continuous layers and low variability at scales larger than 1 m, but not necessarily on smaller scales. Spatial variability at scales smaller than 1 m could not be

recognized in our measurements because the minimum spacing in the grid was 0.5 m. Hard layers in the snow cover can be attributed to high wind speed during deposition (e.g. Seligman, 1936).

Grid-layer 23A was the same surface hoar layer, but identified in the stability tests. Also for the stability test results, there was a significant trend, but the residual drop heights had an additional spatial structure. The spatial variabilities of two different mechanical properties (penetration resistance and stability) measured with different instruments do not have the same spatial structure. This is also due to the stability being a function of slab and weak layer, while the penetration resistance is only a property of the weak layer.

In seven grid-layers of the 21 investigated, the variance increased without bound and no range could be determined. In four other grid-layers, the sill was reached at a range ≥ 10 m, in which case the estimation of the range was poor. The lack of a finite sill could have two reasons. 1) The linear trend was not appropriate to describe the fluctuation of the data at the grid-scale for the eleven layers. A quadratic or higher order trend might have been better. 2) The range might be longer than 10 m. If this had been the case, a better model of the trend would lead to a pure nugget model semi-variogram. In this case, the range could only have been found by increasing the extent of the grid.

For eight grid-layers of 21 investigated, the model semi-variograms reached a sill at a range < 10 m. The ranges varied between 2 m and 8 m (Table 4.9, p. 110). Neither the range, nor the sill and the nugget were related to the observed grain shape and size in the layer. The residual spatial structure (after trend removal), of grid-layers was not similar for grid-layers within a grid. It was therefore not possible to predict the spatial variability of a grid-layer on the slope-scale based on its grain shape and grain size. In view of the individual character of each depositional event (in terms of wind direction, wind speed, temperature and snow fall intensity, which are assumed to vary), it is not surprising that the outcome of each event has a different spatial structure. Metamorphism subsequent to the deposition will further complicate the spatial structure over time. To investigate the influence of factors such as wind, wind speed, temperature and snow fall intensity on the variability of snow layers formed during a depositional event, meteorological data must be investigated in more detail than in the present study. Such a study might show whether certain types of weak layers and slabs (e.g. surface hoar and thick wind slabs) have typical spatial structures. If so, the spatial structure of individual layers could be modeled by using meteorological data.

5.5. Implications for dry snow slab avalanche release

Slab avalanche release starts with an initial fracture in a weak layer. If the initial fracture reaches a certain critical area, the fracture propagates through the weak layer until the unsupported slab above reaches a critical size where the peripheral slab strength is overcome (Schweizer and others, 2003a). Fracture initiation properties of the snow cover for rapid near surface loading were measured with the stability tests. The continuity of the weak layers was investigated with the snow micro-penetrometer. Fracture initiation properties varied over the investigated slopes, primarily in the form of a slope-scale trend. The variation was to a certain degree caused by changes in slab thickness. From areas of a slope where the slab is thicker, it was harder to initiate a fracture in the weak layer. The investigated weak layers were present in all snow micro-penetrometer measurements on the slopes. The weak layers therefore provided potential fracture propagation pathways where propagation would not be halted due to a lack of weak layer. The penetration resistance of the investigated weak layers changed within the grids, mostly as a slope-scale trend with an additional autocorrelated spatial structure. It is not known how well the penetration resistance describes the fracture propagation properties of the weak layer, which likely are determined by a combination of shear strength, compressive strength and fracture toughness. Until such a relation has been established, it is not possible to say whether the variation in weak layer properties is large enough to arrest a fracture. However, once fast fracture propagation has started there will likely be enough energy released at the tip of the fracture to propagate through a weak layer with varying strength and toughness.

5.6. Practical consequences

5.6.1. Grid layout

The layout of the SMP grid was made without knowledge about the spatial structure of the penetration resistance in the layers. With the results presented above, it is possible to estimate how efficiently the grid-layout captured the spatial variability. However, it is important to realize that the variability found was influenced by the grid-layout, thus preventing a completely independent evaluation of the layout. The optimal grid-layout is only possible to design if the spatial variability is

known and grid-design is therefore an iterative process. The semi-variogram was modeled to a distance of 10 m. At larger distances, the number of point pairs in each lag-bin declined (Figure 2.1, p. 31) possibly resulting in erratic semi-variance values. In over half of the grid-layers, the sill was not reached within 10 m. For these layers, a larger extent of the grid (resulting in more point pairs at larger lag-distances) would have made it possible to identify a sill at a longer distance than 10 m. Since the number of measurements per day was limited, a larger extent could have been made by reducing the minimum spacing in the grid. This would increase the nugget variance in the semi-variograms. Four grid-layers had zero nugget variance. In the remaining 16 grid-layers, the grid-layout did not capture the full variability at a scale smaller than 0.5 m, assuming the measurement error was negligible. To capture the small-scale variability, a smaller minimum spacing would have been needed. In summary, the extent of the grid should have been larger for some grid-layers, while for others the minimum spacing should have been smaller. The optimal grid-layout depends on the aim of the study and the available measurement methods and specifically on the number of measurements that can be made. Future studies must decide which scale is more important and change the grid-layout accordingly.

5.6.2. Stability evaluation

The column-type stability tests used in this study did not produce fractures in all test locations, although the weak layer was observed and assumed relevant for slab avalanche release. This is important because stability test methods that do not detect all weak layers relevant for slab release must be used and interpreted carefully. The reason for the lack of fractures in some locations could either be changes in snow cover properties in adjacent measurement locations, or because the stability tests were not reliable as a measure of point stability. Because of the chance of not locating a weak layer with one test (of the type used in this study), a number of tests must be done, and stability test results be supplemented with other stability information (Föhn, 1987a). Föhn (1989), Jamieson and Johnston (1993) and Jamieson (1995) do not report this problem for their grids of rutschblock tests, possibly the rutschblock test integrates a larger area, thereby smoothing any small-scale variations.

Some grid-layers had a large stability trend, causing changes of drop heights of more than 40 cm over a distance of 10 m (Table 4.3). In this case, the stability interpretation based on a single stability test could change from unstable in one point on the slope to stable in a point less

than 10 m away. Typical trends were in the order of a 10 cm change in drop height over 10 m, which would correspond to a change in stability of 0 to 2 RB scores, which corresponds well with results published by Jamieson (1995). This has practical implications for the use of stability tests for field-based stability evaluation. On a single slope, more than one stability test should be done with a considerable distance between them to reveal any trends. This was also suggested by Conway and Abrahamson (1988). Jamieson and Johnston (1993) suggested that the distance between two tests should be at least 10 m. In view of the measurements presented here, 10 m between two tests would be enough to reveal any significant trend in one direction, provided there was no small-scale variation (including error) in the test results. For column-type stability tests, two or more tests should be placed beside each other to reduce the chance of not identifying a weak layer (see discussion above). The stability trends found in this study were more often in the up/down-slope direction. This was also found by Stewart (2002, p. 81). If more than one stability test is done on a slope to reveal a slope-scale trend, it might therefore be better to do the tests along the fall line than across the slope. However, because stability testing is done to identify instabilities in the snow cover, the results from the present study suggest that stability tests should be located towards the top of slopes rather than towards the bottom of slopes. This finding is likely not globally applicable, but rather due to the choice of slopes in this study. On some slopes studied by Jamieson (1995), stability increases towards the top.

The slope-scale trends and variation in point stability at the slope-scale shown in this study interacts with evaluations of regional scale snow stability. Snow stability at the regional scale has been shown to have a certain distribution of stabilities (Schweizer and others, 2003b). Some of this regional variation is due to the variation at the slope-scale. Upscaling of stability-variations found on the slope-scale to the regional scale will be important for further studies of regional stability.

5.6.3. Including spatial variability in models

Schweizer (1999) suggested introducing statistical variation in layer properties in future models of snow stability. Current models do not include such variation. With the spatial variability results described in this study, this is possible for penetration resistance at the slope-scale with the geostatistical descriptors given in Table 4.9, p. 110. The penetration resistance can be related to properties relevant for slab avalanche release: the layer density (Figure 4.14, p. 107), the elastic modulus

(Figure 4.15, p. 108), and the compressive strength (Figure 4.16, p. 109). Other properties of relevance to the slab release process and not investigated here, are the viscosity and the fracture toughness of the snow layers. The spatial variability of these properties must be investigated in the future.

Current models of snow stability use mechanical snow cover parameters that are estimated based on the layer density. As shown by Mellor (1975) and in Figure 4.15, p. 108, there is a relation between density and elastic modulus and compressive strength. However, for a specific density, the values for elastic modulus span at least two orders of magnitude and the values for compressive strength span one order of magnitude. Sturm and others (1997) show that this is also the case for thermal conductivity in snow. Current stability models therefore underestimate the complexity of the snow cover. To improve this, there is a need to include more realistic stratigraphy in the models as well as spatial variability of layer properties.

Presently used snow cover simulation models (e.g. Lehning and others, 1999) are one-dimensional and do not include spatial variation in layer properties. One way to move from a one-dimensional model to a model that predicts an areal snow cover is to run the model at many grid-points and interpolate the layer boundaries. This approach would require highly resolved meteorological input data, which currently does not seem feasible (Raderschall and others, 2003). Alternatively, stochastic variation of layer properties could be introduced to each layer. The size of stochastic component could be controlled by the meteorological conditions, of which wind is likely the most important (Sturm and Benson, in press). In addition to the stochastic variation, the spatial structure of the variation could be modeled by an autocorrelation function for each layer. For such a model, more studies of the influence of wind and other meteorological parameters on the spatial structure of snow layers must be made.

Chapter 6

Conclusions

6.1. Summary

Measurements of penetration resistance and point stability were made on potential avalanche slopes above timber-line. Measurements were distributed in a grid that covered 18 m x 18 m of a slope. In each of the 10 grids analyzed, 24 stability tests, 113 penetration resistance profiles and one stratigraphic profile was done. Based on fractures in the point stability tests, 21 weak layers were identified and analyzed. From the penetration resistance profiles, 20 layers were identified and analyzed. The relation between penetration resistance of layers and measured grain size, measured layer density, and point stability was investigated. Spatial variability of the penetration resistance in each layer was modeled as a linear slope-scale trend and its residuals. The spatial structure of the residuals was characterized by a range, sill and nugget obtained from semi-variograms.

6.2. Conclusions

By combining various measurements methods, it was possible to investigate the spatial variability of an Alpine snow cover on potential avalanche slopes with high spatial resolution. The point stability results from the rammrutsch tests were related to the rutschblock score, which is related to snowpack stability. The stability test results confirm that more than one point stability test should be done in combination with other observations, to evaluate snow stability. The point stability was related to the slab thickness, and to a smaller degree to the slope inclination.

Penetration resistance profiles enabled identification of individual layers in the snow cover. The layer density calculated from the penetration resistance with an empirical formula was found to agree well

with the layer density measured with conventional methods for most grain shapes. The length of microstructural elements and the grain size was calculated from the penetration resistance signal by using a signal-processing algorithm and a mechanical model based on foam penetration theory. The two calculated size-parameters showed a large scatter when compared to the manually observed grain sizes. This was partly attributed to the different way grain size is defined for the manually observed grain size and the calculated grain size, and partly to the simplicity of the mechanical model.

The elastic modulus calculated with the mechanical model agreed qualitatively well with previous data. Good quantitative agreement could be obtained by multiplying with a factor of 150. It was suggested that the discrepancy was due to the signal-processing algorithm and the simple mechanical model used. Towards the end of the study, a less simple model became available. It should be used in future studies. The calculated compressive strength agreed well with previously reported values. There was a large spread in the values of elastic modulus and compressive strength for a narrow range of densities. Independent measurements of elastic modulus and compressive strength must be made for a comparison with the values calculated from the penetration resistance signal. In addition, shear strength is important for avalanche formation and its relation to the penetration resistance should be investigated.

The snow micro-penetrometer is a promising instrument for snow studies where a large number of objective measurements must be made. However, since 50% off all penetration resistance profiles were unusable for analysis due to technical problems, the reliability of the instrument must be improved. The present study is the first to intensively make use of the snow micro-penetrometer in a field-based study. Consequently, this study presents valuable first results on mechanical and structural properties of an Alpine snow cover for individual layers.

In the penetration resistance profiles, it was observed that in most cases, penetration resistance varied gradually between adjacent layers. The thickness over which the penetration resistance gradually changed was 1 to 5 mm. Despite the gradual transition of penetration resistance between layers, it was possible to identify distinct layers based on penetration resistance. These distinct layers, both hard and soft, were found in all measurements within a grid, but less distinct layers could not be identified in all profiles.

One weak layer failed while working on the slope. The slab did not release but it was displaced around 1 cm in the down-slope direction.

Stability tests made after the fracture showed that the weak layer gained strength within 1 to 2 hours. This observation has never previously been made.

The spatial variation of penetration resistance and point stability was found to have spatial structure. Around 40% of the spatial variability of point stability and penetration resistance in the snow layers was accounted for by a linear slope-scale trend. In some layers, a non-linear trend was present. The quartile coefficient of variation around the linear trend was about 20% with a maximum of 50% for the point stability measurements. These values were similar to previous comparable studies. The penetration resistance data were log-normally distributed in the layers, and all analyses were made with transformed penetration resistance data. The quartile coefficient of variation for the transformed penetration resistance was around 15% with a maximum of 60%. No other studies have quantified the variability of individual layers. Layers with larger penetration resistance had larger quartile coefficients of variation. The harder slab layers are likely deposited during windy conditions, suggesting that high wind increases spatial variability of penetration resistance in layers.

The spatial structure of the variation around the slope-scale trend was quantified with the semi-variogram. The 24 point stability tests in each grid did not provide enough data for a complete geostatistical analysis of the residual structure of the point stability variation. The structural analysis of the penetration resistance data showed that individual layers have distinct spatial structures. Adjacent layers also had different spatial structures. The maximum length of autocorrelation varied from around 2 m to a distance longer than 10 m. The complex spatial structure of the penetration resistance in the layers requires a spatial analysis in which trends and semi-variograms are fitted specifically to each individual layer. A description of the spatial structure of variability should accompany or be used instead of classical measures of variation like the coefficient of variation. The present study was the first to characterize the spatial variability of individual layers in the snow cover.

Weak layers of relevance to snow slab avalanche release were identified in all penetration resistance profiles within the grids. The critical size of a crack needed for fast fracture propagation is 1 to 10 m (Schweizer, 1999). Within this length, the variability of penetration resistance was largely in the form of a spatial trend. This suggests that once a fracture starts to propagate fast in a weak layer, the fracture will not be stopped due to the varying properties of the weak layer. The

exact relation between penetration resistance and fracture propagation properties of weak layers requires more investigations.

6.3. Outlook

Regional scale variations in stability are important for the avalanche warning service. The slope-scale variability investigated in this study must be coupled with the regional scale snowpack stability. Results from the present study suggest that trends extend to a larger scale than the grids measured. Increasing the measurement extent will require more measurements if the minimum spacing of 0.5 m between measurements as in this study is used. By using the results of the spatial analysis presented here, the sampling strategy may be enhanced.

The measurements presented here are only a snapshot of the snow cover spatial variability. It is thought that the spatial variability of the snow cover is related to its stability. Because avalanche forecasters have to predict the future avalanche danger, the temporal change of the variability is of interest and should be studied.

The variability of individual layers might be related to the meteorological conditions during the deposition. To test this hypothesis, meteorological conditions during layer formation must be measured and compared with the variability of each layer.

The slope-perpendicular variability of properties within layers in the snow cover must be investigated further. To provide an objective and fast way to classify layers in the snow cover, a study of the boundaries between layers should focus on developing an algorithm that locates layer boundaries automatically. This would enable a more complete investigation of the snow cover than made here, e.g. through the identification of discontinuous lens-like layers.

The geometric properties such as depth and thickness of the snow layers must be characterized to complete the description of the snow cover made in this study. This is possible with the presented data, but remains to be done.

References

- Ashby, M.F., Palmer, A.C., Thouless, M., Goodman, D.J., Howard, M., Hallam, S.D., Murrell, S.A.F., Jones, N., Sanderson, T.J.O. and Ponter, A.R.S., 1986. Nonsimultaneous failure and ice loads on arctic structures, Proceedings of the 18th Annual Offshore Technology Conference. Houston, Texas, USA, May 5-8, 1986: 399-404.
- Bader, H., Haefeli, R., Bucher, E., Neher, J., Eckel, O. and Thams, C., 1939. Der Schnee und seine Metamorphose. Beiträge zur Geologie der Schweiz - Geotechnische Serie - Hydrologie. Zurich, 340 pp.
- Baunach, T., Fierz, C., Satyawali, P.K. and Schneebeili, M., 2000. A model for kinetic grain growth. *Ann. Glaciol.*, **31**, 1-6.
- Benson, C.S. and Sturm, M., 1993. Structure and wind transport of seasonal snow on the Arctic slope of Alaska. *Ann. Glaciol.*, **18**, 261-267.
- Bian, L. and Walsh, S.J., 1993. Scale dependencies of vegetation and topography in a mountainous environment of Montana. *Prof. Geogr.*, **45** (1), 1-11.
- Birkeland, K.W., 1997. Spatial and temporal variations in snowpack stability and snowpack conditions throughout the Bridger Mountains, Montana. Ph.D., Arizona State University, Arizona, U.S.A., 205 pp.
- Birkeland, K.W., 1998. Terminology and predominant processes associated with the formation of weak layers of near-surface faceted crystals in the mountain snowpack. *Arctic and Alpine Research*, **30** (2), 193-199.
- Birkeland, K.W., 2001. Spatial patterns of snow stability throughout a small mountain range. *J. Glaciol.*, **47** (157), 176-186.
- Birkeland, K.W., Hansen, H.J. and Brown, R.L., 1995. The spatial variability of snow resistance on potential avalanche slopes. *J. Glaciol.*, **41** (137), 183-189.
- Birkeland, K.W. and Johnson, R.F., 1999. The stuffblock snow stability test: comparability with the rutschblock, usefulness in different snow climates, and repeatability between observers. *Cold Reg. Sci. Technol.*, **30** (1-3), 115-123.

- Birkeland, K.W., Kronholm, K., Schneebeil, M. and Pielmeier, C., in press. Changes in the shear strength and micro-penetration hardness of a buried surface hoar layer. *Ann. Glaciol.*, **38**.
- Blöschl, G., 1999. Scaling issues in snow hydrology. *Hydrol. Process.*, **13**, 2149-2175.
- Blöschl, G. and Sivapalan, M., 1995. Scale issues in hydrological modelling - a review. *Hydrol. Process.*, **9**, 251-290.
- Bradley, C.C., Brown, R.L. and Williams, T.R., 1977. Gradient metamorphism, zonal weakening of the snowpack and avalanche initiation. *J. Glaciol.*, **19** (81), 335-342.
- Chalmers, T.S. and Jamieson, J.B., 2001. Extrapolating the skier stability of buried surface hoar layers from study plot measurements. *Cold Reg. Sci. Technol.*, **33** (2-3), 163-177.
- Chalmers, T.S. and Jamieson, J.B., 2003. A snow-profile-based forecasting model for skier-triggered avalanches on surface hoar layers in the Columbia Mountains of Canada. *Cold Reg. Sci. Technol.*, **37** (3), 373-383, doi:10.1016/S0165-232X(03)00077-6.
- Chernouss, P.A., 1995. Spatial and time variability of avalanche predictors and accuracy of their estimations. In: Sivardière, F. (Editor), *Les apports de la recherche scientifique à la sécurité neige, glace et avalanche*. Chamonix, France, 30 May-3 June 1995: 123-128.
- Colbeck, S.C., 1991. The layered character of snow covers. *Rev. Geophys.*, **29** (1), 81-96, doi:10.1029/90RG02351.
- Colbeck, S.C., Akitaya, E., Armstrong, R., Gubler, H., Lafeuille, J., Lied, K., McClung, D. and Morris, E., 1990. The international classification for seasonal snow on the ground. International Association of Scientific Hydrology. International Commission on Snow and Ice, Wallingford, Oxfordshire, 23 pp.
- Colbeck, S.C. and Jamieson, J.B., 2001. The formation of faceted layers above crusts. *Cold Reg. Sci. Technol.*, **33** (2-3), 247-252.
- Conway, H. and Abrahamson, J., 1984. Snow stability index. *J. Glaciol.*, **30** (116), 321-327.
- Conway, H. and Abrahamson, J., 1988. Snow-slope stability - a probabilistic approach. *J. Glaciol.*, **34** (117), 170-177.
- Cressie, N.A.C., 1993. *Statistics for spatial data*. Revised edition. Wiley series in probability and mathematical statistics. John Wiley & Sons, New York, 900 pp.

- Cressie, N.A.C. and Hawkins, D.M., 1980. Robust estimation of the variogram, I. *Journal of the International Association for Mathematical Geology*, **12**, 115-125.
- de Quervain, M.R., 1950. Die Festigkeitseigenschaften der Schneedecke und ihre Messung. *Geofisica pura e applicata, Bd. XVIII*, 4-15.
- Dowd, T., and R.L. Brown, 1986. A new instrument for determining strength profiles in snow cover. *J. Glaciol.* **32**(111), 299-301.
- Dozier, J., Davis, R. and Perla, R., 1987. On the objective analysis of snow microstructure. In: Salm, B. and Gubler, H.U. (Editors), *Avalanche Formation, Movement and Effects*. Davos, Switzerland, 14-19 September 1986. IAHS Publication 162, 49-59.
- Durand, Y., Giraud, G., Brun, E., Mérindol, L. and Martin, E., 1999. A computer-based system simulating snowpack structures as a tool for regional avalanche forecasting. *J. Glaciol.*, **45** (151), 469-484.
- Fierz, C., 1998. Field observation and modelling of weak-layer evolution. *Ann. Glaciol.*, **26**, 7-13.
- Föhn, P.M.B., 1987a. The "Rutschblock" as a practical tool for slope stability evaluation. In: Salm, B. and Gubler, H.U. (Editors), *Avalanche Formation, Movement and Effects*. Davos, Switzerland, 14-19 September 1986. IAHS Publication 162: 223-228.
- Föhn, P.M.B., 1987b. The stability index and various triggering mechanisms. In: Salm, B. and Gubler, H.U. (Editors), *Avalanche Formation, Movement and Effects*. Davos, Switzerland, 14-19 September 1986. IAHS Publication 162: 195-214.
- Föhn, P.M.B., 1989. Snow cover stability tests and the areal variability of snow strength, International Snow Science Workshop. Whistler, British Columbia, Canada, 12-15 October 1988: 262-273.
- Gibson, L.J. and Ashby, M.F., 1997. *Cellular Solids: structure and properties*. 2nd edition. Cambridge University Press, Cambridge, 510 pp.
- Good, W., 1987. Thin sections, serial cuts and 3-D analysis of snow. In: Salm, B. and Gubler, H.U. (Editors), *Avalanche Formation, Movement and Effects*. Davos, Switzerland, September 1986, 14-19 September 1986. IAHS Publication 162: 35-48.
- Gubler, H.U., 1975. On the rammsonde hardness equation, IAHS Publication 114: 110-121.
- Gubler, H.U. and Hiller, M., 1984. The use of microwave FMCW radar in snow and avalanche research. *Cold Reg. Sci. Technol.*, **9**, 109-119.

- Hachikubo, A. and Akitaya, E., 1997. Effect of wind on surface hoar growth on snow. *J. Geophys. Res.*, **102** (D4), 4367-4373.
- Haeberli, W., 1975. Untersuchungen zur Verbreitung von Permafrost zwischen Flüelapass und Piz Grialetsch (Graubünden). Ph.D. thesis, ETH, Zurich, 221 pp.
- Haeberli, W., Alean, J.-C., Müller, P. and Funk, M., 1989. Assessing risks from glacier hazards in high mountain regions: some experiences in the Swiss Alps. *Ann. Glaciol.*, **13**, 96-102.
- Harper, J.T. and Bradford, J.H., 2003. Snow stratigraphy over a uniform depositional surface: spatial variability and measurement tools. *Cold Reg. Sci. Technol.*, **37** (3), 289-298.
- Hempel, F., 2003. E-modul Messungen vom Schnee. SLF Internal report.
- Hägeli, P. and McClung, D.M., 2003. Avalanche characteristics of a transitional snow climate—Columbia Mountains, British Columbia, Canada. *Cold Reg. Sci. Technol.*, **37** (3), 255-276, doi:10.1016/S0165-232X(03)00069-7.
- Insightful Corporation, 2001. S-Plus 6 Robust Library User's Guide. Insightful Corporation, Seattle, WA, 182 pp.
- Jamieson, J.B., 1995. Avalanche prediction for persistent snow slabs. Ph.D. thesis, University of Calgary, Calgary AB, Canada, 258 pp.
- Jamieson, J.B., 1999. The compression test - after 25 years. *The Avalanche Review*, **18** (1), 10-12.
- Jamieson, J.B. and Johnston, C.D., 1993. Rutschblock precision, technique variations and limitations. *J. Glaciol.*, **39** (133), 666-674.
- Jamieson, J.B. and Johnston, C.D., 1998. Refinements to the stability index for skier-triggered dry slab avalanches. *Ann. Glaciol.*, **26**, 296-302.
- Jamieson, J.B. and Johnston, C.D., 2001. Evaluation of the shear frame test for weak snowpack layers. *Ann. Glaciol.*, **32**, 59-68.
- Jamieson, J.B. and van Herwijnen, A., 2002. Preliminary results from controlled experiments on the growth of faceted crystals above a wet snow layer. In: Stevens, J.R. (Editor), Proceedings ISSW 2002. International Snow Science Workshop. Penticton BC, Canada, 29 September-4 October 2002: 337-342.
- Johnson, J.B., 2003a, Personal communication.
- Johnson, J.B., 2003b. A statistical micromechanical theory of cone penetration in granular materials. CRREL technical report 03-3: 43 pp.

- Johnson, J.B. and Schneebeli, M., 1999. Characterizing the microstructural and micromechanical properties of snow. *Cold Reg. Sci. Technol.*, **30** (1-3), 91-100.
- Journel, A.G. and Huijbregts, C.J., 1978. Mining geostatistics. Academic Press, London.
- Kaluzny, S.P., Vega, S.C., Cardoso, T.P. and Shelly, A.A., 1998. S+ SpatialStats: user's manual for Windows and UNIX. Springer, New York, 327 pp.
- Kozak, M., Elder, K. and Birkeland, K.W., 2001. The spatial and temporal variability of slab hardness, International Snow Science Workshop. Big Sky, Montana, U.S.A., 1-6 October 2000: 115-120.
- Kozak, M., Elder, K., Birkeland, K.W. and Chapman, P., 2002. Predicting snow layer hardness with meteorological factors. In: Stevens, J.R. (Editor), Proceedings ISSW 2002. International Snow Science Workshop. Penticton BC, Canada, 29 September-4 October 2002: 329-336.
- Kronholm, K., Schneebeli, M. and Schweizer, J., in press-a. Spatial variability of penetration resistance in snow layers on a small slope. *Ann. Glaciol.*, **38**.
- Kronholm, K. and Schweizer, J., 2003. Snow stability variation on small slopes. *Cold Reg. Sci. Technol.*, **37** (3), 453-465, doi:10.1016/S0165-232X(03)00084-3.
- Kronholm, K., Schweizer, J., Pielmeier, C. and Schneebeli, M., in press-b. Spatial variability of snowpack stability on small slopes studied with the stuffblock test. *Data of Glaciological Studies, Institute of Geography of the Russian Academy of Sciences, Glaciological Association*.
- Landry, C.C., 2002. Spatial variations in snow stability on uniform slopes: Implications for extrapolation to surrounding terrain. M.Sc. thesis, Montana State University, Department of Earth Sciences, Bozeman MT, U.S.A., 194 pp.
- Landry, C.C., Birkeland, K.W., Hansen, K., Borkowski, J.J., Brown, R.L. and Aspinall, R., 2003. Variations in snow strength and stability on uniform slopes. *Cold Reg. Sci. Technol.*, in press.
- Landry, C.C., Borkowski, J.J. and Brown, R.L., 2001. Quantified loaded column stability test: mechanics, procedure, sample-size selection, and trials. *Cold Reg. Sci. Technol.*, **33** (2-3), 103-121.
- Lehning, M., Bartelt, P., Brown, R.L., Russi, T., Stöckli, U. and Zimmerli, M., 1999. SNOWPACK model calculations for avalanche warning

- based upon a new network of weather and snow stations. *Cold Reg. Sci. Technol.*, **30** (1-3), 145-157.
- Lehning, M., Fierz, C., Brown, R.L. and Jamieson, B., in press. Modelling instability for the snow cover model SNOWPACK. *Ann. Glaciol.*, **38**.
- Marazzi, A., 1993. Algorithms, routines and S functions for robust statistics. Wadsworth & Brooks/Cole, Pacific Grove, CA.
- MathSoft, 1999. S-PLUS 2000, Professional Release 2.
- McClung, D.M., 1977. Direct simple shear tests on snow and their relation to slab avalanche formation. *J. Glaciol.*, **19** (81), 101-109.
- McClung, D.M., 1987. Mechanics of snow slab failure from a geotechnical perspective. In: Salm, B. and Gubler, H.U. (Editors), *Avalanche Formation, Movement and Effects*. Davos, Switzerland, 14-19 September 1986. IAHS Publication 162: 475-508.
- McClung, D.M., 2000. Predictions in avalanche forecasting. *Ann. Glaciol.*, **31**, 377-381.
- McClung, D.M. and Schaerer, P., 1993. *The Avalanche Handbook*. The Mountaineers, Seattle, Washington, U.S.A., 271 pp.
- Mellor, M., 1975. A review of basic snow mechanics. IAHS Publication 114: 251-291.
- Mock, C.J. and Birkeland, K.W., 2000. Snow avalanche climatology of the Western United States mountain ranges. *Bull. Amer. Meteor. Soc.*, **81** (10), 2367-2392.
- Munter, W., 1997. 3x3 Lawinen - Entscheiden in kritischen Situationen. Agentur Pohl and Schellhammer, Garmisch Partenkirchen, Germany, 220 pp.
- Munter, W., 2003. 3x3 Lawinen - Risikomanagement im Wintersport. Third edition. Verlag Pohl & Schnellhammer, Garmisch-Partenkirchen, Germany, 223 pp.
- Pardo-Igúzquiza, E. and Dowd, P.A., 2003. Testing for constant spatial mean using the global D-statistic. *Computers & Geosciences*, **29**, 1057-1068, doi:10.1016/S0098-3004(03)00095-5.
- Perla, R., 1977. Slab avalanche measurements. *Can. Geotech. J.*, **14** (2), 206-213.
- Pielmeier, C., 2003. Textural and mechanical variability of mountain snowpacks. Ph.D. thesis, University of Berne, Berne, 127 pp.
- Pielmeier, C. and Schneebeli, M., 2003. Stratigraphy and changes in hardness of snow measured by hand, ramsonde and snow micro penetrometer: a comparison with planar sections. *Cold Reg. Sci. Technol.*, **37** (3), 393-405.

- Raderschall, N., Lehning, M. and Schär, C., 2003. Fine-scale modelling of the boundary layer wind field over steep topography. *Boundary-Layer Meteorol.*, submitted.
- Richardson, C. and Holmlund, P., 1999. Spatial variability at shallow snow-layer depths in central Dronning Maud Land, East Antarctica. *Ann. Glaciol.*, **29**, 10-16.
- Sahimi, M., 2003. Large-scale porous media and wavelet transformations. *Computing in Science & Eng.*, **5** (4), 75-87.
- Salm, B., 1975. General discussion, Snow mechanics. Grindelwald, Switzerland, 1-5 April, 1974. IAHS Publication 114: 441-442.
- Schneebeili, M., 2001. High-resolution penetrometry in the low-porosity material snow. In: Kömle, N.I., Kargl, G., Ball, A.J. and Lorenz, R.D. (Editors), International Workshop on Penetrometry in the Solar System. Graz, Austria, 18-20 October 1999: 61-72.
- Schneebeili, M., in press. Numerical simulation of elastic stress in the microstructure of snow. *Ann. Glaciol.*, **38**.
- Schneebeili, M. and Johnson, J.B., 1998. A constant-speed penetrometer for high-resolution snow stratigraphy. *Ann. Glaciol.*, **26**, 107-111.
- Schneebeili, M., Pielmeier, C. and Johnson, J.B., 1999. Measuring snow micro structure and hardness using a high resolution penetrometer. *Cold Reg. Sci. Technol.*, **30** (1-3), 101-114.
- Schweizer, J., 1993. The influence of the layered character of snow cover on the triggering of slab avalanches. *Ann. Glaciol.*, **18**, 193-198.
- Schweizer, J., 1999. Review of dry snow slab avalanche release. *Cold Reg. Sci. Technol.*, **30** (1-3), 43-57.
- Schweizer, J., 2002. The Rutschblock test - Procedure and application in Switzerland. *The Avalanche Review*, **20** (5), 1, 14-15.
- Schweizer, J. and Jamieson, J.B., 2003a. Snow stability measurements. *Proceedings International Seminar on Snow and Avalanche Test Sites, Grenoble, France, 22-23 November 2001*, in press.
- Schweizer, J. and Jamieson, J.B., 2003b. Snowpack properties for snow profile interpretation. *Cold Reg. Sci. Technol.*, **37** (3), 233-241.
- Schweizer, J., Jamieson, J.B. and Schneebeili, M., 2003a. Snow slab avalanche formation. *Rev. Geophys.*, **41** (4), 1016, doi:10.1029/2002RG000123.
- Schweizer, J., Kronholm, K. and Wiesinger, T., 2003b. Verification of regional snowpack stability and avalanche danger. *Cold Reg. Sci. Technol.*, **37** (3), 233-241, doi:10.1016/S0165-232X(03)00067-3.

- Schweizer, J. and Lütschg, M., 2001. Characteristics of human-triggered avalanches. *Cold Reg. Sci. Technol.*, **33** (2-3), 147-162.
- Schweizer, J., Schneebeli, M., Fierz, C. and Föhn, P.M.B., 1995. Snow mechanics and avalanche formation: Field experiments on the dynamic response of the snow cover. *Surv. Geophys.*, **16** (5-6), 621-633.
- Schweizer, J. and Wiesinger, T., 2001. Snow profile interpretation for stability evaluation. *Cold Reg. Sci. Technol.*, **33** (2-3), 179-188.
- Seligman, G., 1936. Snow structure and ski fields. Third edition (reprint 1980). International Glaciological Society, Cambridge, 555 pp.
- Shapiro, L.H., Johnson, J.B., Sturm, M. and Blaisdell, G.L., 1997. Snow mechanics - Review of the state of knowledge and applications. CRREL Report 97-3: 43 pp.
- Sommerfeld, R.A. and King, R.M., 1979. A recommendation for the application of the Roch index for slab avalanche release. *J. Glaciol.*, **22** (88), 547-549.
- Spiegel, M.R. and Stephens, L.J., 1999. Schaum's outline of theory and problems of statistics. Third edition. Schaum's outline series. McGraw-Hill, New York, 538 pp.
- Stenberg, M., Hansson, M., Holmlund, P. and Karlöf, L., 1999. Variability in snow layering and snow chemistry in the vicinity of two drill sites in western Dronning Maud Land, Antarctica. *Ann. Glaciol.*, **29**, 33-37.
- Stewart, W.K., 2002. Spatial variability of slab stability within avalanche start zones. M.Sc. thesis, University of Calgary, Calgary, Alberta, 103 pp.
- Stewart, W.K. and Jamieson, J.B., 2002. Spatial variability of slab stability in avalanche start zones, Proceedings ISSW 2002, International Snow Science Workshop. Penticton BC, Canada, 29 September-4 October 2002: 544-548.
- Stoffel, A., Meister, R. and Schweizer, J., 1998. Spatial characteristics of avalanche activity in an alpine valley - a GIS approach. *Ann. Glaciol.*, **26**, 329-336.
- Sturm, M. and Benson, C.S., in press. Scales of spatial heterogeneity for perennial and seasonal snow layers. *Ann. Glaciol.*, **38**.
- Sturm, M., Holmgren, J., König, M. and Morris, K., 1997. The thermal conductivity of seasonal snow. *J. Glaciol.*, **43** (143), 26-41.

- Sturm, M., Holmgren, J. and Liston, G.E., 1995. A seasonal snow cover classification system for local to global applications. *J. Clim.*, **8** (5), 1261-1283.
- Sturm, M., Morris, K. and Massom, R., 1998. The winter snow cover of the west Antarctic pack ice: its spatial and temporal variability. *Antarc. Res. Series*, **74**, 1-18.
- Takeuchi, Y., Nohguchi, Y., Kawashima, K. and Izumi, K., 1998. Measurement of snow-hardness distribution. *Ann. Glaciol.*, **26**, 27-30.
- Tschirky, F., Brabec, B. and Kern, M., 2000. Lawinenunfälle in den Schweizer Alpen - Eine statistische Zusammenstellung mit den Schwerpunkten Verschüttung, Rettungsmethoden und Rettungsgeräte. In: Ammann, W.J. (Editor), *Durch Lawinen verursachte Unfälle im Gebiet der Schweizer Alpen*. Eidgenössisches Institut für Schnee- und Lawinenforschung SLF, Davos, Switzerland, pp. 125-136.
- Vanmarke, E.H., 1977. Probabilistic modeling of soil profiles. *J. Geotech. Engg. Div.*, **103** (GT 11), 1227-1246.
- Webster, R. and Oliver, M.A., 2001. *Geostatistics for environmental scientists*. Statistics in practice. John Wiley and Sons, Chichester, 271 pp.
- Yohai, V., Stahel, W.A. and Zamar, R.H., 1991. A procedure for robust estimation and inference in linear regression. In: Stahel, W.A. and Weisberg, S.W. (Editors), *Directions in robust statistics and diagnostics, Part II*. Springer.

Appendix A

Snow profiles

A.1. Notes

Most of the German phrases in the figures of the manual snow cover profiles should be rather self-explanatory, while a few might require a translation, given in the table below.

Table A.1. English translation of selected German terms in the stratigraphic profiles.

	German	English
Header	Beobachter	Observer
	Höhe ü. M.	m a.s.l.
	LKNr	Map number
	Bemerkungen	Comments
	Ort	Location
	Neigung	Slope inclination
	Temp.	Air temperature
	Windrichtung	Wind direction
	-stärke	Wind speed
	Gesamtwasserwert	Snow water equivalent
	Mittl. Raumgew.	Average density
	Mittl. Rammwiderstand	Average rammsonde penetration resistance
Grain shape	Kristalle	Crystals after Colbeck and others (1990) except crusts (see text)
	Durchm.	Grain size (mm)
Hardness	FA (Faust)	Fist
	4F	4 Fingers
	1F	1 Finger
	B (Bleistift)	Pencil
	M (Messer)	Knife
Rutschblock: fracture type	ganzer Block	Complete block
	Teilbruch	Part of the block (typically below skis)
	nur ein Eck	Only corner broken off
Rutschblock: fracture plane type	glatt	Planar
	rauh	Rough
	unregelmäßig	Irregular

A.2. Grid 14

Handprofil

Beobachter: Schweizer
 Höhe ü. M. 2515 m
 Exposition: ESE
 Wetter/Niederschlag: sonnig
 LKNr: 1197 Bemerkungen: Profil bei Grid#1 / unterhalb. leichter Kruste, n. abgerutscht, erst beim 1. Sprung / nur unterhalb Ski

Ort: GR Chorbsshorn NE-Grat

Datum/Zeit: 09.01.2002 11:00
 Station: 164
 Koordinaten: 778225 / 185175
 Neigung: 31 Grad

Profilnr: 1
 Temp.: 0.0 °C
 sonnig (0/8)
 Windrichtung:
 -stärke: 0 km/h

Gesamtwasserwert: 354.4 mm (HS: 113.0 cm)

Mittl. Raungew.: 314 kg/m³

Mittl. Rannwiderstand: 157 N

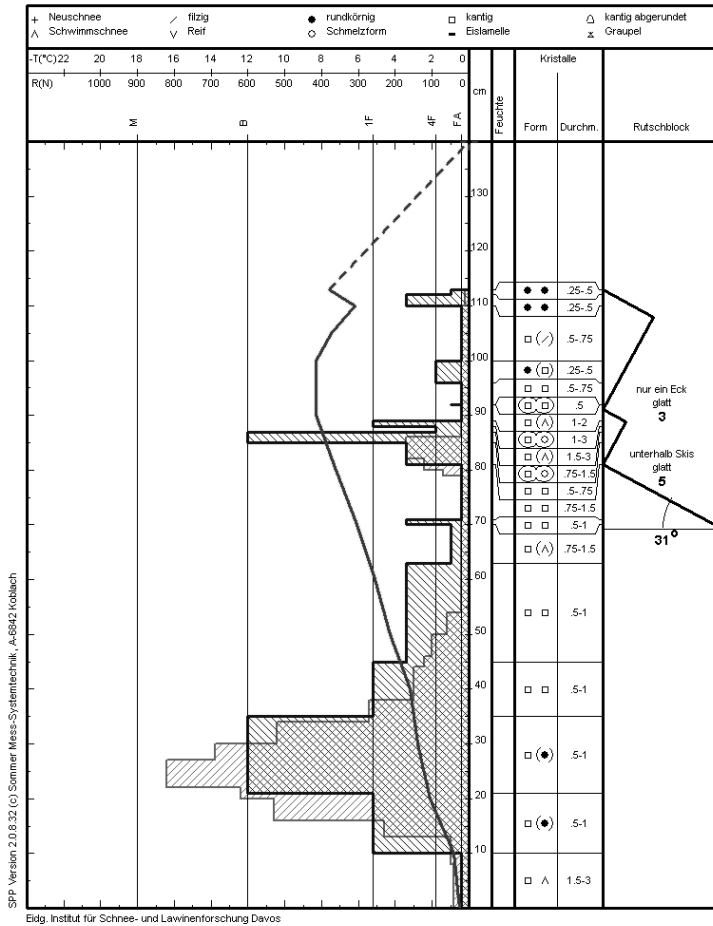


Figure A.1. Stratigraphic snow cover profile from grid 14.

A.3. Grid 15

Handprofil

Ort: **GR Steintälli - Strela - Davos**

Beobachter: Schweizer/Fierz

Datum/Zeit: **15.01.2002 10:00**

Profilnr: 1

Höhe ü. M. 2415 m

Station: 164

Temp.: -9.0 °C

Exposition: NNE

Koordinaten: 779510 / 186525

sonnig (0/8)

Wetter/Niederschlag: sonnig

Neigung: 28 Grad

Windrichtung:

-stärke: 0 km/h

LKNr: 1197 Bemerkungen: bei Grid #2 / unterhalb Ski

Gesamtwasserwert: 355.1 mm (HS: 126.0 cm)

Mittl. Raungew.: 282 kg/m³

Mittl. Rammwiderstand: 54 N

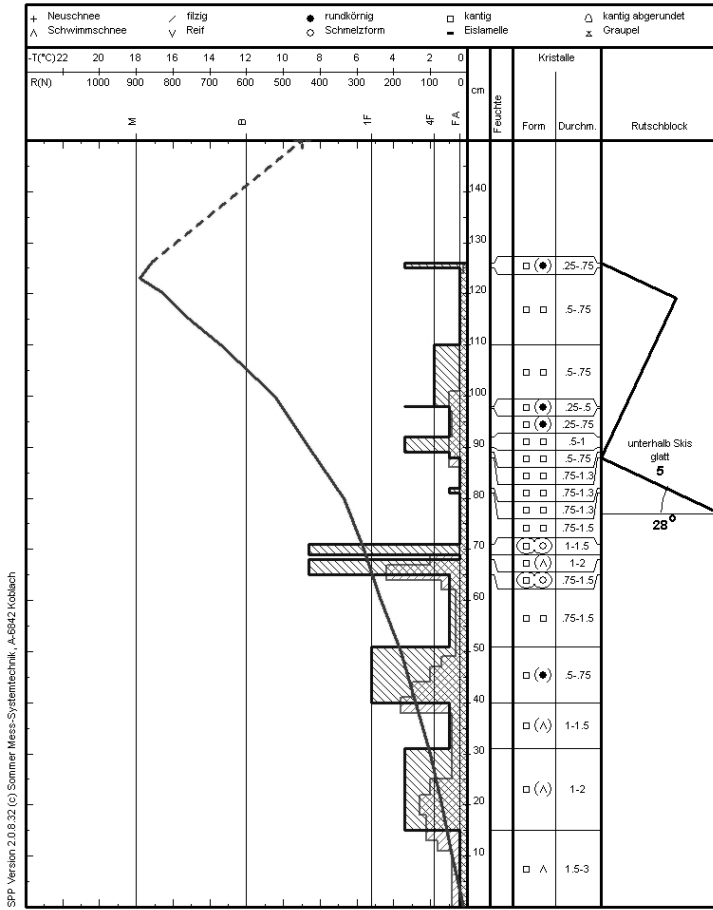


Figure A.2. Stratigraphic snow cover profile from grid 15.

A.4. Grid 16

Handprofil

Ort: GR Hanengretji - Davos

Datum/Zeit: 29.01.2002 11:10

Profintr.: 1

Beobachter: Schweizer/Fierz

Station: 164

Temp.: 1.5 °C

Höhe ü. M. 2495 m

Koordinaten: 778325 / 184940

wolkig (2/8-3/8)

Exposition: ENE

Neigung: 25 Grad

Windrichtung: SW

Wetter/Niederschlag: zeitweise Schneefegen, sonst hohe Bewölkung

-stärke: 5 km/h

LKNr.: 1197 Bemerkungen: Profil bei Grid / nur unterhalb Ski, oberhalb leichter Kruste

Gesamtwasserwert: 442.6 mm (HS: 155.0 cm)

Mittl. Raumbew.: 286 kg/m³

Mittl. Rammwiderstand: 72 N

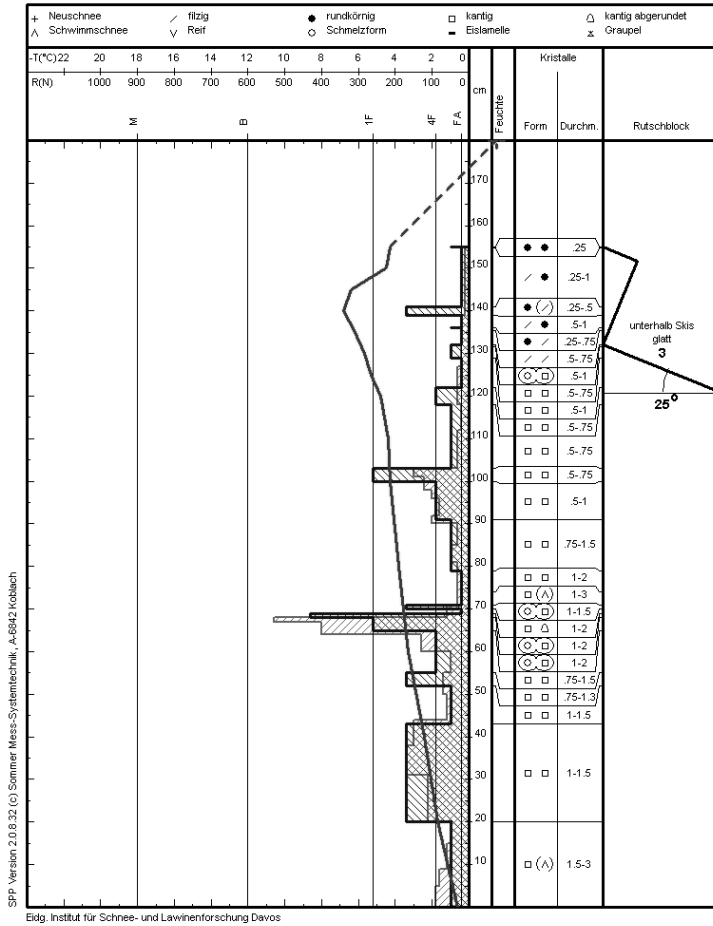


Figure A.3. Stratigraphic snow cover profile from grid 16.

A.5. Grid 17

Handprofil

Ort: GR Hanengretji - Davos

Datum/Zeit: 18.02.2002 10:45

Profilnr: 1

Beobachter: Schweizer/Hendrikx

Station: 164

Temp.: -7.0 °C

Höhe ü. M. 2500 m

Koordinaten: 778425 / 184900

stark bewölkt (6/8-7/6)

Exposition: NNW

Nelgung: 28 Grad

Windrichtung: NNW

Wetter/Niederschlag: zeitweise leichter Schneefall, zeitweise sonnig

-stärke: 2 km/h

LfNr: 1197 Bemerkungen: Profil bei Grid #4

Gesamtwassergehalt: 295.3 mm (HS: 115.0 cm)

Mittl. Raungew.: 257 kg/m³

Mittl. Rammwiderstand: 32 N

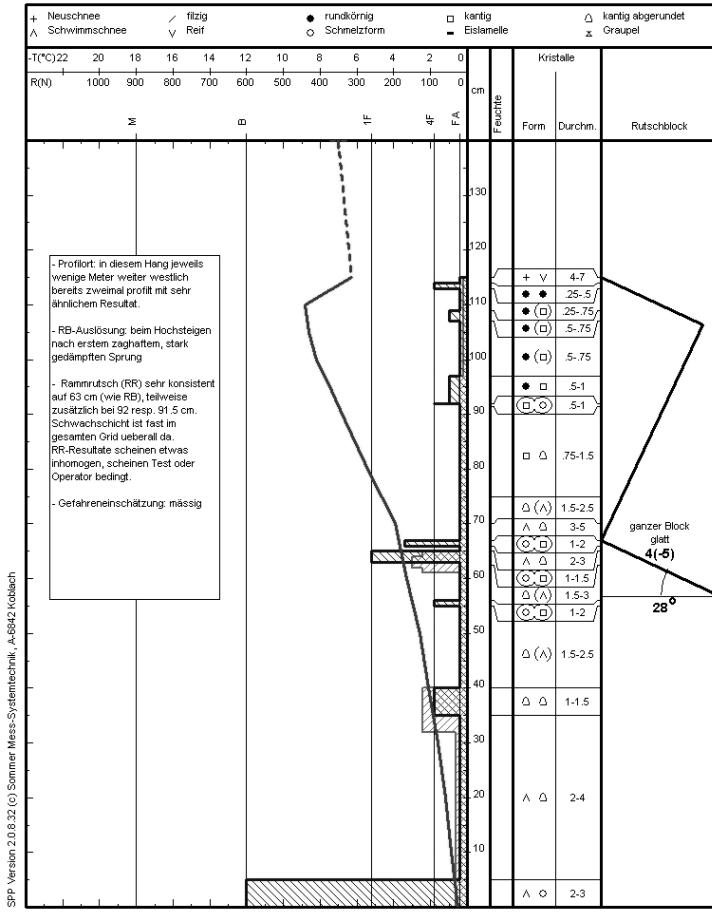


Figure A.4. Stratigraphic snow cover profile from grid 17.

A.6. Grid 18

Handprofil

Ort: GR Hanengretjji - Davos

Datum/Zeit: 01.03.2002 11:00

Profitorf: 1

Beobachter: Schweizer/Hendrickx

Station: HGR

Temp.: -2.8 °C

Höhe ü. M. 2495 m

Koordinaten: 778460 / 184935

wechsellnd bewölkt (4/8-5/8)

Exposition: NW

Neigung: 29 Grad

Windrichtung: S

Wetter/Niederschlag: zeitweise Schneefegen

-stärke: 10 km/h

LKNr: 350 Bemerkungen: Profil bei Grid #5

Gesamtwasserwert: 245.0 mm (HS: 103.0 cm)

Mittl. Raugew.: 238 kg/m³

Mittl. Rammwiderstand: 20 N

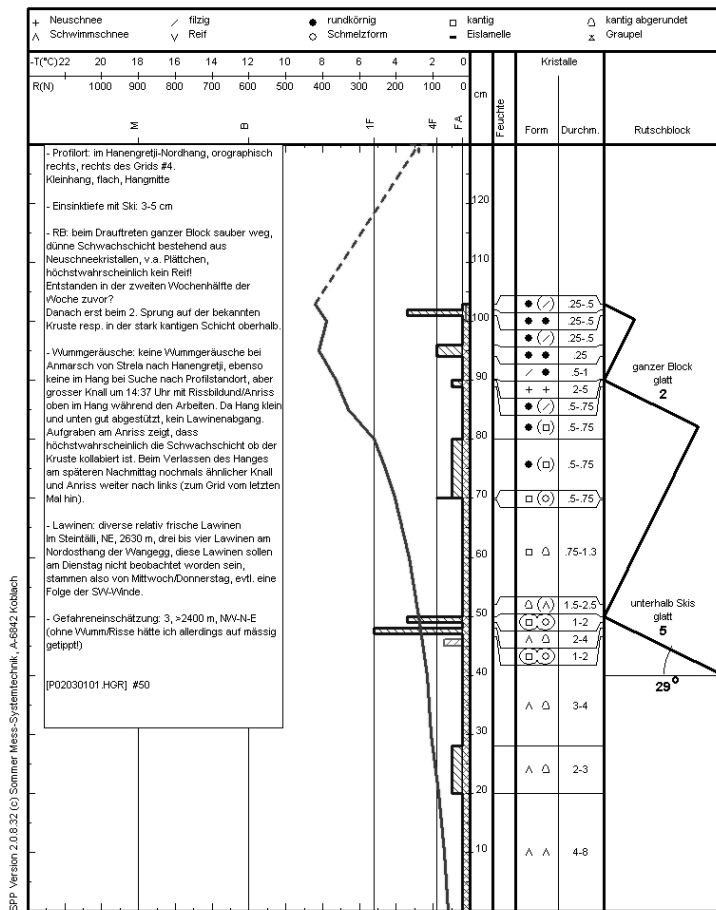


Figure A.5. Stratigraphic snow cover profile from grid 18.

A.7. Grid 19

Handprofil

Ort: GR Choerbsch Horn NE-Grat, Davos

Datum/Zeit: 05.03.2002 11:10

Profilnr: 1

Beobachter: Fierz/Hellig

Station: HGR

Temp.: -1.3 °C

Höhe ü. M. 2520 m

Koordinaten: 778155 / 185230

wechselnd bewölkt (4/8-5/8)

Exposition: N

Nelgung: 25 Grad

Windrichtung: SW

Wetter/Niederschlag: anfangs sonnig, später zunehmende Bewölkung

-stärke: 3 km/h

LKNr: 1197 Bemerkungen: / Uebergang Alt-Neuschnee an sehr kleiner Kruste

Gesamtwasserwert: 209.4 mm (HS: 87.0 cm)

Mittl. Raungew.: 241 kg/m³

Mittl. Rammwiderstand: 41 N

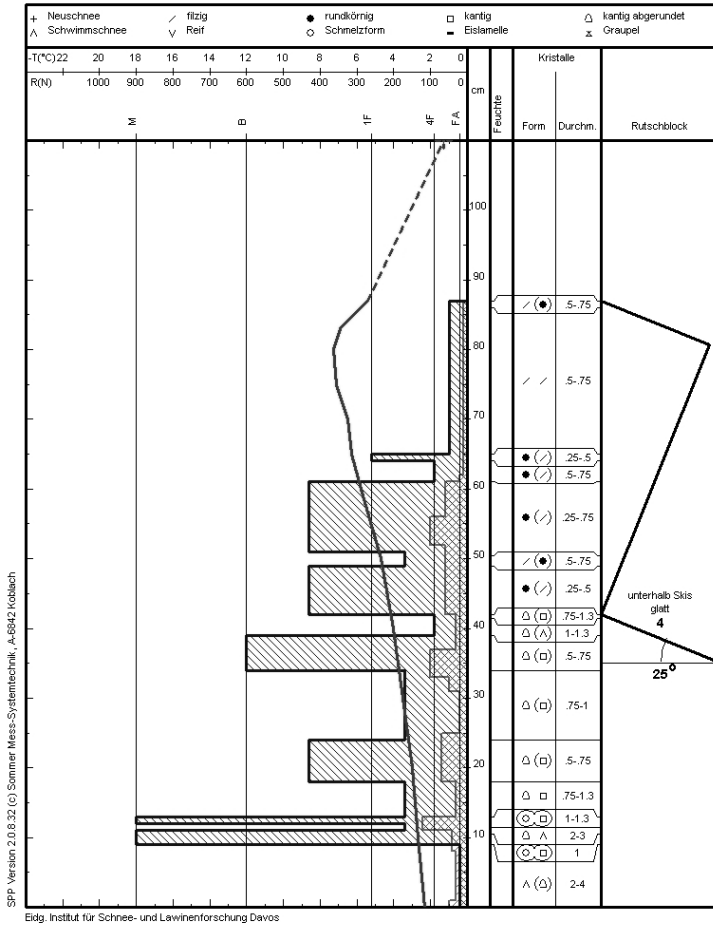


Figure A.6. Stratigraphic snow cover profile from grid 19.

A.8. Grid 20

Handprofil

Ort: GR Hanengretj, Davos

Datum/Zeit: 08.03.2002 11:05

Profnr.: 1

Beobachter: Kronholm/Hellig

Station: HGR

Temp.: -0.5 °C

Höhe ü. M. 2495 m

Koordinaten: 778485 / 184950

helter (1/8)

Exposition: N

Neigung: 26 Grad

Windrichtung:

Wetter/Niederschlag: sonnig

-stärke: km/h

LKNr: 1197 Bemerkungen: / 1. Wippen auf Verhaertung / unter 2. Verhaertung, gleichzeitig

Gesamtwasserwert: --- mm (HS: --- cm)

Mittl. Rauegew.: --- kg/m³

Mittl. Rammwiderstand: 33 N

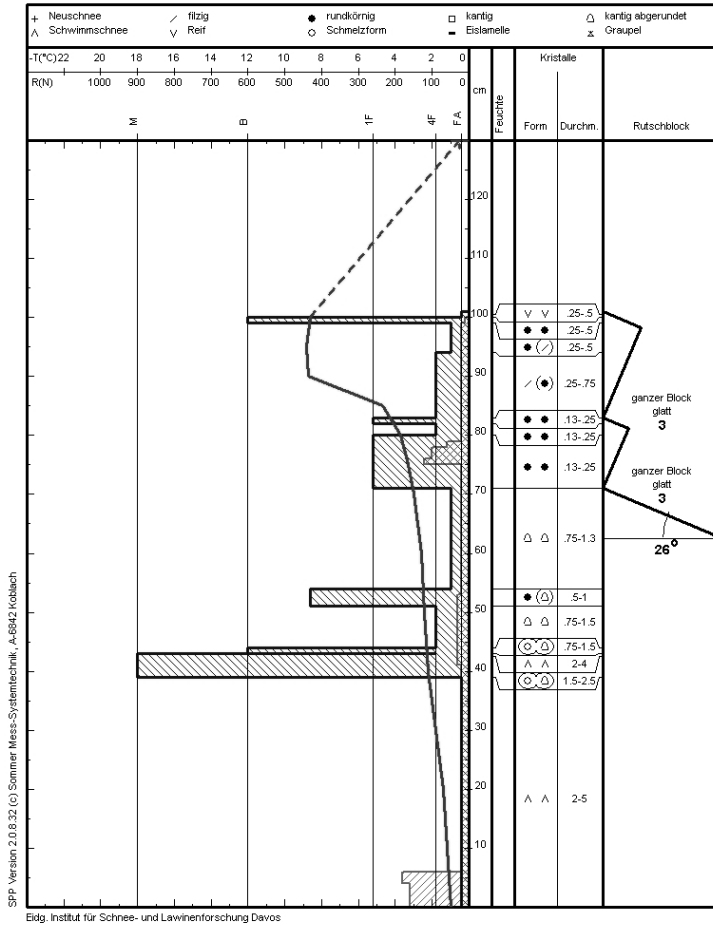


Figure A.7. Stratigraphic snow cover profile from grid 20.

A.10. Grid 22

Handprofil

Ort: **GR Hanengretj - Davos**

Datum/Zeit: **13.01.2003 10:00**

Profintr: 104

Beobachter: Fierz / Landl

Station: HGR

Temp.: -10.5 °C

Höhe ü. M. 2525 m

Koordinaten: 778475 / 184888

6

Exposition: NNW

Neigung: 35 Grad

Windrichtung: E

Wetter/Niederschlag: Vm Altostratus mit Löchern, am Nn ab ca. 15:00 Schneefall

-stärke: 15 km/h

LKNr: 1196 Bemerkungen: Profil zu Grid #1

Gesamtwasserwert: 351.9 mm (HS: 123.0 cm)

Mittl. Rauegew.: 286 kg/m³

Mittl. Rammwiderstand: 84 N

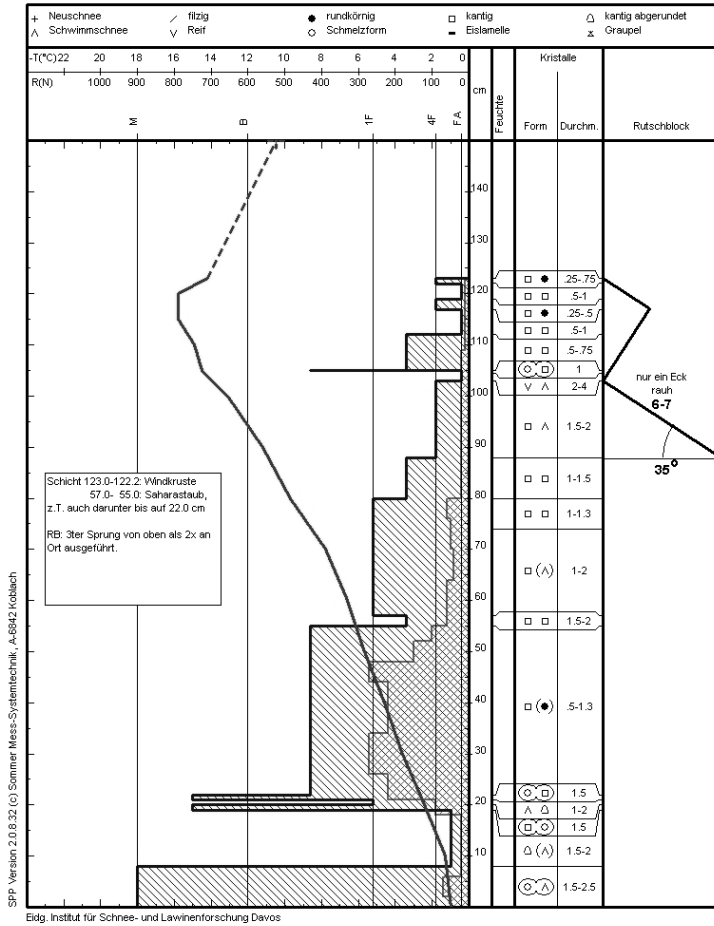


Figure A.9. Stratigraphic snow cover profile from grid 22.

A.11. Grid 23

Handprofil

Ort: GR Hanengretji - Davos

Datum/Zeit: 17.01.2003 08:50

Profiltirn: 180

Beobachter: Schweizer / Hegglin

Station: HGR

Temp.: -5.0 °C

Höhe ü. M. 2478 m

Koordinaten: 778439 / 185036

0

Exposition: NE

Nelgung: 33 Grad

Windrichtung: S

Wetter/Niederschlag: schön

-stärke: 2 km/h

LKNr: 1197 Bemerkungen: Profil bei Grid #2, nahe Lawinenanriss vom 10-12.1.2003

Gesamtwasserwert: 521.0 mm (HS: 180.0 cm)

Mittl. Raungew.: 289 kg/m³

Mittl. Rammwiderstand: 123 N

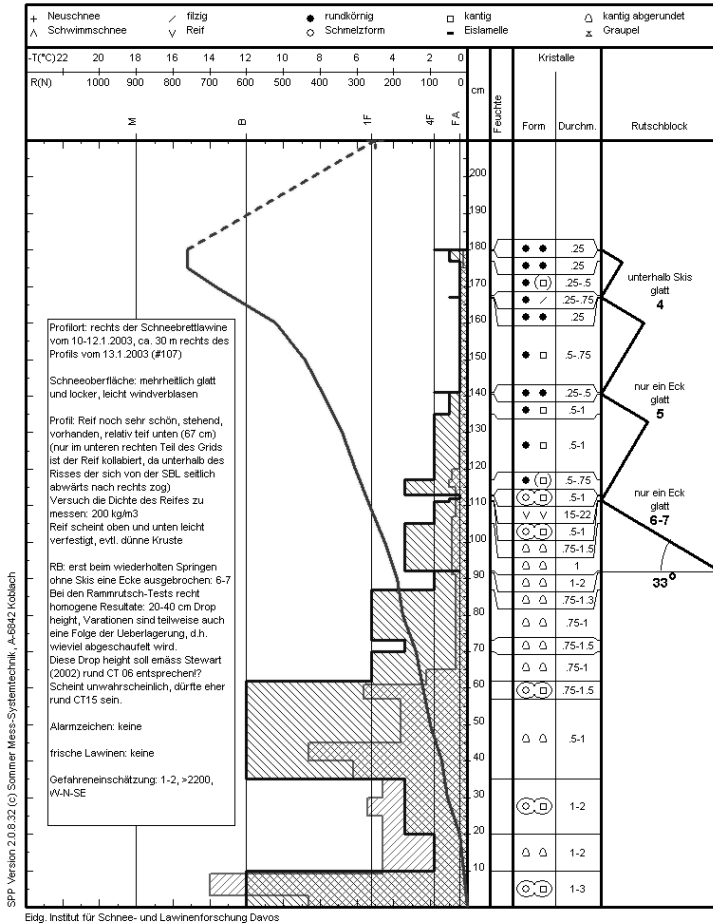


Figure A.10. Stratigraphic snow cover profile from grid 23.

A.12. Grid 24

Handprofil

Beobachter: Schweizer / Odermatt

Höhe ü. M. 2586 m

Exposition: SW

Wetter/Niederschlag:

LKNr: 1197 Bemerkungen: Profil bei Grid #3

Gesamtwasserwert: 724.3 mm (HS: 228.0 cm)

Ort: GR Chörbschhorn - Chörb - Stafier Berg - Davos

Datum/Zeit: 19.02.2003 09:25

Station: HGR

Koordinaten: 777589 / 184804

Neigung: 35 Grad

Mittl. Raugew.: 318 kg/m³

Profintr: 380

Temp.: -3.2 °C

0

Windrichtung: -

-stärke: 0 km/h

Mittl. Rammwiderstand: 165 N

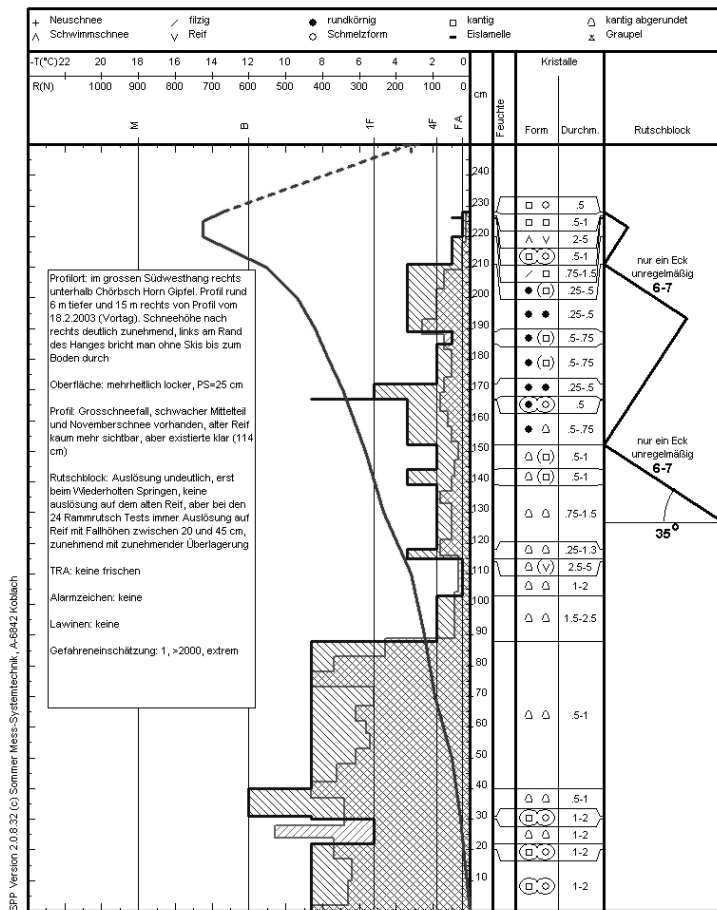


Figure A.11. Stratigraphic snow cover profile from grid 24.

Appendix B

Stability test data

B.1. Notes

The figures in this appendix show the data from the stability tests. All figures have on the left side the drop heights DH and fracture depths FD with the modeled linear trend shown with contours. On the right side, the semi-variograms of residuals from the linear trend regression. On each semi-variogram a scale shows the number of point pairs for each lag-distance bin.

B.2. Grid 14

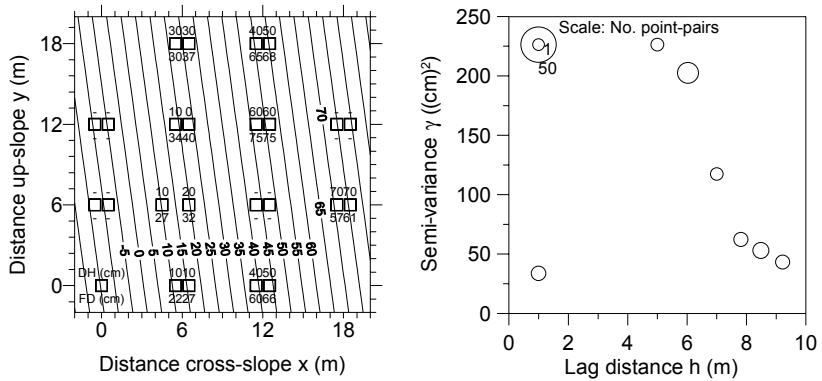


Figure B.1. Stuffblock test results in grid-layer 14A.

B.3. Grid 15

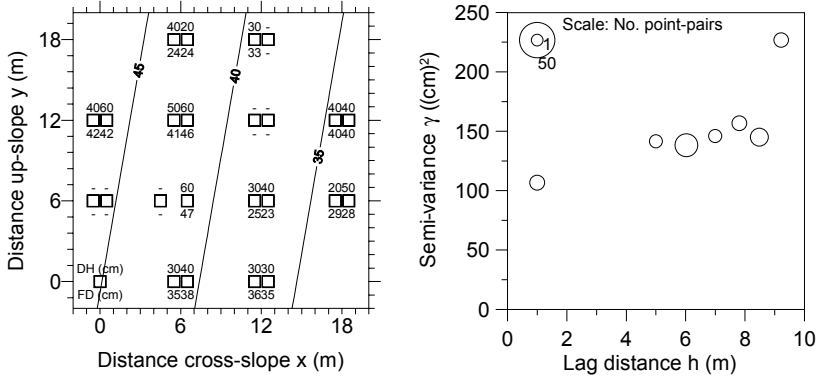


Figure B.2. SB test results in grid-layer 15A.

B.4. Grid 16

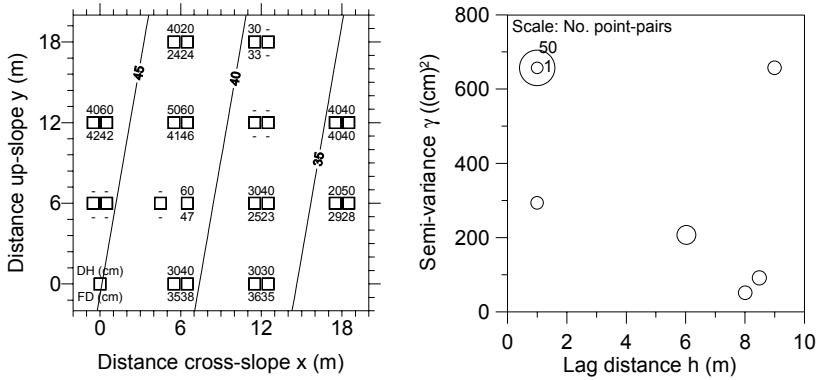


Figure B.3. SB test results in grid-layer 16A.

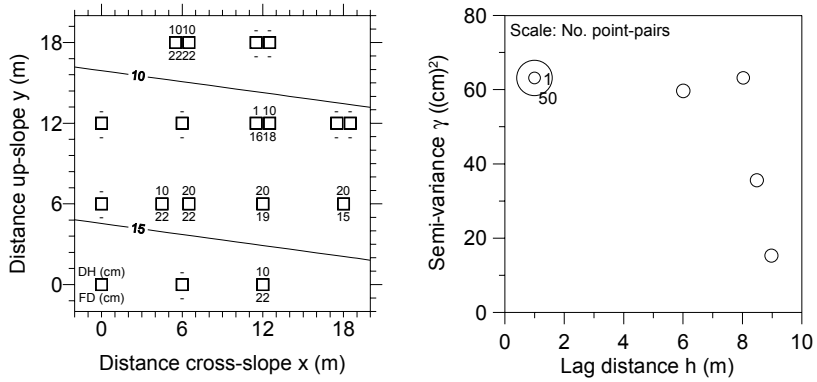


Figure B.4. SB test results in grid-layer 16B.

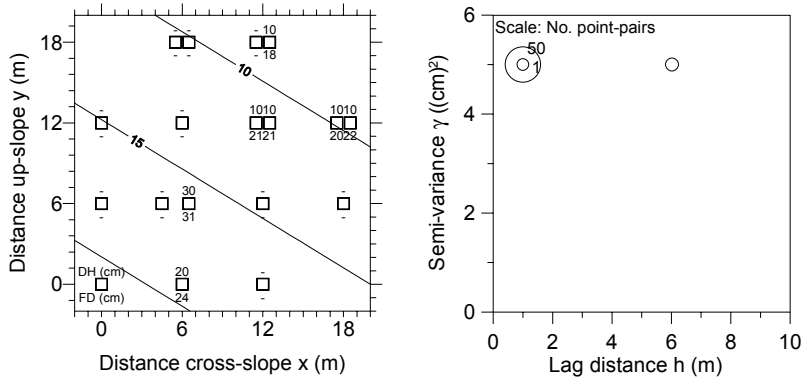


Figure B.5. SB test results in grid-layer 16C.

B.5. Grid 17

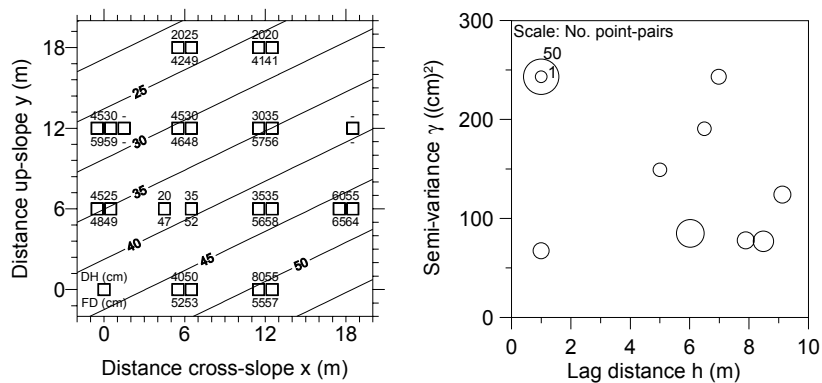


Figure B.6. RR test results in grid-layer 17A.

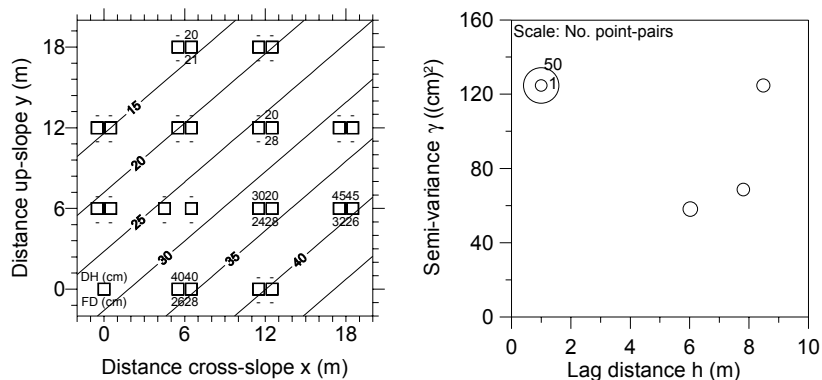


Figure B.7. RR test results in grid-layer 17B.

B.6. Grid 18

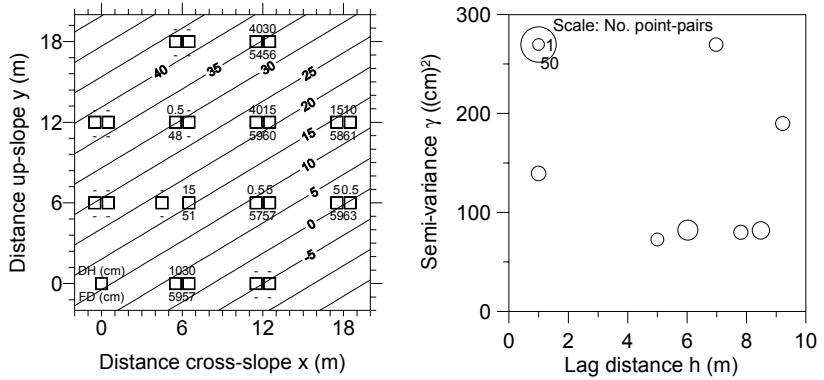


Figure B.8. RR test results in grid-layer 18A.

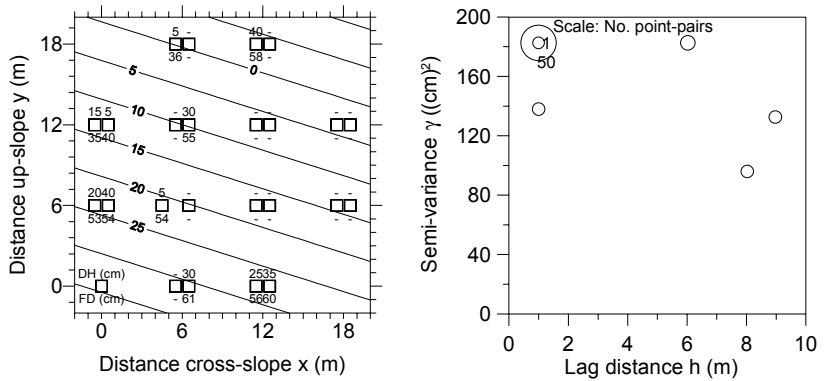


Figure B.9. RR test results in grid-layer 18B.

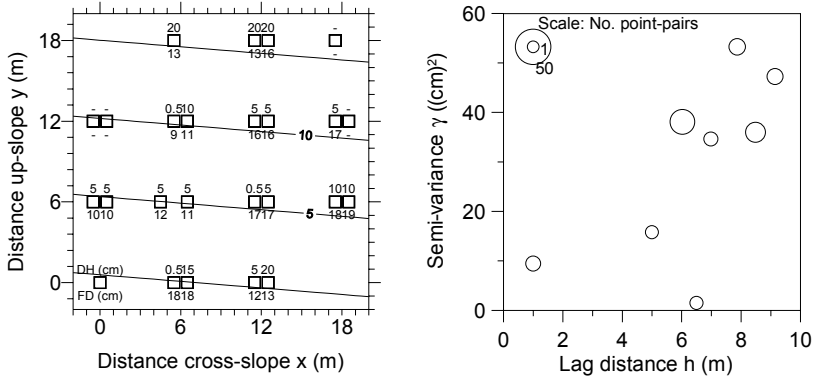


Figure B.10. RR test results in grid-layer 18C.

B.7. Grid 19

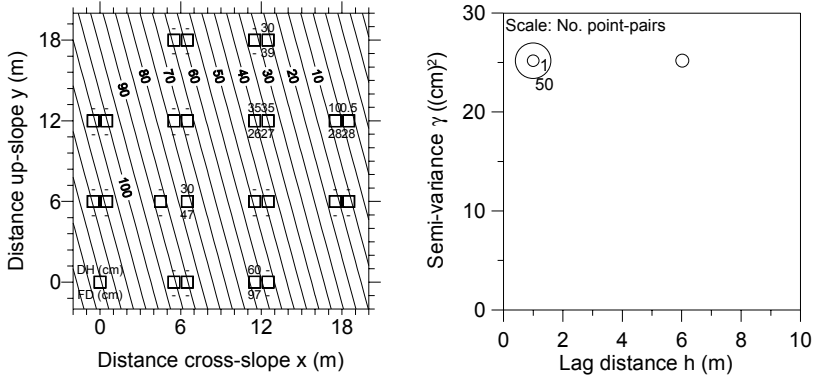


Figure B.11. RR test results in grid-layer 19A.

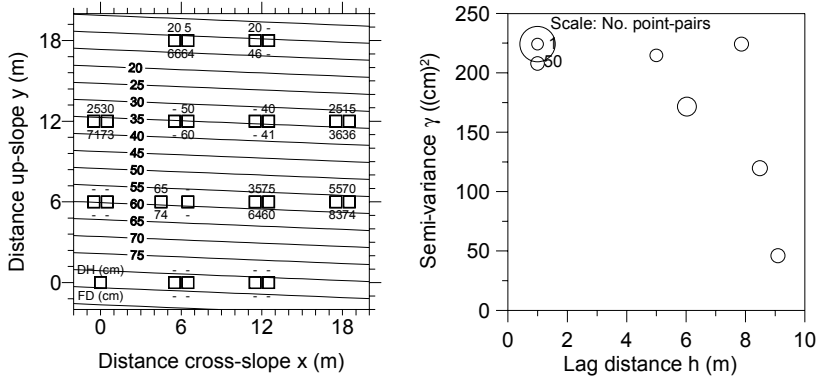


Figure B.12. RR test results in grid-layer 19B.

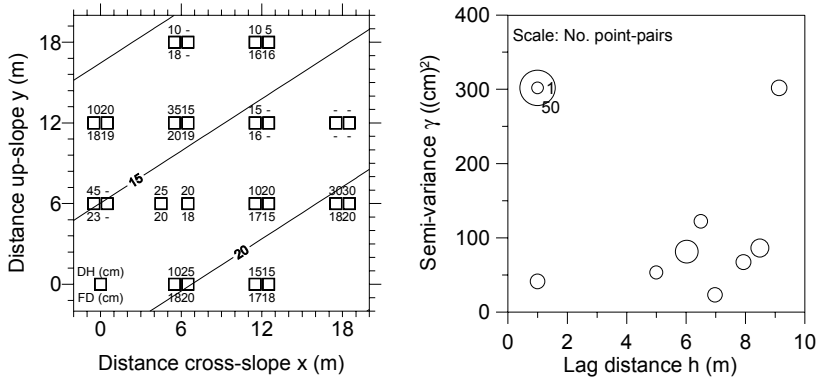


Figure B.13. RR test results in grid-layer 19C.

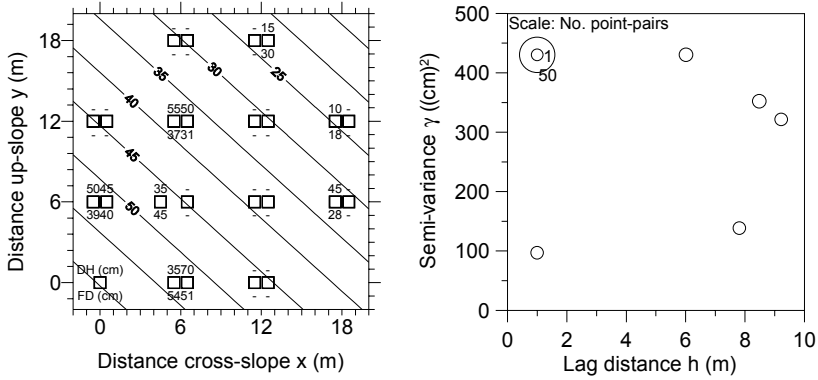


Figure B.14. RR test results in grid-layer 19D.

B.8. Grid 20

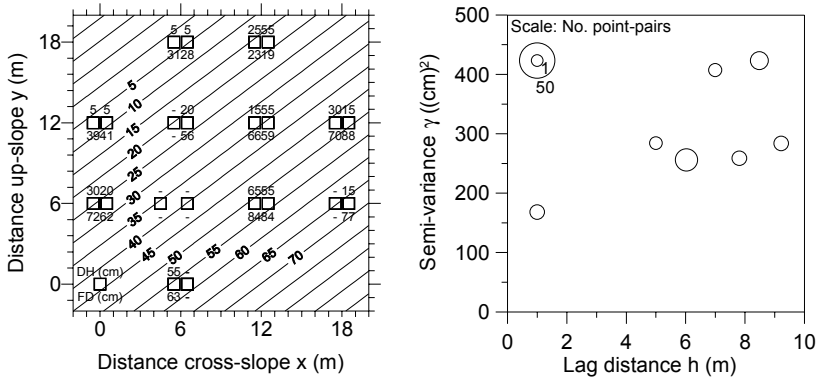


Figure B.15. RR test results in grid-layer 20A.

B.9. Grid 21

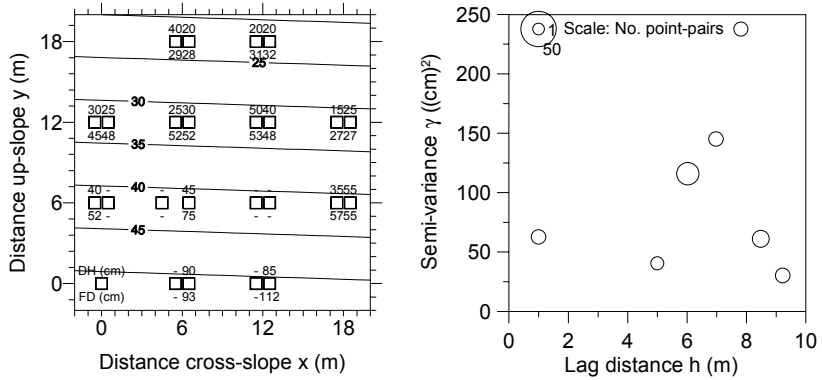


Figure B.16. RR test results in grid-layer 21A.

B.10. Grid 22

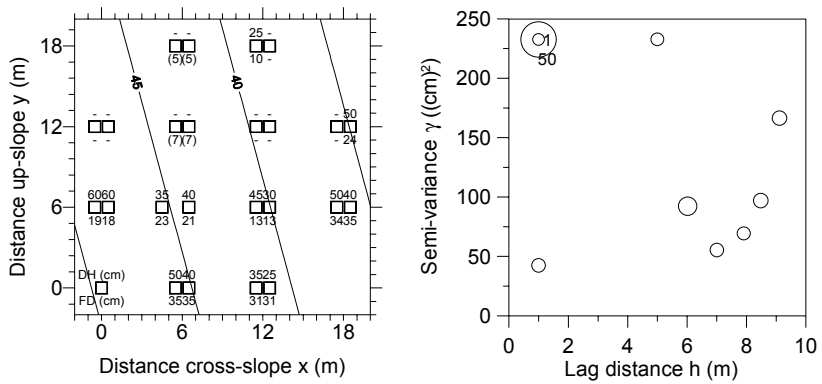


Figure B.17. RR test results in grid-layer 22A.

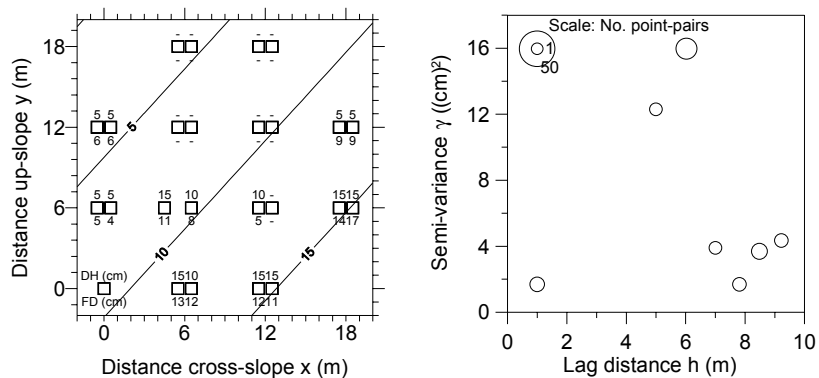


Figure B.18. RR test results in grid-layer 22B.

B.11. Grid 23

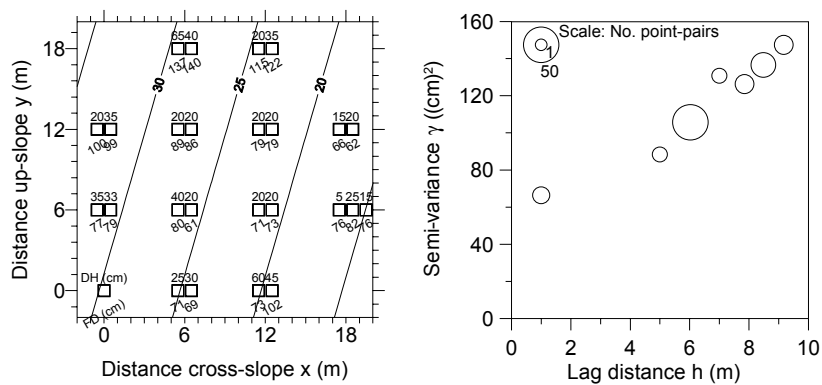


Figure B.19. RR test results in grid-layer 23A.

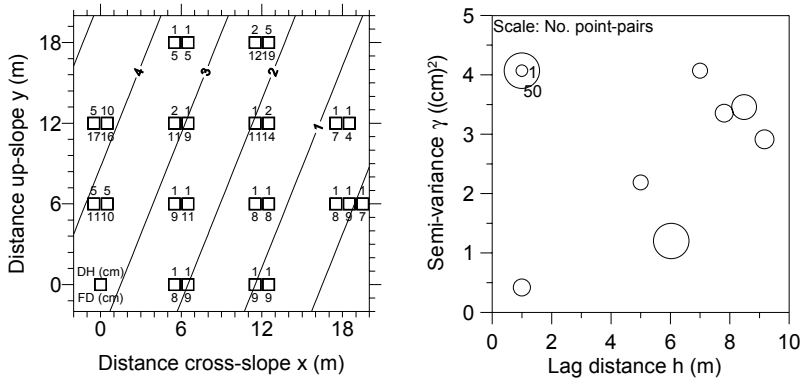


Figure B.20. RR test results in grid-layer 23B.

B.12. Grid 24

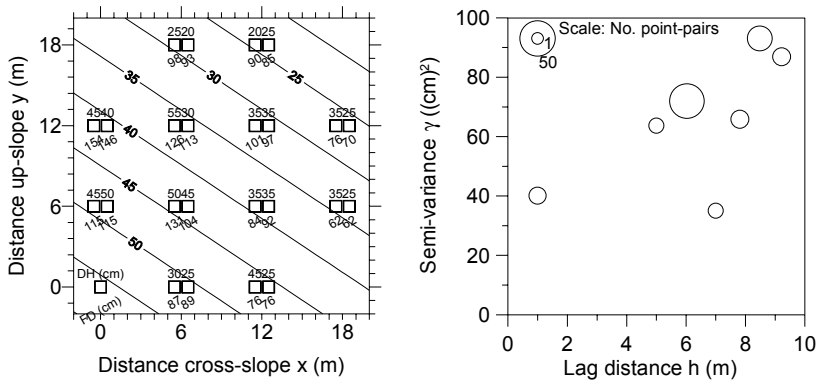


Figure B.21. RR test results in grid-layer 24A.

Appendix C

SMP data

C.1. Notes

The following figures all show the semi-variograms for the \log_{10} -transformed penetration resistance within a grid-layer. The size of the circle for each lag-distance bin is scaled with the number of point pairs in the bin. The scale is shown on each figure.

C.2. Grid 14

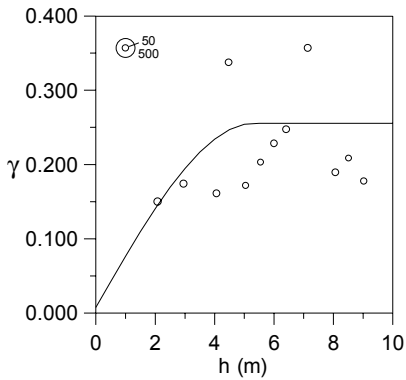


Figure C.1. Sample and model semi-variograms for grid-layer 14a.

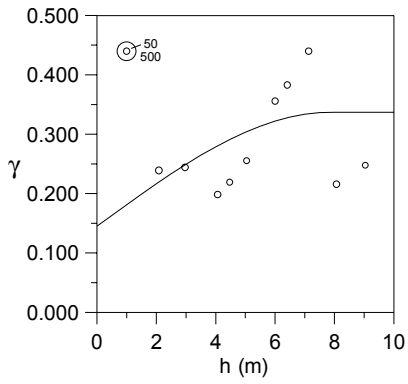


Figure C.2. Sample and model semi-variograms for grid-layer 14b.

C.3. Grid 15

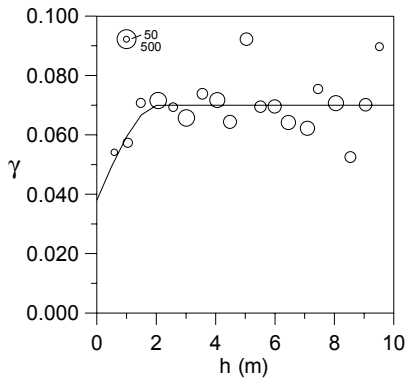


Figure C.3. Sample and model semi-variograms for grid-layer 15a.

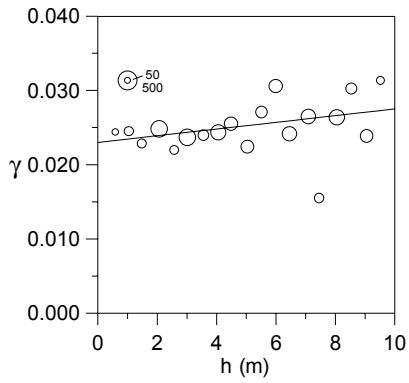


Figure C.4. Sample and model semi-variograms for grid-layer 15b.

C.4. Grid 16

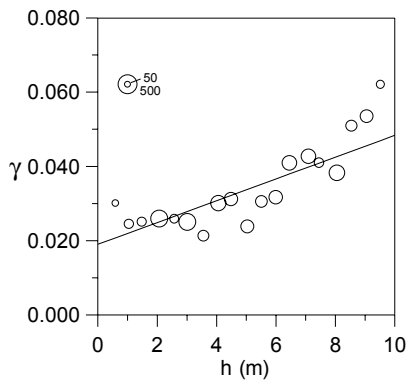


Figure C.5. Sample and model semi-variograms for grid-layer 16a.

C.5. Grid 20

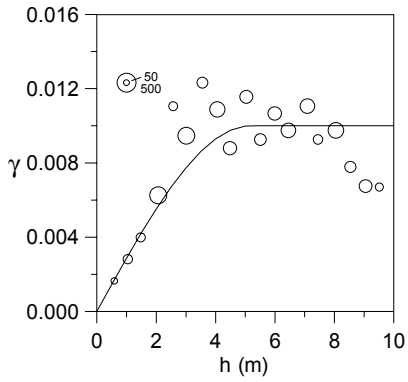


Figure C.6. Sample and model semi-variograms for grid-layer 20a.

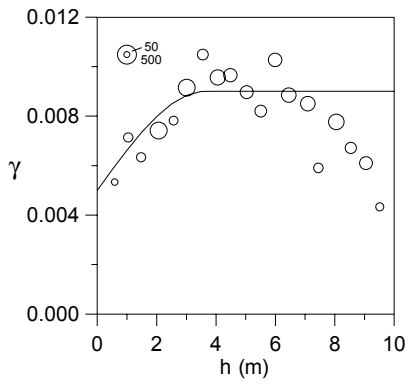


Figure C.7. Sample and model semi-variograms for grid-layer 20b.

C.6. Grid 21

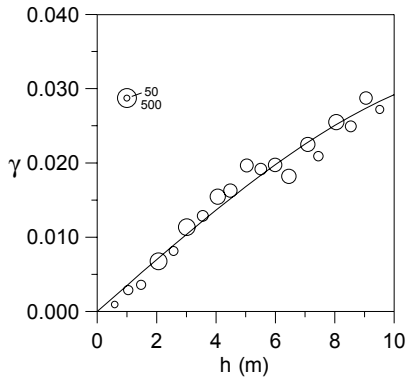


Figure C.8. Sample and model semi-variograms for grid-layer 21a.

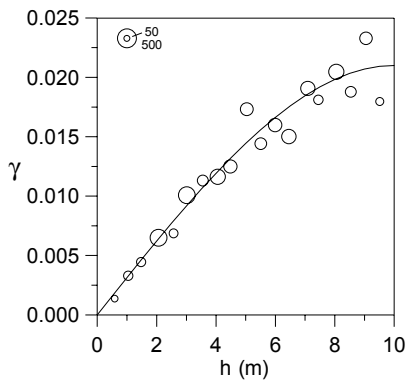


Figure C.9. Sample and model semi-variograms for grid-layer 21b.

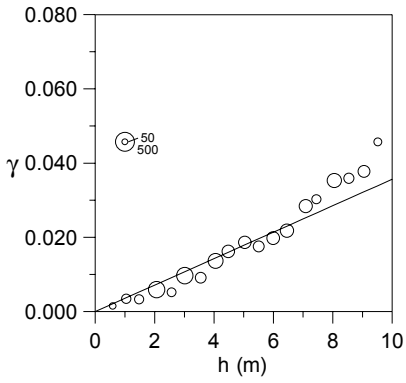


Figure C.10. Sample and model semi-variograms for grid-layer 21c.

C.7. Grid 22

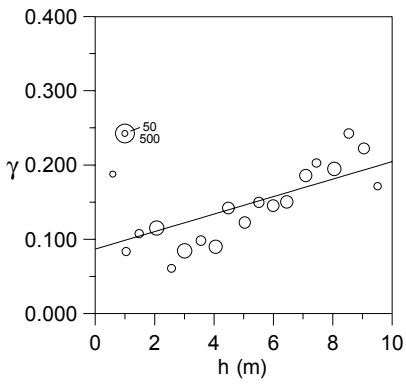


Figure C.11. Sample and model semi-variograms for grid-layer 22b.

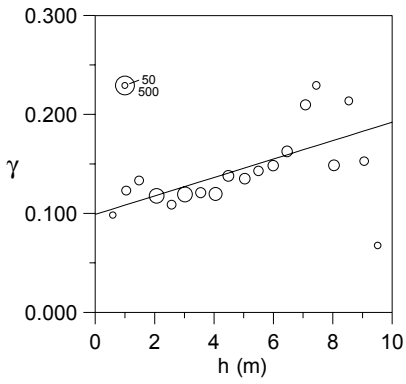


Figure C.12. Sample and model semi-variograms for grid-layer 22c.

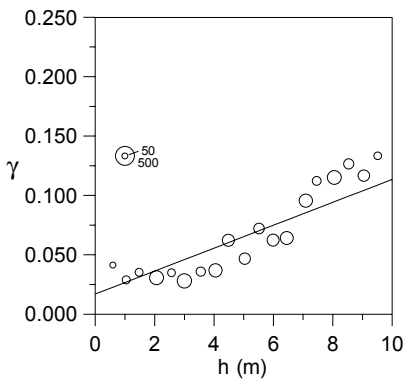


Figure C.13. Sample and model semi-variograms for grid-layer 22d.

C.8. Grid 23

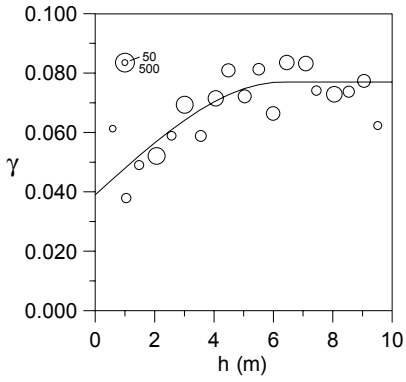


Figure C.14. Sample and model semi-variograms for grid-layer 23a.

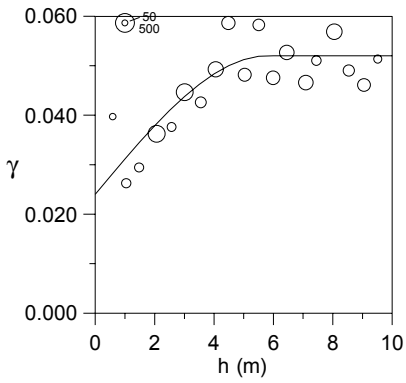


Figure C.15. Sample and model semi-variograms for grid-layer 23b.

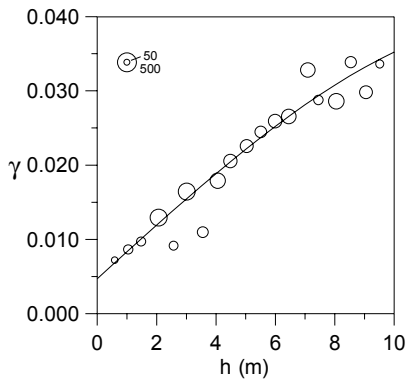


Figure C.16. Sample and model semi-variograms for grid-layer 23c.

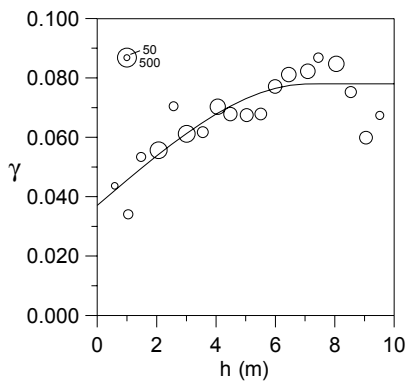


Figure C.17. Sample and model semi-variograms for grid-layer 23d.

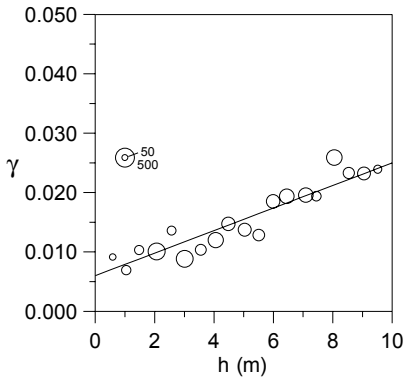


Figure C.18. Sample and model semi-variograms for grid-layer 23e.

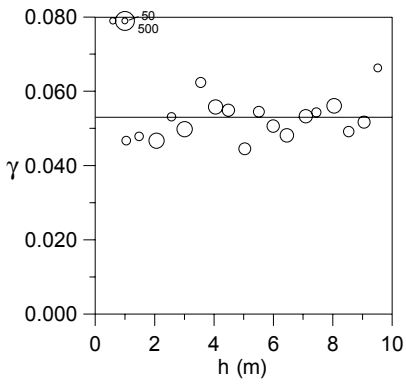


Figure C.19. Sample and model semi-variograms for grid-layer 23f.

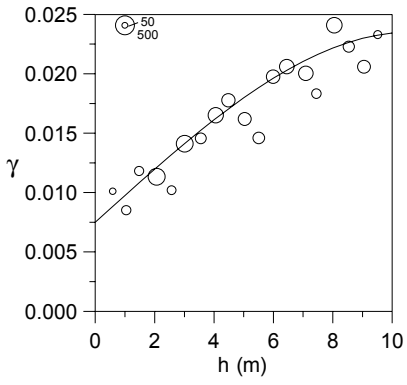


Figure C.20. Sample and model semi-variograms for grid-layer 23g.

Curriculum Vitae

Personal Details

<i>Name</i>	Kalle Kronholm
<i>Date of Birth</i>	11 July 1972
<i>Place of Birth</i>	Nakuru, Kenya
<i>Nationality</i>	Danish

Education

<i>1979 – 1986</i>	Primary school. Visborg, Hadsund, Denmark
<i>1986 – 1988</i>	Secondary school. Hadsund, Denmark
<i>1988 – 1989</i>	Gymnasium. Hobro, Denmark
<i>1989 – 1991</i>	International Baccalaureate in Victoria, Canada
<i>1992 – 1999</i>	Student at University of Copenhagen, Geographical Institute. Specialization in glaciology and coastal morphodynamics. Thesis: "Sediment transport in the inner surf zone; a comparison of the Bailard formulation with field measurements". Glaciological and hydrological fieldwork in Greenland.
<i>2000 – 2003</i>	PhD student at SLF, Davos and University of Zurich, Department of Geography

Abstract

The spatial variability of snowpack mechanical properties strongly influences the fracture initiation and fracture propagation properties of the snowpack, thereby largely controlling the avalanche formation process. The slope-scale spatial variability of the snowpack was investigated on small potential avalanche slopes above timberline near Davos, Switzerland. The characterization of variability was accomplished by combining classical and new measurement methods. The sampling strategy was to optimize the measurement layout for geostatistical analysis. The fracture initiation properties of the snow cover were measured with stuffblock and rammrutsch point stability tests at 24 locations on each slope. High-resolution profiles of penetration resistance were recorded with a novel snow micro-penetrometer, the "SnowMicroPen", at more than 100 locations on each slope. On each slope, a classical stratigraphic profile was made and samples of weak layers were taken. The spatial structure of stability and penetration resistance was modeled as a trend plus residual variation that was described with the semi-variogram. The trend was modeled as a linear regression on the measurement coordinates. A spherical semi-variogram model was used to describe the residual variation.

Twenty weak layers were identified by fractures in point stability tests. The spatial variability of point stability had a spatial structure, mainly in the form of slope-scale trends. The trends accounted for around 40% of the observed spread. The quartile coefficient of variation around the linear trend was around 20% with a maximum of around 50%. This variation around the trend had little spatial structure and was within the measurement error of the tests. The weak layer depth partly explained the variation in stability.

The snow cover stratigraphy was reconstructed from the snow micro-penetrometer profiles. The 21 investigated layers were both weak layers and wind-slabs. The weak layers were identified in all penetrometer profiles on a slope, i.e. they were spatially continuous. A significant spatial trend in penetration resistance was found in most layers. The quartile coefficient of variation around the linear trend was around 15% with a maximum of around 60%. Spatial structure around the linear trend was found in all layers except in a layer of buried surface hoar. The range of spatial auto-correlation varied between 2 m and more than 10 m. The layer depth partly explained the spatial variation in penetration resistance. Each layer had unique geostatistical properties with regard to penetration resistance. These were likely caused by the different depositional processes acting during each depositional event, thus emphasizing the sedimentary nature of the snow cover.

Similar slope scale spatial trends were found when comparing the results from the point stability tests and the micro-penetrometer profiles.

For the first time, the three-dimensional variability of the snow cover was quantified. The results can be used to improve snow cover models that currently do not reflect the spatial variability observed in the field. With regard to the avalanche formation process, the study showed that the weak layers were continuous (through going) at the slope-scale, and that their penetration resistance had a spatial structure with typical length scales of a few meters. Likewise, results from snowpack stability tests had a spatial structure. Therefore, stability tests will not give random results and are useful to assess snow cover stability. The type of variability found suggests that once initiated, a fracture is likely to propagate through the weak layer without being arrested before reaching the critical size where a snow slab avalanche is released.